ERDC TR-04-6

Engineer Research and Development Center

US Army Corps of Engineers®

Characterization of Soils from the Night Vision and Electronic Sensors Directorate Mine Lane Facility, Fort Belvoir, VA

John O. Curtis, Dan Leavell, Charles Weiss,
Ryan North, Eric Smith, Javier Cortes, Ray Castellane,
and Morris Fields

December 2004

ERDC TR-04-6
December 2004

Characterization of Soils from the Night Vision and Electronic Sensors Directorate Mine Lane Facility, Fort Belvoir, VA

John O. Curtis, Javier Cortes, and Morris Fields

Environmental Laboratory
U.S. Army Engineer Research and Development Center
3909 Halls Ferry Road
Vicksburg, MS 39180-6199

Dan Leavell, Charles Weiss, Ryan North, Eric Smith, and Ray Castellane

Geotechnical and Structures Laboratory
U.S. Army Engineer Research and Development Center
3909 Halls Ferry Road
Vicksburg, MS 39180-6199

Final report

Prepared for U.S. Army Corps of Engineers
Washington, DC 20314-1000

ABSTRACT: In support of mine detection sensor development programs at the U.S. Army Night Vision and Electronic Sensors Directorate, both onsite and laboratory measurements of soil properties were conducted on soils from the Fort Belvoir, VA, indoor mine lane facility. The lanes contain six distinctly different soils. In an effort to characterize these soils for both current and anticipated sensor technologies, measurement activities included onsite seismic refraction data collection and laboratory measurements of physical property data, complex dielectric constants, magnetic susceptibilities, visual specular reflectances, broadband infrared reflectances, and soil mineralogy and chemistry.

Contents

List of Figures

List of Tables

Preface

The work reported in this document was performed for the U.S. Army RDECOM CERDEC, Night Vision and Electronic Sensors Directorate (NVESD), located at Fort Belvoir, VA. It was done at the request of Mr. Ian McMichael, an engineer in the NVESD Science and Technology Division, Countermine Team, in support of multiple mine detection sensor test and development programs.

Dr. John O. Curtis, Environmental Systems Branch (ESB), Ecosystem Evaluation and Engineering Division (EE), Environmental Laboratory (EL), Engineer Research and Development Center (ERDC), Vicksburg, MS, had overall responsibility for conducting this study. Other ERDC employees who made significant contributions included Dr. Charles Weiss, Geotechnical and Structures Laboratory (GSL); Messrs. Dan Leavell, Ryan North, Ray Castellane, and Eric Smith from GSL; and Messrs. Morris Fields and Javier Cortes from EL.

This investigation was conducted under the direct supervision of Mr. Wade West, Chief, ESB, and the general supervision of Dr. Dave Tazik, Chief, EE.

At the time of publication of this report, Dr. Edwin A. Theriot was Director, EL, and Dr. James R. Houston was Director of ERDC. Commander and Executive Director of ERDC was COL James R. Rowan, EN.

1 Introduction

Background

The U.S. Army Night Vision and Electronic Sensors Directorate (NVESD) maintains a land mine technology test facility at Fort Belvoir, VA, where mine detection sensors can be tested in a variety of controlled environmental conditions. Building 353 at Fort Belvoir contains two sets of six mine lanes (troughs that are each filled with a different type of soil). Analysis of seismic refraction data collected for this project, along with information gathered in conversations with the staff at NVESD, clearly indicated that the depth of these lanes varied from one end of the building to the other. The northern lanes, pictured in Figure 1-1, are 1.2 m deep, 32.7 m long, and approximately 3.0 m wide. The southern lanes, pictured in Figure 1-2, are 1.8 m deep, 18.9 m long, and approximately 3.0 m wide. Depths were not confirmed with core samples because of the risk of disturbing the structure of the lanes.

A sprinkler system, moisture sensors, and a buried drainage system can be utilized on the southern lanes to control moisture content of the soils. The sidewalls of all of the lanes are wooden planks, while the bottom of each lane is on top of approximately 0.5 m of gravel which, in turn, lies on top of compacted native soil. Each of the lanes is surrounded by plastic sheeting on all sides.

Objective of This Study

The staff at NVESD expressed a desire to fully characterize all of the soils in their mine lane facility to support their own test projects as well as those of numerous contractors who use the facility to test prototype mine detection and/or discrimination sensor systems. Throughout the history of this facility, various measurements of soil properties have been conducted by users for their own measurement programs. However, no compilation of these measurements has ever been attempted. Therefore, the objective of this study was to produce a single document containing as much soil characterization data as might be useful to any sensor developer making use of the facility.

Figure 1-1. Long mine lanes in the north end of building 353, lane 1 to the right

Figure 1-2. Short mine lanes in the south end of building 353, lane 1 to the left

Acquisition of Samples

Three sealed plastic bag samples of soil were collected from each mine lane and shipped to the U.S. Army Engineer Research and Development Center (ERDC) laboratories in Vicksburg, MS, where all of the characterization measurements were performed (with the obvious exception of the seismic refraction surveys). The samples were surface soils and were collected at the following locations: those that will later be labeled "North End" were collected at a spot about 10 m south of the extreme north boundary of each lane; those labeled "Middle" were scooped up from a spot about 20 m south of the north boundary; and those labeled "South End" were collected in the middle of the short mine lanes at the south end of building 353. Eighteen sample bags were shipped to ERDC; sixteen survived shipment, while the other two broke open and the soils were mixed in the shipping container.

Report Content

This report is divided into seven chapters of soil characterization data collected by the authors and edited by the first author. Mr. Leavell supervised the collection of physical property data found in Chapter 2. Information presented there includes grain-size distribution curves, plasticity indices, specific gravities, and soil classifications. Soil mineralogy and chemistry data were collected by Dr. Weiss. Results are contained in Charter 3. Chapter 4 presents the results of seismic refraction surveys performed on each lane at NVESD by Mr. North and Dr. Curtis, the final result being tables of shear wave (S-wave) and pressure (P-wave) wave speeds for the lane soils and the underlying gravel layer. Electrical properties of the soils are found in Chapter 5. These data, collected by Dr. Curtis, include the complex dielectric constants, loss tangents, equivalent electrical conductivities, power losses, and phase velocities as a function of signal frequency and volumetric moisture content. Chapter 6 contains magnetic susceptibility measurements at two frequencies made by Mr. Smith. Mr. Cortes collected specular reflectance data in the visual portion (380 to 730 nm) of the electromagnetic spectrum, which is presented in Chapter 7. The report concludes with broadband (2.5 to 24 μm) infrared reflectance data measured by Messrs. Castellane and Fields and reported in Chapter 8.

For additional details on how the data in this report were collected, please contact the first author at the U.S. Army Engineer Research and Development Center (ERDC), Environmental Laboratory, Vicksburg, MS, (voice: 601-634-2855, FAX: 601-634-2575, e-mail: *John.O.Curtis@erdc.usace.army.mil*).

2 Physical Property Data

Physical property data were collected on the 16 NVESD samples that survived shipment to the ERDC laboratories. These data include soil classifications by the Unified Classification System,[1] Atterberg limits, specific gravities, and gradation curves. Laboratory measurements were conducted using standard procedures (Headquarters, Department of the Army 1970).

Table 2-1 contains a summary of classification data and is followed by all of the gradation curves developed for the 16 samples being examined (Figures 2-1 through 2-16). The high specific gravity of the lane 1 samples is due to the presence of a substantial amount of magnetite (Fe_2O_3). The six mine lane soils classify into only three different types: poorly graded sand (SP), silty sand (SM), and low-plasticity clay (CL).

Table 2-1
Classification of NVESD Mine Lane Soils

Sample Identification	Sample No.	Atterberg Limits Liquid Limit/Plastic Limit	Classification	Specific Gravity
Lane 1 - North	1	NP	SAND (SP), GRAY	3.04
Lane 1 - South	2	NP	SAND (SP), GRAY	3.04
Lane 2 - North	3	27 / 17	CLAY (CL), BROWN	2.68
Lane 2 - Middle	4	25 / 16	CLAY (CL), GRAY	2.68
Lane 2 - South	5	29 / 18	CLAY (CL), BROWN	2.69
Lane 3 - North	6	NP	GRAVELLY SILTY SAND (SM), BROWN	2.7
Lane 3 - Middle	7	NP	GRAVELLY SILTY SAND (SM), BROWN	2.7
Lane 3 - South	8	NP	GRAVELLY SILTY SAND (SM), BROWN	2.7
Lane 4 - North	9	41 / 24	CLAY (CL), REDDISH BROWN	2.74
Lane 4 - Middle	10	45 / 27	CLAY (CL), REDDISH BROWN	2.74
Lane 5 - North	11	NP	SILTY SAND (SM), REDDISH BROWN; WITH GRAVEL	2.72
Lane 5 - Middle	12	NP	SILTY SAND (SM), REDDISH BROWN; WITH GRAVEL	2.72
Lane 5 - South	13	NP	GRAVELLY SILTY SAND (SM), REDDISH BROWN	2.72
Lane 6 - North	14	NP	SAND (SP), LIGHT GRAY; TRACE OF GRAVEL	2.65
Lane 6 - Middle	15	NP	SAND (SP), LIGHT GRAY; TRACE OF GRAVEL	2.64
Lane 6 - South	16	NP	SAND (SP), LIGHT GRAY	2.65

[1] U.S. Army Corps of Engineers, Waterways Experiment Station. (1953, revised 1960). "The Unified Soil Classification System," Technical Memorandum 3-357, Vicksburg, MS.

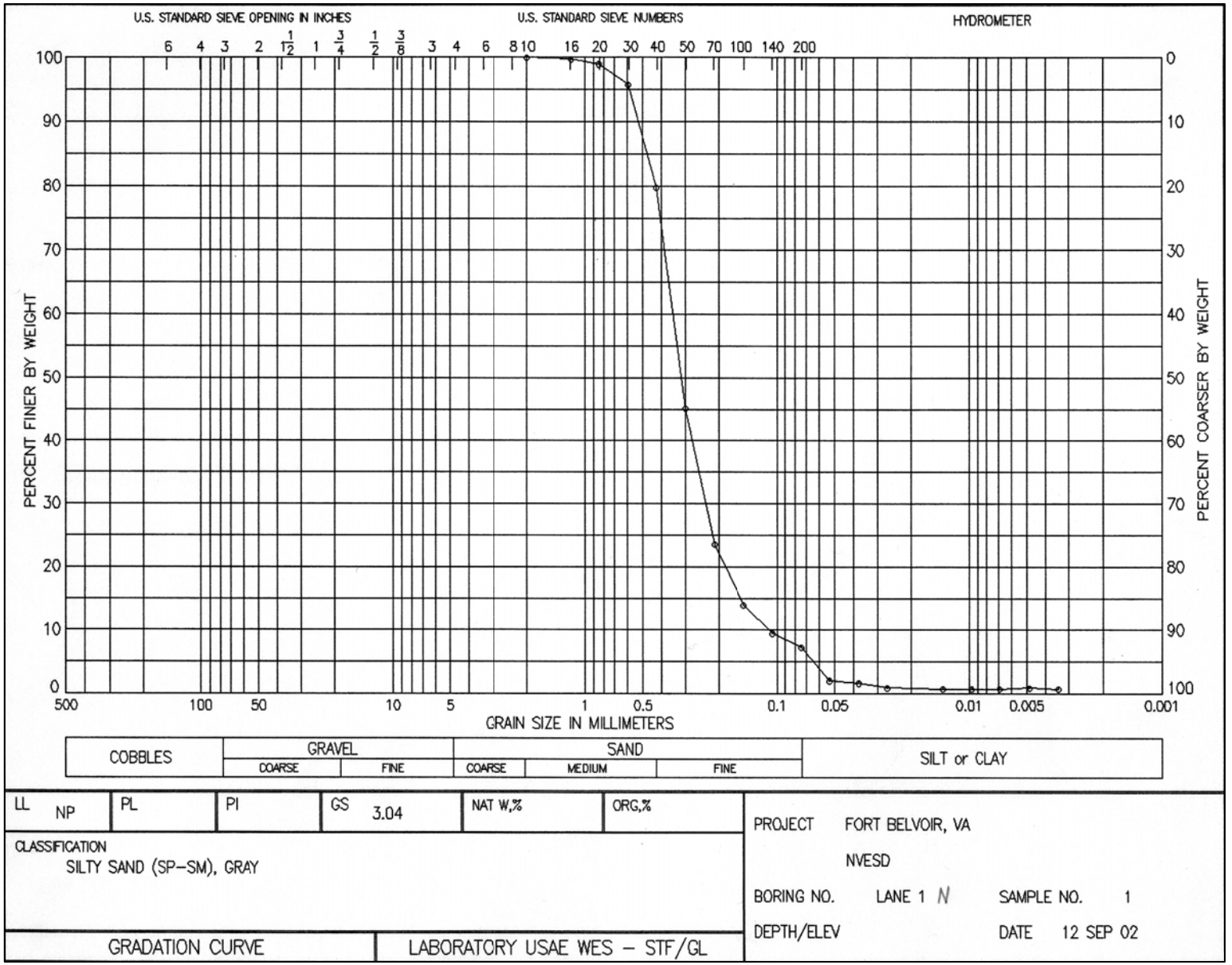

Figure 2-1. Gradation curve, Sample 1

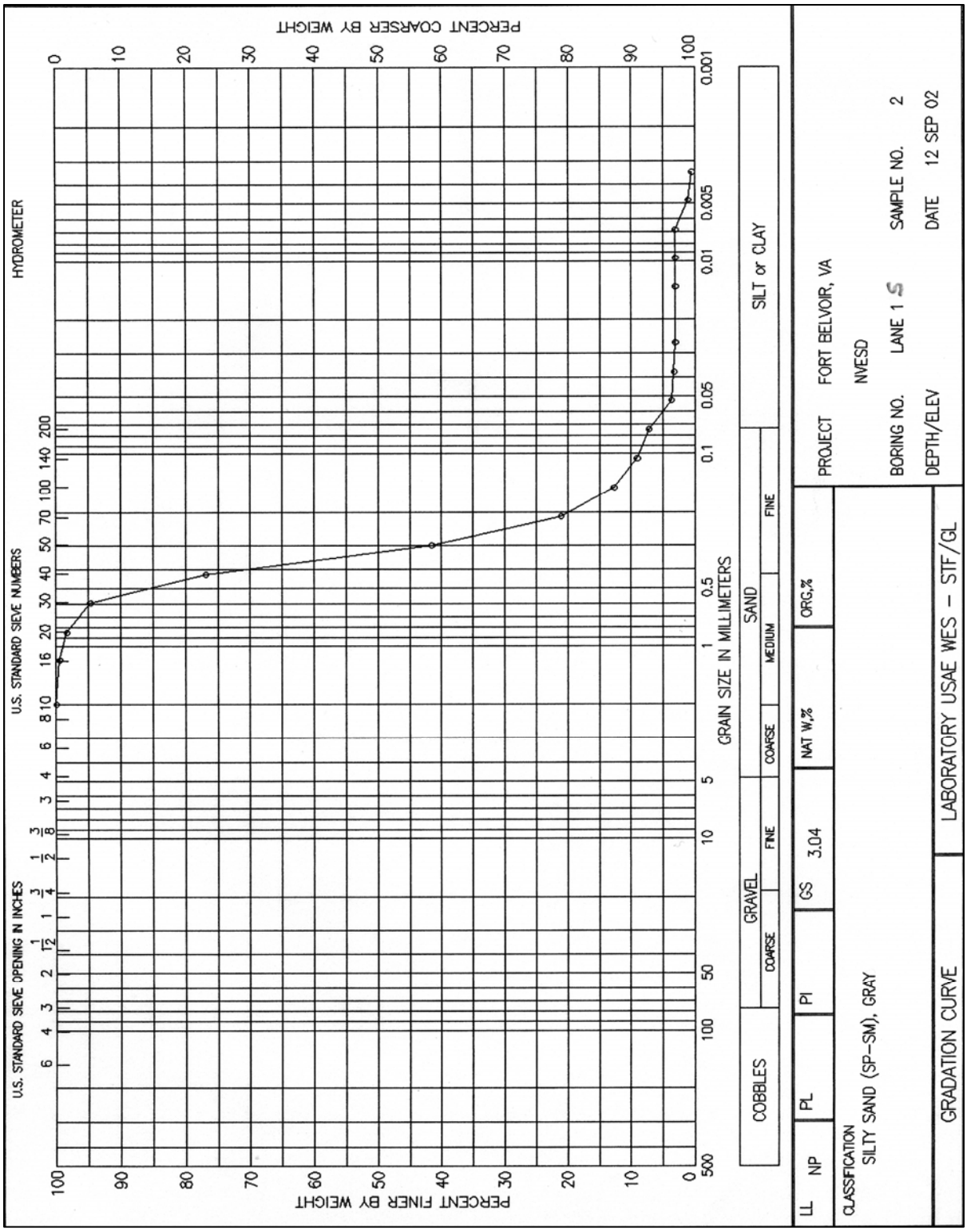

Figure 2-2. Gradation curve, Sample 2

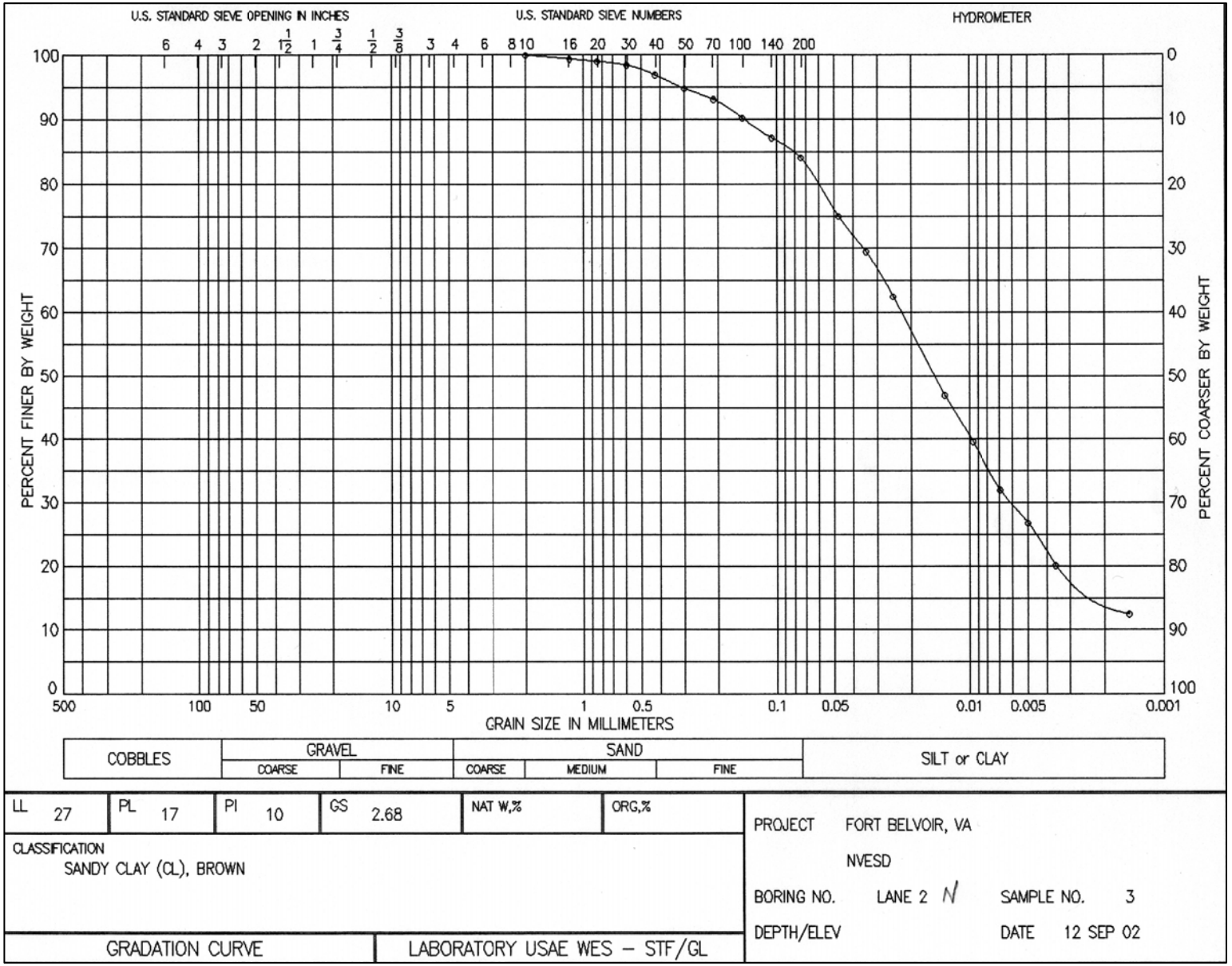

Figure 2-3. Gradation curve, Sample 3

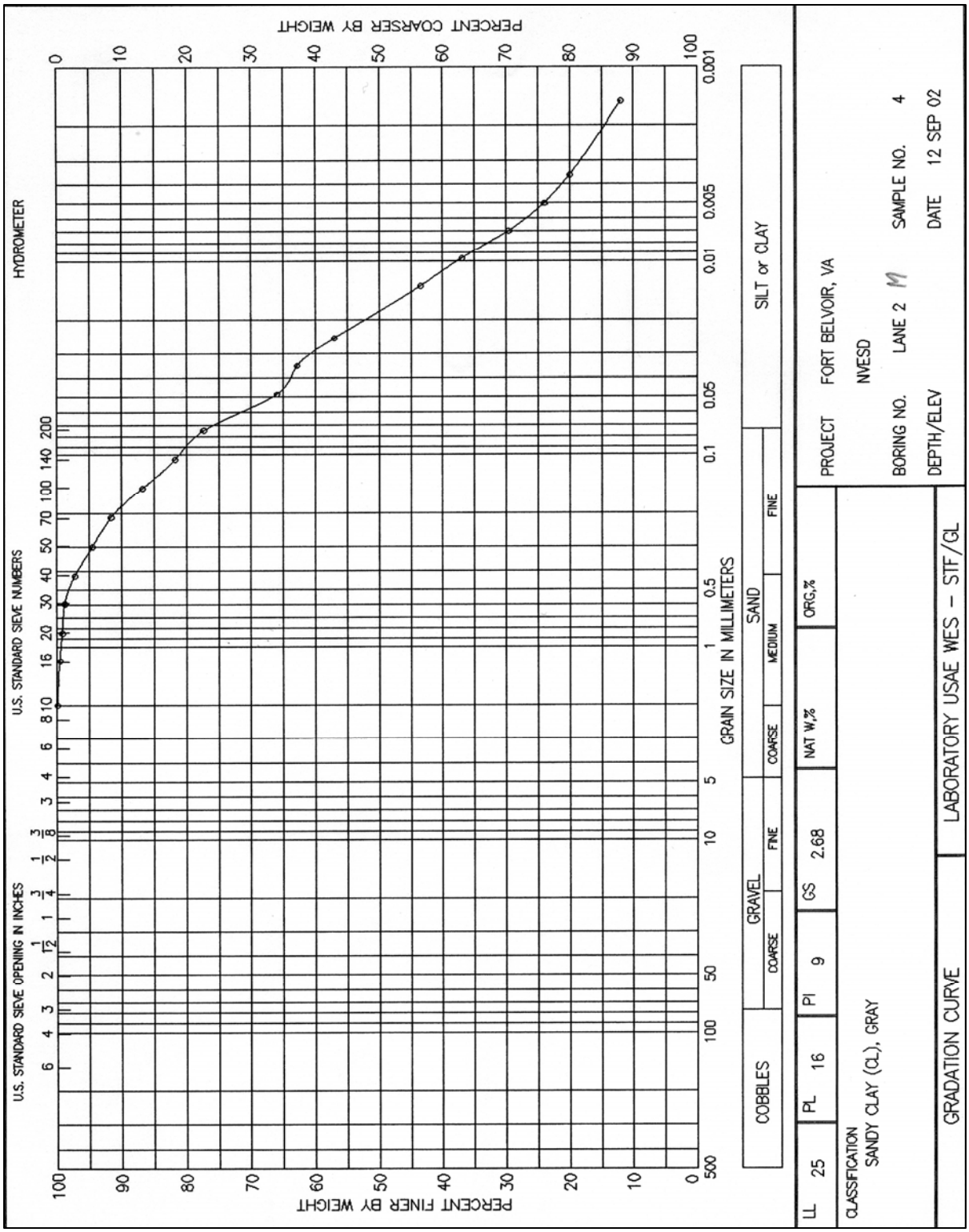

Figure 2-4. Gradation curve, Sample 4

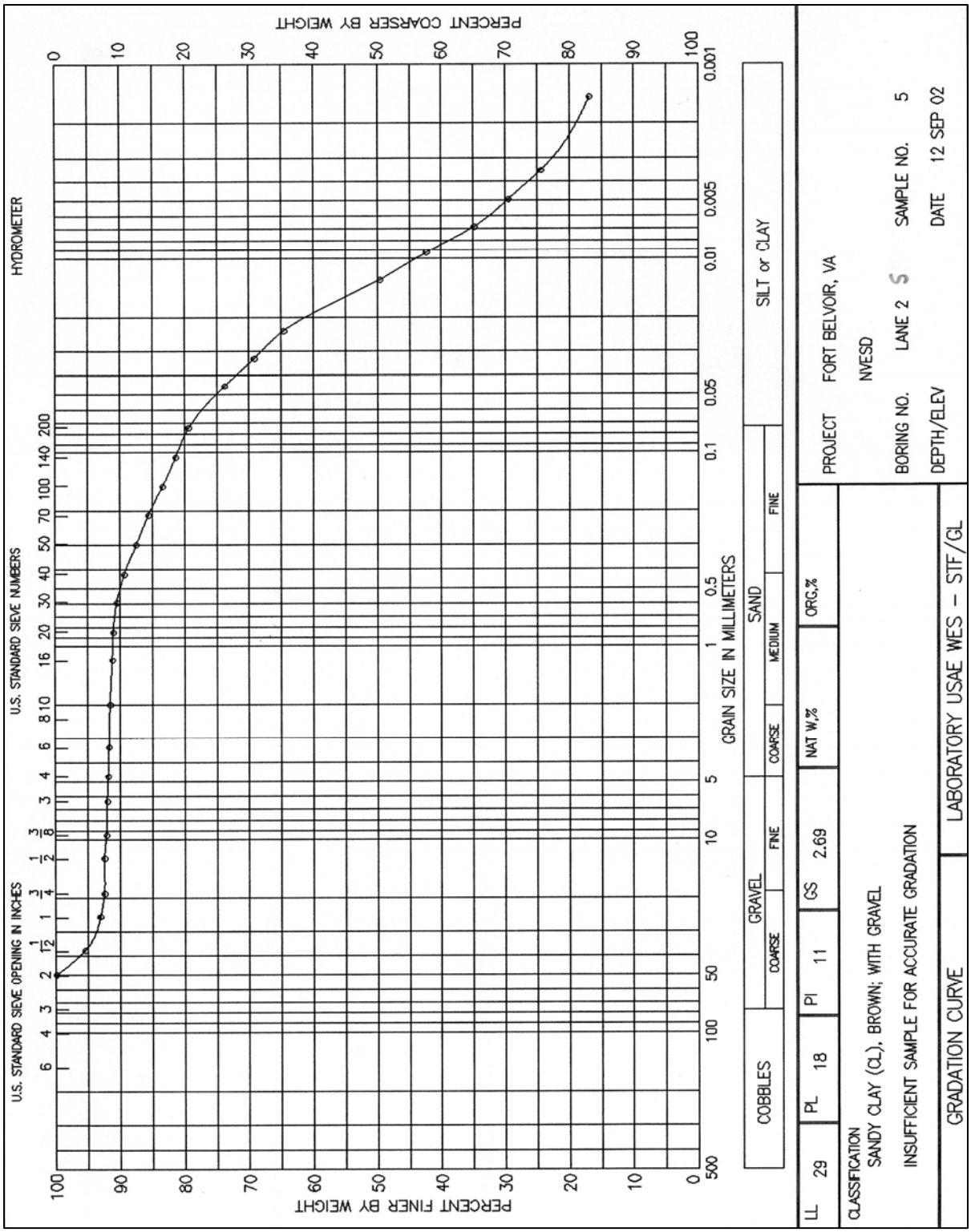

Figure 2-5. Gradation curve, Sample 5

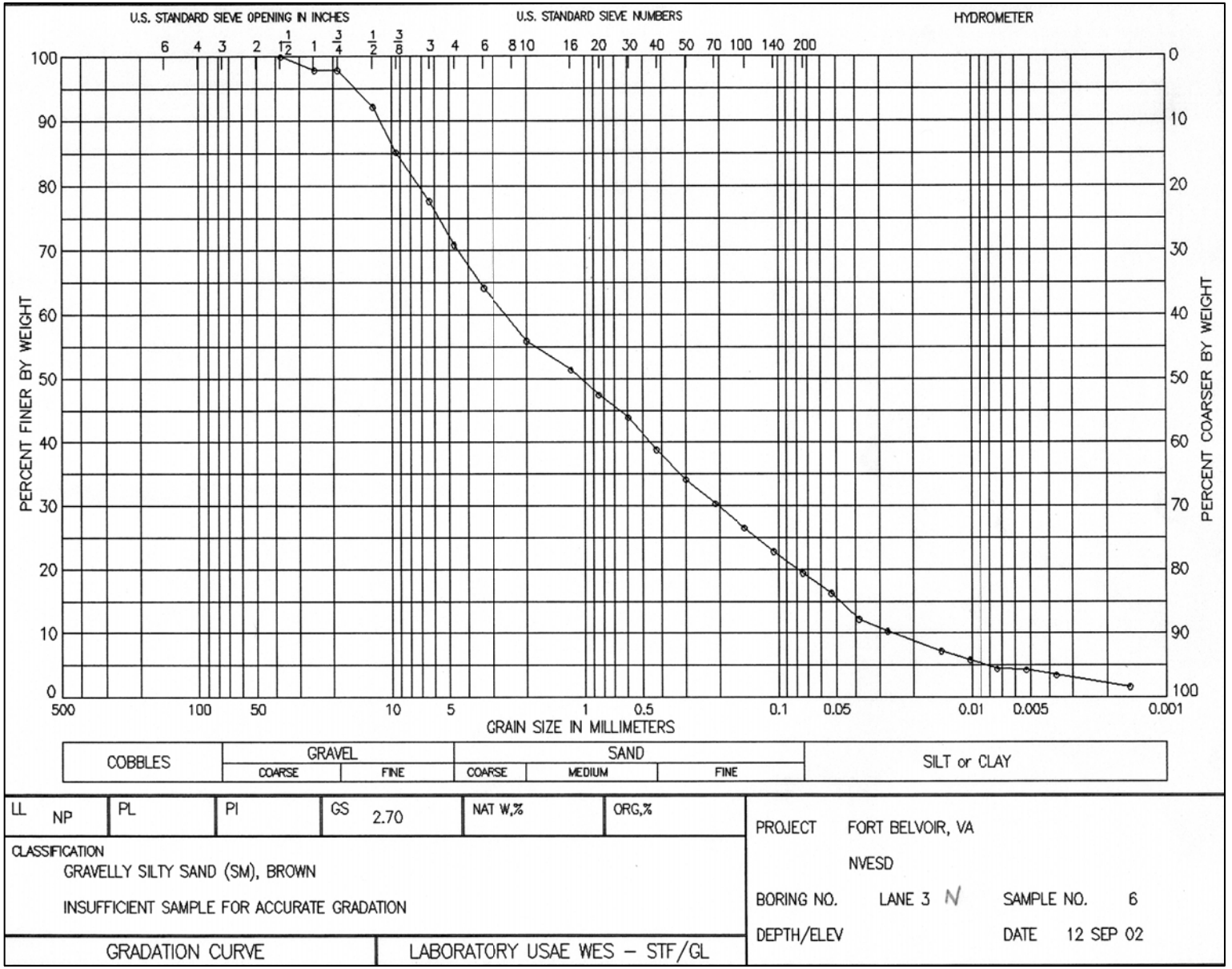

Figure 2-6. Gradation curve, Sample 6

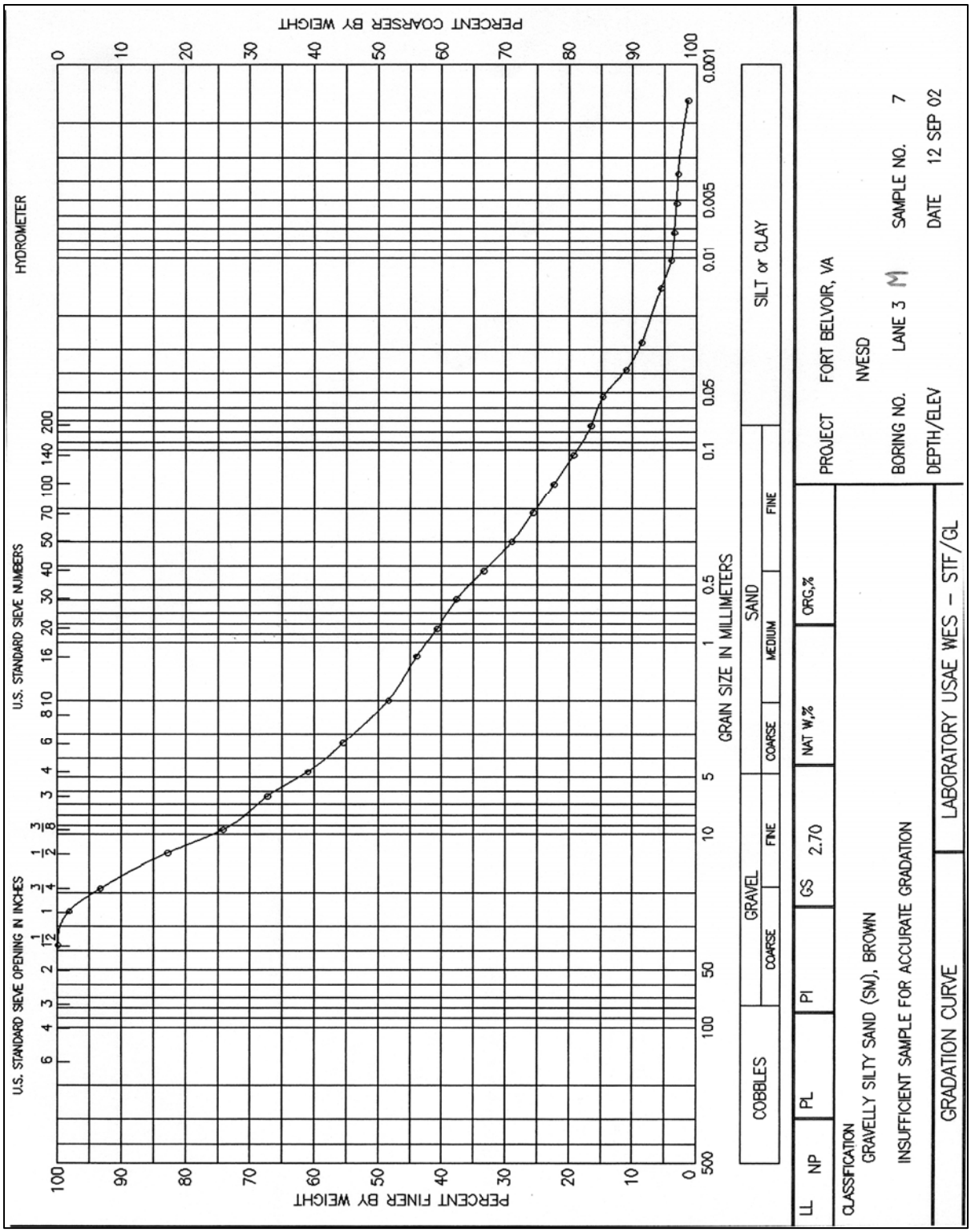

Figure 2-7. Gradation curve, Sample 7

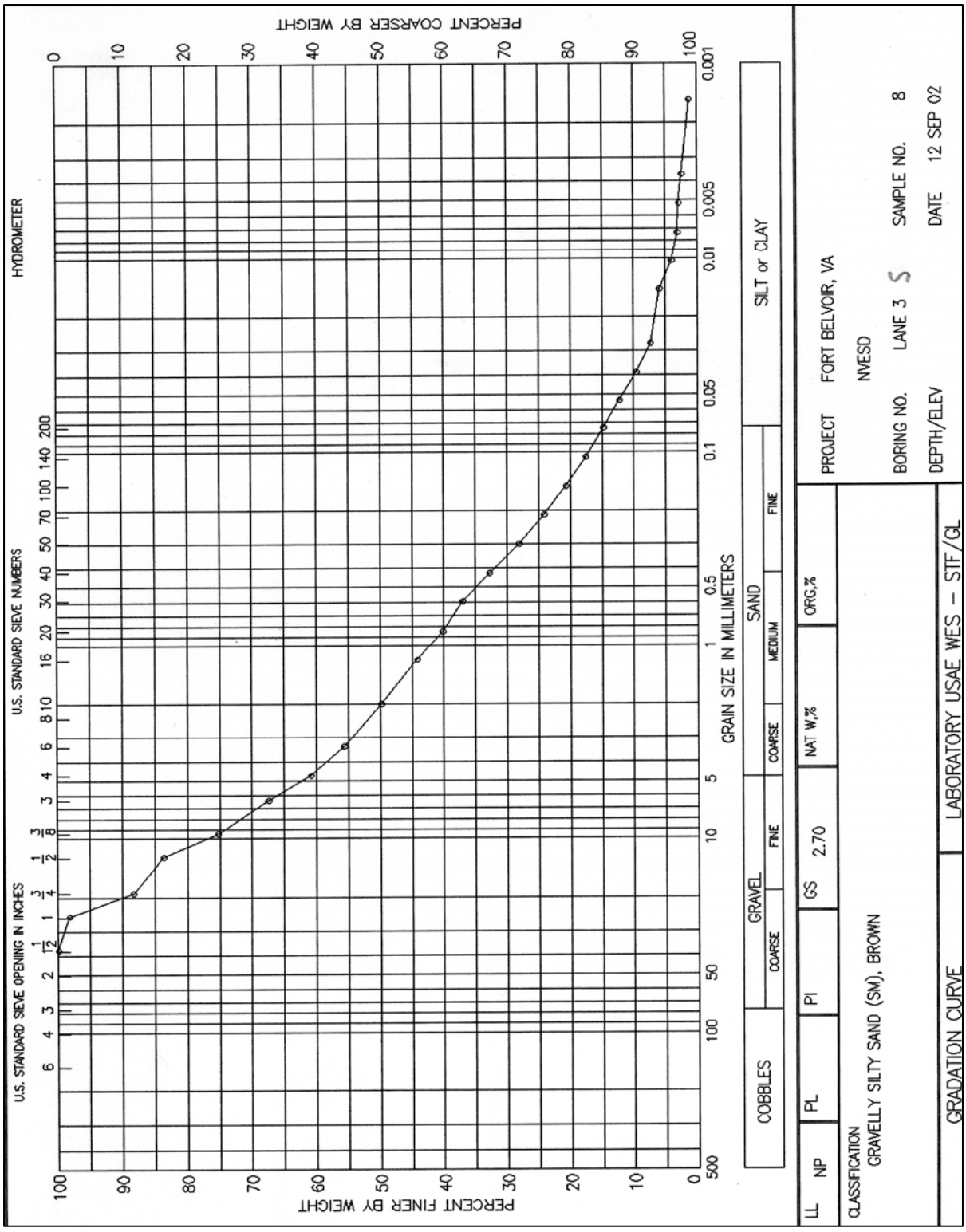

Figure 2-8. Gradation curve, Sample 8

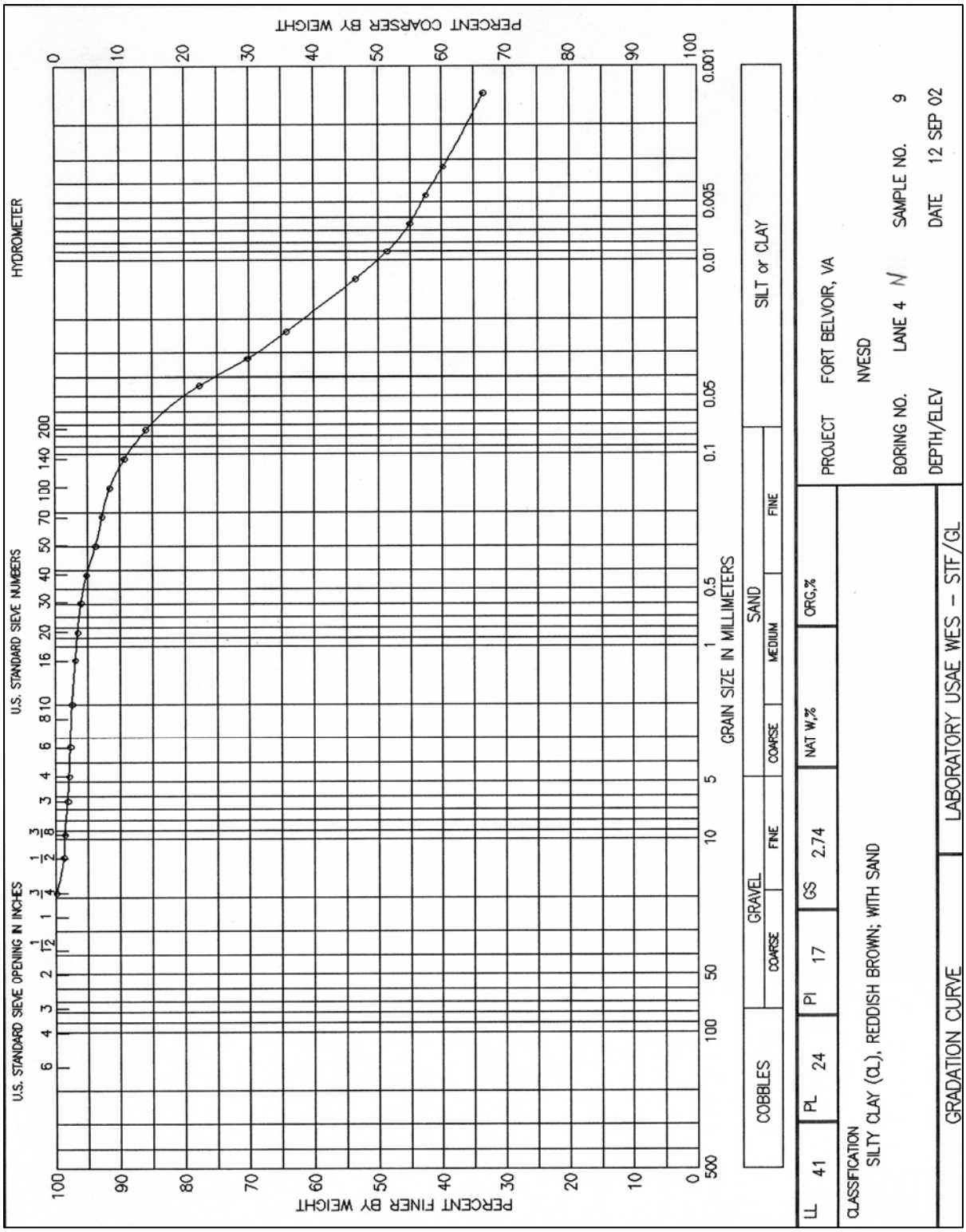

Figure 2-9. Gradation curve, Sample 9

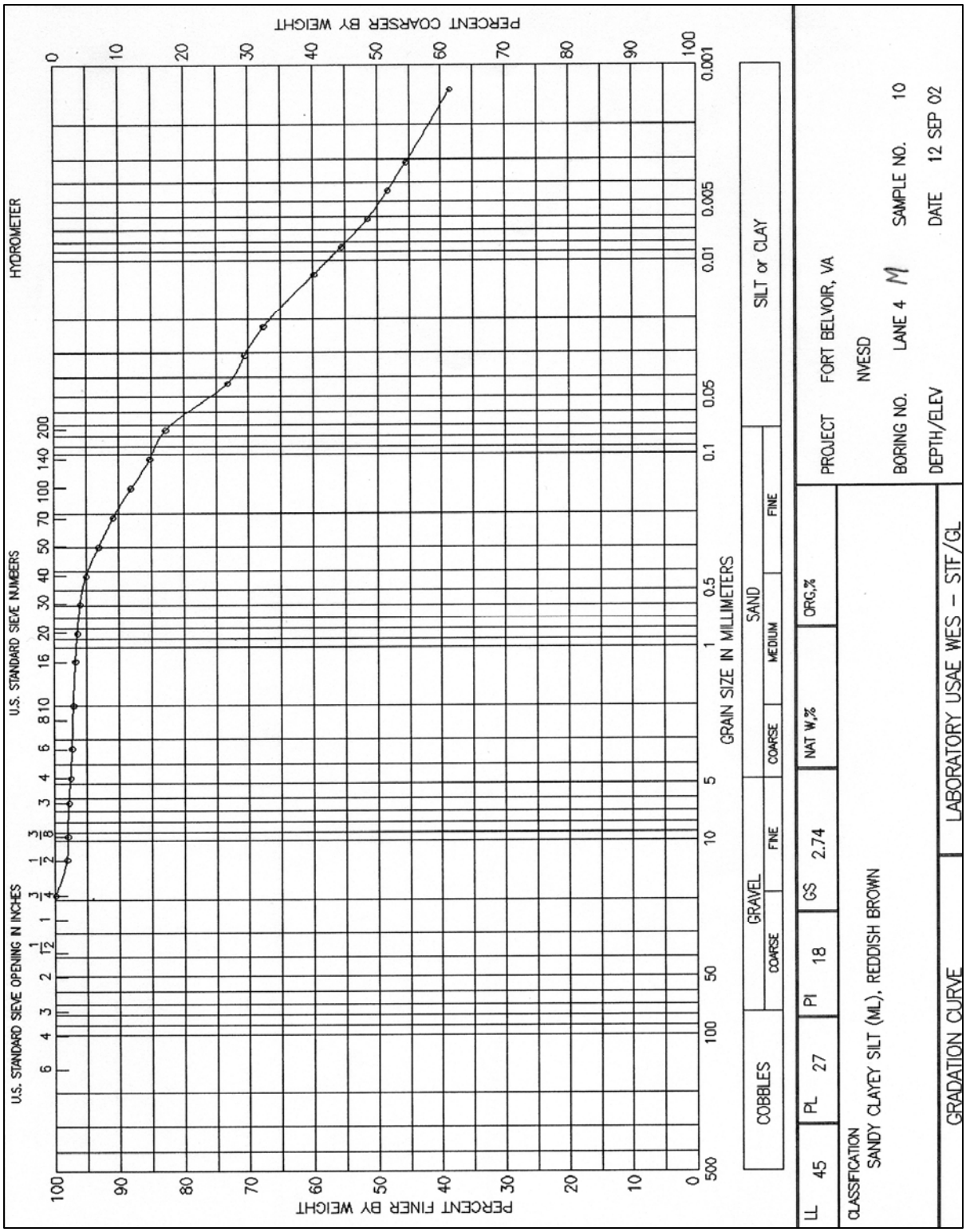

Figure 2-10. Gradation curve, Sample 10

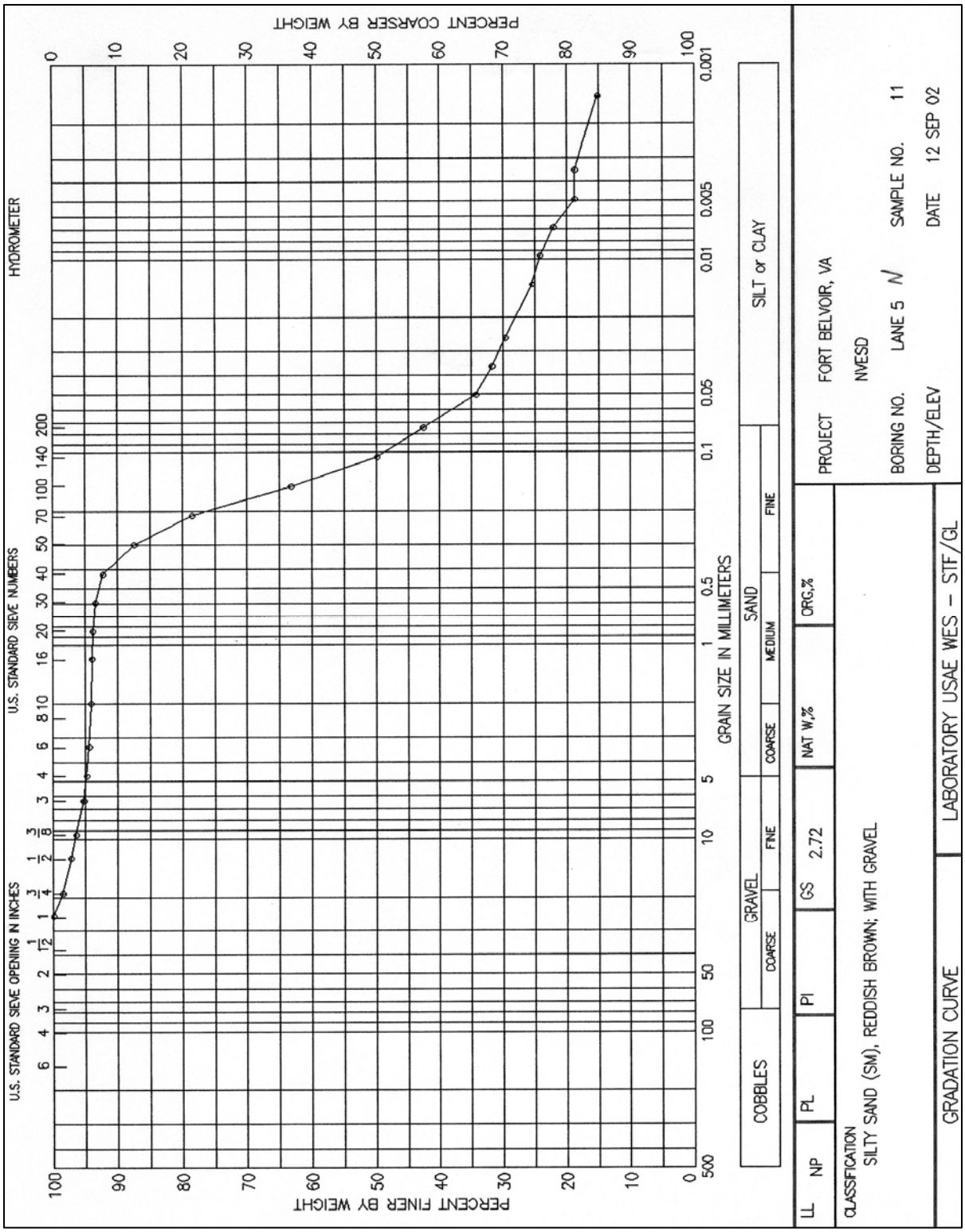

Figure 2-11. Gradation curve, Sample 11

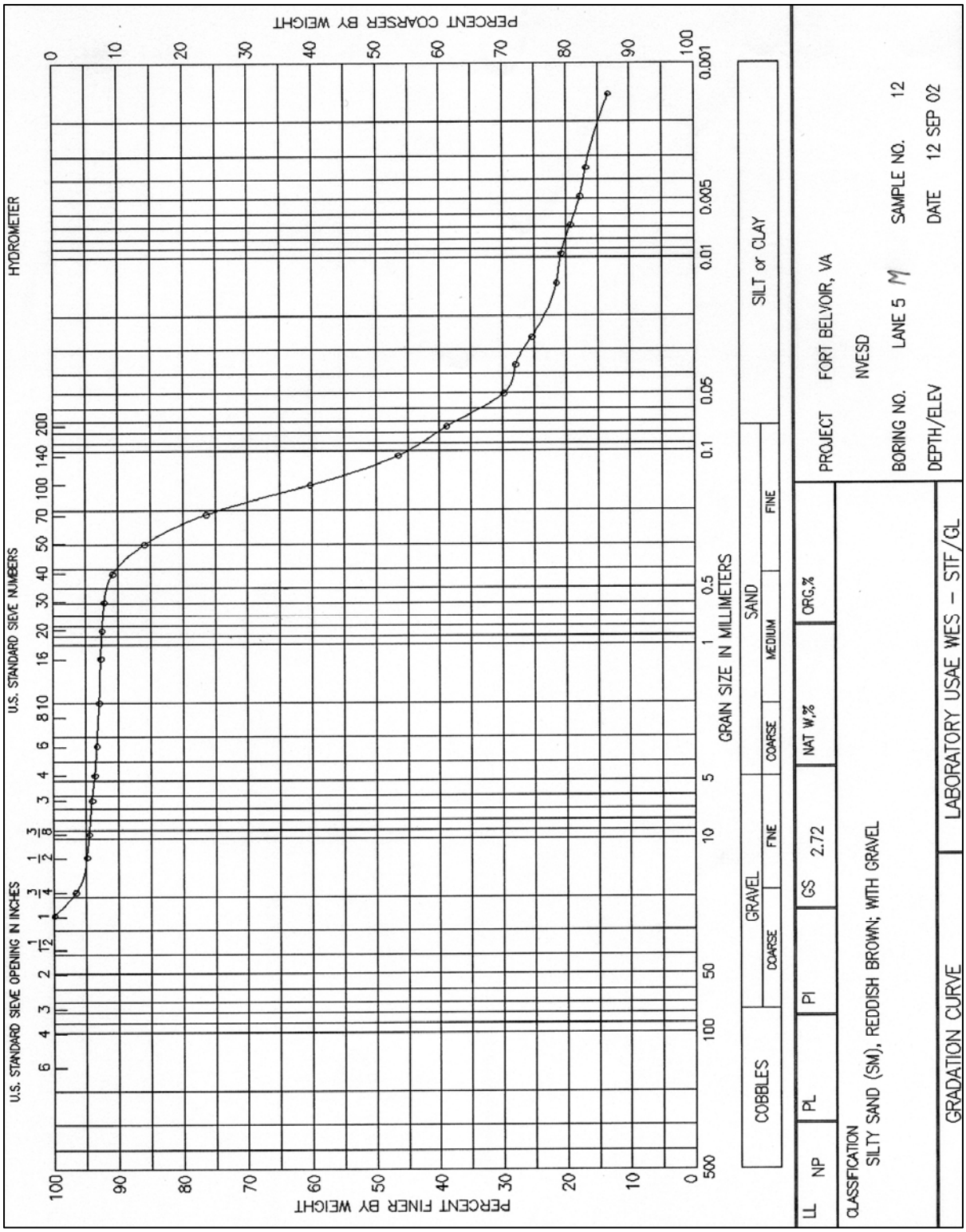

Figure 2-12. Gradation curve, Sample 12

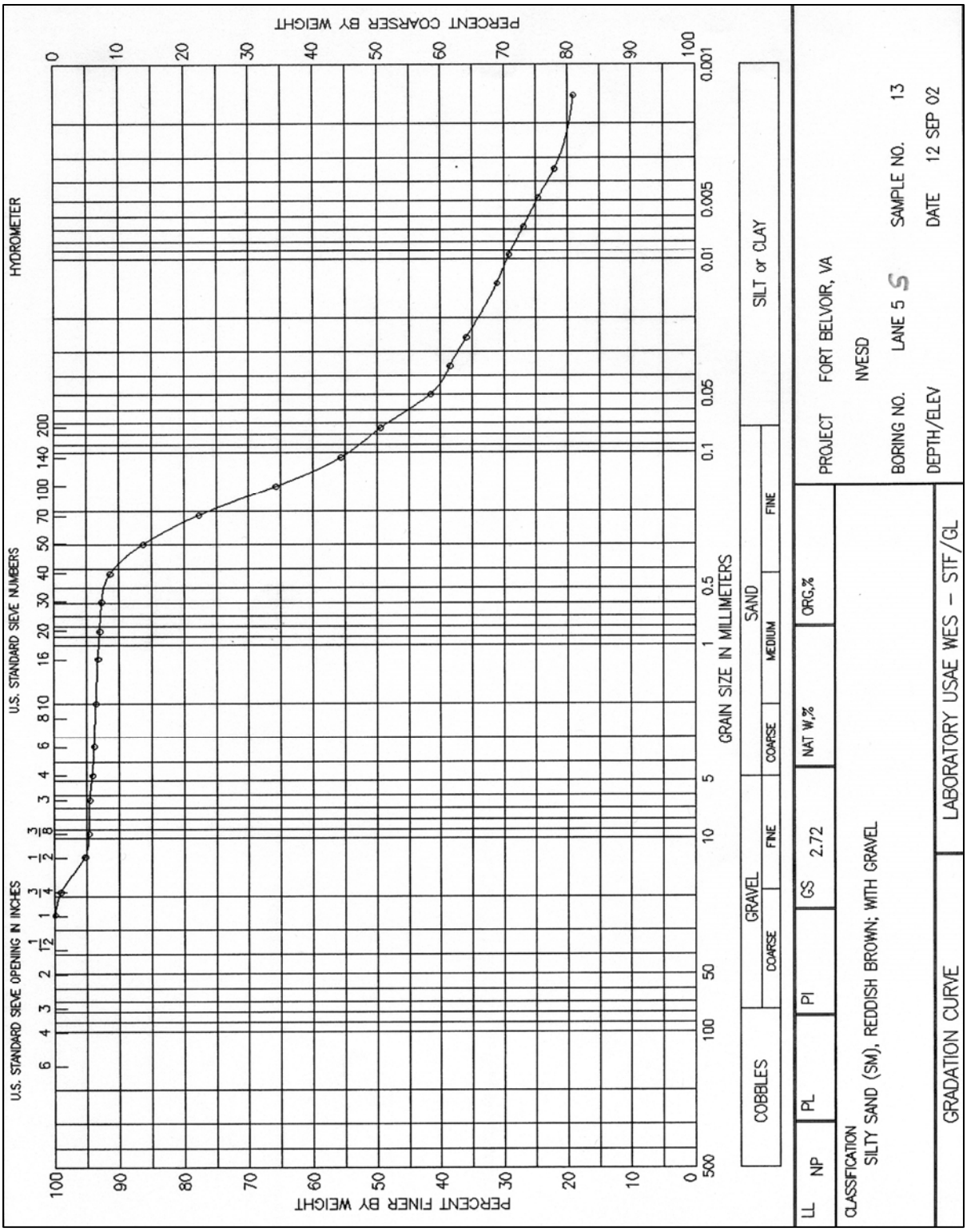

Figure 2-13. Gradation curve, Sample 13

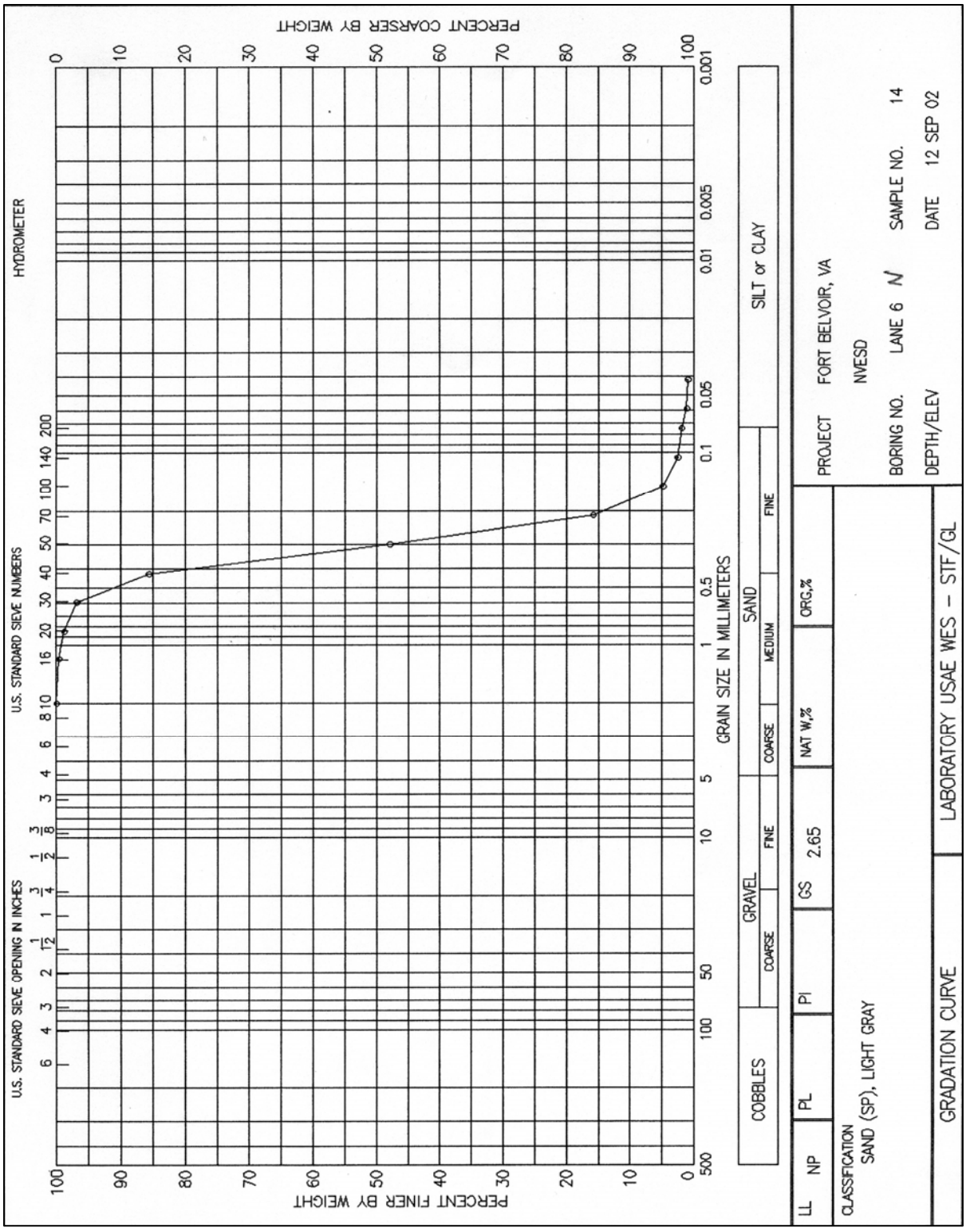

Figure 2-14. Gradation curve, Sample 14

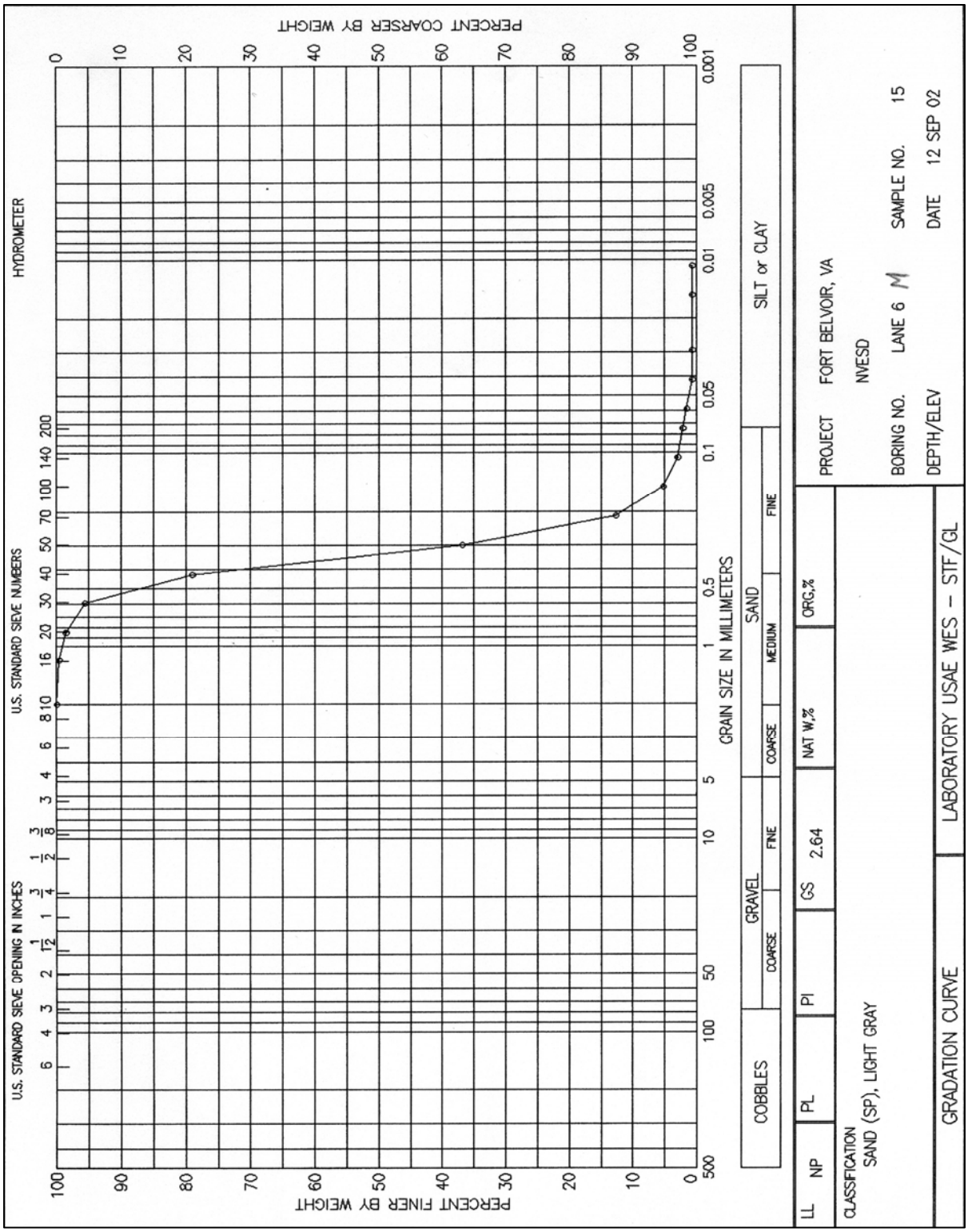

Figure 2-15. Gradation curve, Sample 15

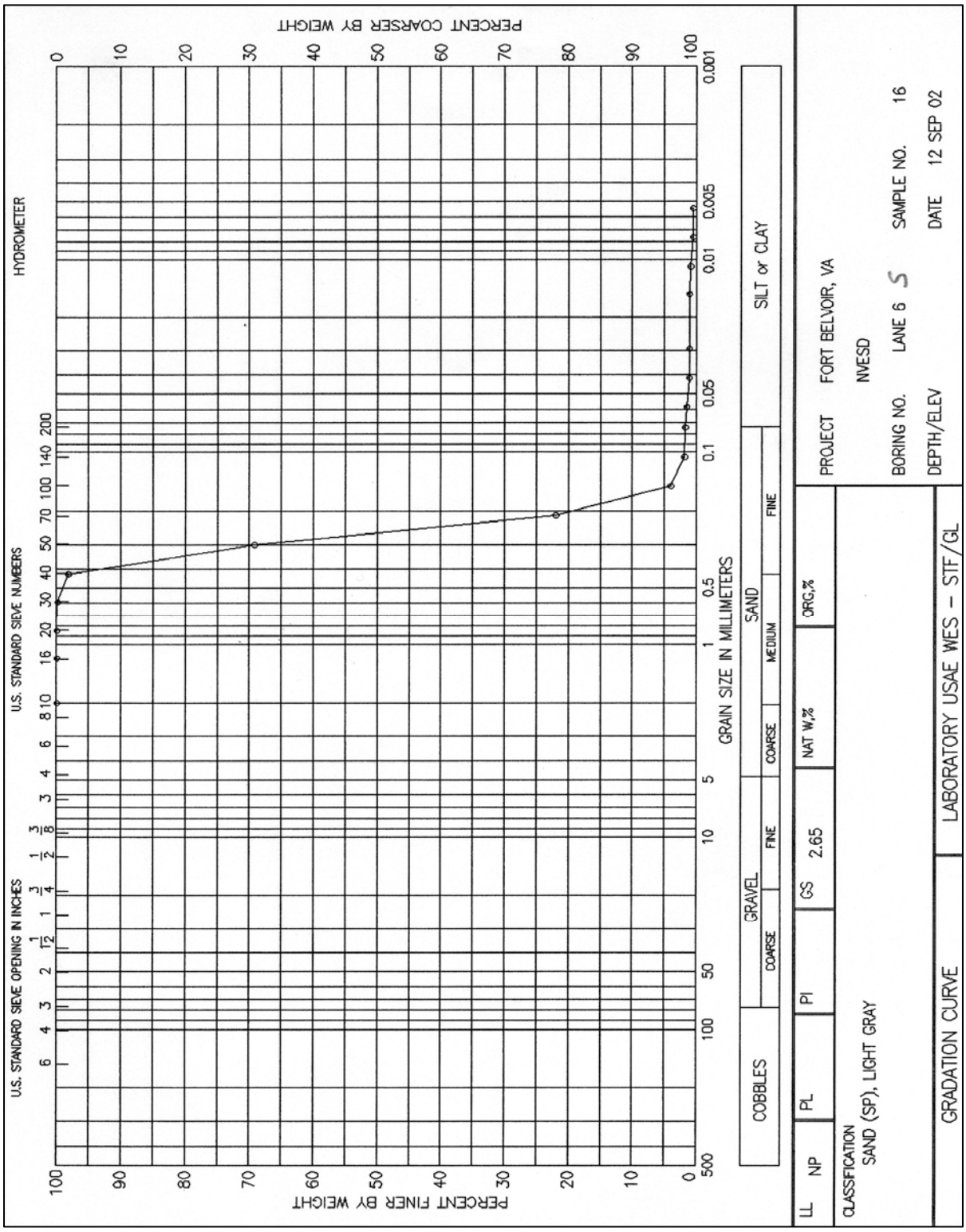

Figure 2-16. Gradation curve, Sample 16

3 Soil Mineralogy and Chemistry

Soil mineralogy and chemistry data were collected using X-ray diffraction and energy-dispersive X-ray chemical analyzer equipment housed in the ERDC Petrology Laboratory. The following sections include both tabulated data and diffraction spectra for 12 of the 16 soil samples obtained from NVESD.

X-ray Diffraction Analysis (Mineralogy)

The X-ray diffraction samples were run as randomly oriented packed powders. A Philips PW1800 Automated Powder Diffractometer system was utilized to collect X-ray diffraction (XRD) patterns employing standard techniques for phase identification. The run conditions included Cu K_{α} radiation and scanning from 2 to 65 º2θ with collection of the diffraction patterns accomplished using the PC-based, Windows-based version of Datascan, and analysis of the patterns using the Jade program (both from Materials Data, Inc.). In preparation for XRD analysis, a portion of the sample was ground in a mortar and pestle to pass a 45-µm mesh sieve (No. 325). Bulk sample random powder mounts were analyzed using XRD to determine the mineral constituents present in each sample (Figures 3-1 through 3-6).

To determine the type of phyllosilicates present, oriented samples of the <4-µm-size fraction of each sample were prepared and XRD patterns were obtained. These samples were then placed in an ethylene glycol atmosphere overnight at room temperature, and an X-ray diffraction pattern was collected for each sample. Samples that show expansion of the crystal structure after exposure to an ethylene glycol atmosphere compared to air-dried pattern indicate expandable smectic clays. Comparisons of patterns obtained before and after exposure to ethylene glycol were used to determine the amount of expandable clay present.

Semiquantitative determinations of whole-rock mineral amounts are done utilizing integrated peak areas (derived from peak-decomposition/profile-fitting methods) and empirical reference intensity ratio (RIR) factors determined specifically for the diffractometer used in data collection. The total phyllosilicate (clay and mica) abundance of the samples is determined on the whole-rock XRD patterns using combined {001} and {hkl} clay mineral reflections and suitable empirical RIR factors.

The bulk mineralogy of each sample is given in Figures 3-1 through 3-6. A complete summary of the mineral phases found in each sample and their relative abundances can be seen in Table 3-1.

Chemical Analysis

Bulk chemical composition of each sample was analyzed using an energy-dispersive X-ray analyzer (Table 3-2). The samples were prepared by making a pellet using a portion of the <45-µm fraction and a methylcellulose binder. The equipment used was a Fisons-Kevex 771 EDX chemical analyzer for bulk samples running the XRF Toolbox II version 4.4 software on a PC. These analyses were made using the software package EXACT — Energy-dispersive X-ray analysis Computation Technique (Kevex Instruments XRF Toolbox II Reference Manual, San Carlos, California, 1990) and a plastic clay standard (Source Reference Material from the National Institute of Standards and Technology, Standard Reference Material 98b). In this procedure, the standard is analyzed, and the intensity obtained for each element is calibrated to the known chemical composition.

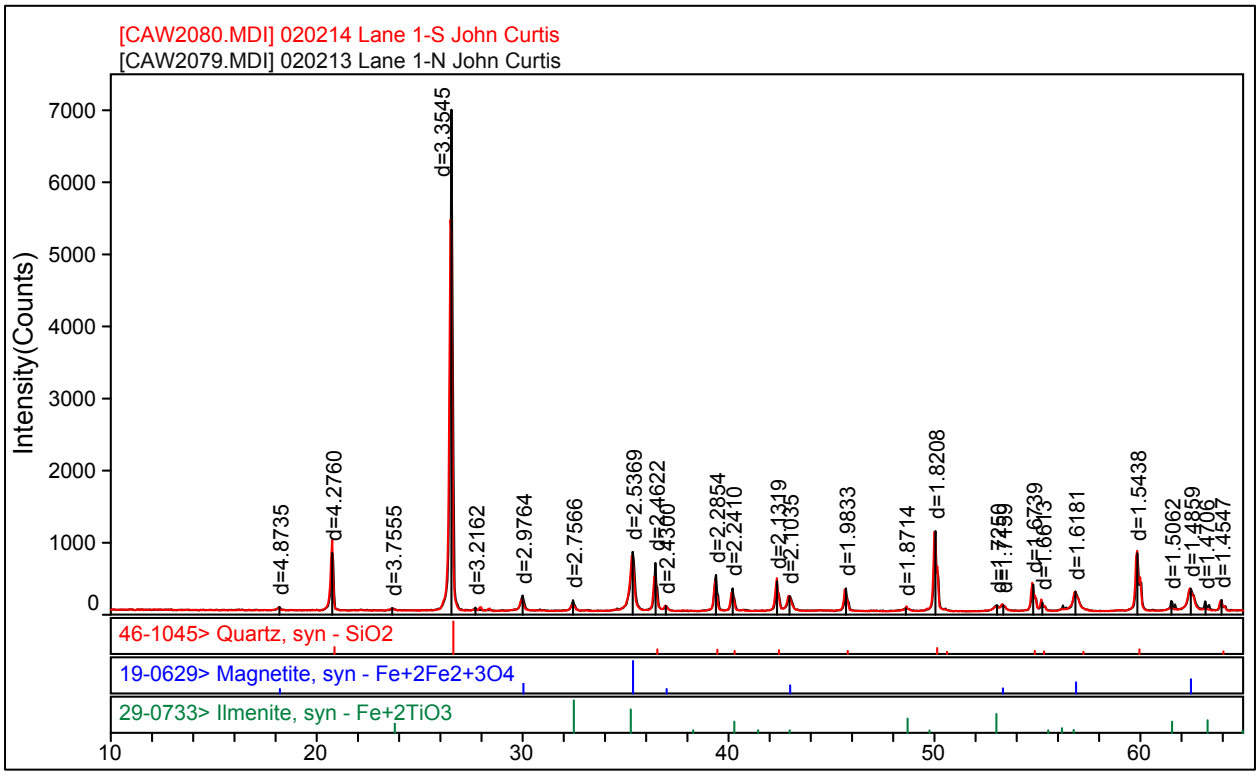

Figure 3-1. X-ray diffraction pattern of bulk samples of lanes 1N and 1S

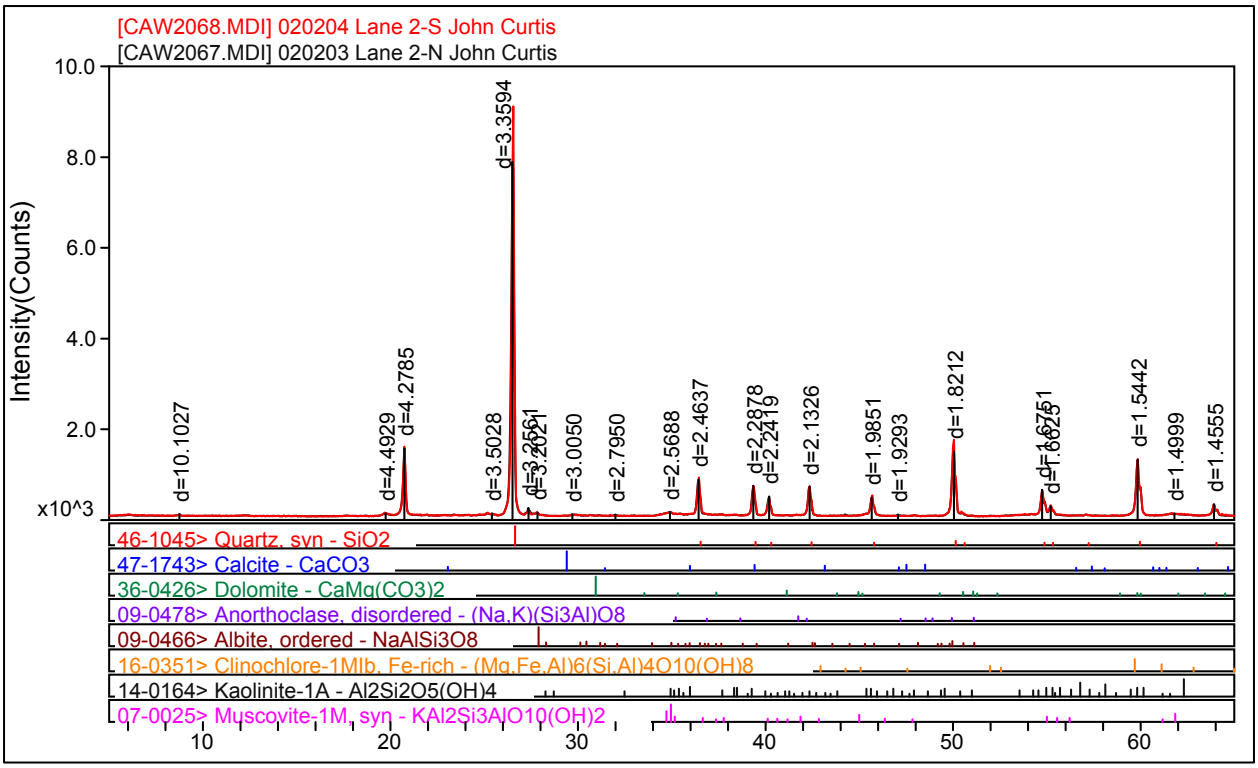

Figure 3-2. X-ray diffraction pattern of bulk samples of lanes 2N and 2S

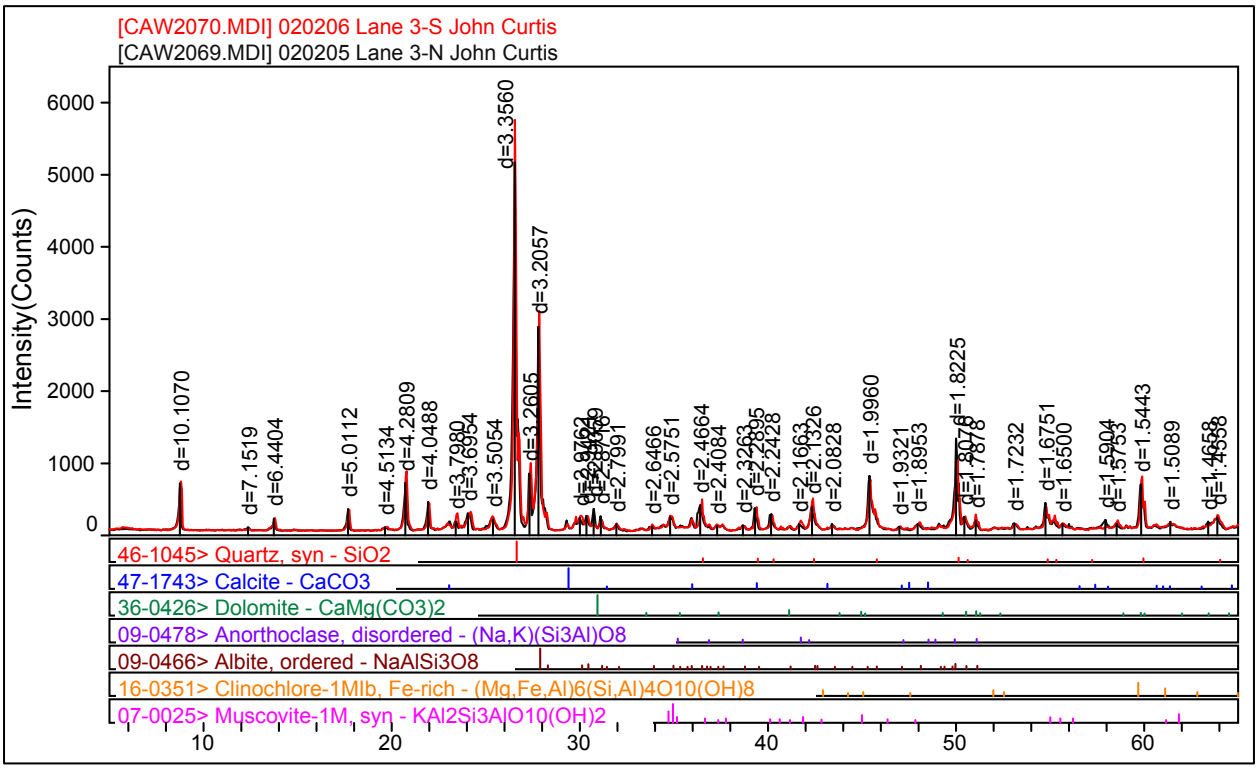

Figure 3-3. X-ray diffraction pattern of bulk samples of lanes 3N and 3S

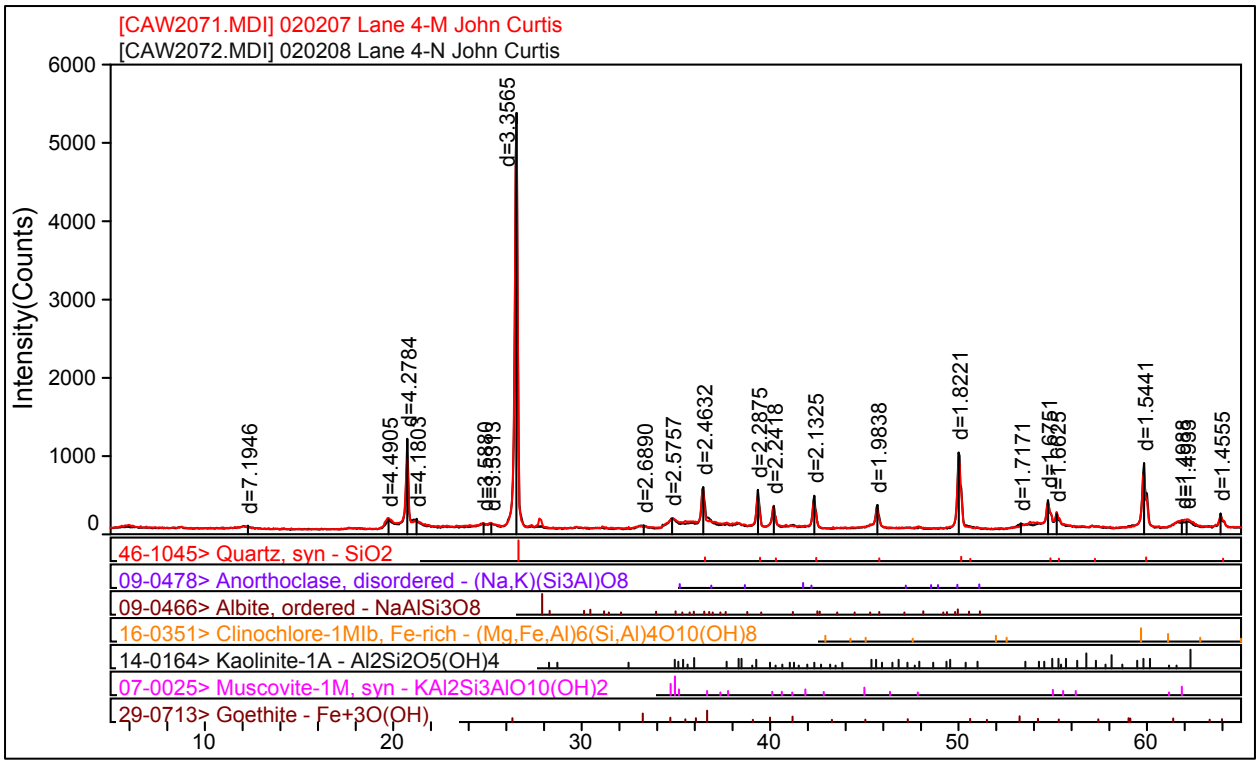

Figure 3-4. X-ray diffraction pattern of bulk samples of lanes 4N and 4M

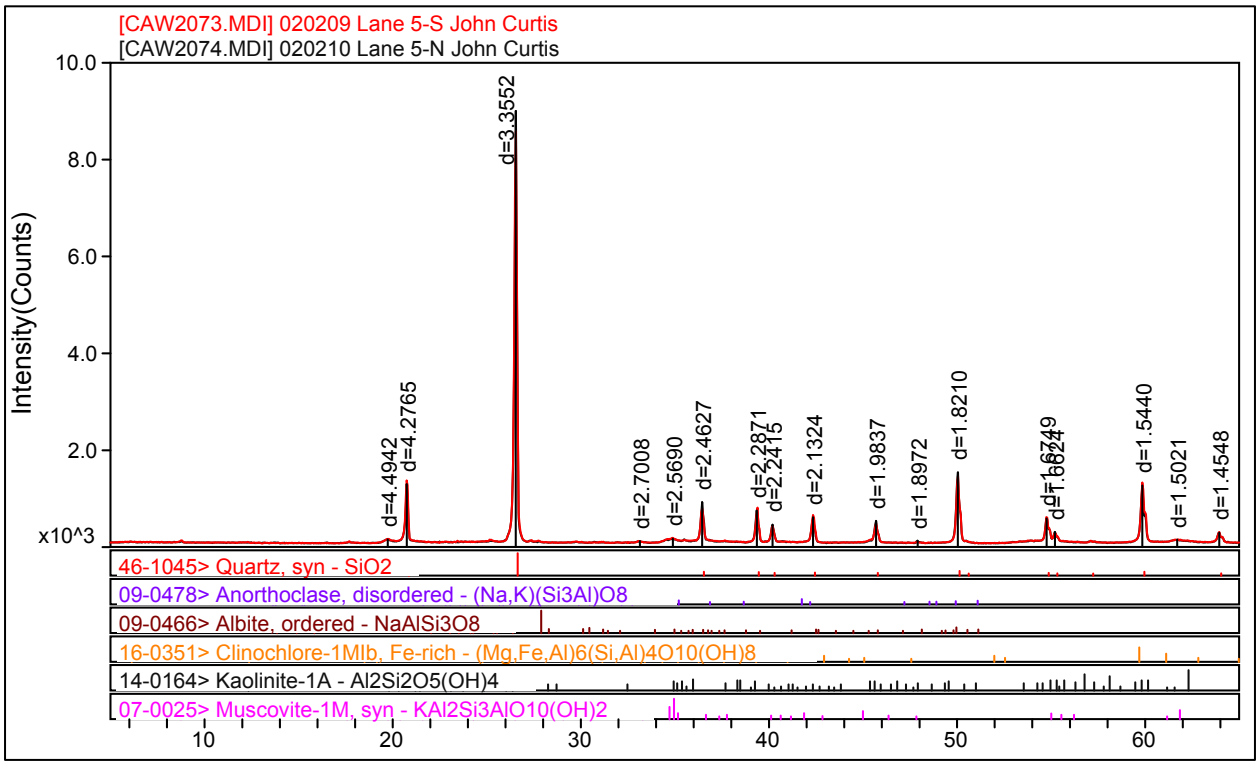

Figure 3-5. X-ray diffraction pattern of bulk samples of lanes 5N and 5S

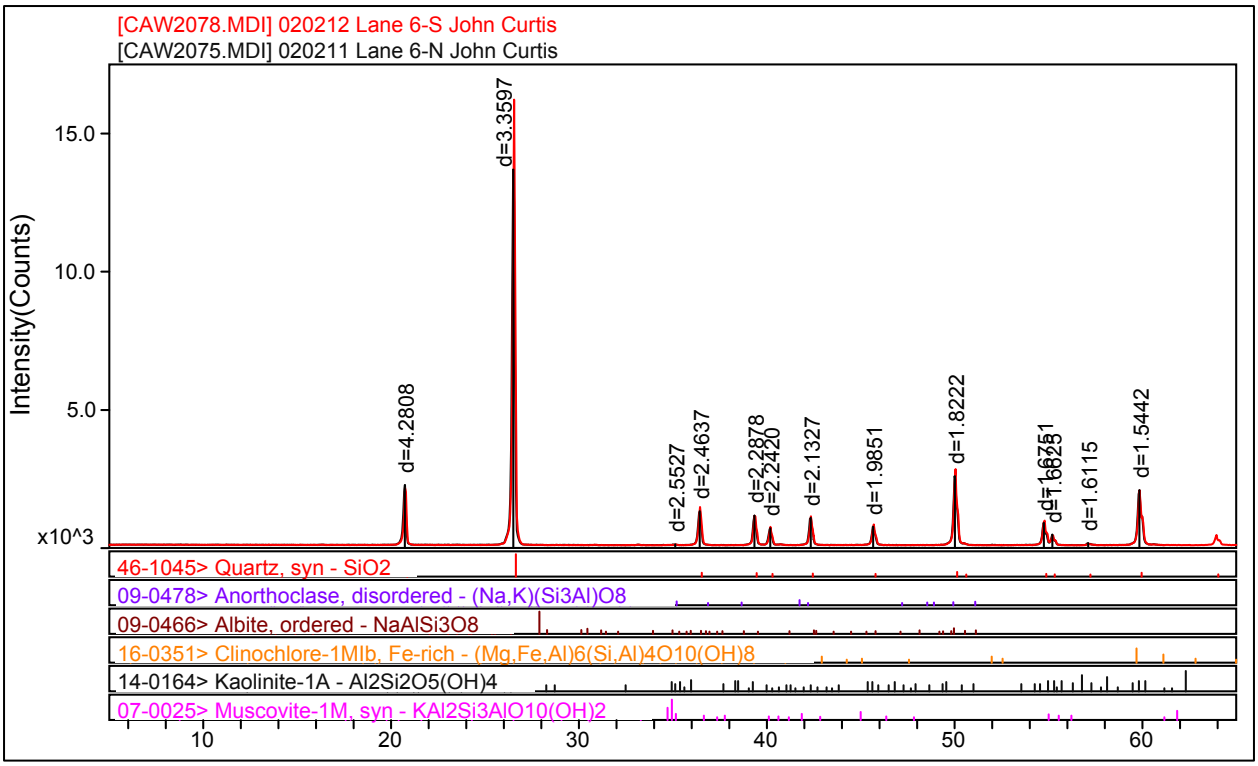

Figure 3-6. X-ray diffraction pattern of bulk samples of lanes 6N and 6S

Table 3-1
Bulk Mineralogy and Phyllosilicate Mineralogy for the Samples Examined in This Study

Description	Lane 1N	Lane 1S	Lane 2N	Lane 2S	Lane 3N	Lane 3S	Lane 4N	Lane 4M	Lane 5S	Lane 5N	Lane 6N	Lane 6S
Whole Rock Mineralogy (mass %)												
Quartz	85%	74%	89%	89%	31%	22%	71%	73%	90%	89%	98%	98%
K-Feldspar	0%	0%	3.7%	2.6%	8.6%	9.2%	1.2%	2.7%	0.8%	1.9%	0%	0%
Plagioclase	0.4%	1.1%	1.2%	1.8%	38%	46%	0.9%	1.5%	2.1%	0.5%	0%	0%
Calcite	0%	0%	0%	0%	1.6%	1.1%	0%	0%	0%	0%	0%	0%
Dolomite	0%	0%	0%	0%	0.5%	2.8%	0%	0%	0%	0%	0%	0%
Goethite	0%	0%	0%	0%	0%	0%	11%	7.2%	0%	0%	0%	0%
Ilmenite	1.5%	4.1%	0%	0%	0%	0%	0%	0%	0%	0%	0%	0%
Magnetite	11%	20%	0%	0%	0%	0%	0%	0%	0%	0%	0%	0%
Total Phyllosilicates	1.9%	1.0%	6.1%	6.2%	20%	18%	15%	16%	7.0%	8.4%	2.2%	1.8%
Total	100%	100%	100%	100%	100%	100%	100%	100%	100%	100%	100%	100%
Phyllosilicate Mineralogy (Relative Abundance)												
Smectite	0%	0%	0%	0%	6%	5%	0%	0%	0%	0%	0%	0%
R=0 M-L C/S (10-20%S)[1]	0%	0%	20%	20%	0%	0%	5.9%	18%	11%	12%	0%	0%
Illite&Mica	70%	63%	43%	40%	91%	94%	38%	29%	55%	59%	71%	76%
Kaolinite	20%	18%	16%	23%	0.0%	0.0%	41%	36%	24%	22%	23%	17%
Chlorite	10%	19%	21%	18%	3.1%	1.4%	16%	17%	9.7%	6.8%	5.9%	6.9%
Total	100%	100%	100%	100%	100%	100%	100%	100%	100%	100%	100%	100%

(Continued)

Table 3-1 (Concluded)

Description	Lane 1N	Lane 1S	Lane 2N	Lane 2S	Lane 3N	Lane 3S	Lane 4N	Lane 4M	Lane 5S	Lane 5N	Lane 6N	Lane 6S
Summary Mineralogy (mass %)												
Quartz	85%	74%	89%	89%	31%	22%	71%	73%	90%	89%	98%	98%
K-Feldspar	0%	0%	3.7%	2.6%	8.6%	9.2%	1.2%	2.7%	0.8%	1.9%	0%	0%
Plagioclase	0.4%	1.1%	1.2%	1.8%	38%	46%	0.9%	1.5%	2.1%	0.5%	0%	0%
Calcite	0%	0%	0%	0%	1.6%	1.1%	0%	0%	0%	0%	0%	0%
Dolomite	0%	0%	0%	0%	0.5%	2.8%	0%	0%	0%	0%	0%	0%
Goethite	0%	0%	0%	0%	0%	0%	11%	7.2%	0%	0%	0%	0%
Ilmenite	1.5%	4.1%	0%	0%	0%	0%	0%	0%	0%	0%	0%	0%
Magnetite	11%	20%	0%	0%	0%	0%	0%	0%	0%	0%	0%	0%
Smectite	0%	0%	0%	0%	1.1%	0.9%	0%	0%	0%	0%	0%	0%
R=0 M-L C/S (10-20%S)	0%	0%	1.2%	1.2%	0%	0%	0.9%	3.0%	0.7%	1.0%	0%	0%
Illite&Mica	1.3%	0.6%	2.6%	2.5%	18%	17%	5.8%	4.7%	3.9%	4.9%	1.6%	1.4%
Kaolinite	0.4%	0.2%	1.0%	1.4%	0.0%	0.0%	6.3%	5.7%	1.7%	1.8%	0.5%	0.3%
Chlorite	0.2%	0.2%	1.3%	1.1%	0.6%	0.3%	2.4%	2.7%	0.7%	0.6%	0.1%	0.1%
Total	100%	100%	100%	100%	100%	100%	100%	100%	100%	100%	100%	100%

[1] Mixed-layer chlorite/smectite (with 10-20% expandable smectite layers)

The oxides listed on Table 3-2 are the choice of the person conducting the analysis and may not reflect the exact chemical composition of the metal oxide, as the oxidation state of some of the metals is unknown. For example, although the iron in a sample is listed as Fe_2O_3, it may actually be Fe_3O_4 as in the case for lane 1 where the mineralogy indicated an appreciable amount of magnetite (Fe_3O_4).

Table 3-2
Chemistry of the Samples Examined in This Study (expressed in percent of sample mass)

Element	Lane 1N	Lane 1S	Lane 2N	Lane 2S	Lane 3N	Lane 3S	Lane 4N	Lane 4M	Lane 5N	Lane 5S	Lane 6N	Lane 6S
(mass %)	20213	20214	20203	20204	20205	20206	20208	20207	20210	20209	20211	20212
Na_2O	1.79	1.99	0.80	0.55	3.57	7.46	1.16	0.78	0.87	0.85	2.06	2.55
MgO	0.45	0.61	0.84	0.77	1.18	0.74	1.06	1.11	0.85	0.65	0.35	0.37
Al_2O_3	2.29	4.00	8.57	9.70	15.59	14.57	14.50	17.37	9.30	9.26	1.64	2.42
SiO_2	62.04	65.28	83.37	82.90	72.46	70.86	73.89	70.61	82.26	81.63	95.29	94.11
SO_3	0.54	0.32	0.23	0.17	0.17	0.26	0.16	0.23	0.18	0.27	0.39	0.34
K_2O	0.03	0.04	1.16	1.00	3.14	3.19	0.94	0.94	1.00	1.12	0.02	0.03
CaO	0.26	0.10	0.13	0.08	1.31	0.96	0.09	0.05	0.06	0.14	0.03	0.05
TiO_2	3.61	2.57	1.30	1.34	0.24	0.21	0.79	1.16	0.91	0.97	0.04	0.03
Mn_2O_3	0.17	0.17	0.10	0.03	0.07	0.05	0.04	0.03	0.03	0.03	0.00	0.00
Fe_2O_3	28.83	24.92	3.50	3.45	2.27	1.70	7.35	7.71	4.53	5.07	0.17	0.10

Consistency of Analyses

The mineralogy and chemistry of these samples agree with each other. Samples such as lanes 1N, 1S, 4N, and 4M, which have abundant Fe phases as determined by XRD analysis, also show high Fe contents in the chemical analysis. Lanes 5N, 5S, 6N, and 6S, which have the highest amount of SiO_2, also have the greatest amounts of total silica by chemical analysis. Lanes 3N, 3S, 4N, and 4M, which have the highest amount of plagioclase feldspar and clays present, also have the greatest amounts of total Al_2O_3 by chemical analysis. In addition, sample 3S has by far the greatest amount of Na present by chemical analysis and also has the most plagioclase feldspar compared with the other samples.

4 Seismic Properties

The goal of this effort was to determine the seismic velocities of each of the six mine lanes, pictured in Figures 1-1 and 1-2, in building 353 at Fort Belvoir, VA. Each lane contains a different type of soil that will be used to test new mine discrimination technologies. This fieldwork was performed for the NVESD at Fort Belvoir, VA, during 15 – 19 July 2002.

Data Acquisition

The desired characteristic properties are the P-wave (Primary or Pressure wave) and S-wave (Secondary or Shear wave) velocities for each of the mine lanes. To acquire the seismic data, geophone lines were set up with 30-cm receiver spacing as seen in Figure 4-1. This receiver spacing was chosen based on prior knowledge of the layer thickness. All of the lines were centered on the 10-m marks of each lane (the north boundary of each lane is designated as the 0.0-m mark). The shot point was offset 90 cm from the first receiver for the P-wave surveys, but only offset 30 cm for the S-wave surveys. Mark Products (now Sercel) geophones and a Geometrics Strataview seismograph were used to acquire the data. For P-wave surveys, a sledgehammer was utilized to input seismic energy into the ground by striking a steel plate placed on the ground surface. The sledgehammer had an accelerometer attached to the handle, which triggered the seismograph to start recording when the hammer contacted the steel plate. For the S-wave surveys, a source was fabricated onsite using a 4- by 4-in. piece of lumber with carriage bolts bolted through it (as seen in Figure 4-2). The bolts were driven into the ground at each end of the geophone line, and the energy was input horizontally into the ground by placing the steel plate on one end and striking the steel plate with the sledgehammer.

For the P-wave surveys, the source was set at one end of the receiver line and then at the other end. That allowed for a check of true wave speeds and dipping layers. For the S-wave surveys, a source was also used at both ends of the line. In addition, the source was struck from both sides perpendicular to the receiver line so that there would be two data files that should be 180 deg out of phase. The data were stacked until the quality of the traces on the screen of the StrataView seemed to be no longer improving.

Figure 4-1. Geophone line on long mine lane 2. P-wave source plate is at the bottom of the photo

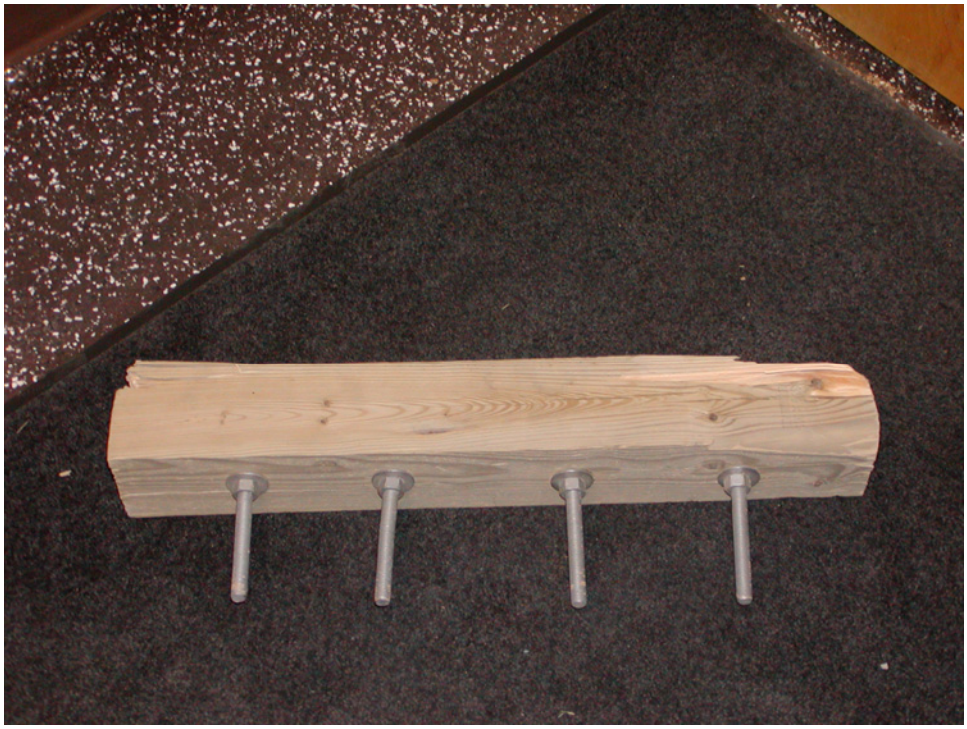

Figure 4-2. Shear wave source fabricated onsite

Data Processing

The processing was begun with several assumptions based on the information provided by NVESD: that there were two layers of material; that the depths to the interface were known; and that the wave velocities should be the same for the second layer in every lane. Some of these assumptions were later found to be incorrect.

Two methods were used to process and interpret the data. All of the P-wave data were processed with Rimrock Geophysics' SIP package for DOS and SIPwin for Windows. The software allows the user to pick the first break of each trace and saves those times to another file. Figures 4-3 and 4-4 are representative displays of the processing procedure. The numbers on the left side of each plot indicate the receiver number and the time, in milliseconds, for the first arrival of a P-wave. The numbers along the bottom of the plot trace times in milliseconds, and the inset boxes are windows that zoom in on the red-dotted box, showing early results for the first geophone.

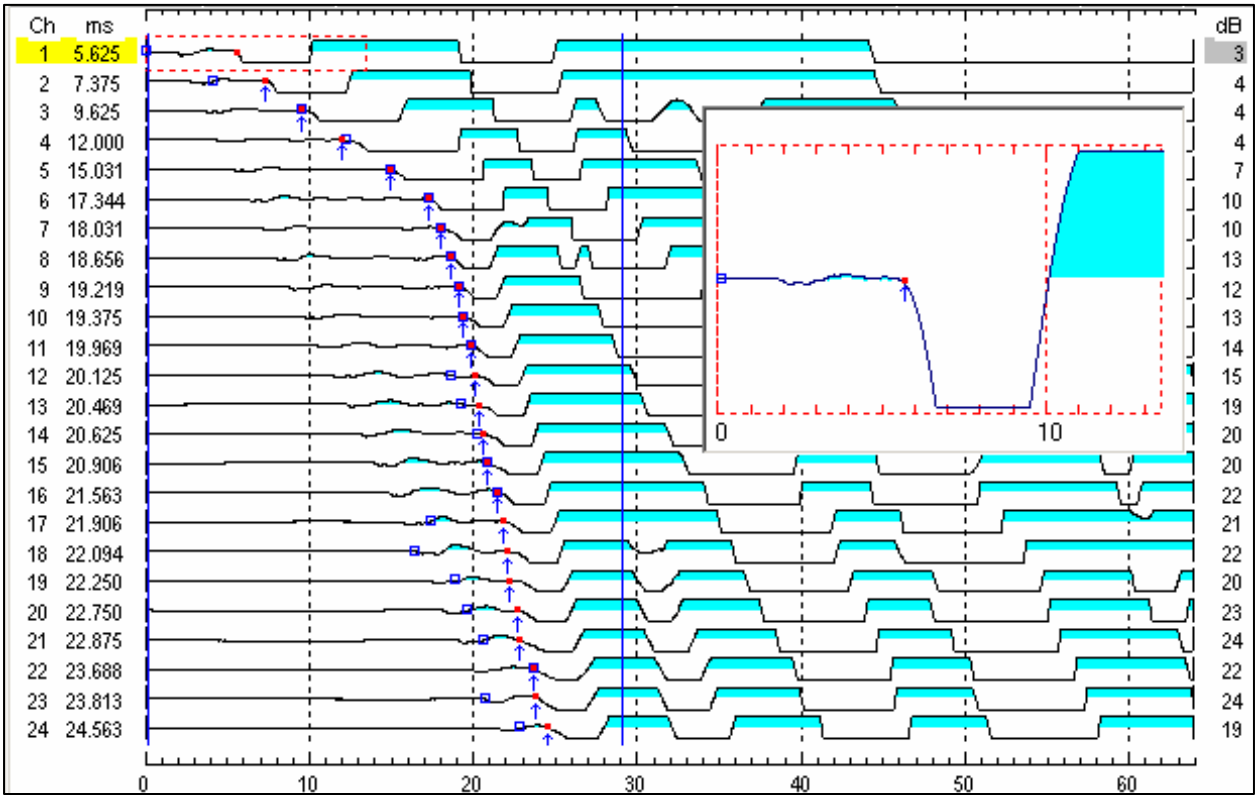

Figure 4-3. Long lane 6, P-wave seismic traces, source to left

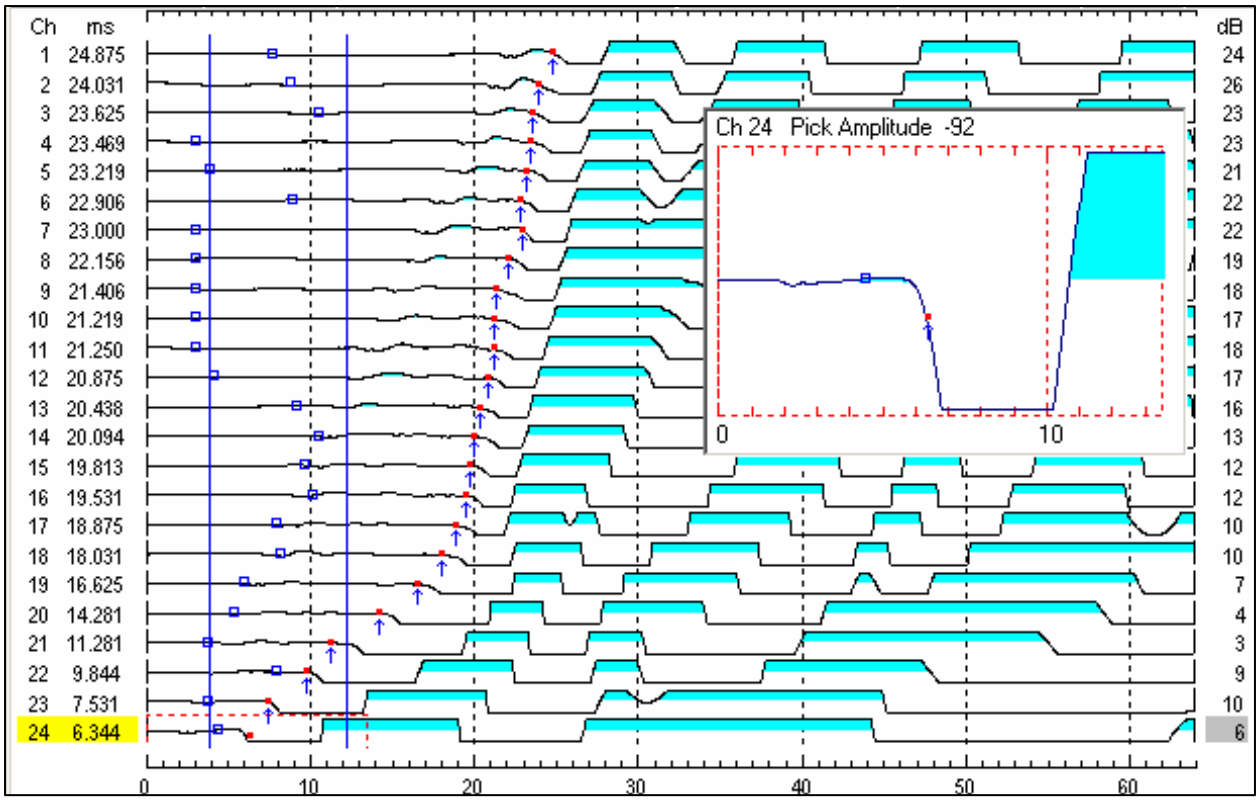

Figure 4-4. Long lane 6, P-wave seismic traces, source to right

The times of the first breaks combined with the geometry of the receivers and sources allows the program's algorithm to determine the velocities as seen in Figure 4-5. The left and right axes of Figure 4-5 are time in milliseconds, while the bottom axis shows the actual source and receiver locations. This chart shows a two-layer structure for lane 6 and the P-wave velocities of each layer.

A final example of processed data is shown in Figure 4-6, which reveals the depth to the bottom of the first layer as determined by the computer software. Both the horizontal and vertical axes on this figure are in meters. The plot shows the calculated depth to the interface below each shot point and receiver. This figure shows that the calculated thickness of the top soil layer is constant along the entire receiver line (in this case, about 1.2 m), meaning that the layer is flat and horizontal. If the depth output by the program matches the known depth, the confidence in the data increases.

The S-wave data were interpreted by hand. The S-wave energy arrival times were hand-picked on each trace, and a best-fit line was chosen with a ruler.

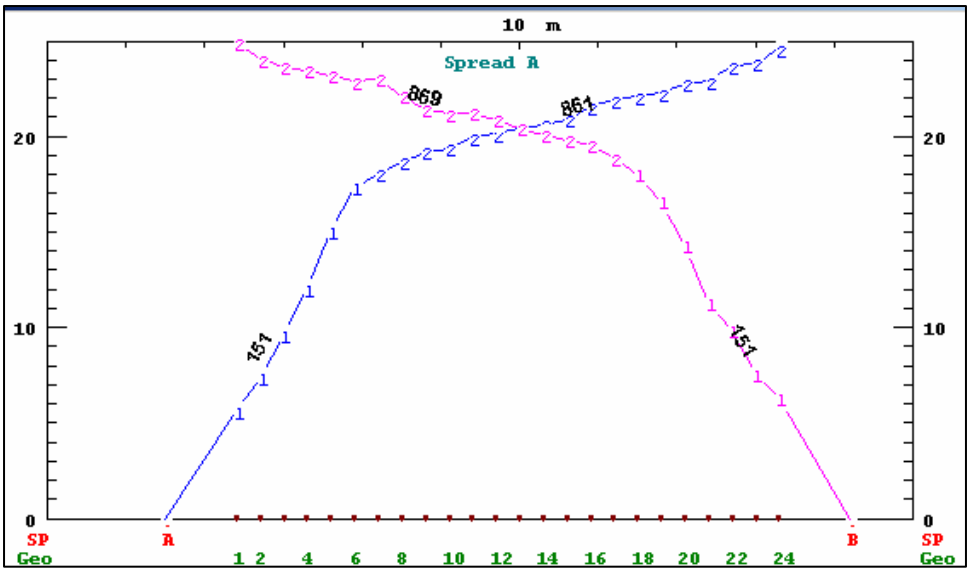

Figure 4-5. Long lane 6, P-wave velocity plot

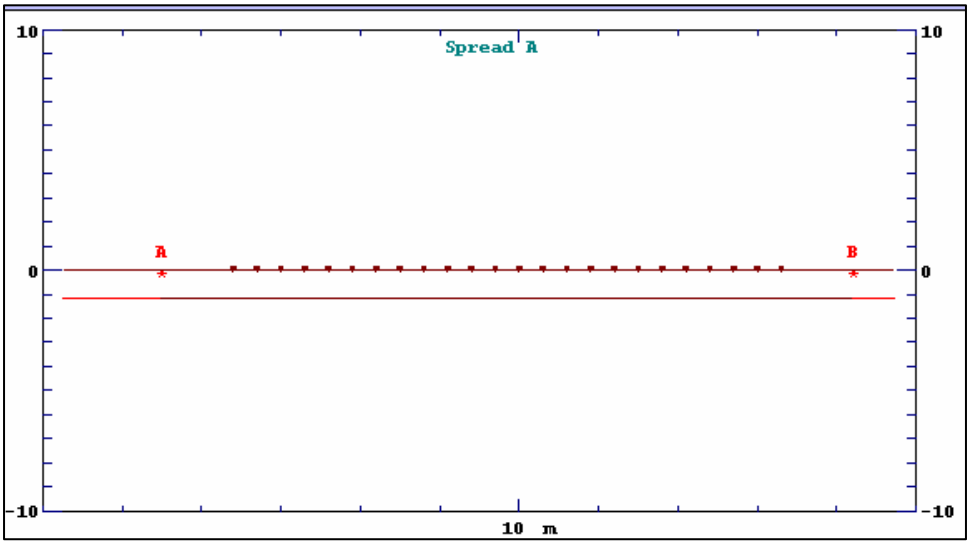

Figure 4-6. Long lane 6, P-wave layer plot

Results

The results of the P-wave and S-wave surveys can be seen in Tables 4-1 and 4-2. Table 4-1 contains the wave velocities for the lanes located on the north end of the building (the long lanes), while Table 4-2 contains the wave velocities for the short lanes located on the south end of the building. There are no results for short lane 1, because it was in the process of being sifted, and no data could be collected. Other N/A entries indicate unreliable results. Calculated depths for each mine lane soil are shown in the tables as well as the "known" depth; i.e., the value provided by NVESD.

Initial analysis of data to compute P-wave speeds using a two-layer model (mine lane fill over another deep layer) resulted in all of the lane soils having P-wave speeds less than the speed of sound in air. While that result is not surprising for the loose dry sands in lanes 1 and 6 (Burger 1972), it is less probable for the more compacted soils found in lanes 2-5. For example, Figure 4-3 shows a low-amplitude disturbance whose arrival times correspond to a wave speed of about 355 m/s. The air temperature at ground level in building 353 was about 40 ºC on the day of these measurements. Acoustic wave speed at 40 ºC is about 355 m/s.

As a result of these inconsistencies, the seismic refraction data were reprocessed with a three-layer assumption, the first layer nearest the surface being one where the density profile might indicate very slow P-wave speeds. The second layer would represent the bulk of the lane fill, and the third layer would represent the underlying native soil or some other base material. The average velocities for the base layer are also included in these tables.

Agreement among the wave speeds of the base layers is generally good. If, in fact, the underlying layer is the same material for all lanes, and environmental conditions are the same, then all base-layer speeds should be very similar. However, the P-wave speed for the base layer under lanes 1 and 2 on the north end of the building, as well as the S-wave speed for the base layer beneath lane 4 (also at the north end), are clearly different from those of the other layers, indicating that either they are different materials, or their density and moisture conditions were quite different from the other lanes at the time that these data were collected.

Bulk fill layer depths were determined by the P-waves only. Conversations with NVESD personnel during the time when these data were collected indicated that the true depths of each mine lane fill were unknown. In fact, it was initially understood that lanes on both ends of the building had the same depth. Clearly, the analysis of seismic refraction data indicates substantially different fill depths. In light of these contradictions, and particularly in light of the research on seismic/acoustic sensors being conducted at this facility, it is strongly recommended that at least one depth profile be measured in each lane. One should measure *in situ* densities, moisture contents, and depths to the layer boundaries.

Table 4-1
Long Lane Seismic Velocities and Depths

Lane #	Soil Designation	P-Wave (m/s)			Shear-Wave (m/s)		Depth (m)
		Slow Surface Layer	Bulk Fill	Base Layer	Bulk Fill	Base Layer	
1	Magnetite	N/A	149	970	123	466	1.180
2	Loam	195	278	736	154	445	1.550
3	21A	200	352	834	275	N/A	1.290
4	Bank Run Gravel	139	391	858	129	643	1.140
5	Virginia Clay	172	389	846	169	438	1.050
6	White Beach Sand	N/A	151	857	118	399	1.180
Averages				**850**		**478**	**1.232**

Table 4-2
Short Lane Seismic Velocities and Depths

Lane #	Soil Designation	P-Wave (m/s)			Shear-Wave (m/s)		Depth (m)
		Slow Surface Layer	Bulk Fill	Base Layer	Bulk Fill	Base Layer	
1	Magnetite	N/A	N/A	N/A	N/A	N/A	N/A
2	Loam	172	357	835	155	N/A	1.640
3	21A	229	301	973	125	277	1.620
4	Bank Run Gravel	N/A	220	786	146	315	1.940
5	Virginia Clay	220	334	900	184	N/A	1.460
6	White Beach Sand	N/A	137	893	123	308	1.490
Averages				**877**		**300**	**1.630**

5 Dielectric Properties

This chapter contains dielectric property measurement results for soils. These data were collected utilizing a Hewlett-Packard 8753E Network Analyzer System with a coaxial sample holder. An earlier, but similar, methodology is described elsewhere (Curtis 2001a). The section entitled "Laboratory Experimental Procedures" contains more detail on sample preparation and data collection.

S-parameter measurements were transformed into complex dielectric constant values as a function of frequency. Other useful electromagnetic properties were calculated from the dielectric constant, including an equivalent electrical conductivity, power attenuation, and a normalized phase velocity. The section entitled "Fundamental Relationships" contains the formulae used to calculate these properties. Additional physical parameters of the soil samples that are included in the report include their wet and dry densities and their gravimetric and volumetric moisture contents.

In the section entitled "Results," charts are presented that display the frequency-dependent nature of the soil response. Additional data are presented in tabular form for several selected frequencies and graphically displayed as a function of volumetric moisture content.

Laboratory Experimental Procedures

To begin the experimental procedure, soil was first taken from the source container and packed into a brass coaxial sample holder using small spatulas and other utensils. Unfortunately, this methodology for sample preparation allows no control over sample dry density. Furthermore, it is highly unlikely that the densities achieved in the laboratory will ever exceed *in situ* densities. Nevertheless, the sample holders were packed with soil as tightly as possible given the *in situ* moisture content of the sample. The brass holders used in these measurements were 25 cm in length and had a square cross section whose dimension was 0.75 cm, resulting in total sample volumes of about 13.8 cm^3.

After enclosing the sample in the holder with a brass cover plate, the holder was connected to the HP8753E Network Analyzer test ports with precision flexible cables. Laboratory data were normally first collected on soil that had been taken directly from the sample bag. All of the soil samples collected at NVESD for this measurement program were relatively dry. Therefore, the first measurement on each sample was typically under the driest conditions. Following the

initial measurement, a small amount of distilled, deionized water was added to the sample and more data collected. The amount of time allowed for reaching equilibrium was about an hour. For this study, one more measurement was made after nearly saturating the sample in the holder. In summary, the electrical properties of each sample were measured three times, at three different moisture conditions, without any additional physical disturbance.

Sample masses were recorded prior to each measurement. Following the last data collection, the soil was scraped and flushed from the sample holder and dried in an oven to obtain its dry mass. Once the sample dry mass was known along with the sample volume, it was possible to calculate sample densities (wet and dry) and moisture contents (both weight-based and volume-based) for each measurement conducted in the laboratory. Table 5-1 lists each of the laboratory measurements that were made on these samples, including a unique file name for each set of frequency-domain data, sample wet density, sample dry density, gravimetric moisture content (mass of the water in the sample/mass of the dried sample), and volumetric moisture content (volume of water in the sample/volume of the sample holder).

Table 5-1
Moisture Content and Sample Density Calculations – NVESD Mine Lane Samples

File Name	Sample Description	Empty Holder (g)	Holder + Sample (g)	Drying Can (g)	Can + Dried Sample (g)	Wet Sample (g)	Dry Sample (g)	Water (g)	Wet Density (g/cc)	Dry Density (g/cc)	Gravimetric Moisture (%)	Volumetric Moisture (%)
5Sep21504	Lane 1, N end	493.95	519.30	52.80	77.98	25.35	25.18	0.17	1.84	1.82	0.7	1.2
6Sep21144	Lane 1, N end	493.95	520.80	52.80	77.98	26.85	25.18	1.67	1.95	1.82	6.6	12.1
6Sep21237	Lane 1, N end	493.95	523.60	52.80	77.98	29.65	25.18	4.47	2.15	1.82	17.8	32.4
6Sep21601	Lane 1, N end	493.95	523.70	52.80	77.98	29.75	25.18	4.57	2.16	1.82	18.1	33.1
17Sep21539	Lane 1, S end	492.10	517.07	51.92	76.87	24.97	24.95	0.02	1.81	1.81	0.1	0.1
13Sep21550	Lane 1, S end	492.10	517.17	51.92	76.87	25.07	24.95	0.12	1.82	1.81	0.5	0.9
13Sep21642	Lane 1, S end	492.10	*519.58*	51.92	76.87	27.48	24.95	2.53	1.99	1.81	10.1	18.3
13Sep21648	Lane 1, S end	492.10	521.35	51.92	76.87	29.25	24.95	4.30	2.12	1.81	17.2	31.2
6Sep21150	Lane 2, N end	489.70	508.90	51.25	70.08	19.20	18.83	0.37	1.39	1.36	2.0	2.7
5Sep21511	Lane 2, N end	489.70	510.35	51.25	70.08	20.65	18.83	1.82	1.50	1.36	9.7	13.2
6Sep21244	Lane 2, N end	489.70	513.60	51.25	70.08	23.90	18.83	5.07	1.73	1.36	26.9	36.7
6Sep21607	Lane 2, N end	489.70	513.62	51.25	70.08	23.92	18.83	5.09	1.73	1.36	27.0	36.9
17Sep21547	Lane 2, Middle	492.15	511.73	54.20	73.48	19.58	19.28	0.30	1.42	1.40	1.6	2.2
13Sep21556	Lane 2, Middle	492.15	513.30	54.20	73.48	21.15	19.28	1.87	1.53	1.40	9.7	13.6
13Sep21654	Lane 2, Middle	492.15	517.10	54.20	73.48	24.95	19.28	5.67	1.81	1.40	29.4	41.1
20Sep21127	Lane 2, S end	493.98	512.20	52.25	70.25	18.22	18.00	0.22	1.32	1.30	1.2	1.6
19Sep21511	Lane 2, S end	493.98	513.71	52.25	70.25	19.73	18.00	1.73	1.43	1.30	9.6	12.5
19Sep21557	Lane 2, S end	493.98	516.18	52.25	70.25	22.20	18.00	4.20	1.61	1.30	23.3	30.4
6Sep21157	Lane 3, N end	492.00	516.76	54.58	79.00	24.76	24.42	0.34	1.79	1.77	1.4	2.5
5Sep21517	Lane 3, N end	492.00	518.60	54.58	79.00	26.60	24.42	2.18	1.93	1.77	8.9	15.8
6Sep21613	Lane 3, N end	492.00	520.60	54.58	79.00	28.60	24.42	4.18	2.07	1.77	17.1	30.3
17Sep21556	Lane 3, Middle	492.65	515.00	52.71	74.95	22.35	22.24	0.11	1.62	1.61	0.5	0.8
13Sep21602	Lane 3, Middle	492.65	516.03	52.71	74.95	23.38	22.24	1.14	1.69	1.61	5.1	8.3
13Sep21659	Lane 3, Middle	492.65	519.46	52.71	74.95	26.81	22.24	4.57	1.94	1.61	20.5	33.1

(Continued)

Table 5-1 (Concluded)

File Name	Sample Description	Empty Holder (g)	Holder + Sample (g)	Drying Can (g)	Can + Dried Sample (g)	Wet Sample (g)	Dry Sample (g)	Water (g)	Wet Density (g/cc)	Dry Density (g/cc)	Gravimetric Moisture (%)	Volumetric Moisture (%)
20Sep21146	Lane 3, S end	489.60	513.07	51.83	75.20	23.47	23.37	0.10	1.70	1.69	0.4	0.7
19Sep21518	Lane 3, S end	489.60	514.30	51.83	75.20	24.70	23.37	1.33	1.79	1.69	5.7	9.6
19Sep21602	Lane 3, S end	489.60	517.06	51.83	75.20	27.46	23.37	4.09	1.99	1.69	17.5	29.6
6Sep21204	Lane 4, N end	492.20	513.62	54.58	75.25	21.42	20.67	0.75	1.55	1.50	3.6	5.4
5Sep21523	Lane 4, N end	492.20	519.17	54.58	75.25	26.97	20.67	6.30	1.95	1.50	30.5	45.7
17Sep21525	Lane 4, N end	493.95	510.48	53.55	69.80	16.53	16.25	0.28	1.20	1.18	1.7	2.0
13Sep21537	Lane 4, N end	493.95	512.58	53.55	69.80	18.63	16.25	2.38	1.35	1.18	14.6	17.2
13Sep21625	Lane 4, N end	493.95	515.40	53.55	69.80	21.45	16.25	5.20	1.55	1.18	32.0	37.7
17Sep21603	Lane 4, Middle	492.72	509.94	51.68	68.26	17.22	16.58	0.64	1.25	1.20	3.9	4.6
13Sep21614	Lane 4, Middle	492.72	512.10	51.68	68.26	19.38	16.58	2.80	1.40	1.20	16.9	20.3
13Sep21707	Lane 4, Middle	492.72	515.43	51.68	68.26	22.71	16.58	6.13	1.65	1.20	37.0	44.4
6Sep21211	Lane 5, N end	492.90	515.15	52.85	74.68	22.25	21.83	0.42	1.61	1.58	1.9	3.0
5Sep21529	Lane 5, N end	492.90	517.58	52.85	74.68	24.68	21.83	2.85	1.79	1.58	13.1	20.7
6Sep21626	Lane 5, N end	492.90	518.68	52.85	74.68	25.78	21.83	3.95	1.87	1.58	18.1	28.6
6Sep21225	Lane 5, Middle	491.72	512.80	51.00	71.52	21.08	20.52	0.56	1.53	1.49	2.7	4.1
5Sep21541	Lane 5, Middle	491.72	515.70	51.00	71.52	23.98	20.52	3.46	1.74	1.49	16.9	25.1
6Sep21637	Lane 5, Middle	491.72	517.30	51.00	71.52	25.58	20.52	5.06	1.85	1.49	24.7	36.7
17Sep21608	Lane 5, S end	491.62	510.58	54.80	73.22	18.96	18.42	0.54	1.37	1.33	2.9	3.9
13Sep21620	Lane 5, S end	491.62	512.30	54.80	73.22	20.68	18.42	2.26	1.50	1.33	12.3	16.4
13Sep21713	Lane 5, S end	491.62	515.25	54.80	73.22	23.63	18.42	5.21	1.71	1.33	28.3	37.8
5Sep21535	Lane 6, N end	492.85	515.20	53.50	75.60	22.35	22.10	0.25	1.62	1.60	1.1	1.8
6Sep21217	Lane 6, N end	492.85	517.42	53.50	75.60	24.57	22.10	2.47	1.78	1.60	11.2	17.9
6Sep21631	Lane 6, N end	492.85	521.03	53.50	75.60	28.18	22.10	6.08	2.04	1.60	27.5	44.1
6Sep21312	Lane 6, N end	492.85	521.22	53.50	75.60	28.37	22.10	6.27	2.06	1.60	28.4	45.4
13Sep21544	Lane 6, N end	489.62	512.80	51.89	75.08	23.18	23.19	-0.01	1.68	1.68	0.0	-0.1
17Sep21534	Lane 6, N end	489.62	512.80	51.89	75.08	23.18	23.19	-0.01	1.68	1.68	0.0	-0.1
13Sep21631	Lane 6, N end	489.62	515.58	51.89	75.08	25.96	23.19	2.77	1.88	1.68	11.9	20.1
13Sep21637	Lane 6, N end	489.62	518.02	51.89	75.08	28.40	23.19	5.21	2.06	1.68	22.5	37.8
19Sep21524	Lane 6, Middle	492.11	515.26	54.11	77.19	23.15	23.08	0.07	1.68	1.67	0.3	0.5
19Sep21629	Lane 6, Middle	492.11	517.49	54.11	77.19	25.38	23.08	2.30	1.84	1.67	10.0	16.7
20Sep21036	Lane 6, Middle	492.11	518.78	54.11	77.19	26.67	23.08	3.59	1.93	1.67	15.6	26.0
19Sep21531	Lane 6, S end	492.10	514.68	54.88	77.20	22.58	22.32	0.26	1.64	1.62	1.2	1.9
19Sep21635	Lane 6, S end	492.10	517.38	54.88	77.20	25.28	22.32	2.96	1.83	1.62	13.3	21.4
20Sep21051	Lane 6, S end	492.10	518.38	54.88	77.20	26.28	22.32	3.96	1.90	1.62	17.7	28.7

Fundamental Relationships Used in Data Collection and Data Processing

Complex dielectric and complex magnetic property measurements

The idealized measurement geometry used in this study is a sample of length, ***d***, in a coaxial holder. The complex relative dielectric constant and complex

relative magnetic permeability of a sample are labeled $\boldsymbol{\varepsilon}$ and $\boldsymbol{\mu}$, respectively. The parameter, $\boldsymbol{S_{11}}$, is the complex ratio of reflected voltage to incident voltage at one end of the sample (with the other end electronically shorted), while the parameter, $\boldsymbol{S_{21}}$, is the complex ratio of voltage measured on the other end of the sample to the same incident voltage (an idealized transmission coefficient).

The use of S-parameters as measurement tools for electronic devices was introduced in the 1960s. In 1970, a paper was published that described the use of coaxial samples and S-parameter measurements to determine the complex dielectric and magnetic properties of a material (Nicolson and Ross 1970). The model can be summarized:

$$\varepsilon = \sqrt{\frac{c_2}{c_1}} \tag{1}$$

and

$$\mu = \sqrt{c_1 c_2} \tag{2}$$

where

$$c_1 = \frac{\mu}{\varepsilon} = \left(\frac{1 + \Gamma}{1 - \Gamma}\right)^2 \tag{3}$$

$$c_2 = \varepsilon\mu = -\left\{\frac{c}{\omega d} ln\left(\frac{1}{z}\right)\right\}^2 \tag{4}$$

$$z = \frac{V_1 - \Gamma}{1 - V_1\Gamma} \tag{5}$$

$$\Gamma = X \pm \sqrt{X^2 - 1} \text{ (smallest value)} \tag{6}$$

$$X = \frac{1 - V_1V_2}{V_1 - V_2} \tag{7}$$

$$V_1 = S_{21} + S_{11} \tag{8}$$

and

$$V_2 = S_{21} - S_{11} \quad (9)$$

c is the speed of light in a vacuum, and ***ω*** is the angular frequency of the signal. Implied in this model is the assumption that the sample holder has no intrinsic magnetic properties, which is not true for the measurements made in this study. In fact, if the holders were ideal, laboratory measurements of empty holders would produce real relative dielectric constants and relative permeabilities with unit magnitudes. Data taken in this and previous studies reveal non-unity results for empty sample holders. The reasons are probably that the center conductor for the sample holders is made of a steel alloy and that the connectors at the ends of the sample holders are not precision, low-loss devices.

If one is able to confidently assume that the material being measured is non-magnetic, then the complex dielectric constant can be calculated directly from Equation 4, and that was done for all of the measurements reported here. As a result, dielectric constant data for magnetite samples (lane 1) must be referred to as "apparent dielectric constant data," where it is recognized that the magnetic properties are reported in a later section.

Calculation of additional parameters

While the complex dielectric constant and complex magnetic permeability are, by themselves, meaningful properties of any material, it is possible to generate from them other useful parameters that are more readily utilized by engineers and scientists. For example, in the design of ground-penetrating radar systems, what may be most useful to the engineer is how rapidly the soil attenuates the signal. Attenuation, coupled with the sensitivity of the receiver, determines the effective depth of penetration for the radar in a particular soil. Similarly, a clear understanding of how the speed of an electromagnetic wave varies with depth and lateral position at any given test site, determines how well the radar data can be processed to produce an accurate assessment of subsurface conditions. The following paragraphs outline the generation of several useful parameters from complex dielectric and magnetic properties, including power attenuation, phase velocity, and an equivalent electrical conductivity.

Assuming plane harmonic wave propagation in a lossy, unbounded medium, the wave amplitude function may be written:

$$e^{i(kx - \omega t)}$$

where

$k = \beta + i\alpha = \omega N/c$ = the complex propagation constant,

β = the phase constant,

α = the amplitude attenuation factor,

ω = the radial frequency,

N = the complex index of refraction,

c = the velocity of light in a vacuum,

i = the symbol designating an imaginary quantity = $\sqrt{-1}$,

x = a space coordinate, and

t = time.

For the sake of simplicity, let the medium be *nonmagnetic*. Then,

$$N^2 = \varepsilon = \varepsilon' + i\varepsilon'' \tag{10}$$

where, as stated above, $\boldsymbol{\varepsilon}$ is the relative complex dielectric constant. The dielectric constant, along with the electrical conductivity from Ohm's Law, represents the electrical properties of the medium. Conductivity, $\boldsymbol{\sigma}$, accounts for current flow in the sample because of free charged particle motion; whereas, the real part of the dielectric constant, $\boldsymbol{\varepsilon'}$, accounts for Maxwell's "displacement currents" because of the electric polarization of the medium and to the time rate-of-change of the electric field. When both conduction and displacement currents are considered, one finds two terms in Ampere's law for current flow that represent losses (or a shift in phase), one containing the electrical conductivity and one containing the imaginary part of the dielectric constant. While these two terms account for different loss mechanisms, most researchers use only one term or the other to identify losses. Many users prefer to deal with the concept of electrical conductivity. However, the algorithm used in this laboratory to measure dielectric properties assumes that all losses are contained in the $\boldsymbol{\varepsilon''}$ term. Upon observing how the two loss terms appear in Maxwell's equations, one can choose to use them interchangeably through the relationship (in MKS units),

$$\sigma = \varepsilon'' \varepsilon_0 \omega \tag{11}$$

where the units of the "equivalent" conductivity (Kraus 1984) are mhos/meter (or siemens/meter) and $\boldsymbol{\varepsilon_0}$ is the permittivity of free space (8.85×10^{-12} farads/meter).

Squaring the expression for the complex propagation constant, substituting the expression for the square of the complex index of refraction, and equating real and imaginary components, one obtains two algebraic equations that relate the amplitude attenuation factor and phase constant to the complex dielectric constant:

$$\beta^2 - \alpha^2 = \frac{\omega^2}{c^2}\varepsilon' \tag{12}$$

and

$$\alpha\beta = \frac{\omega^2 \varepsilon''}{2c^2} \tag{13}$$

Solving these equations for the amplitude attenuation factor and for the phase constant results in the following expressions:[1]

$$\alpha = \frac{\omega}{c}\left[\frac{\varepsilon'}{2}\left(\sqrt{1+\left(\frac{\varepsilon''}{\varepsilon'}\right)^2}-1\right)\right]^{\frac{1}{2}} \tag{14}$$

and

$$\beta = \frac{\omega}{c}\left[\frac{\varepsilon'}{2}\left(\sqrt{1+\left(\frac{\varepsilon''}{\varepsilon'}\right)^2}+1\right)\right]^{\frac{1}{2}} \tag{15}$$

The $\varepsilon''/\varepsilon'$ ratio is also referred to as the loss tangent. Keep in mind that some researchers prefer to work with the electrical conductivity in place of the dielectric loss term, so that the radicand might look different in other references (e.g., $\varepsilon''/\varepsilon'$ may be replaced by $\sigma/(\varepsilon'\varepsilon_0\omega)$).

Plane waves of constant phase will propagate with a velocity

$$v = \frac{\omega}{\beta} = c\left[\frac{\varepsilon'}{2}\left(\sqrt{1+\left(\frac{\varepsilon''}{\varepsilon'}\right)^2}+1\right)\right]^{-\frac{1}{2}} \tag{16}$$

This phase velocity is not necessarily the speed with which the energy of the wave propagates through the medium. The latter is referred to as the group velocity and can be calculated as the rate of change of radial frequency with respect to the phase constant. However, as long as the phase velocity is relatively constant over the range of frequencies of interest, then there is little difference between phase velocity and group velocity.

The power intensity of the plane electromagnetic wave decreases exponentially with depth of penetration by the factor, $e^{-2\alpha x}$, or, in one unit of distance

---

[1] Had magnetic permeability been included, then the phase constant would have been: $\beta^2 = \frac{\omega^2}{2c^2}\left[\left(\varepsilon'\mu' - \varepsilon''\mu''\right) \pm \sqrt{\left(\varepsilon'\mu'\right)^2 + \left(\varepsilon'\mu''\right)^2 + \left(\varepsilon''\mu'\right)^2 + \left(\varepsilon''\mu''\right)^2}\right]$ and the attenuation coefficient would have been: $\alpha = \frac{\omega^2\left(\varepsilon'\mu'' + \varepsilon''\mu'\right)}{2\beta\ c^2}$

traveled, a decrease of $e^{-2\alpha}$. Power attenuation expressed in decibels per meter can then be written as:

$$power\ \ loss = -8.6859\ \frac{\omega}{c}\left[\frac{\varepsilon'}{2}\left(\sqrt{1+\left(\frac{\varepsilon''}{\varepsilon'}\right)^2}\ -\ 1\right)\right]^{\frac{1}{2}} \qquad (17)$$

Results

Frequency dependence

Appendix A contains charts of dielectric constant values and calculated parameters plotted against frequency for every sample at every moisture content condition produced in the laboratory. For this study, data were collected and displayed over a frequency range of 1 MHz to 2,000 MHz. The key at the top of each figure shows the sample dry density and volumetric moisture content for each string of data that was collected. These charts are grouped by mine lane number and are ordered by increasing volumetric moisture.

The charts in Appendix A represent the best visualization of all the data collected for each sample condition. They clearly show the dispersive nature of these soils; i.e., that soil dielectric properties are, indeed, frequency dependent. Power attenuation and phase velocity both increase with increasing frequency. While low-frequency data indicate that simple ionic conductivity is the dominant loss mechanism (constant conductivity and a linear imaginary part of the complex dielectric constant plotted on a log-log scale), some of the high-frequency results highlight the beginning of dielectric relaxation losses (above 500 MHz). It is possible that for some samples, the physical and chemical properties of the soils result in other loss mechanisms as well (e.g., Maxwell-Wagner losses).

Moisture dependence at fixed frequencies

While the frequency-domain charts in Appendix A clearly reveal how signal frequency affects soil electromagnetic properties, they do not provide a clear picture of how those properties vary with sample moisture, nor do they provide an easily visual comparison of different soils. Soil moisture has been shown to be the most influential factor in controlling soil dielectric property values (Curtis 2001b). Therefore, it is quite useful to plot these properties against volumetric moisture content in a way that brings various soil sample results together on single charts. This has been done in the following pages, where one finds charts of electromagnetic properties versus volumetric moisture content at four different frequencies: 1 MHz (Figures 5-1 through 5-6), 10 MHz (Figures 5-7 through 5-12), 100 MHz (Figures 5-13 through 5-18), and 1,000 MHz (Figures 5-19 through 5-25).

Presenting data in chart form also allows one to easily recognize if there is any sample dependence on measured and calculated electromagnetic properties.

In this study, six different soil types were examined. If one is able to produce laboratory samples whose dry densities are comparable with what is found in the field, or whose densities, relative to one another, have the same trend as the *in situ* soils, then differences in soil chemistry might be easily observed on the charts found in the following pages. Unfortunately, analyses of other soil property data for samples taken from many different locations around the country and whose dry densities covered a wide range of values has not led this researcher to a definitive model for predicting sample density effects.

From a sensor design and data processing point of view, the most relevant data are probably the power attenuation numbers and the values of normalized phase velocity. Attenuation controls the depth of penetration of a ground-penetrating radar system. Phase velocity determines beam patterns (Snell's Law effects) and the ability to determine depth to a target from time-domain data. Focusing on those results for each of the four selected frequencies, one can make several generalized observations.

Consider, first, the attenuation charts in Figures 5-5, 5-11, 5-17a,b, and 5-24. One immediately sees that, for all of the soils taken as a group, attenuation can vary by at least an order of magnitude at any fixed moisture content. Furthermore, with the exception of the highest frequency data shown (1,000 MHz), attenuation for any soil type can increase by two orders of magnitude as the moisture content varies from nearly dry conditions to very wet soils (30 percent, or more, moisture content by volume). In a normal range of soil moisture values (10 to 20 percent by volume) and at 1,000 MHz, attenuation values for these soils easily vary from 10 to 100 dB per meter, indicating serious limitations on probing depth in unfrozen soils for ground-penetrating radar systems.

A practical question that can be asked is whether or not attenuation values are predictable for each soil as a function of moisture content. To help answer that question, attenuation data for 100 MHz were reproduced on Figure 5-17b along with power function fits to the data for each soil type. Certainly there is a difference in the gross response of each different mine lane soil type. One could make the observation that the clean white sand in lane 6 is the least lossy of the six soils. Lane 3 material (21A, gravelly silty sand (SM)) appears to be the most lossy soil.

Normally, one might expect the magnetite/sand mixture from lane 1 to exhibit the most bizarre behavior. However, results for this soil are difficult to assess, because its dielectric properties were measured under the assumption that the soil is non-magnetic. It is not clearly understood how such an assumption affects the final data.

Turning to the normalized phase velocity results in Figures 5-6, 5-12, 5-18, and 5-25, one can see that there is considerable change in phase velocity as moisture content increases. Taken as a group, wave speeds in these soils can vary by a factor or two or three at any fixed moisture content. As moisture content increases from nearly dry conditions to very wet conditions, phase velocity can drop from 50 to 60 percent of the speed of light to less than 10 percent of the speed of light at low frequencies.

As with attenuation data, trendlines were fit to the 100-MHz phase velocity data in Figure 5-19. These are not power functions, but rather are second and third order polynomials. Except for the oddball material in lane 1, phase velocity data at this frequency are fairly tight for all soil types and have very little variance. Lane 4 soil (Bank Run Gravel, clay (CM)), reveals an unusual linear relationship between phase velocity and moisture content.

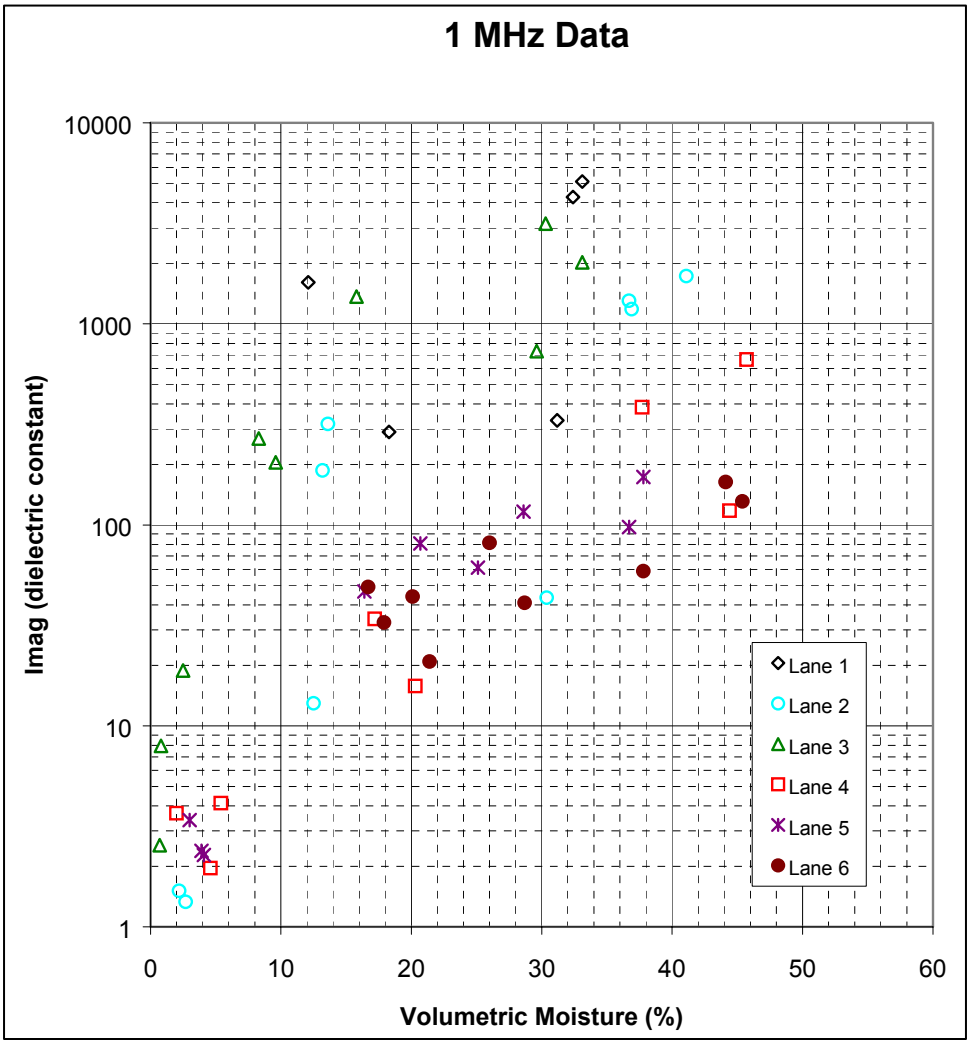

Figure 5-1. Real (dielectric constant) vs volumetric moisture, 1 MHz

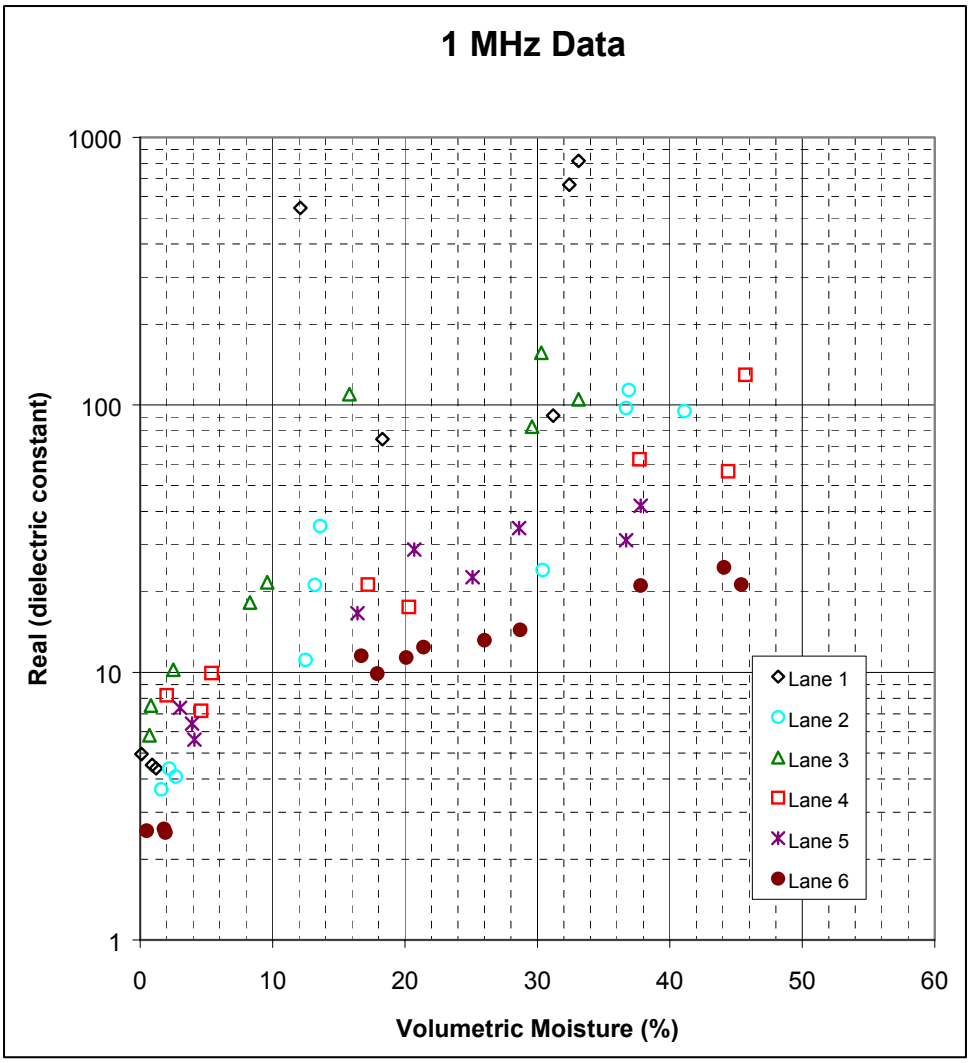

Figure 5-2. Imaginary (dielectric constant) vs volumetric moisture, 1 MHz

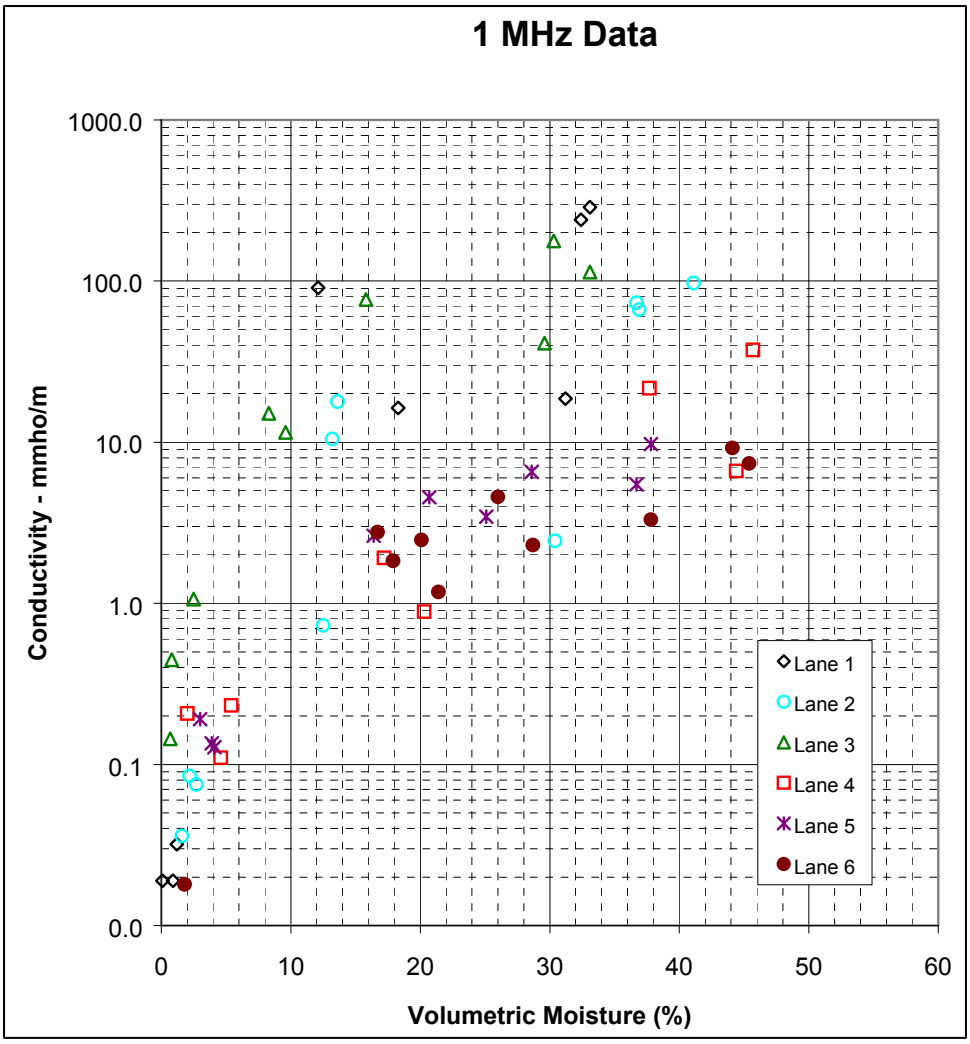

Figure 5-3. Conductivity vs volumetric moisture, 1 MHz

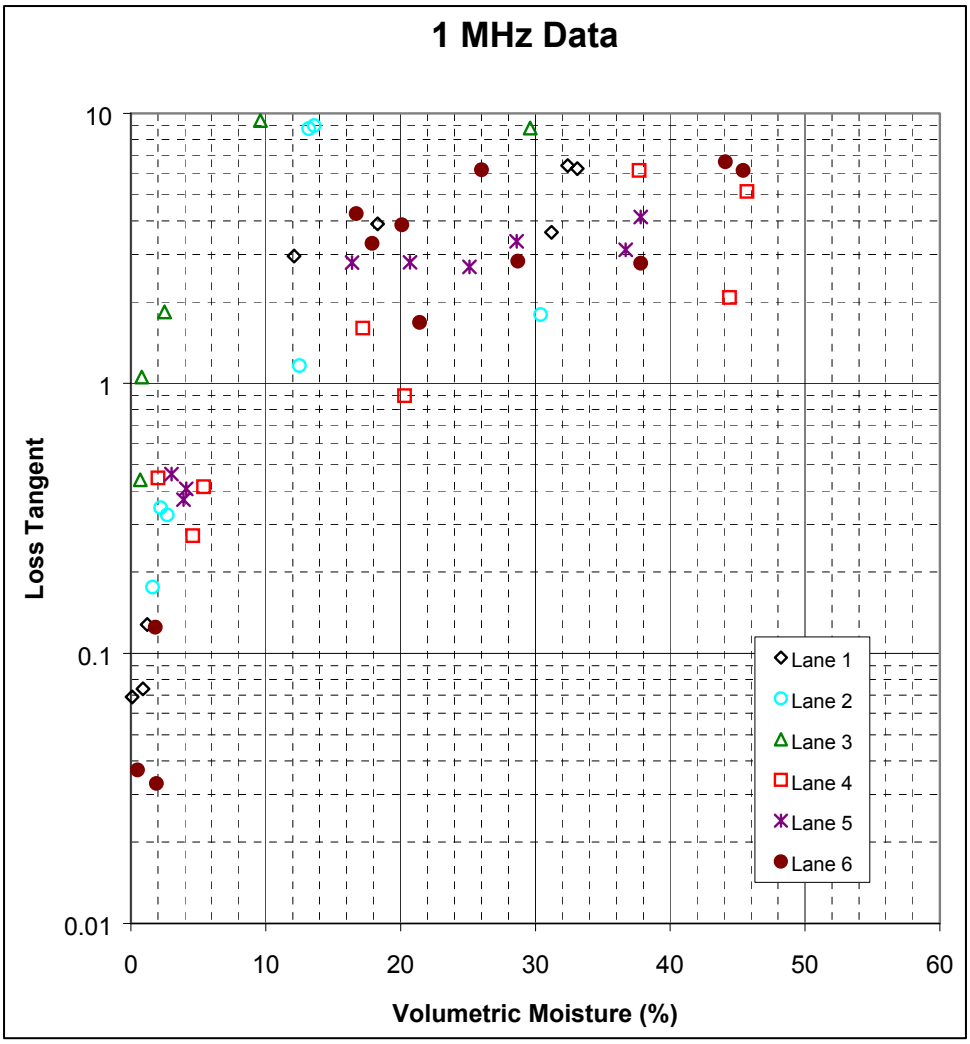

Figure 5-4. Loss tangent vs volumetric moisture, 1 MHz

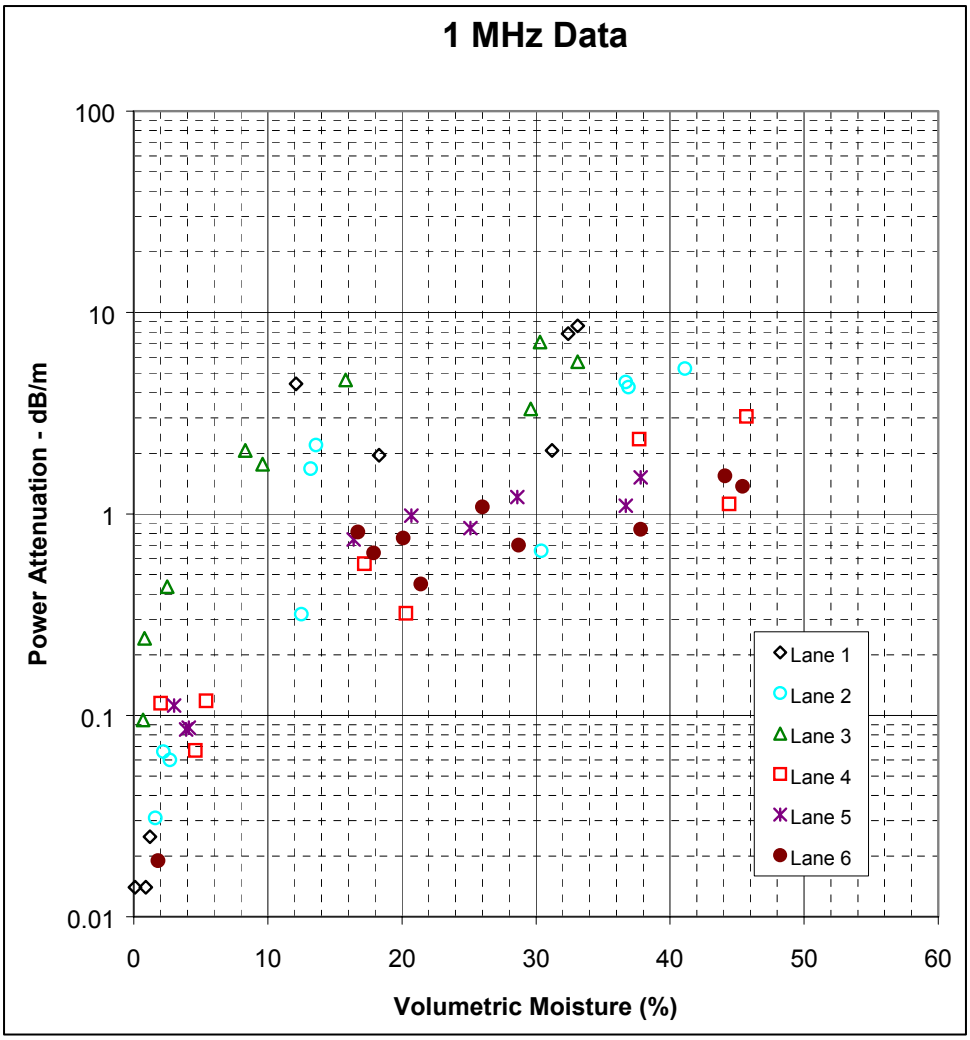

Figure 5-5. Power attenuation vs volumetric moisture, 1 MHz

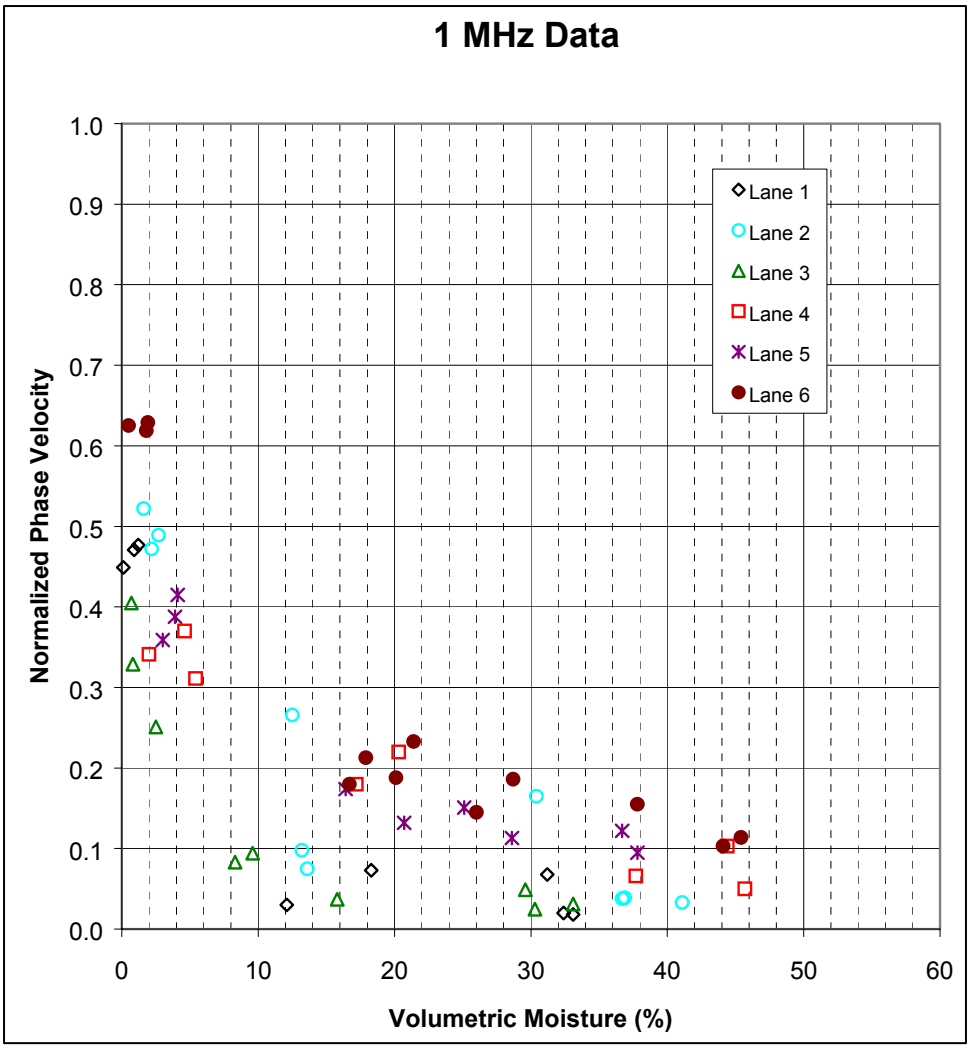

Figure 5-6. Normalized phase velocity vs volumetric moisture, 1 MHz

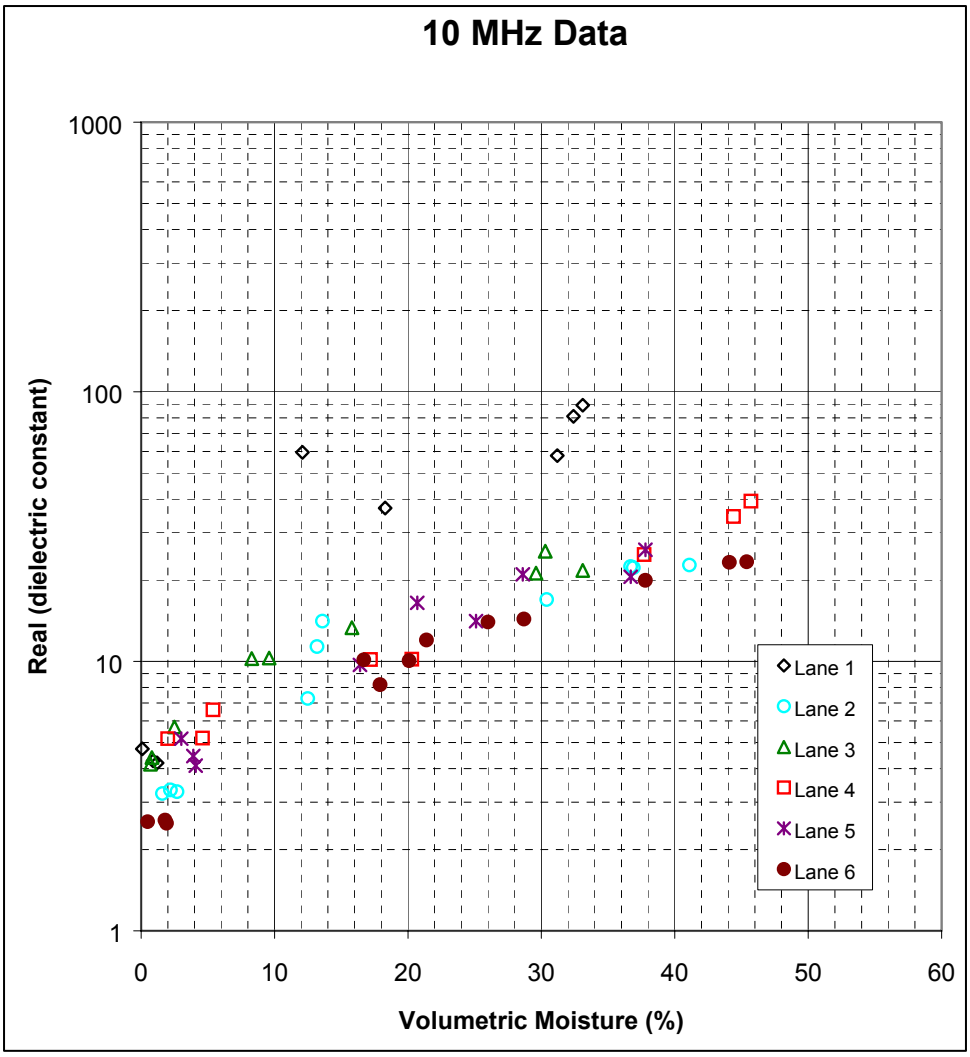

Figure 5-7. Real (dielectric constant) vs volumetric moisture, 10 MHz

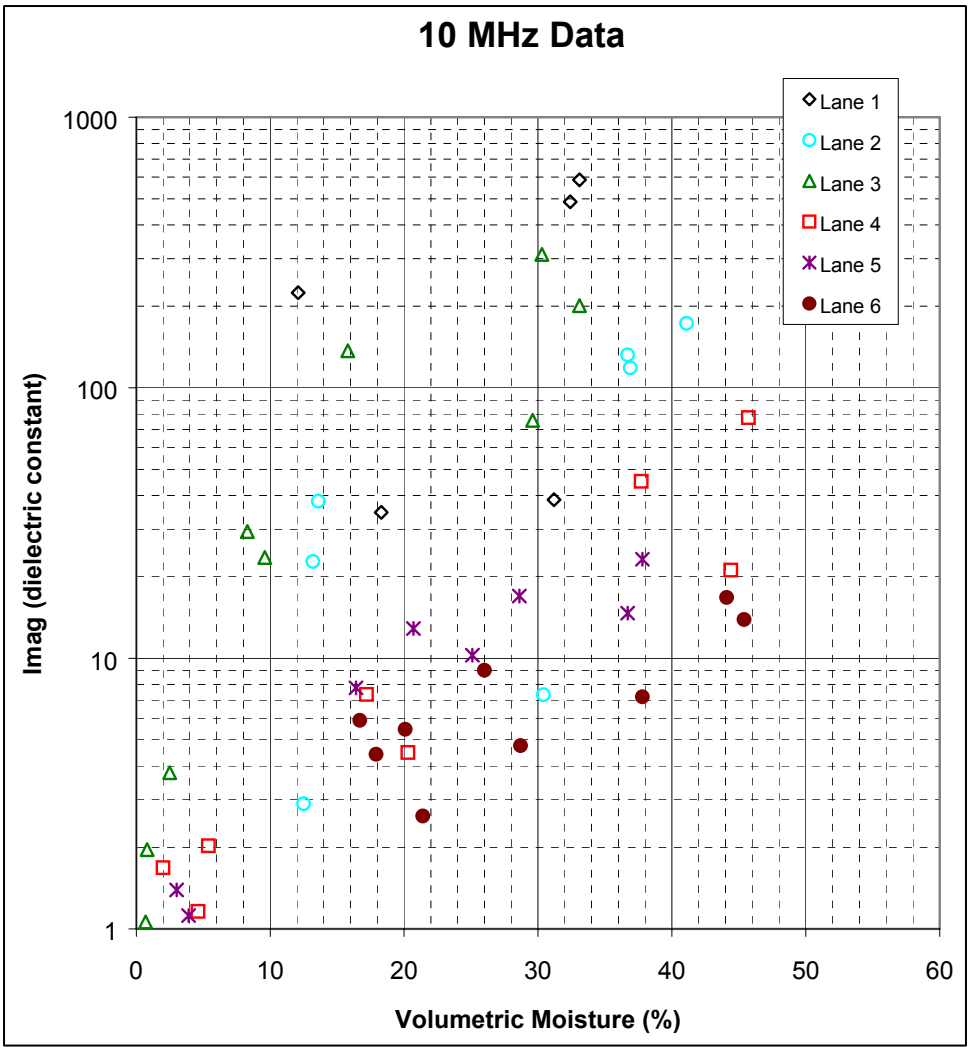

Figure 5-8. Imaginary (dielectric constant) vs volumetric moisture, 10 MHz

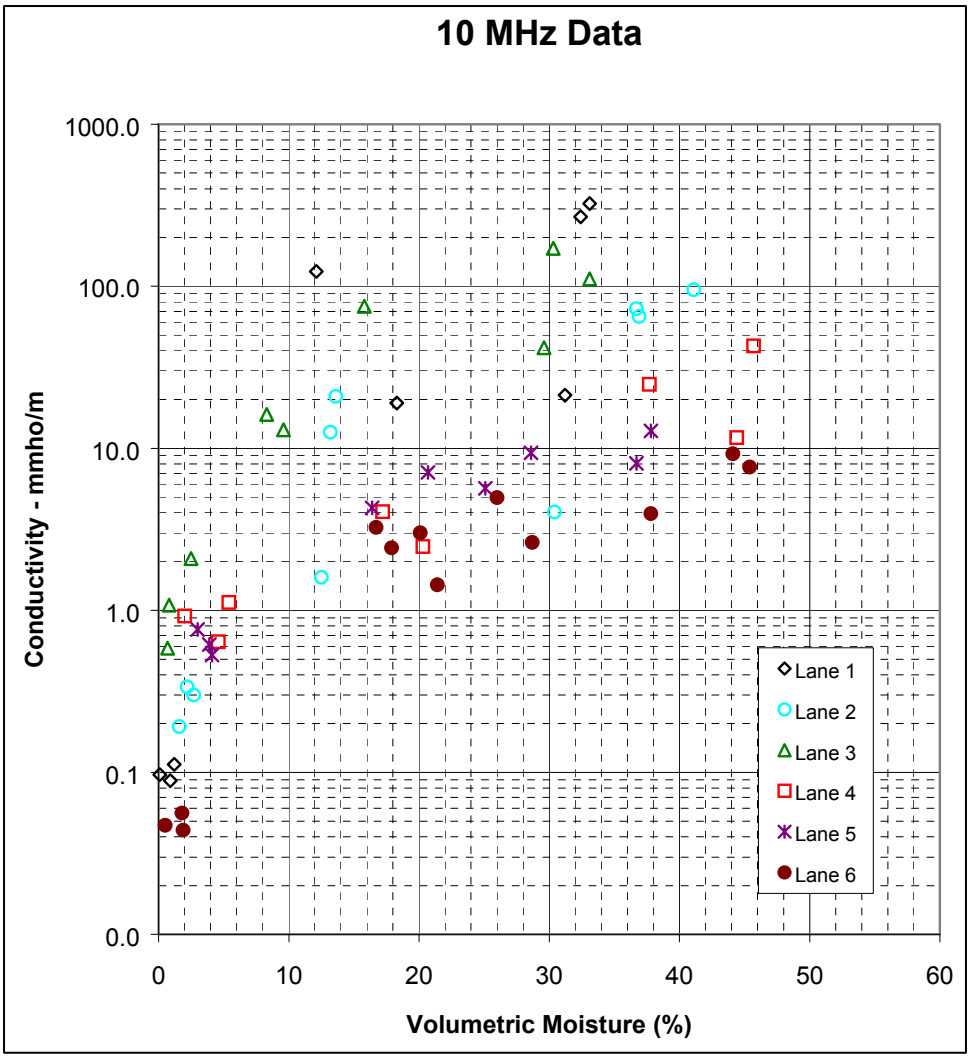

Figure 5-9. Conductivity vs volumetric moisture, 10 MHz

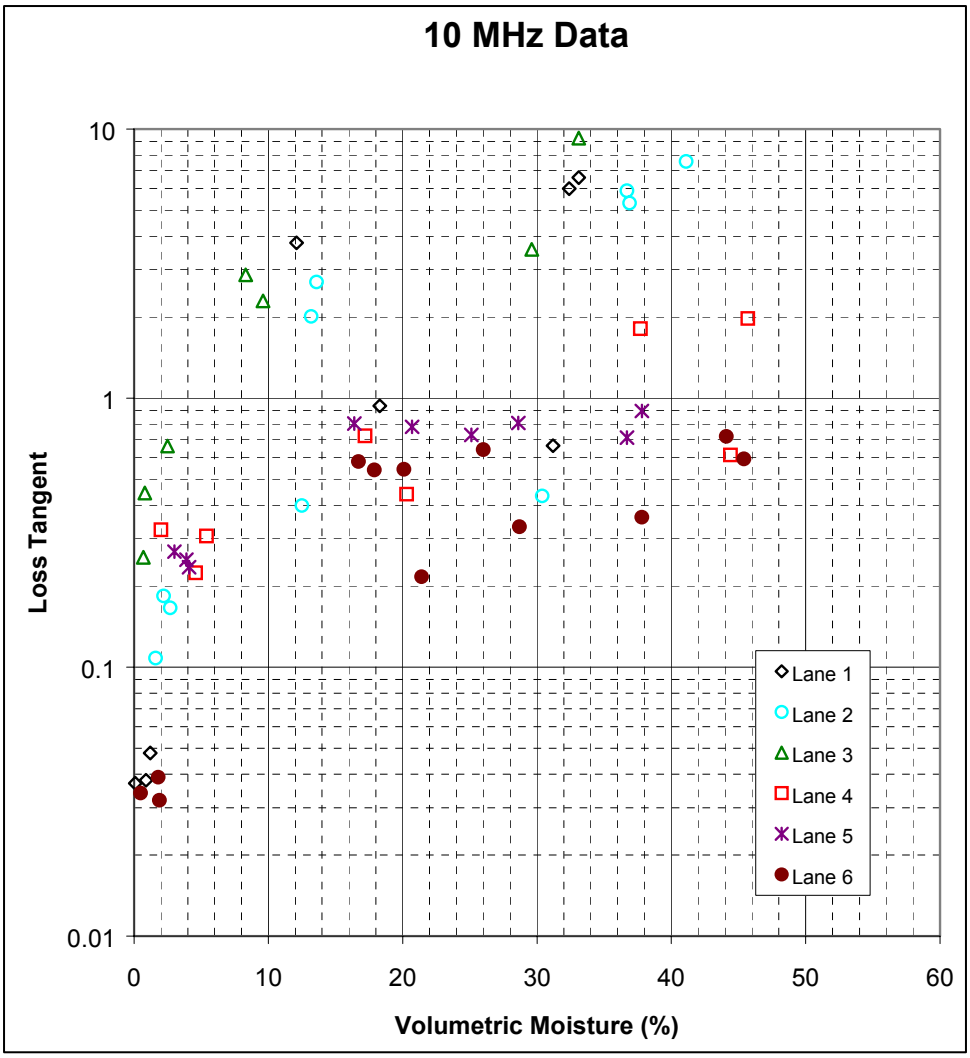

Figure 5-10. Loss tangent vs volumetric moisture, 10 MHz

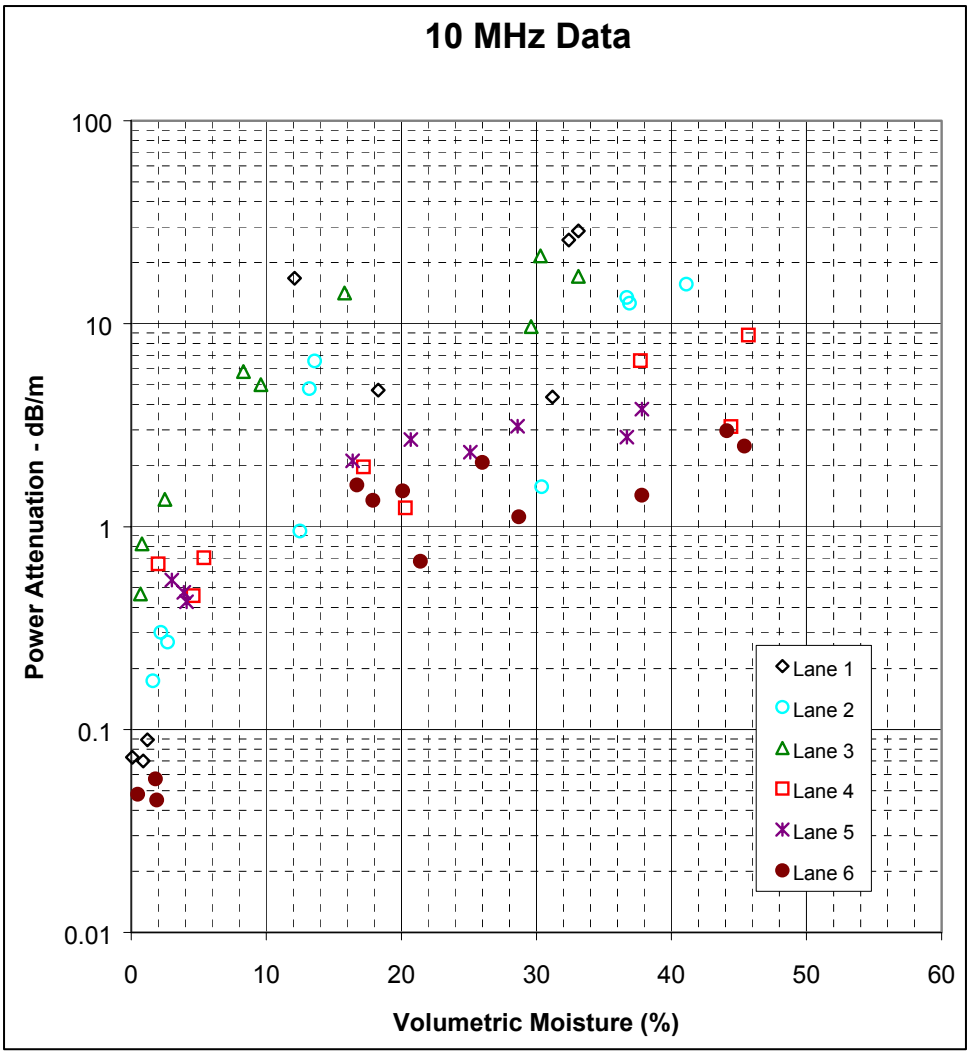

Figure 5-11. Power attenuation vs volumetric moisture, 10 MHz

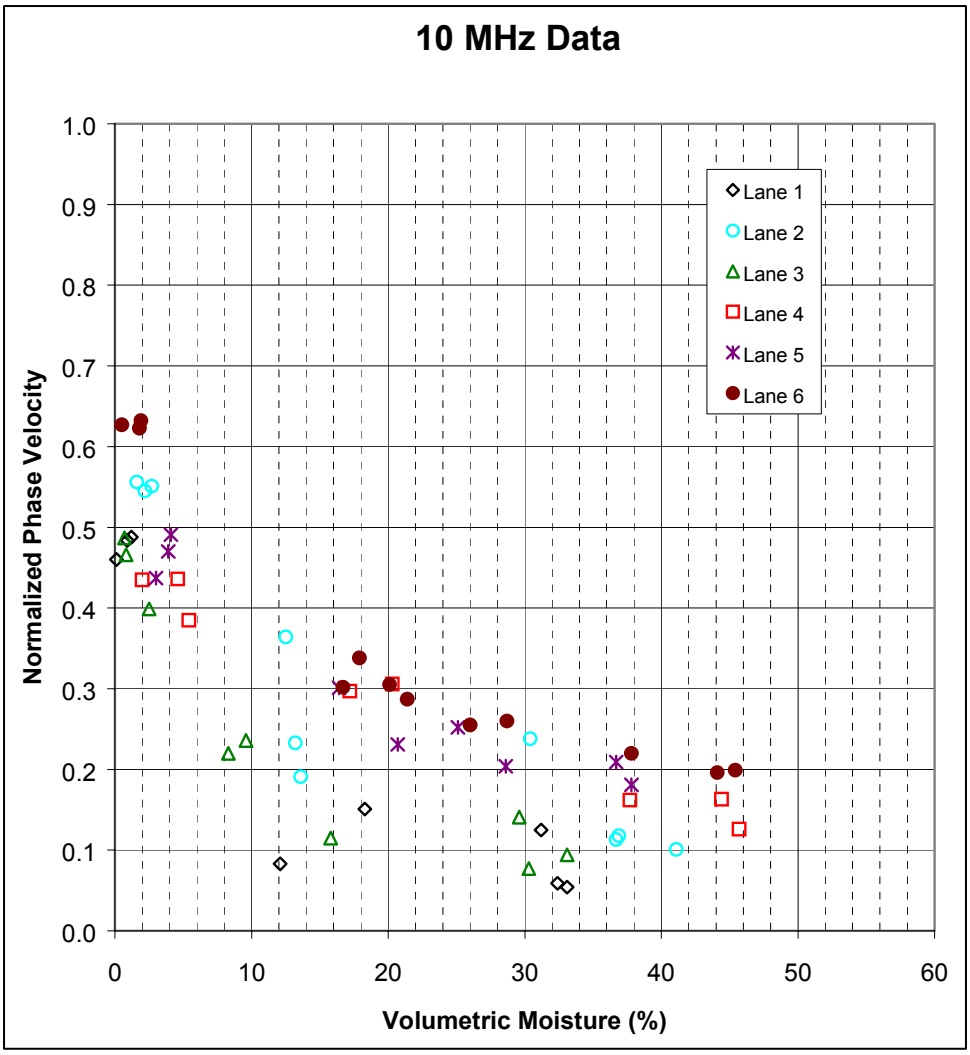

Figure 5-12. Normalized phase velocity vs volumetric moisture, 10 MHz

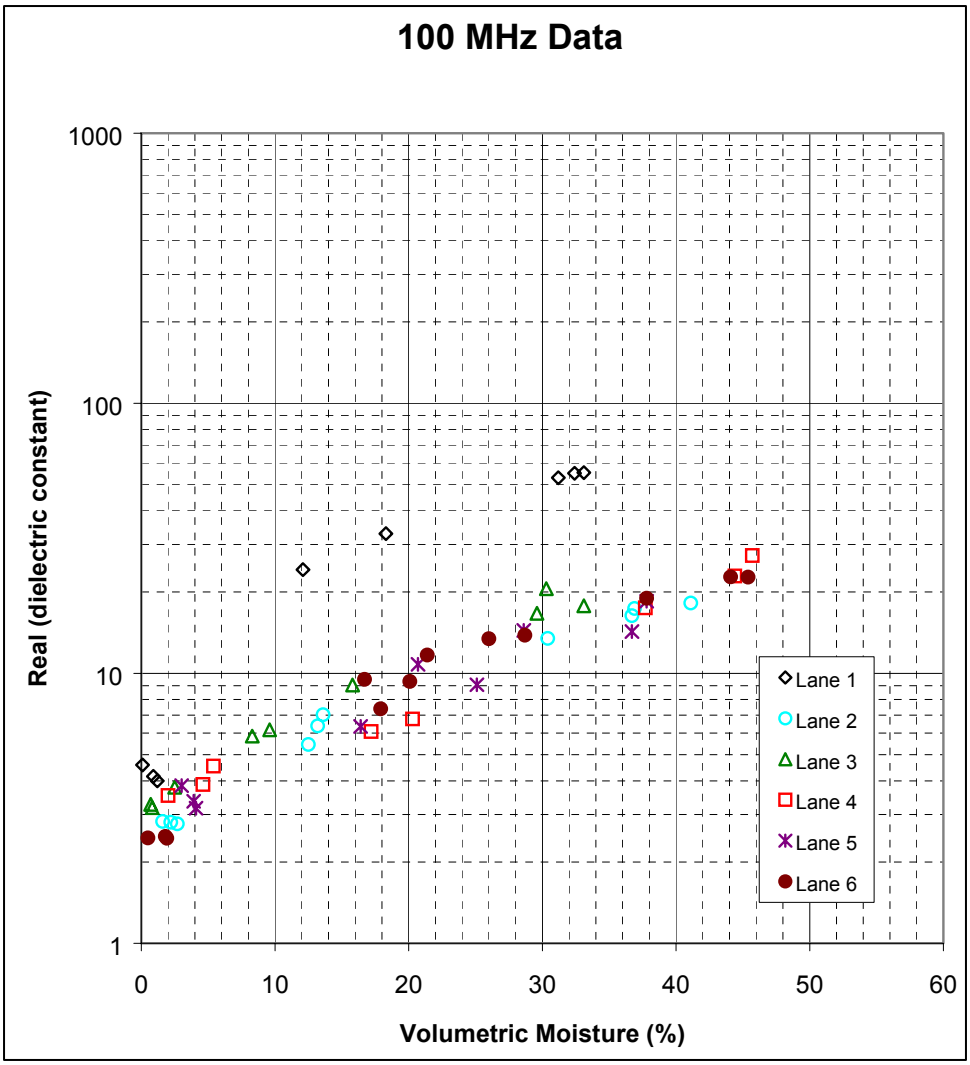

Figure 5-13. Real (dielectric constant) vs volumetric moisture, 100 MHz

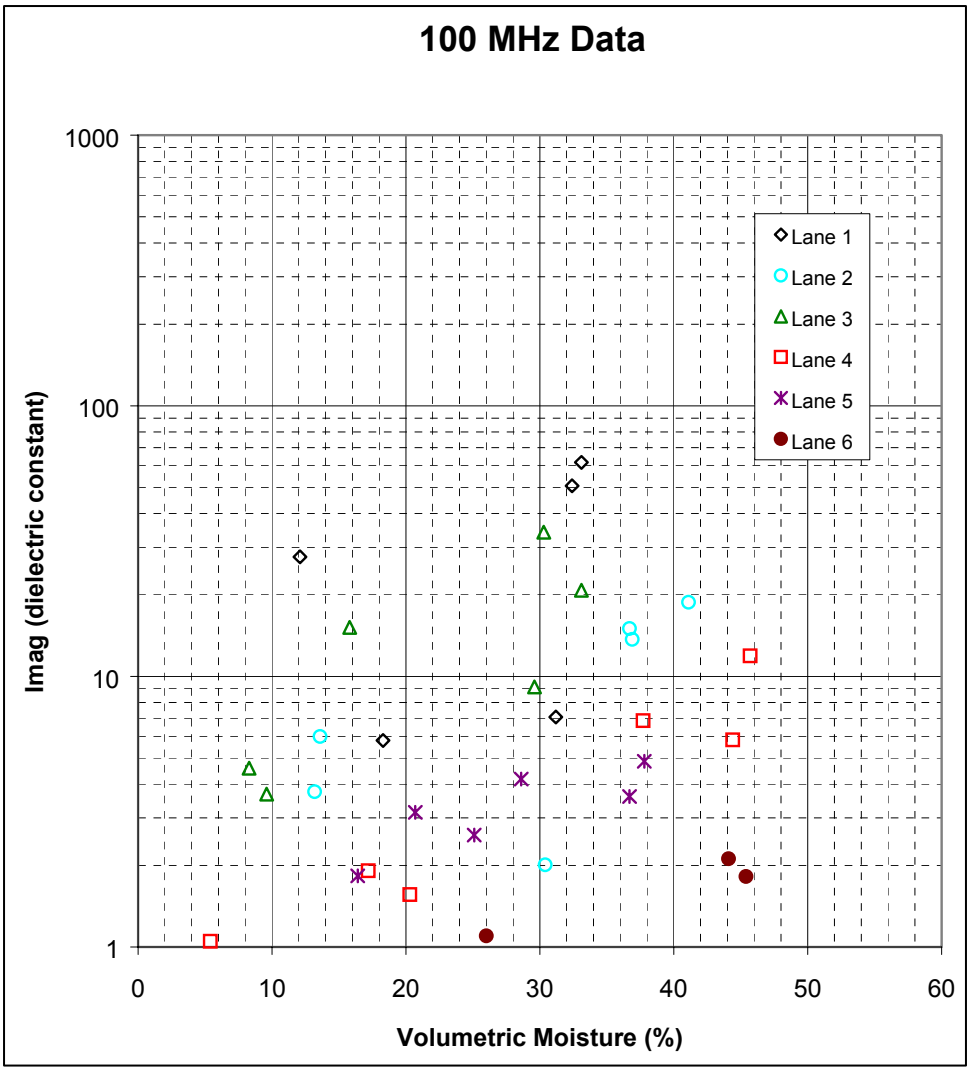

Figure 5-14. Imaginary (dielectric constant) vs volumetric moisture, 100 MHz

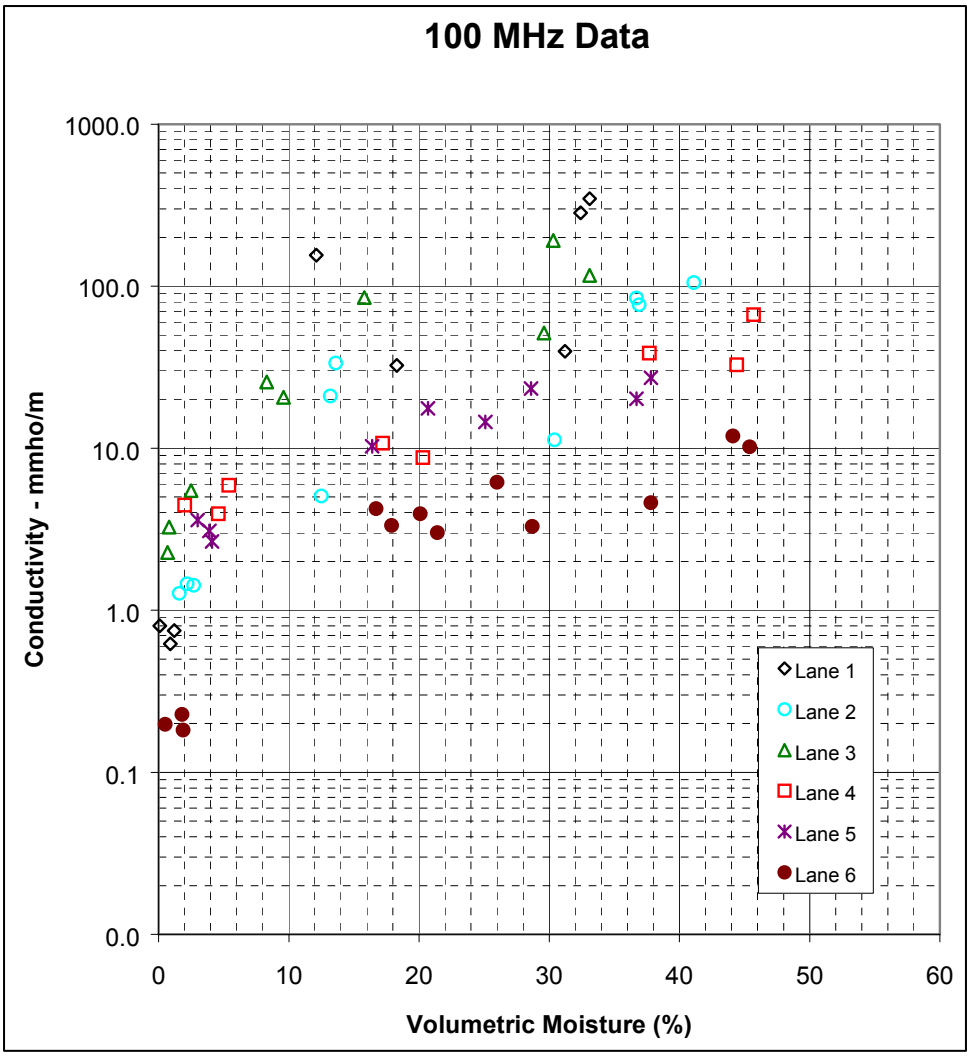

Figure 5-15. Conductivity vs volumetric moisture, 100 MHz

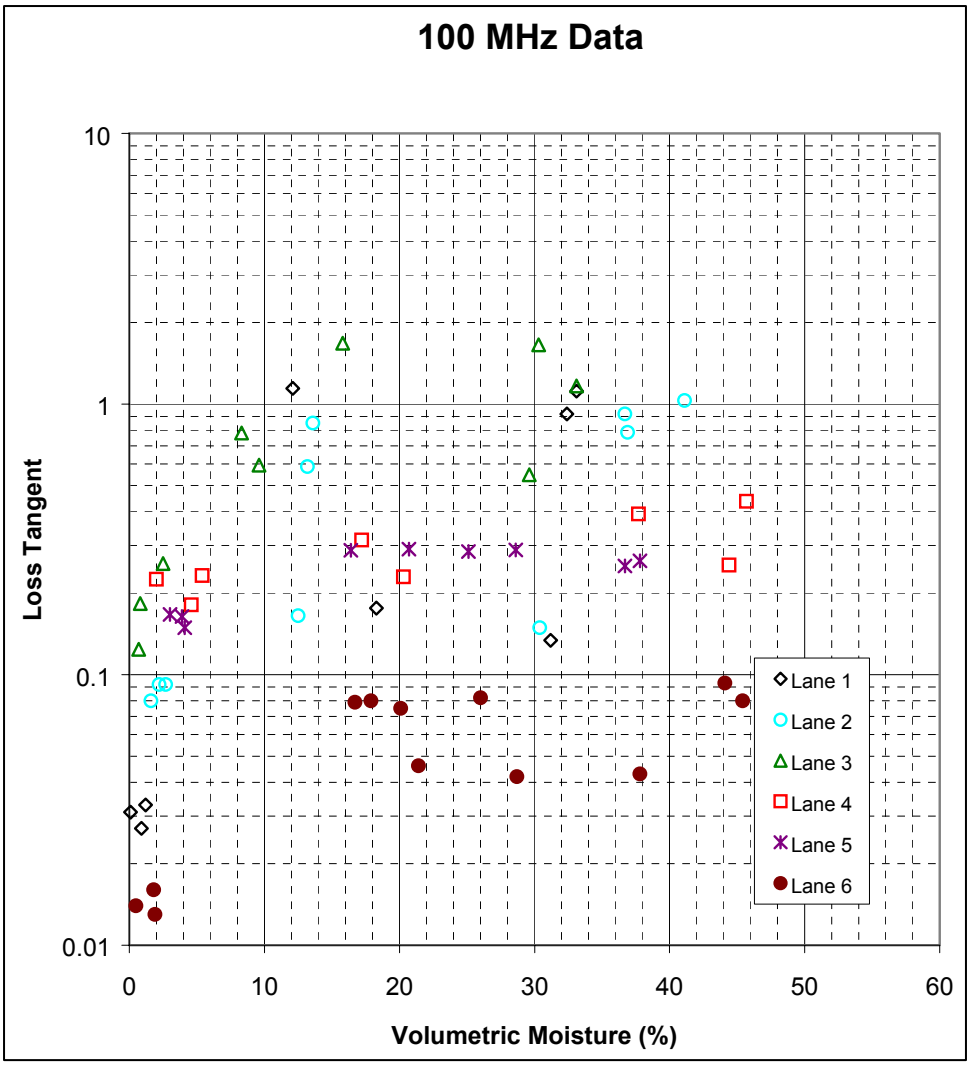

Figure 5-16. Loss tangent vs volumetric moisture, 100 MHz

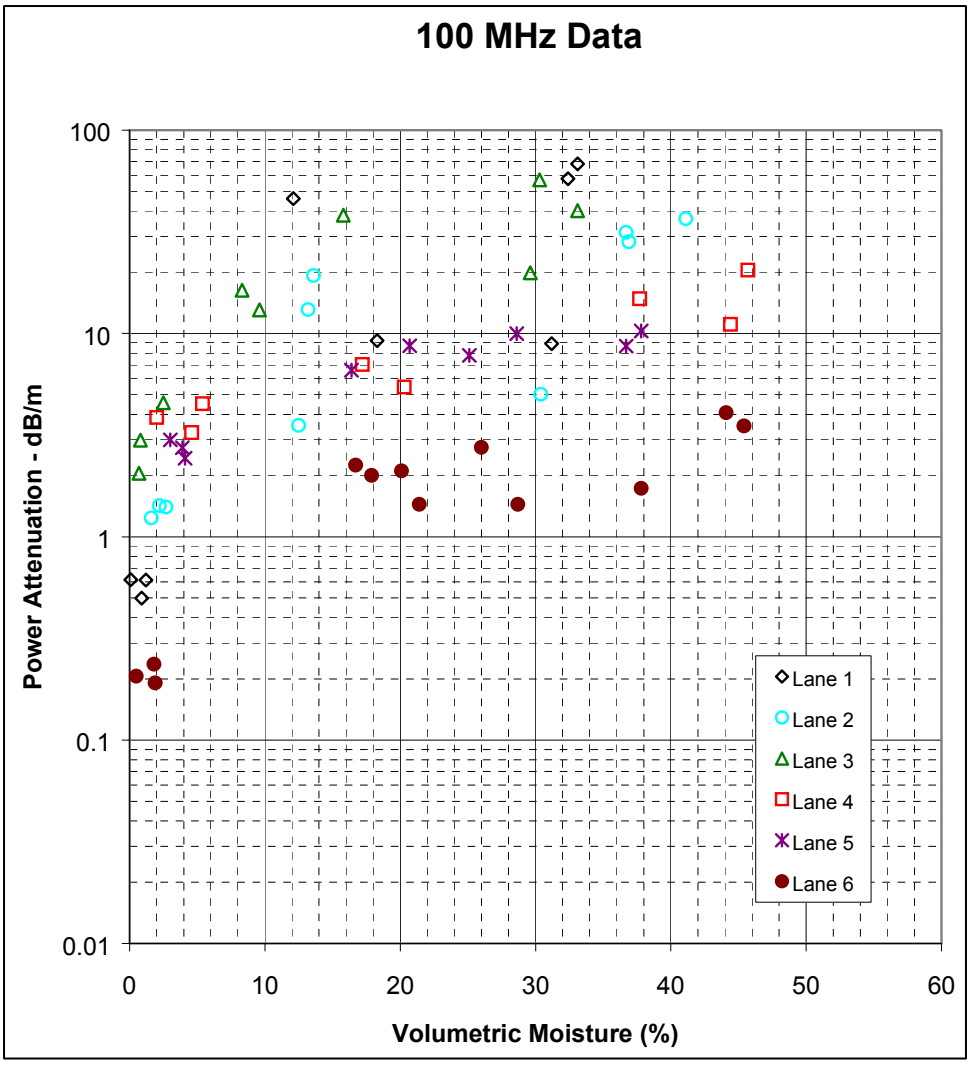

Figure 5-17a. Power attenuation vs volumetric moisture, 100 MHz

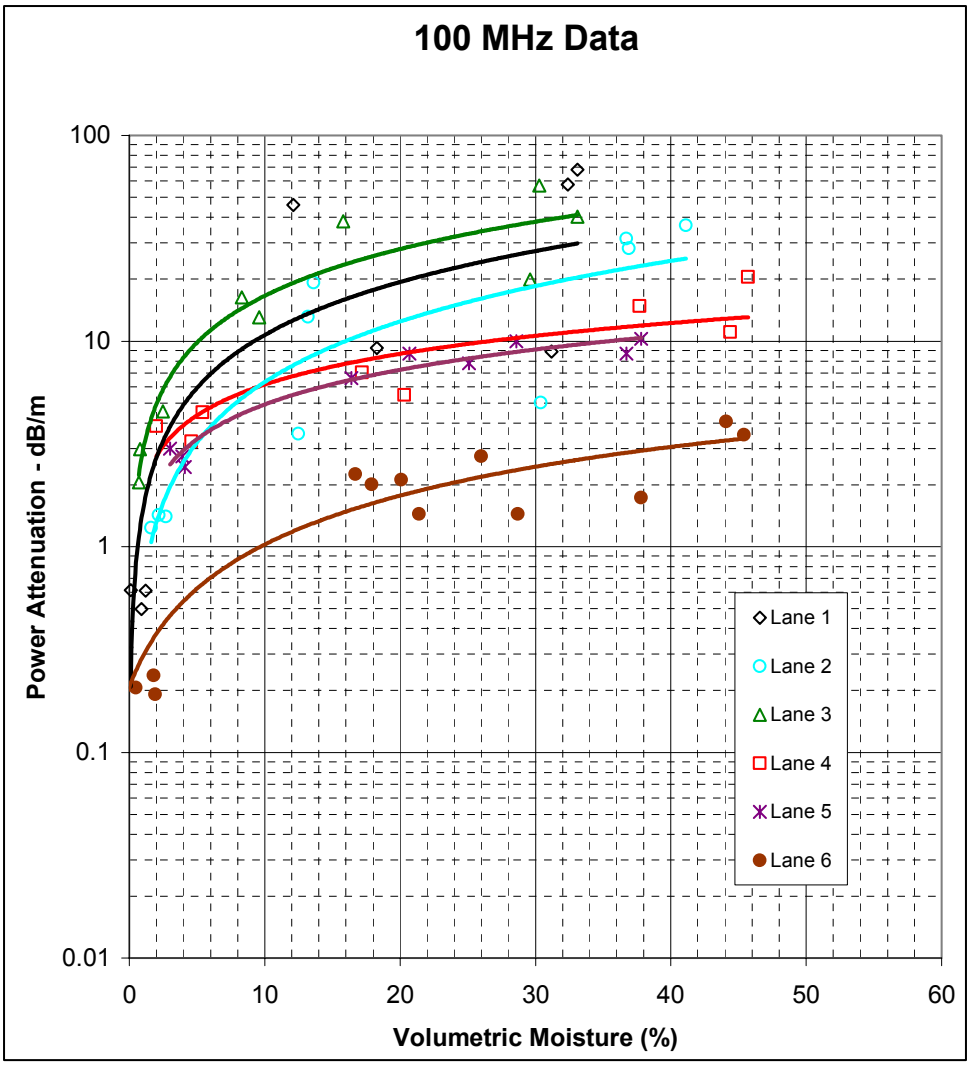

Figure 5-17b. Power attenuation vs volumetric moisture, 100 MHz, trendlines added

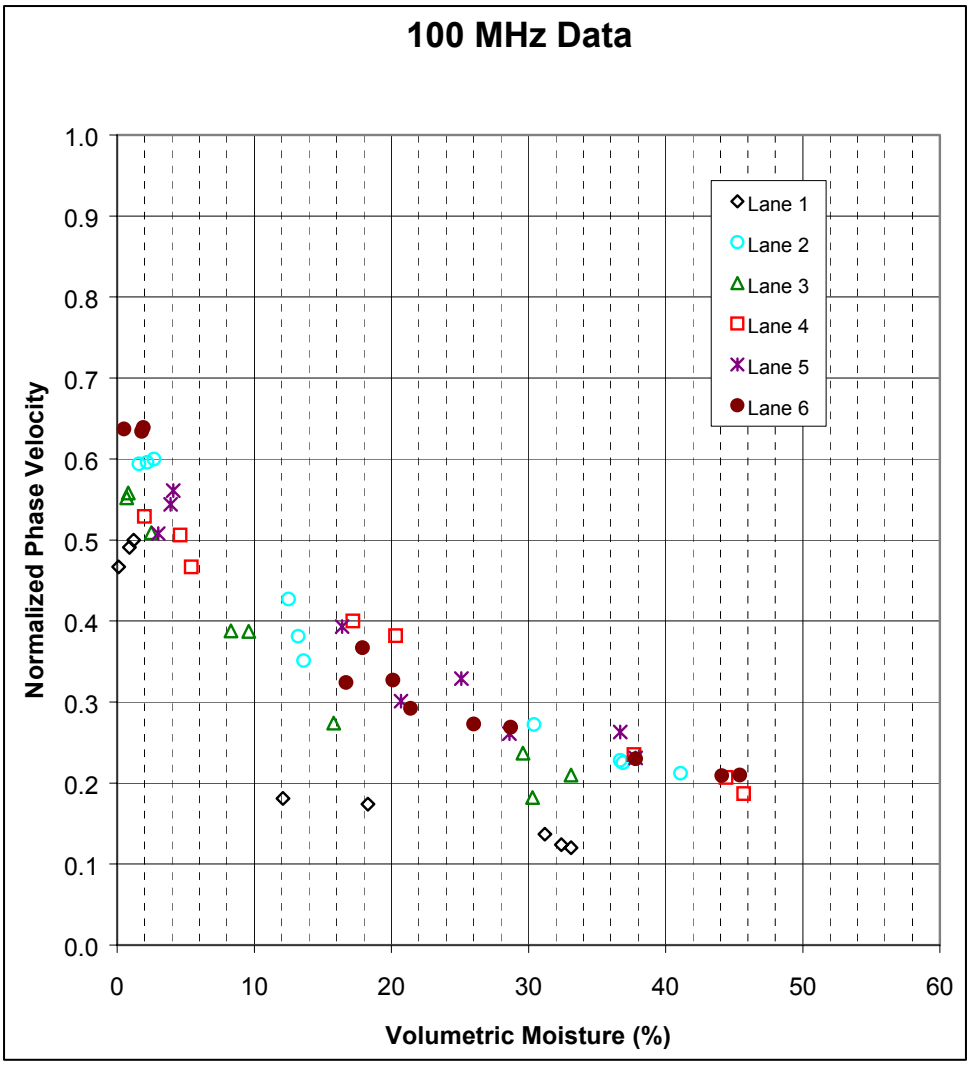

Figure 5-18. Normalized phase velocity vs volumetric moisture, 100 MHz

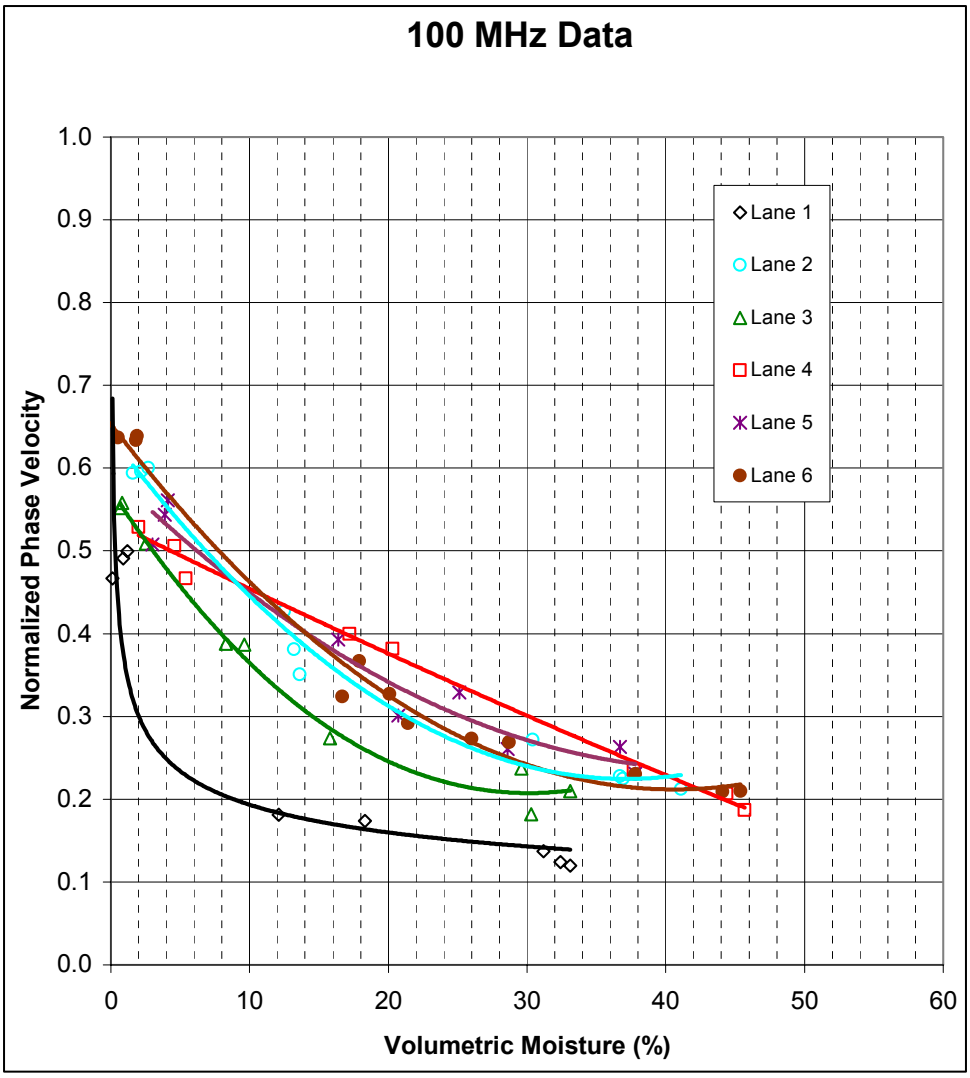

Figure 5-19. Normalized phase velocity vs volumetric moisture, 100 MHz, trendlines added

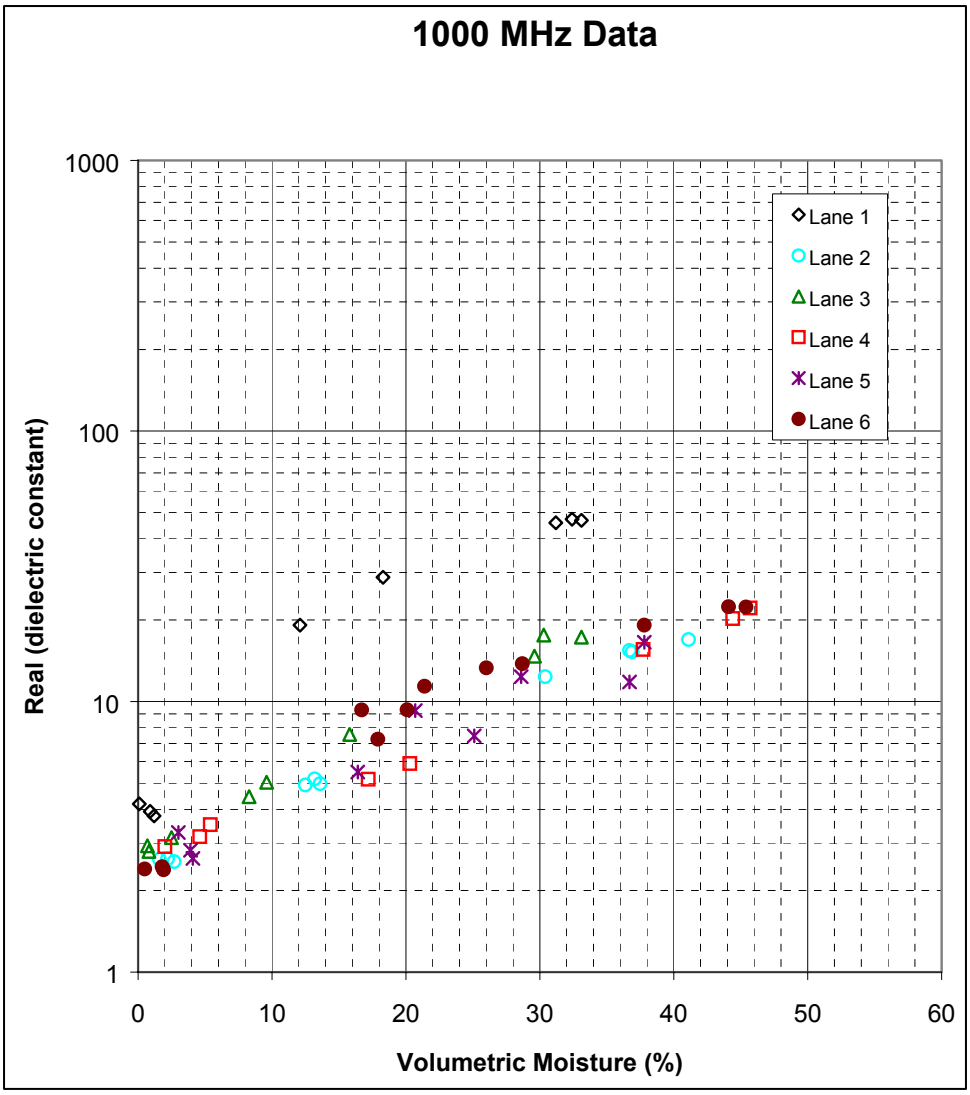

Figure 5-20. Real (dielectric constant) vs volumetric moisture, 1,000 MHz

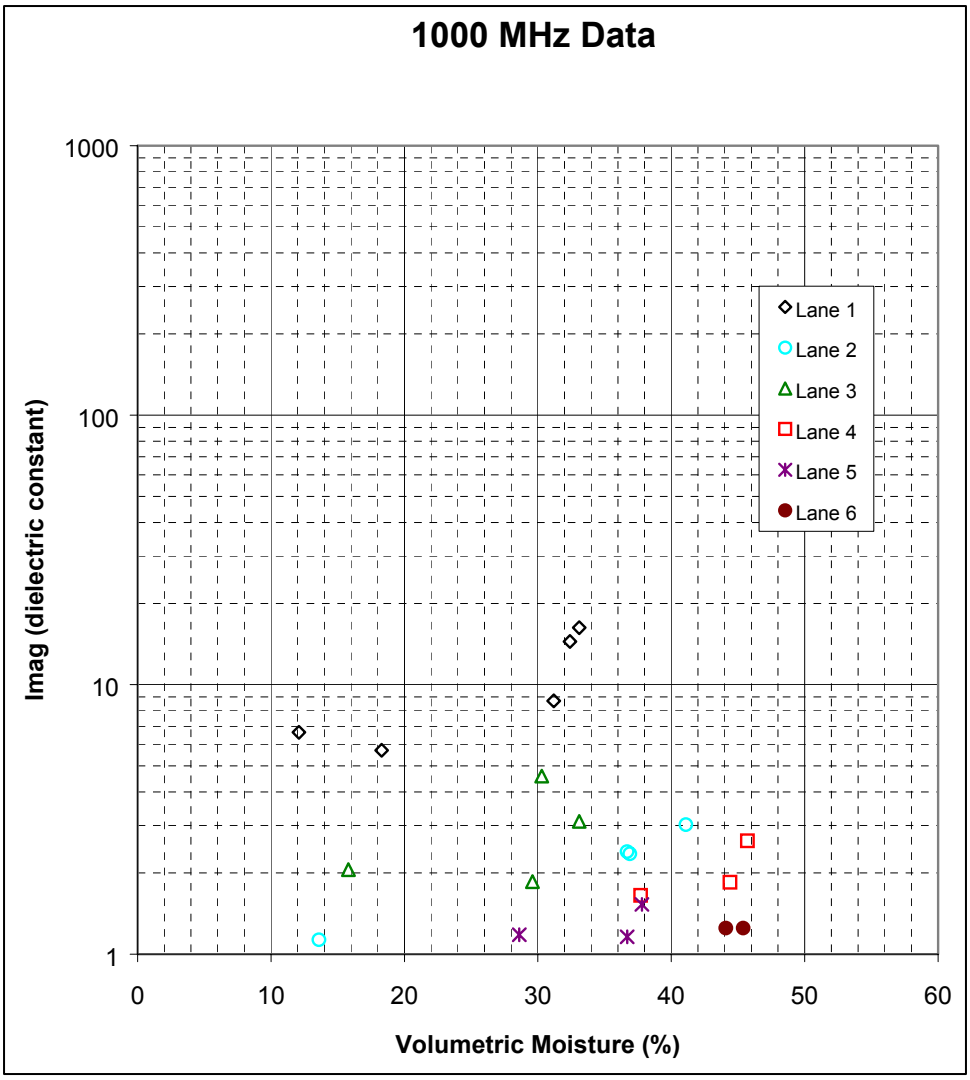

Figure 5-21. Imaginary (dielectric constant) vs volumetric moisture, 1,000 MHz

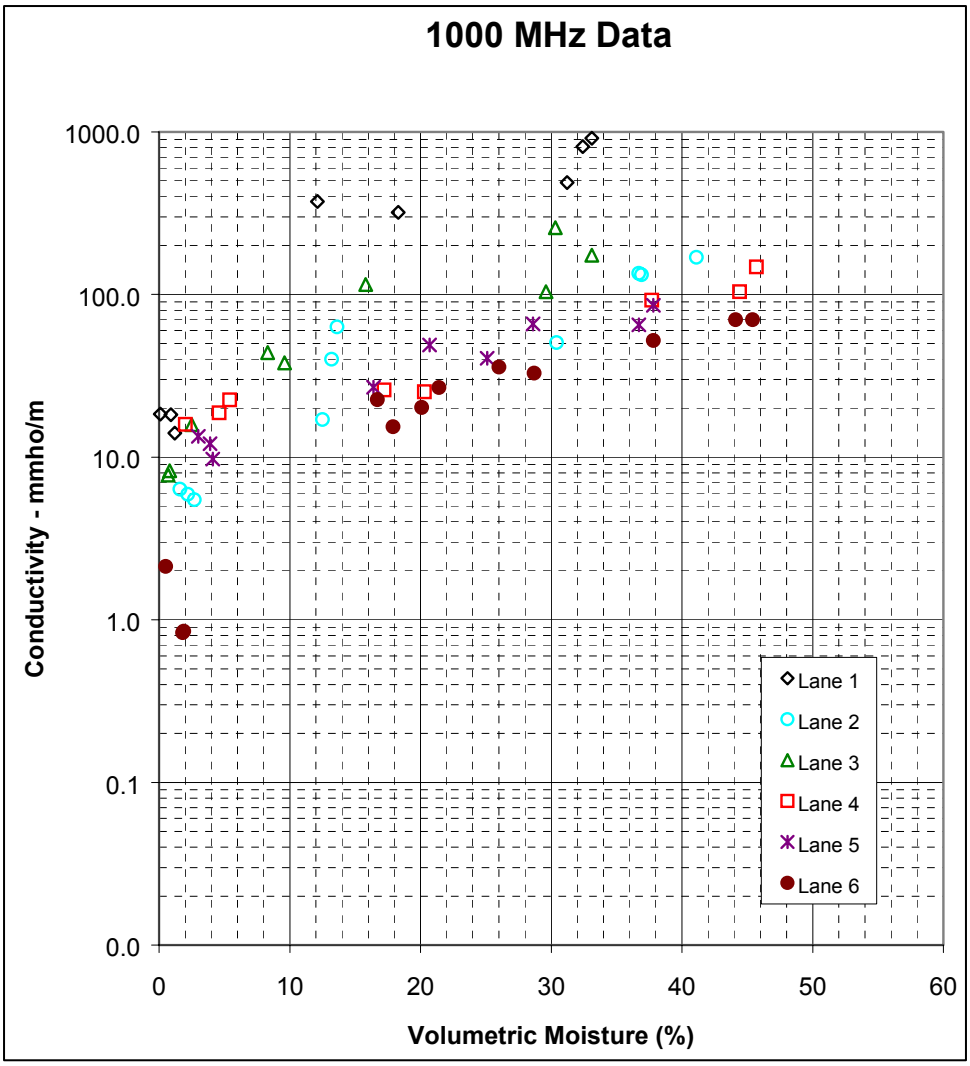

Figure 5-22. Conductivity vs volumetric moisture, 1,000 MHz

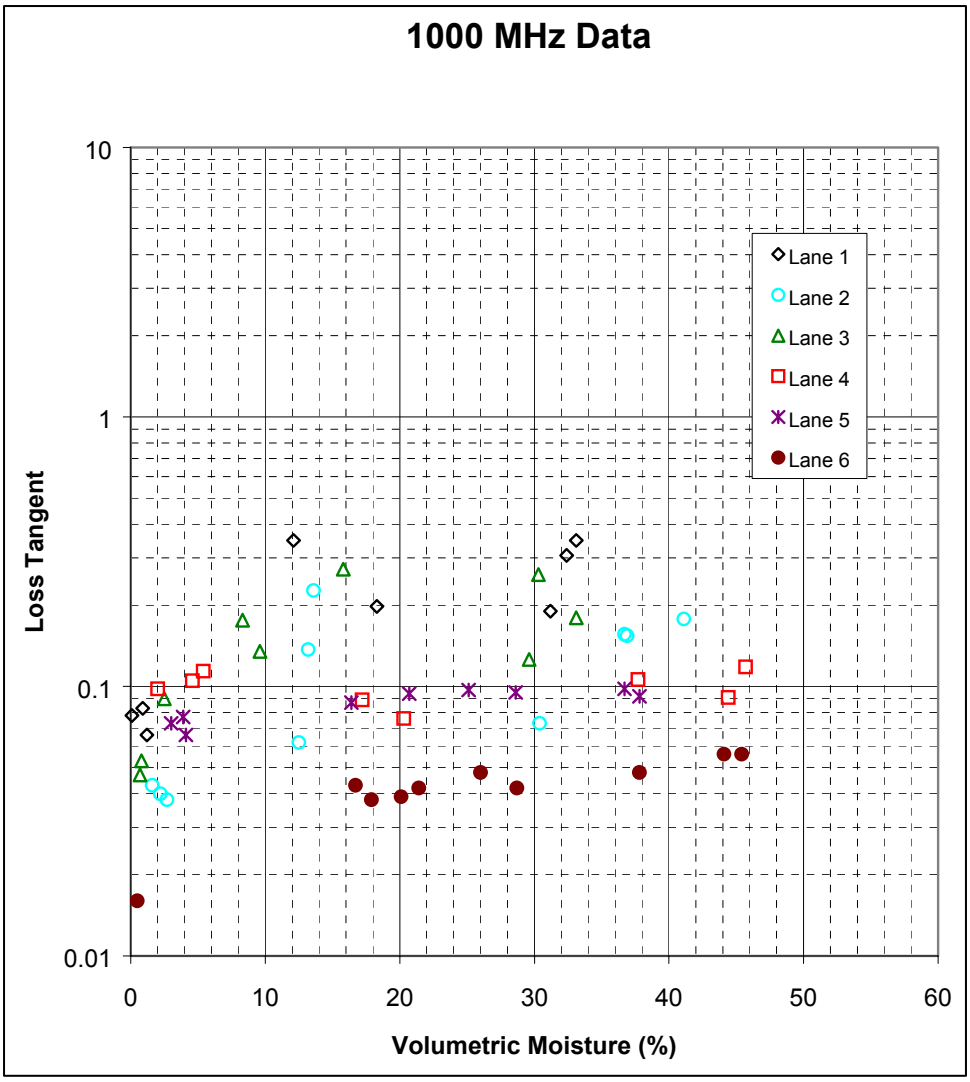

Figure 5-23. Loss tangent vs volumetric moisture, 1,000 MHz

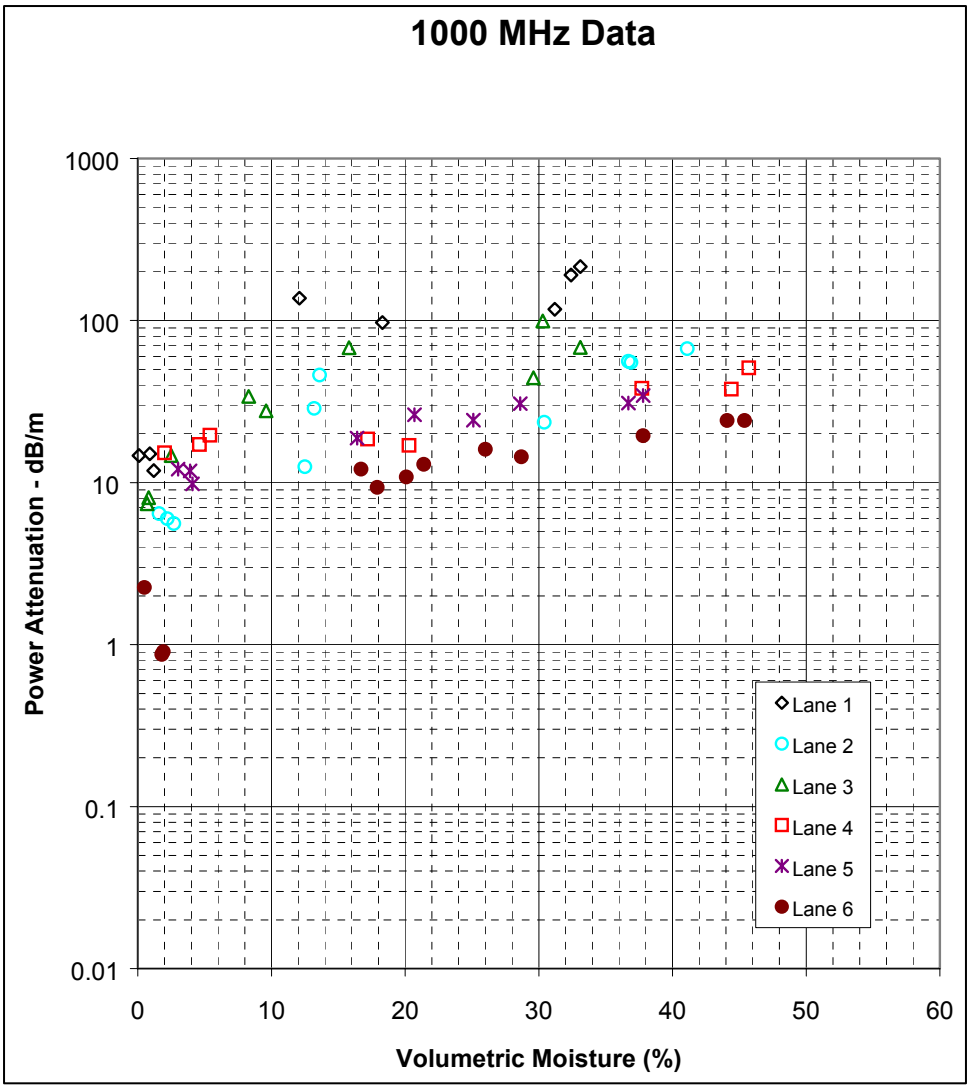

Figure 5-24. Power attenuation vs volumetric moisture, 1,000 MHz

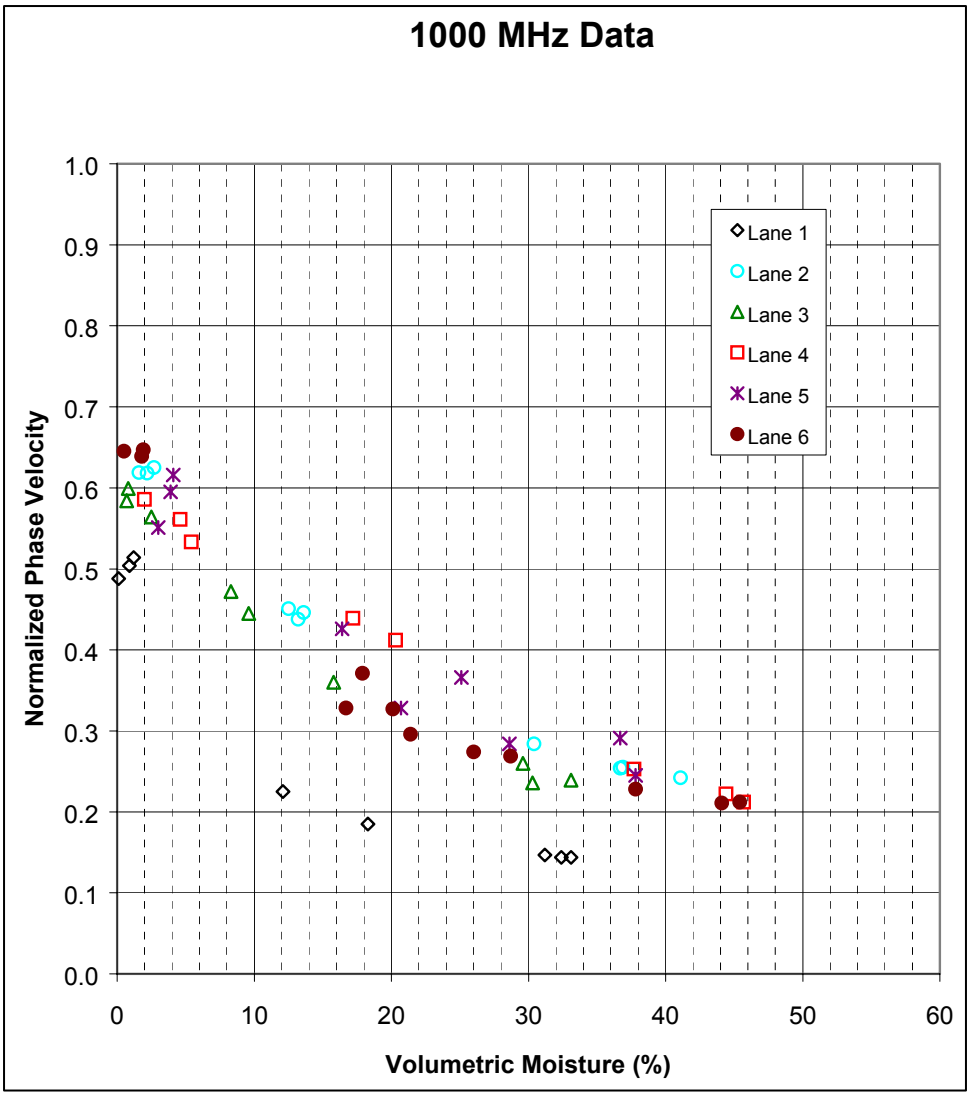

Figure 5-25. Normalized phase velocity vs volumetric moisture, 1,000 MHz

6 Magnetic Susceptibility Data

Instrument Description and Operation

The Bartington MS2 measurement system (Dearing 1999) uses a variety of sensors to determine the magnetic susceptibility (the ratio of magnetization to magnetic field in a sample) of soil and rock, both *in situ* and in the laboratory. The MS2B sensor was utilized for this work, because it is applicable for measuring loose soil samples. The MS2 meter directly displays the volume magnetic susceptibility values in SI or CGS units. Mass magnetic susceptibility values are obtained knowing the sample volume and mass of each sample. Two different frequency measurements can be made with the MS2B sensor, one at 0.465 kHz and one at 465kHz. The lower frequency is applicable for soils having weak magnetic susceptibility; whereas, the higher frequency is used for soils exhibiting stronger susceptibilities. The sensor is fitted with a moving platen to allow for easy insertion and removal of samples. The sensor is specifically calibrated for use with a 10-cc sample container with internal dimensions 24 mm diameter x 23 mm height and a base external diameter of 26 mm maximum. A calibration sample is provided with the MS2B system to ensure the sensor is functioning properly.

Sample Preparation and Data Acquisition

Details of sample preparation are included here, because there is no standard method established for this test. The soil test samples were prepared using a minimum of 100 g of soil. Each of the 16 samples was initially laid out to air dry at room temperature for a day. The samples were then sieved through a 1.18-mm #16 sieve. The 10-cc plastic containers that would contain the soil were labeled and weighed without any soil. The containers were then filled with soil. Each container was tapped on the counter 10 times, and additional soil was added to fill the container completely. The containers were weighed again with soil included.

Using the calibration sample provided with the instrument, the sensor calibration was checked. The measurement of the calibration sample should be within 1 percent of the calibration value on the sample. Prior to acquiring any measurements, the background interference of the laboratory was checked with

no sample in the sensor, the selector switch on the (x) 1.0 range, and on continuous measure.

Susceptibility measurements made with the MS2B measurement system were entirely menu driven. The susceptibility of each container was obtained by taking a measurement of air (no container), an empty container, and air again on the low-frequency setting, only. Air measurements accounted for instrument drift. The average container susceptibility was $-0.3 \times 10^{-8} m^3 kg^{-1}$ (plastic is diamagnetic). Following the empty container measurement, a sample was prepared, as described above, and measurements made of the sample using the same air-sample-air method to account for drift. A given sample was measured at both frequencies before moving on to the next holder/sample. All corrections for holder susceptibility and instrument drift were made internally by the MS2B system. The final output of the instrument was the mass susceptibility for each sample, at each frequency, in SI units. Volume susceptibility could be calculated by multiplying the mass susceptibility by the sample density.

Discussion of Results

Tables 6-1 and 6-2 list the data collected on 23 soil samples from the NVESD mine lane facility at 0.465 kHz and 465 kHz, respectively. Figures 6-1 and 6-2 are bar charts of the same data. According to Dearing (1999), soils showing purely paramagnetic behavior rarely have values greater than $10 \times 10^{-8} m^3 kg^{-1}$. Lanes 1, 2, and 4 have susceptibility values that are consistent with ferrimagnetic behavior, normally attributed to the presence of iron oxides such as magnetite. Returning to the mineralogy of these lanes, found in Table 3-1, one sees that magnetite is indeed a major component of the lane 1 soil. Magnetization in the soil of lane 4 could be accounted for by a large amount of the iron-rich mineral, goethite. Lane 2 susceptibility values are more difficult to explain. While lane 2 soil contains neither magnetite nor goethite, it does contain some chlorite, which has the potential for iron cations. However, the presence of chlorite in lane 2 is not sufficient to explain relatively high susceptibility values, since lane 4 soil contains a higher percentage of chlorite, without correspondingly higher susceptibility values. The low-frequency susceptibility values were slightly larger than the high-frequency susceptibility values for these measurements.

Table 6-1
Magnetic Susceptibility of NVESD Mine Lane Soil Samples 0.465 kHz – Air Dried

Location	Sample	Container Mass (gm)	Sample Mass w/Container (gm)	Sample Mass (gm)	Mass Susceptibility (x $10^8 m^3 kg^{-1}$)
Lane 1 N end	1	4.264	23.541	19.277	461.2
	2	4.196	23.767	19.571	332.0
Lane 1 S end	1	4.281	22.433	18.152	376.4
	2	4.200	23.173	18.973	276.3
	3	4.337	23.613	19.276	350.3
				lane 1 average	**359.2**
Lane 2 N end	1	4.173	17.168	12.995	120.9
	2	4.163	16.895	12.732	119.1
	3	4.264	17.352	13.085	109.7
Lane 2 middle	1	4.253	17.992	13.739	110.6
	2	4.118	17.773	13.655	101.4
	3	4.145	17.943	13.798	103.5
Lane 2 S end	1	4.264	18.155	13.891	121.4
	2	4.269	18.381	14.112	130.2
	3	4.218	18.002	13.784	111.2
				lane 2 average	**114.2**
Lane 3 N end	1	4.224	20.177	15.953	11.6
	2	4.179	20.692	16.513	13.1
	3	4.160	21.069	16.909	11.1
Lane 3 middle	1	4.278	20.642	16.364	44.7
	2	4.230	20.321	16.091	48.7
	3	4.191	20.613	16.422	46.3
Lane 3 S end	1	4.240	20.704	16.464	15.1
	2	4.163	21.493	17.330	15.7
	3	4.101	20.631	15.530	13.1
				lane 3 average	**24.4**
Lane 4 N end	1	4.142	17.405	13.263	135.3
	2	4.122	17.190	13.068	95.1
	3	4.245	17.222	12.977	105.1
Lane 4 middle	1	4.156	16.549	12.393	30.0
	2	4.192	17.081	12.889	27.0
	3	4.161	16.564	12.403	24.9
				lane 4 average	**69.6**
Lane 5 N end	1	4.163	18.612	14.449	25.2
	2	4.237	18.882	14.645	25.9
	3	4.115	19.052	14.937	26.2
Lane 5 middle	1	4.316	18.890	14.574	24.8
	2	4.273	18.496	14.223	24.6
	3	4.246	19.105	14.859	25.2
Lane 5 S end	1	4.257	18.967	14.71	24.5
	2	4.139	18.601	14.462	24.3
	3	4.255	18.742	14.487	29.0
				lane 5 average	**25.5**

(Continued)

Table 6-1 (Concluded)					
Location	**Sample**	**Container Mass (gm)**	**Sample Mass w/Container (gm)**	**Sample Mass (gm)**	**Mass Susceptibility (x $10^{8}m^{3}kg^{-1}$)**
Lane 6 N end	1	4.276	20.793	16.517	1.9
	2	4.291	21.132	16.841	1.3
	3	4.146	20.875	16.729	1.3
Lane 6 middle	1	4.132	20.343	16.211	1.5
	2	4.226	21.028	16.802	2.4
	3	4.126	20.705	16.579	1.9
Lane 6 S end	1	4.189	20.648	16.459	0.5
	2	4.130	20.267	16.137	0.2
	3	4.266	20.220	15.954	1.3
				lane 6 average	**1.4**

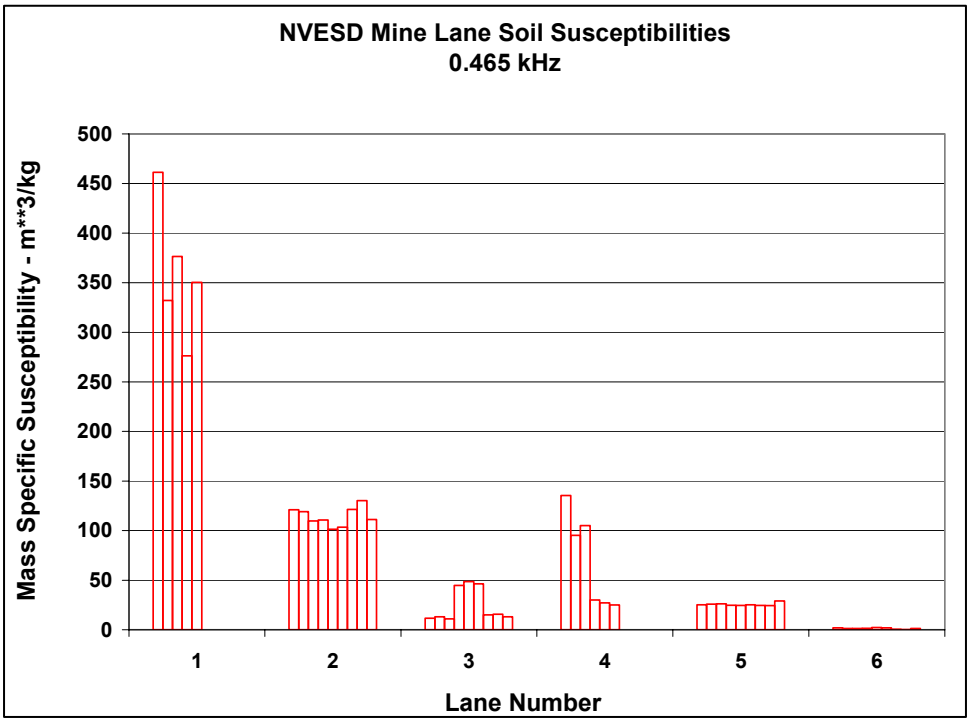

Figure 6-1. NVESD mine lane soil susceptibilities at 0.465 kHz

Table 6-2
Magnetic Susceptibility of NVESD Mine Lane Soil Samples 465 kHz – Air Dried

Location	Sample	Container Mass (gm)	Sample Mass w/Container (gm)	Sample Mass (gm)	Mass Susceptibility (x $10^8 m^3 kg^{-1}$)
Lane 1 N end	1	4.264	23.541	19.277	440.7
	2	4.196	23.767	19.571	317.1
Lane 1 S end	1	4.281	22.433	18.152	409.7
	2	4.200	23.173	18.973	244.9
	3	4.337	23.613	19.276	327.1
				lane 1 average	**347.9**
Lane 2 N end	1	4.173	17.168	12.995	114.5
	2	4.163	16.895	12.732	113.1
	3	4.264	17.352	13.085	104.4
Lane 2 middle	1	4.253	17.992	13.739	105.8
	2	4.118	17.773	13.655	97.8
	3	4.145	17.943	13.798	98.4
Lane 2 S end	1	4.264	18.155	13.891	120.3
	2	4.269	18.381	14.112	129.6
	3	4.218	18.002	13.784	110.1
				lane 2 average	**110.4**
Lane 3 N end	1	4.224	20.177	15.953	11.3
	2	4.179	20.692	16.513	12.8
	3	4.160	21.069	16.909	11.2
Lane 3 middle	1	4.278	20.642	16.364	44.1
	2	4.230	20.321	16.091	48.4
	3	4.191	20.613	16.422	46.0
Lane 3 S end	1	4.240	20.704	16.464	14.8
	2	4.163	21.493	17.330	15.7
	3	4.101	20.631	15.530	12.4
				lane 3 average	**24.1**
Lane 4 N end	1	4.142	17.405	13.263	134.5
	2	4.122	17.190	13.068	93.5
	3	4.245	17.222	12.977	103.7
Lane 4 middle	1	4.156	16.549	12.393	29.8
	2	4.192	17.081	12.889	26.5
	3	4.161	16.564	12.403	24.0
				lane 4 average	**68.7**
Lane 5 N end	1	4.163	18.612	14.449	25.6
	2	4.237	18.882	14.645	24.9
	3	4.115	19.052	14.937	24.8
Lane 5 middle	1	4.316	18.89	14.574	24.8
	2	4.273	18.496	14.223	24.1
	3	4.246	19.105	14.859	25.1
Lane 5 S end	1	4.257	18.967	14.710	23.7
	2	4.139	18.601	14.462	23.2
	3	4.255	18.742	14.487	29.6
				lane 5 average	**25.1**

(Continued)

Table 6-2 (Concluded)					
Location	**Sample**	**Container Mass (gm)**	**Sample Mass w/Container (gm)**	**Sample Mass (gm)**	**Mass Susceptibility (x $10^{8}m^{3}kg^{-1}$)**
Lane 6 N end	1	4.276	20.793	16.517	1.6
	2	4.291	21.132	16.841	1.4
	3	4.146	20.875	16.729	0.5
Lane 6 middle	1	4.132	20.343	16.211	0.7
	2	4.226	21.028	16.802	2.3
	3	4.126	20.705	16.579	2.2
Lane 6 S end	1	4.189	20.648	16.459	0.4
	2	4.130	20.267	16.137	0.3
	3	4.266	20.220	15.954	1.4
				lane 6 average	1.2

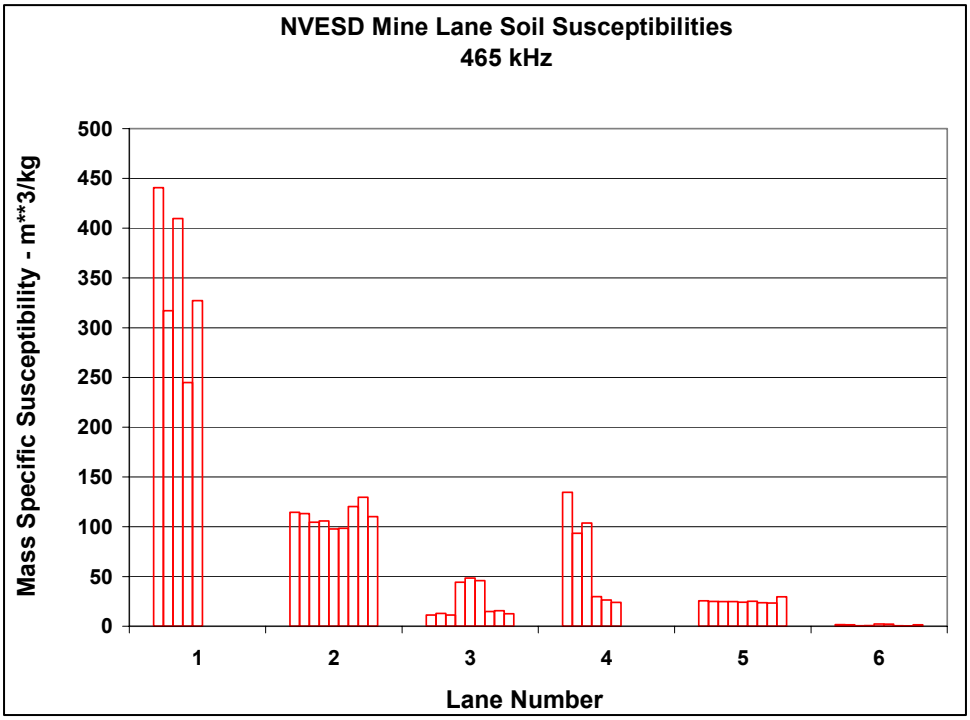

Figure 6-2. NVESD mine lane soil susceptibilities at 465 kHz

7 Visual Reflectance Data

Instrument Description and Operation

Visual reflectance data for the NVESD soil samples were obtained using a Jobin Yvon HR640 Scanning Monochromator. The optical mount is a Czerny-Turner design, meaning that it consists of a plane grating illuminated by collimated light. The light source for these measurements was a 300W halogen bulb. Reflected light was collected by an optical fiber pointing at approximately 45 deg from the normal to each sample surface. This energy was fed to the collimator mirror. Rotation of the grating generated data for different wavelengths.

Sample Preparation and Data Acquisition

Soil samples were prepared by spooning soil into aluminum covers of soil drying cans and then crushing the sample and smoothing its surface with a metal straight edge. The moisture content of the samples was unknown; however, all of the soils were visibly dry, and measurements were conducted in an air-conditioned laboratory.

Experience showed that the illumination source became slightly hotter with time. Therefore, a measurement of the source spectrum was made once prior to soil data collection, once at the halfway point in measurements, and one final time at the completion of the measurements. The source spectra were measured from energy reflected off a 100 percent reflectance standard. Figure 7-1 shows the final result of the source measurements, in which all three spectra were averaged and then smoothed with a five-point averaging filter. The maximum spread of the source data was no more than about a 1,000 counts at the peak intensity.

The room in which measurements were conducted was a windowless facility. Data were collected with all lights out in the room to yield instrument noise which would be used in data processing. These “dark current” data were remarkably flat across the spectrum at a level of about 380 counts.

Discussion of Results

Figures 7-2 through 7-17 contain the spectra collected on each of the soil samples collected from the NVESD mine lanes. Each chart shows two data

curves. One represents the simple ratio of the measured reflectance counts to the averaged source reflectance counts and is labeled “w/o dark current correction.” The other curve is labeled “dark current corrected” and represents the ratio of the soil reflectance less the “dark current” counts to the source reflectance less the “dark current.” The uncorrected data are shown to demonstrate the impact of not accounting for system noise.

Visual reflectance measurement results are consistent with human observation of the color of each mine lane soil. Referring to the photo in Figure 1-1, lane 1 is almost black in color, and the data show less than 10-percent reflectance across the entire spectrum. Soils from lanes 2 and 3 are the lightest color of the normal silty soils and have reflectances that peak at about 40 percent. Lanes 4 and 5 contain darker normal soils with maximum reflectances on the order of 30 percent. Finally, the soil in lane 6 is a pure white beach sand, which shows a very high peak reflectance on the order of 55 percent.

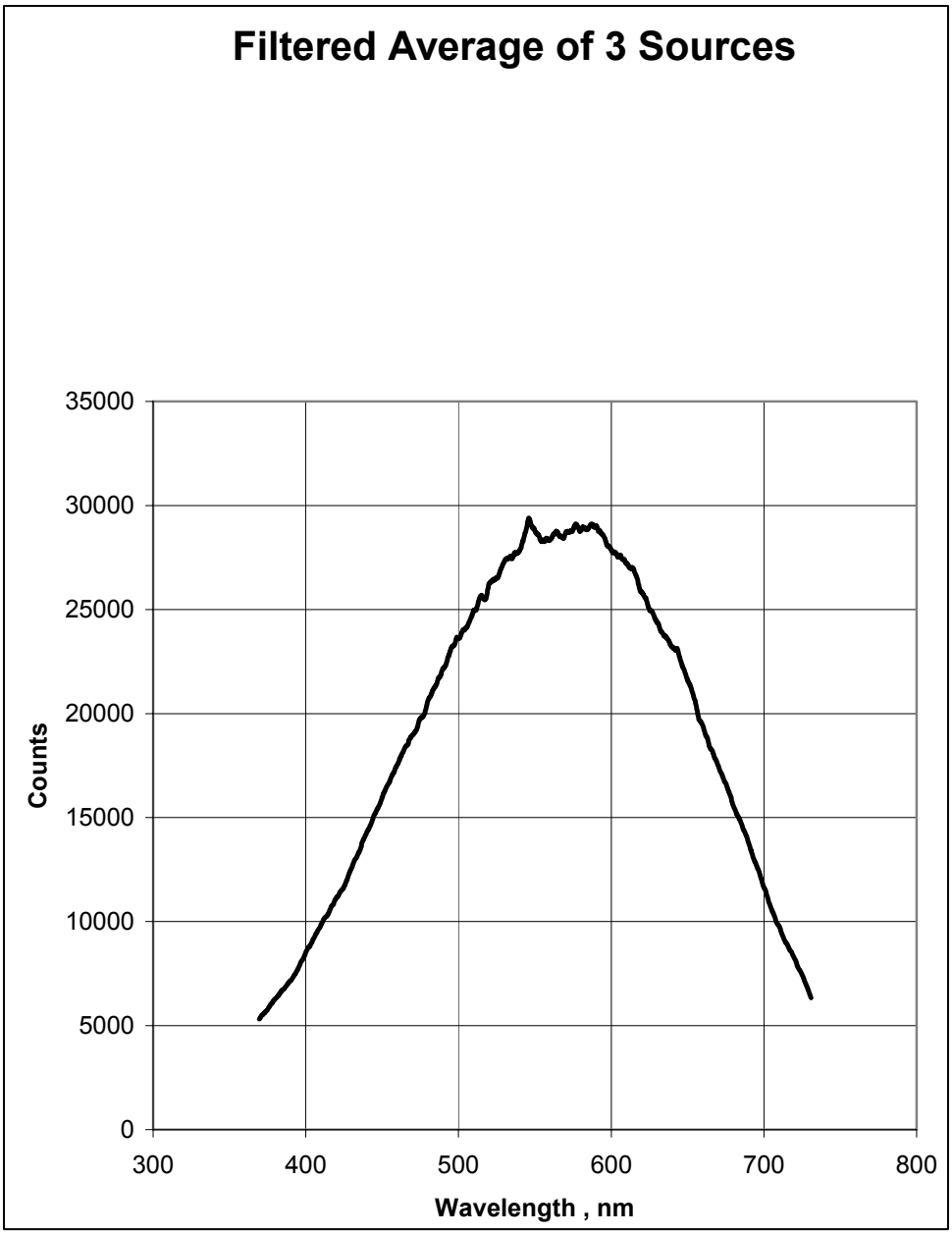

Figure 7-1. Visual reflectance light source spectrum

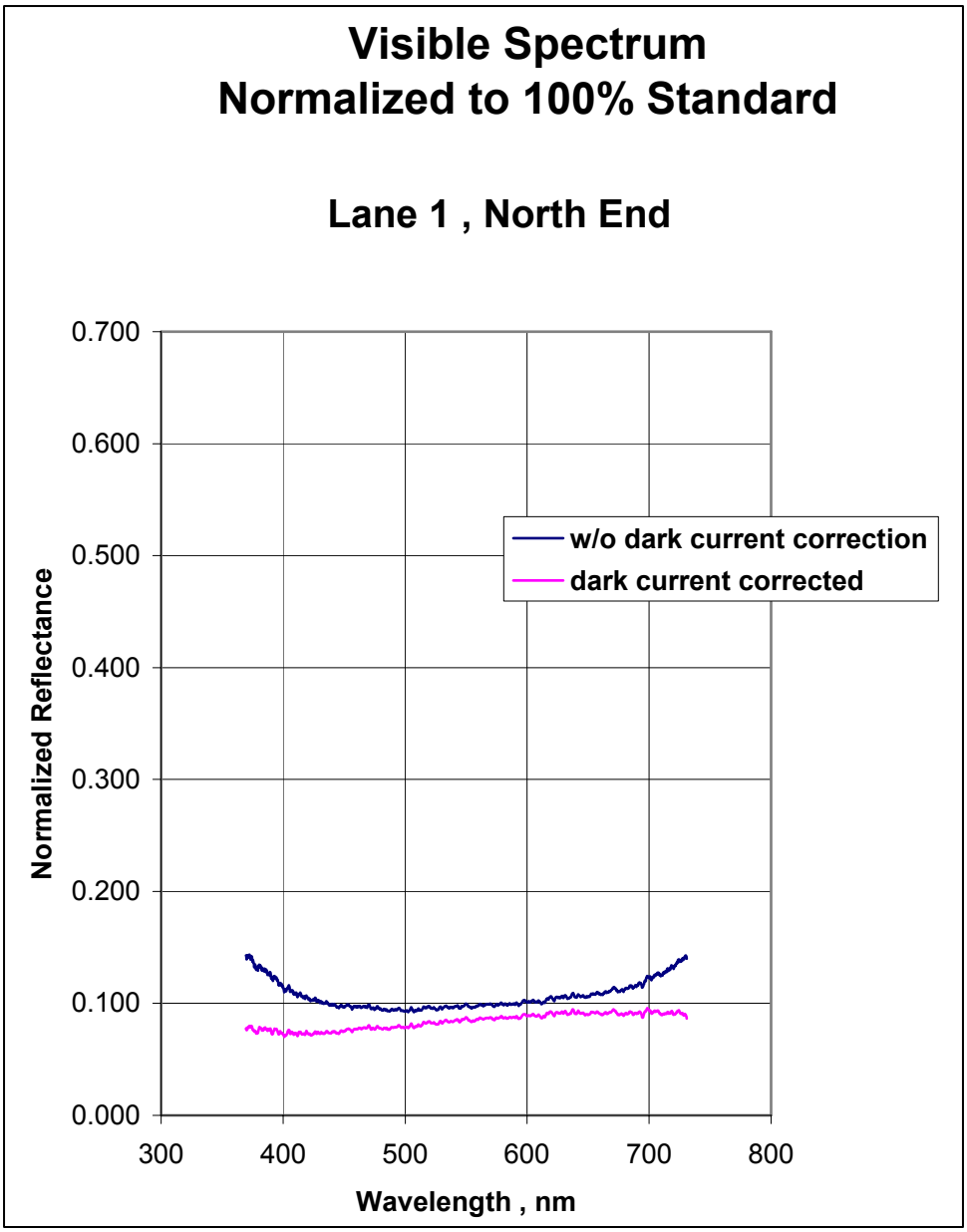

Figure 7-2. Visual reflectance spectrum of lane 1, North soil

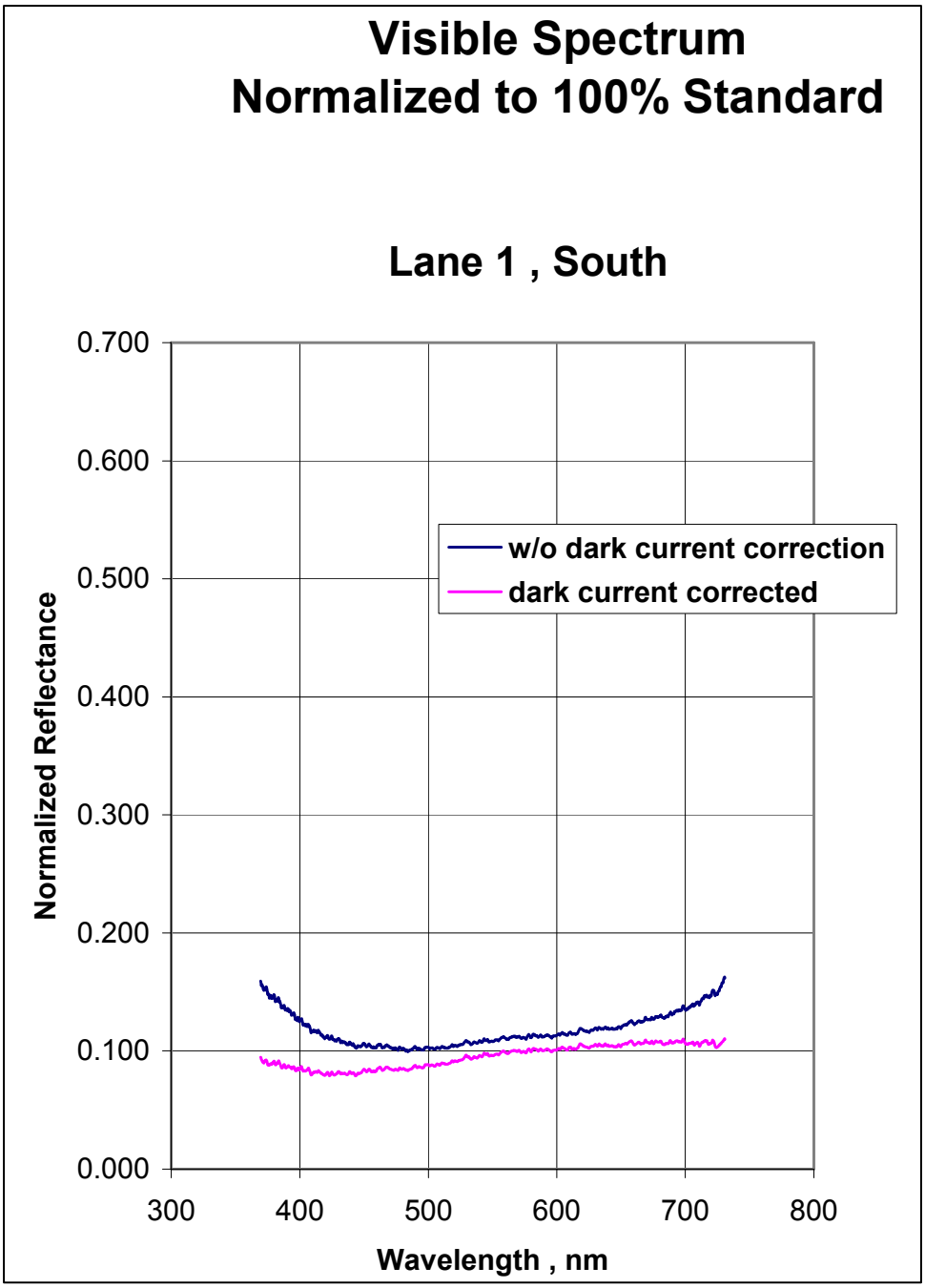

Figure 7-3. Visual reflectance spectrum of lane 1, South soil

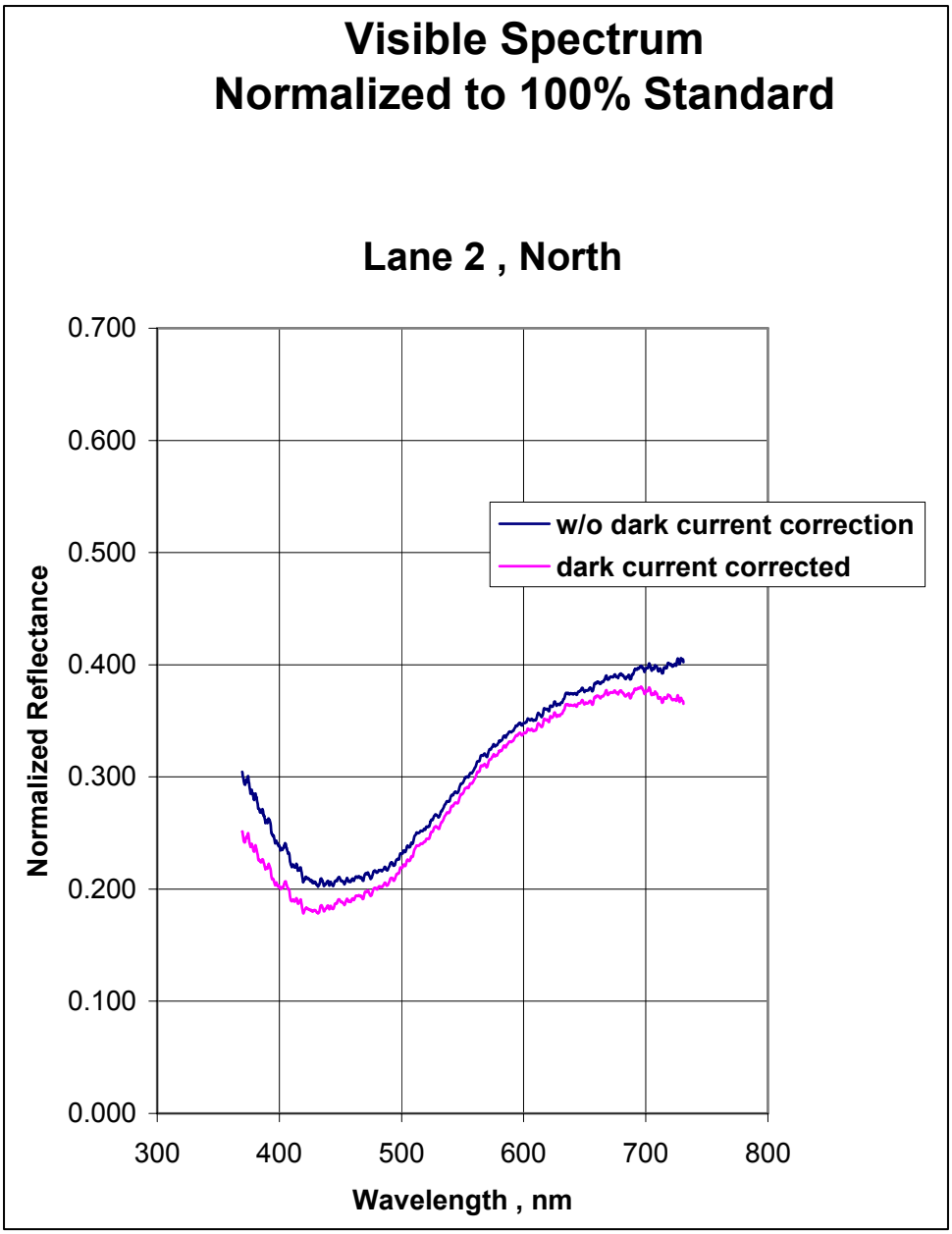

Figure 7-4. Visual reflectance spectrum of lane 2, North soil

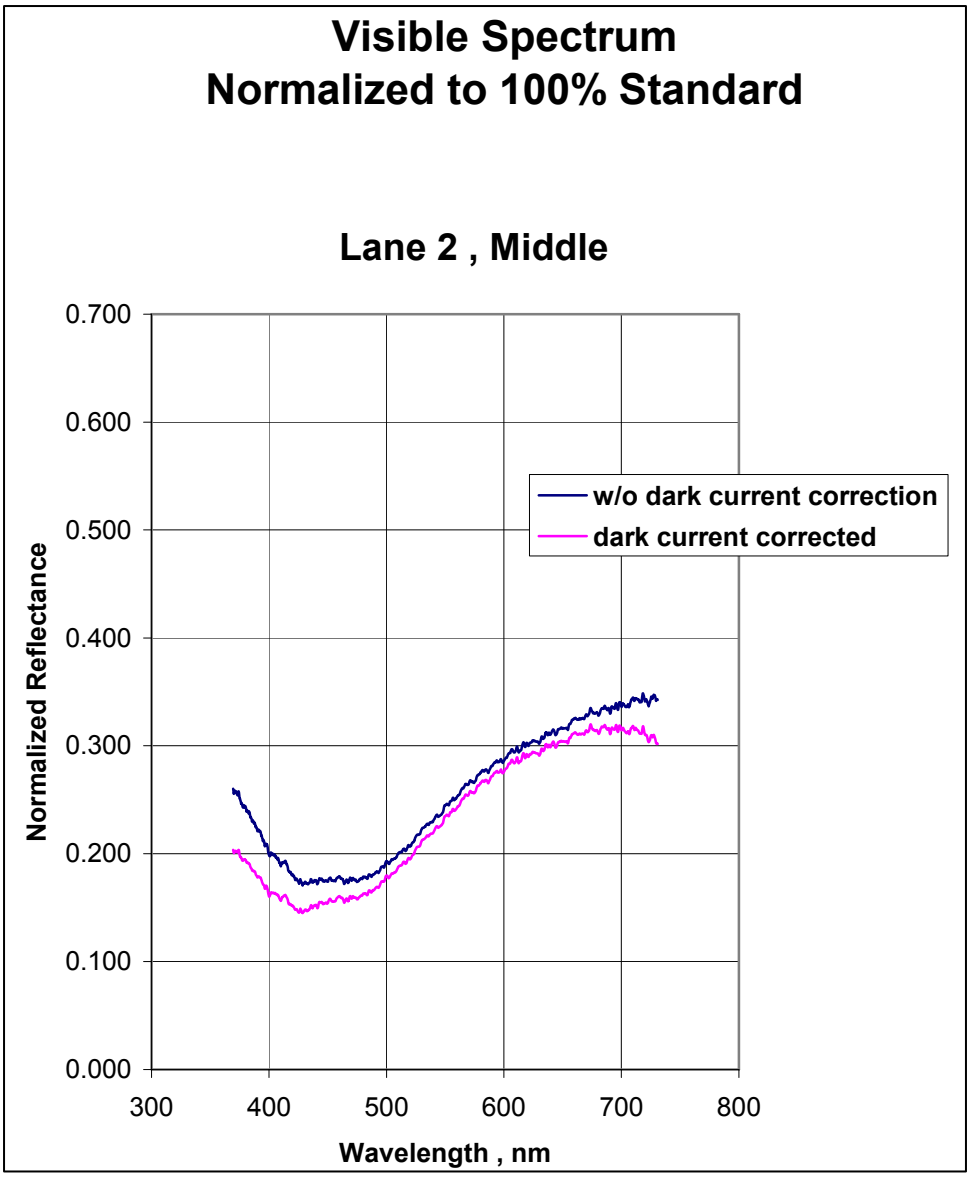

Figure 7-5. Visual reflectance spectrum of lane 2, Middle soil

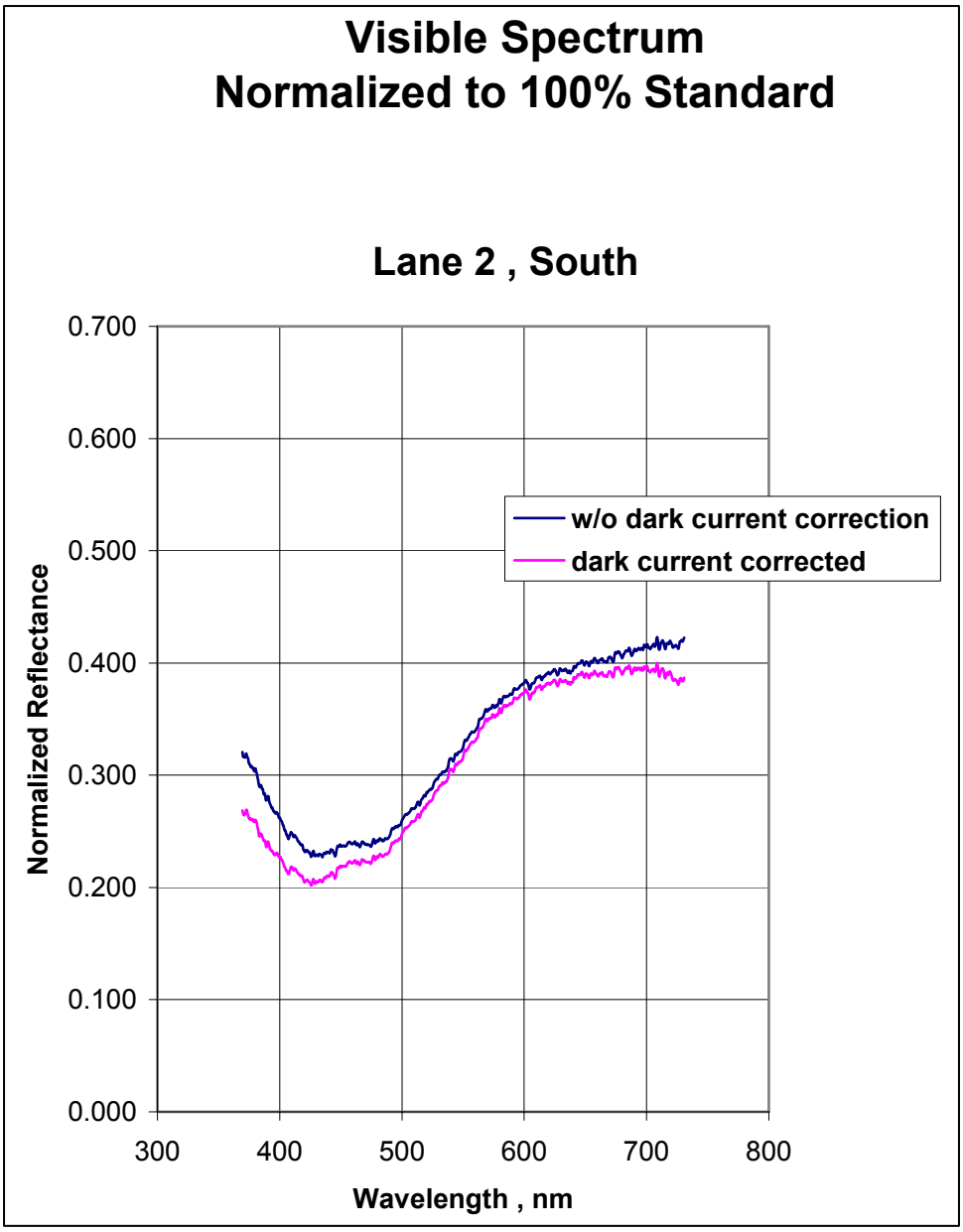

Figure 7-6. Visual reflectance spectrum of lane 2, South soil

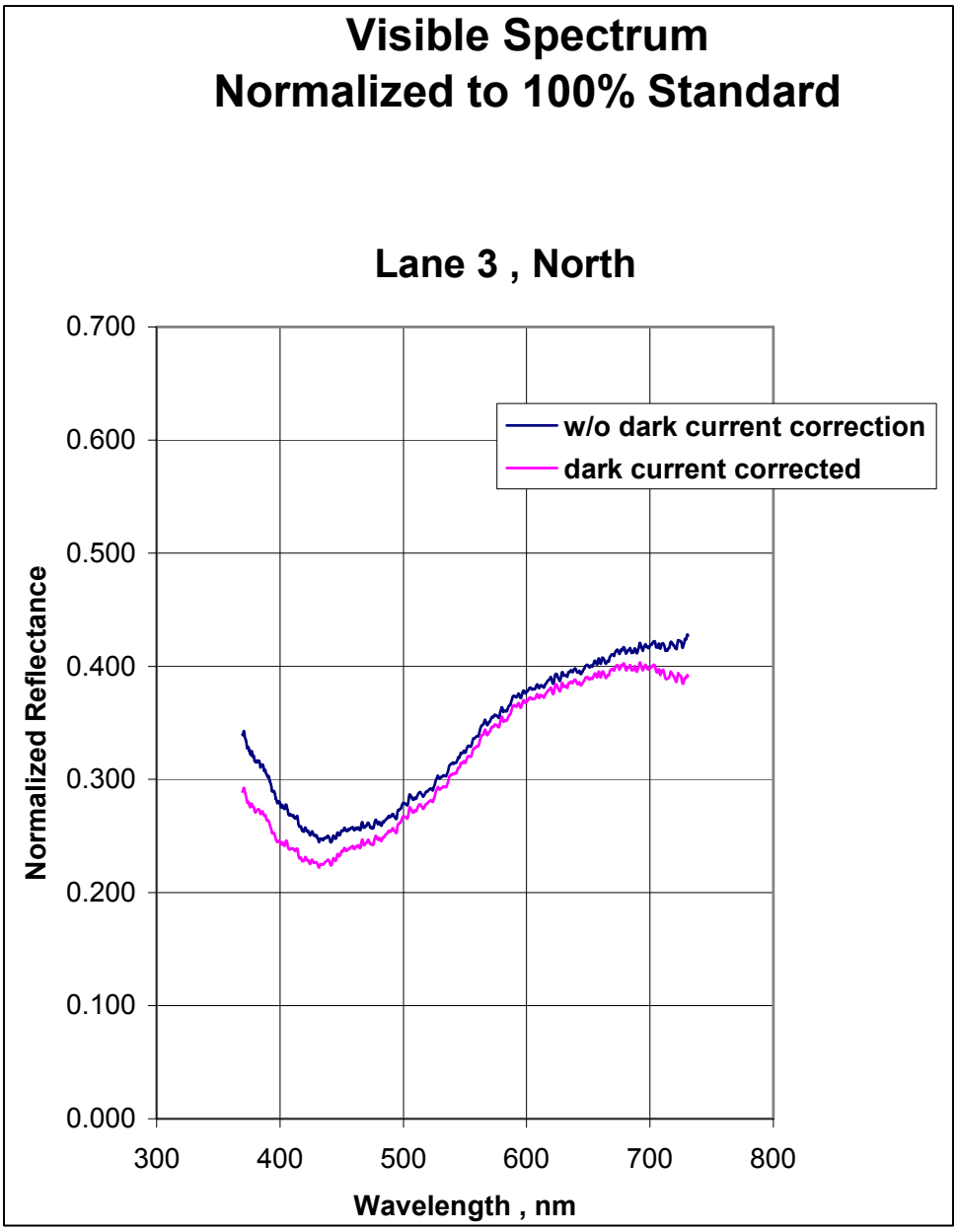

Figure 7-7. Visual reflectance spectrum of lane 3, North soil

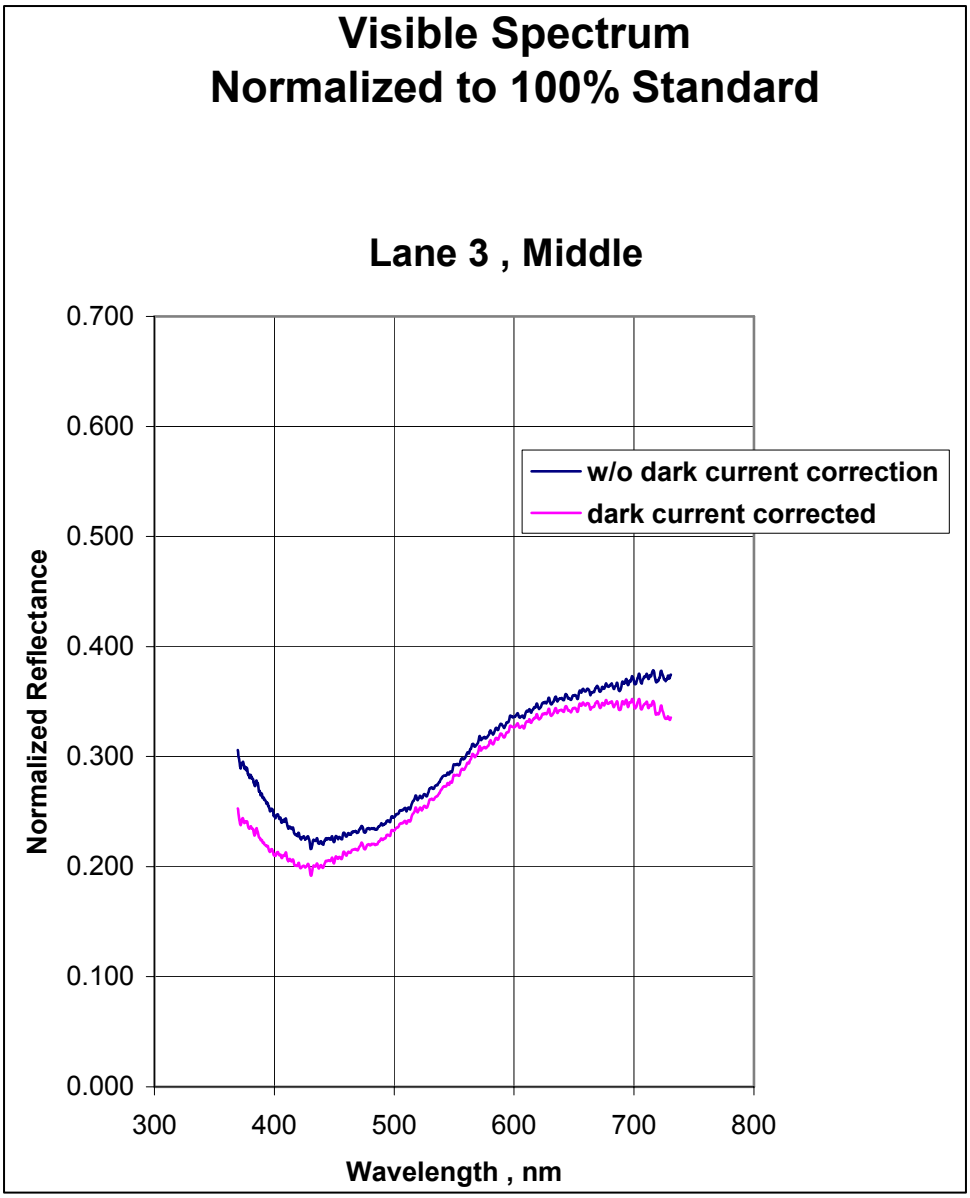

Figure 7-8. Visual reflectance spectrum of lane 3, Middle soil

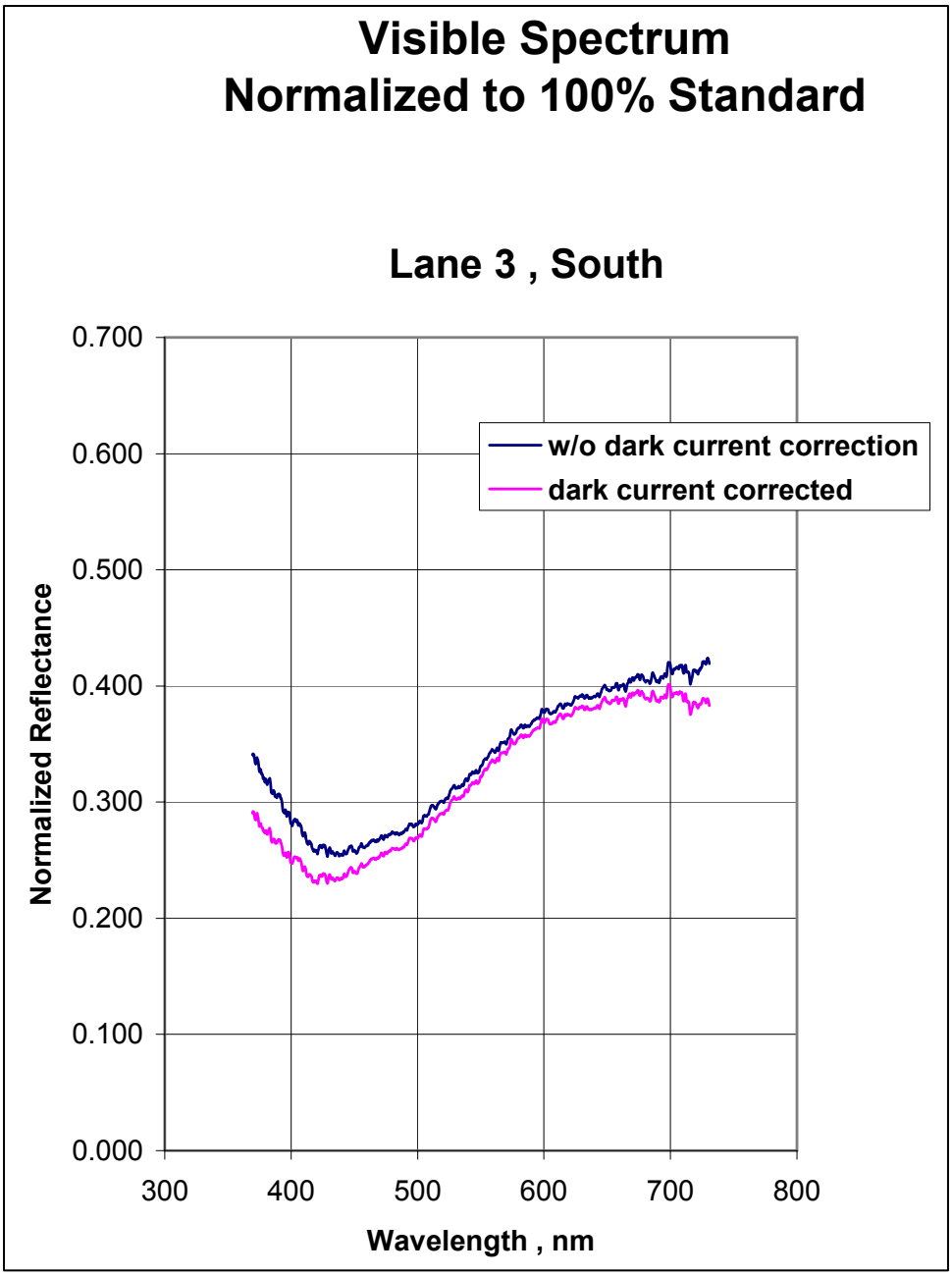

Figure 7-9. Visual reflectance spectrum of lane 3, South soil

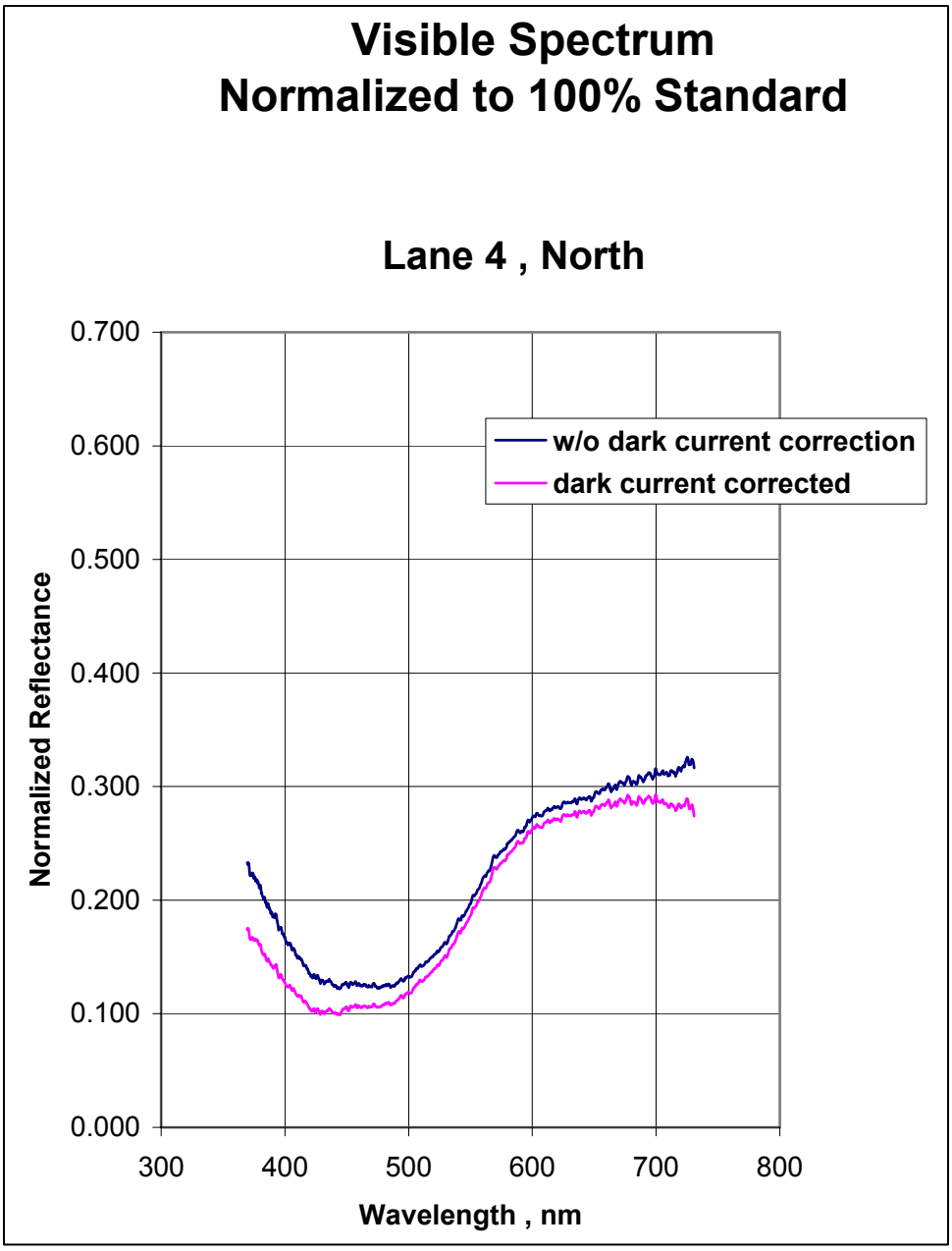

Figure 7-10. Visual reflectance spectrum of lane 4, North soil

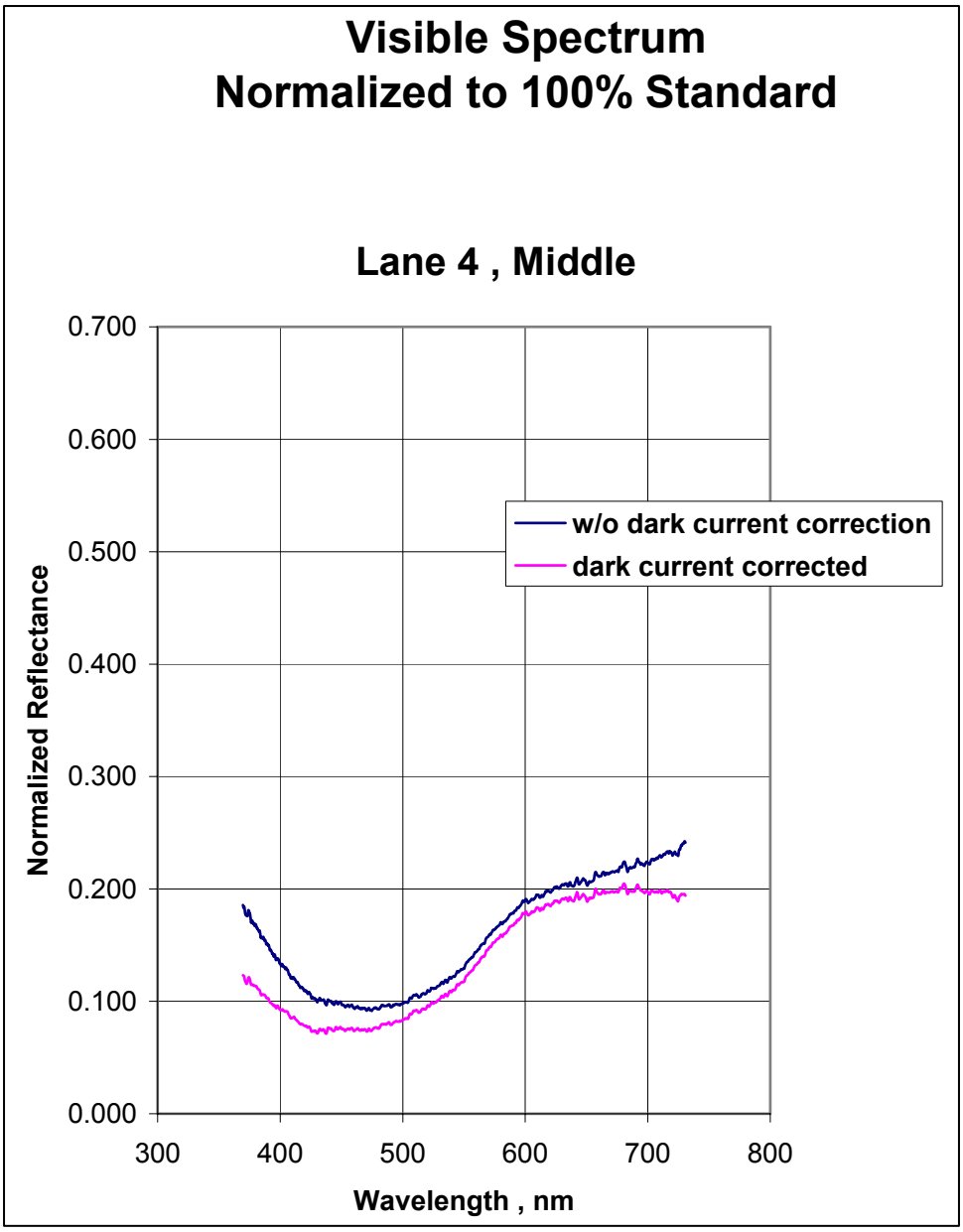

Figure 7-11. Visual reflectance spectrum of lane 4, Middle soil

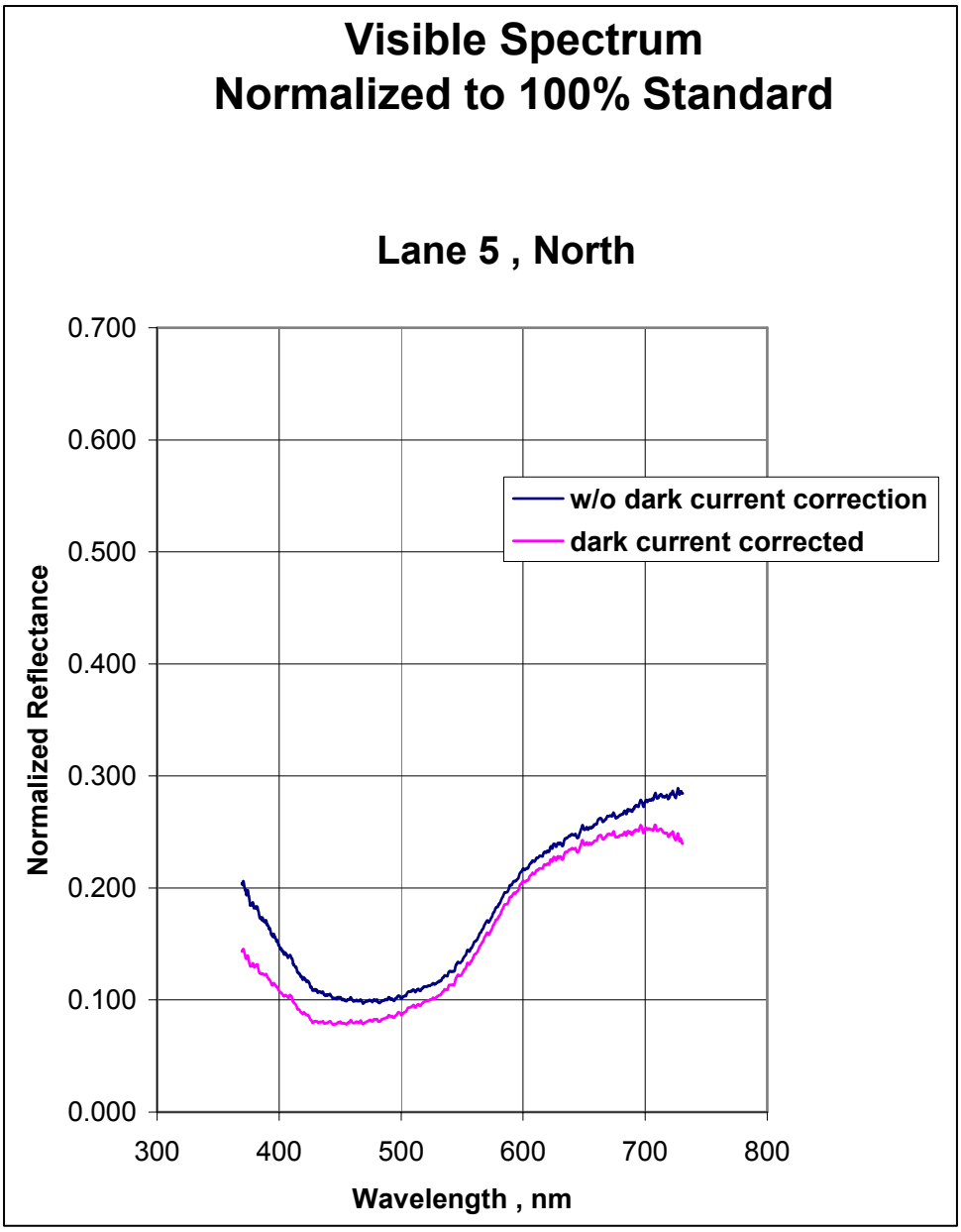

Figure 7-12. Visual reflectance spectrum of lane 5, North soil

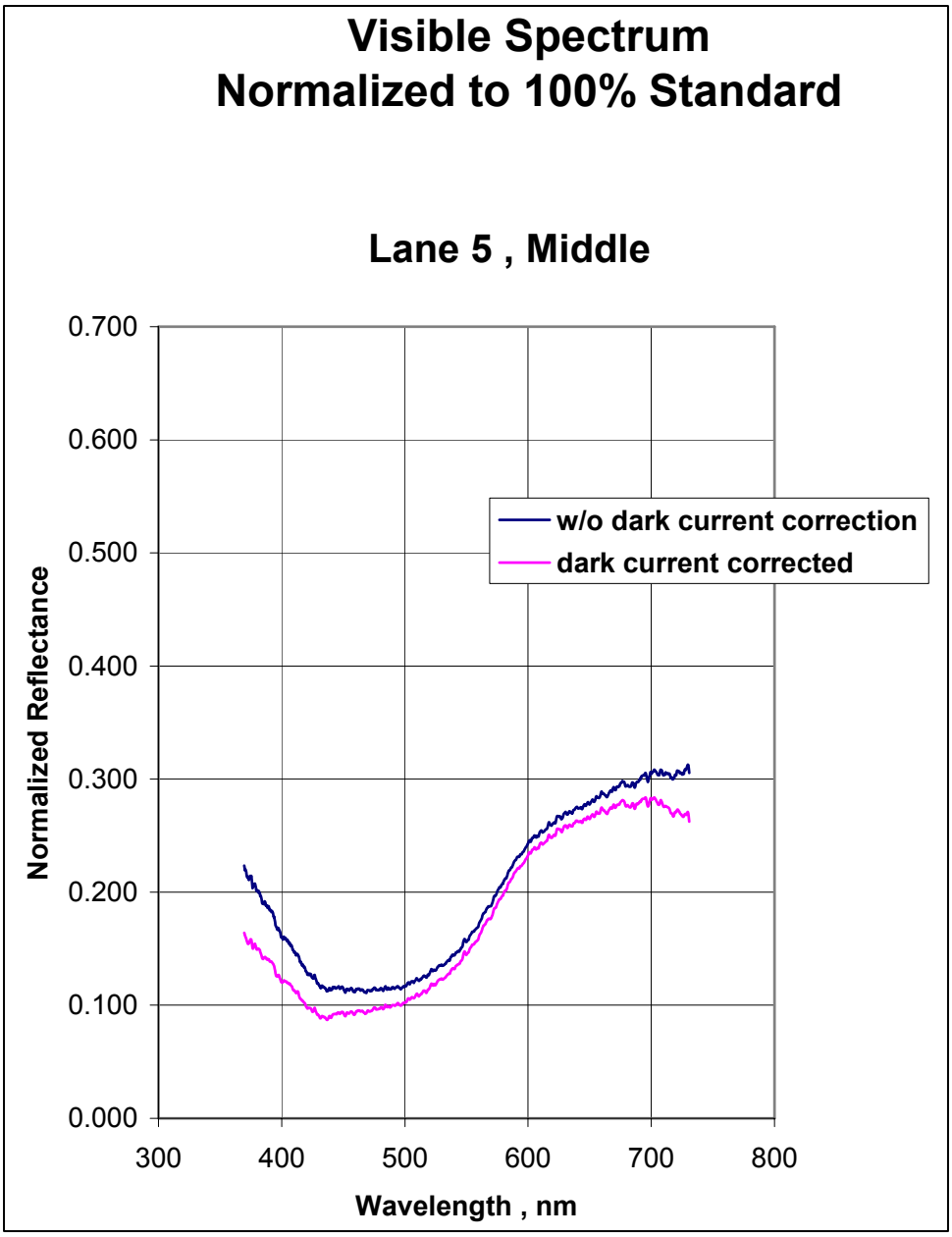

Figure 7-13. Visual reflectance spectrum of lane 5, Middle soil

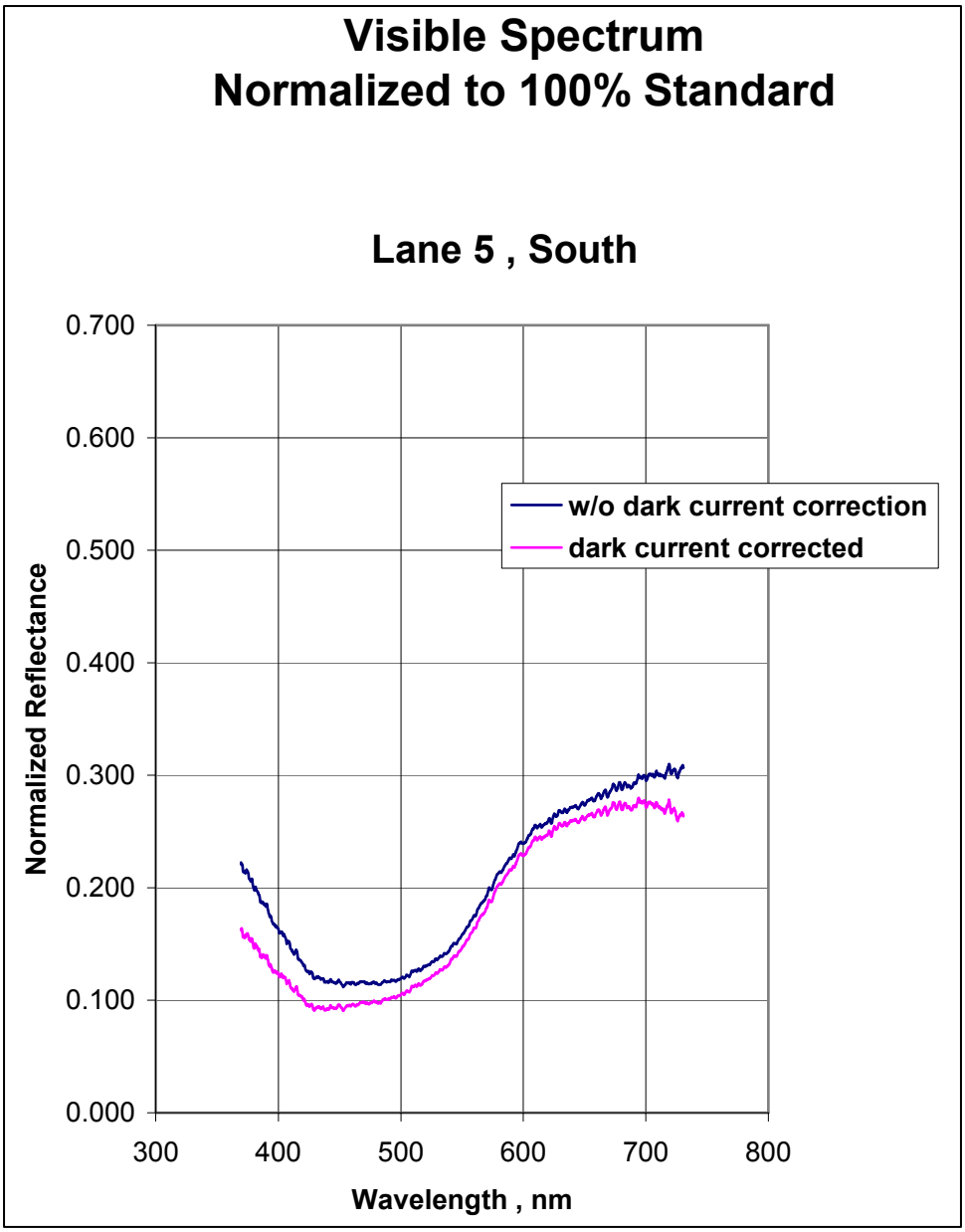

Figure 7-14. Visual reflectance spectrum of lane 5, South soil

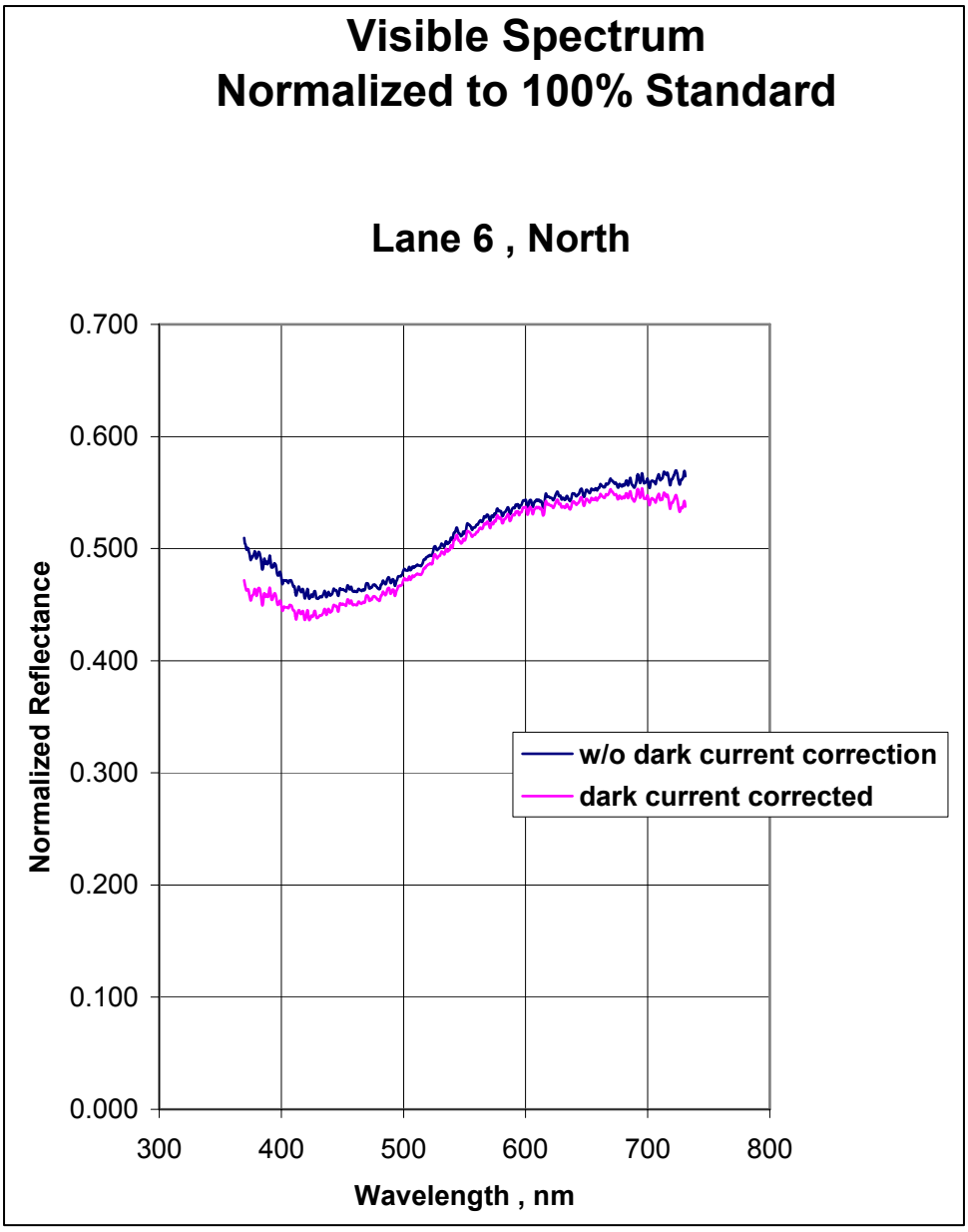

Figure 7-15. Visual reflectance spectrum of lane 6, North soil

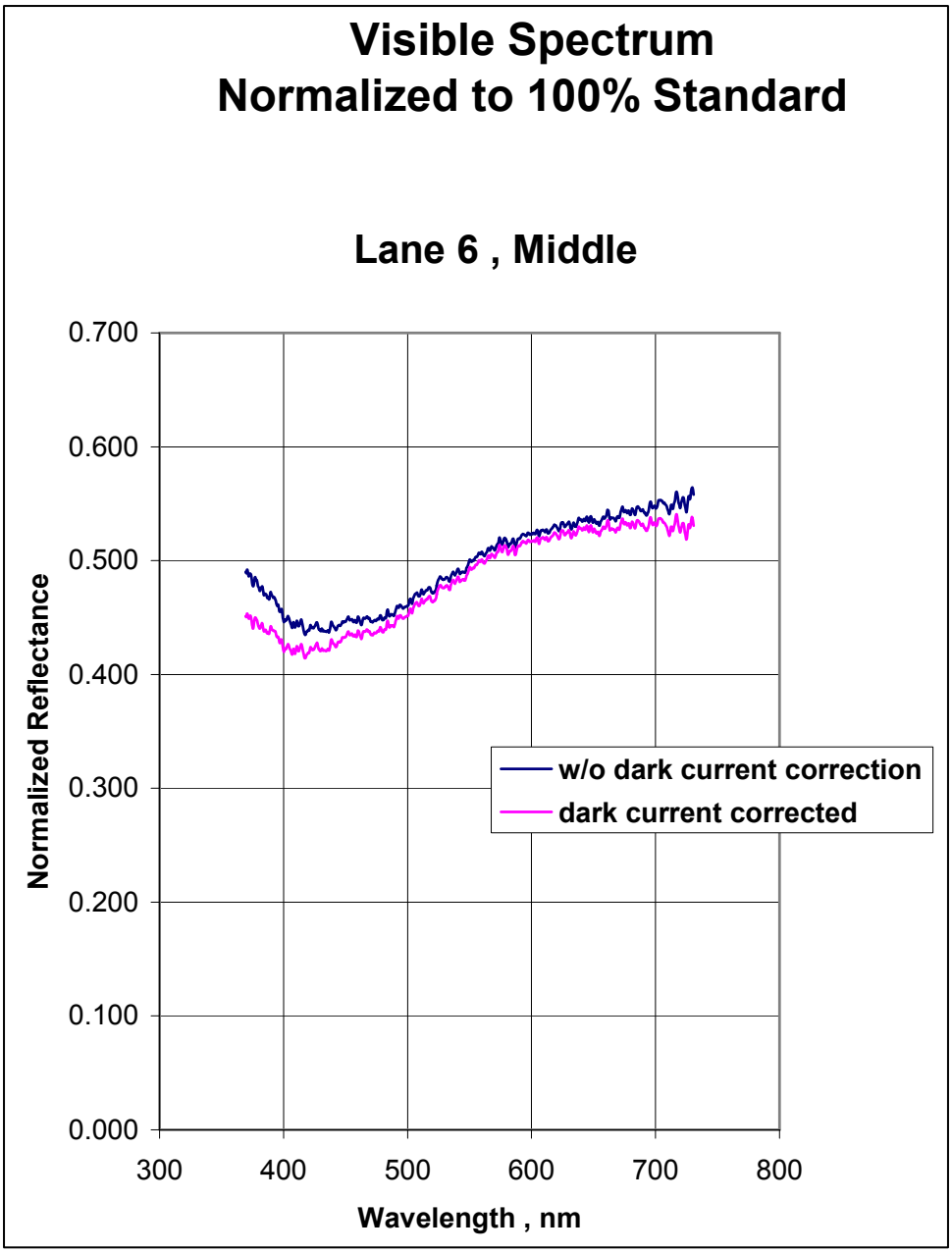

Figure 7-16. Visual reflectance spectrum of lane 6, Middle soil

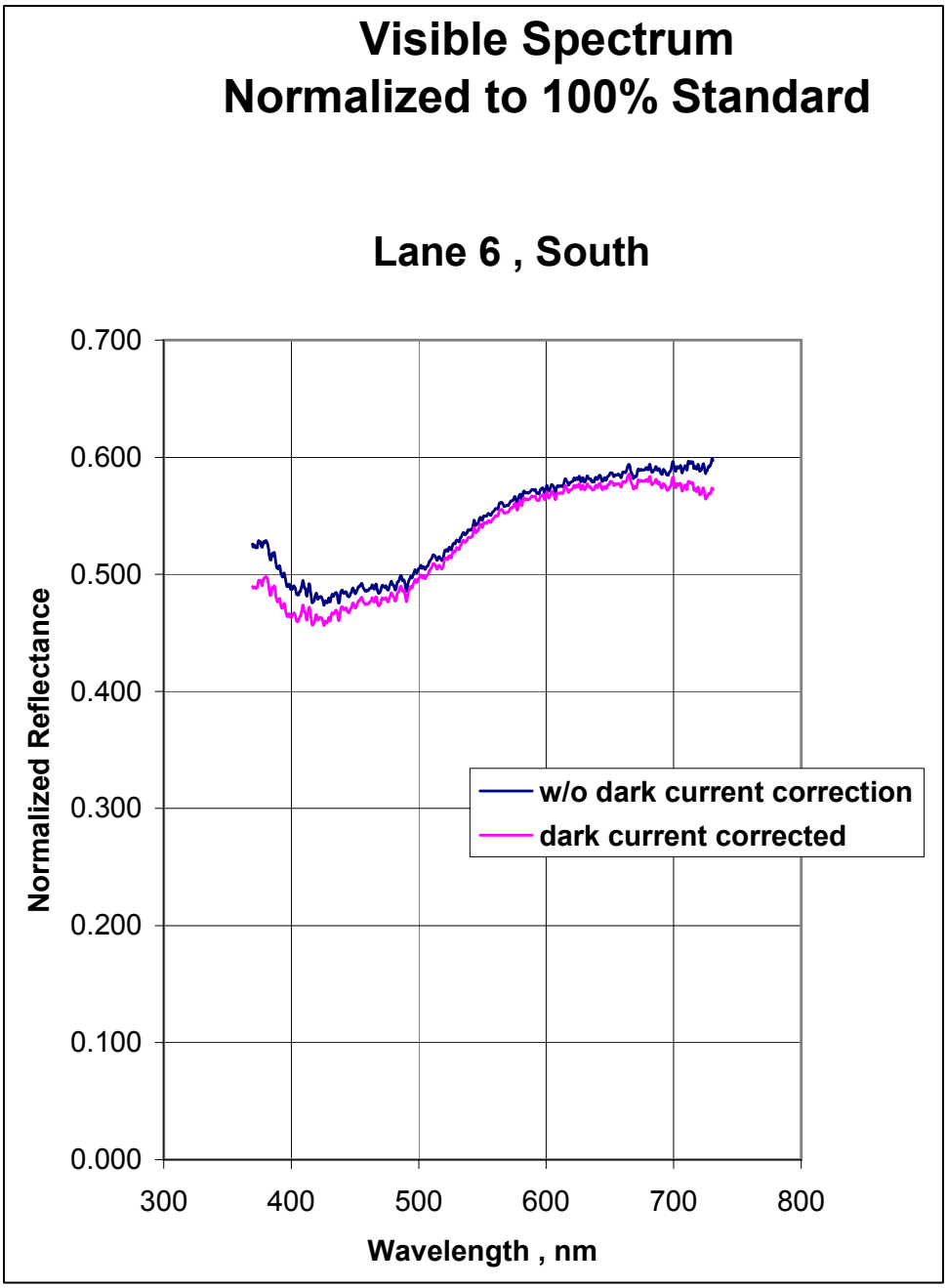

Figure 7-17. Visual reflectance spectrum of lane 6, South soil

8 Broadband IR Reflectance Data

Instrument Description and Operation

Broadband infrared reflectance data for the NVESD soil samples were obtained using a Nicolet Magna 750 Fourier Transform Infrared (FTIR) Spectrometer with a deuterated triglycine sulfate (DTGS) detector. Samples were illuminated and scattered energy collected by a "praying mantis" diffuse reflectance accessory. Dried air is circulated through the spectrometer to eliminate water absorption lines.

Data were collected at a spectral resolution of about 4 cm^{-1} over a range of values from 413 to 4,000 cm^{-1} (or 24 to 2.5 μm). Signal-to-noise was reduced by averaging 64 scans to produce each sample's interferogram.

Sample Preparation and Data Acquisition

Measurement samples were prepared by grinding air-dried soil in a granite mortar until the soil had a talc-like consistency. Grinding stopped when test samples resulted in a relatively clean spectrum. Sand crystals could not be crushed effectively; however, the resulting spectra were still relatively clean. The sample holder for the diffuse reflectance accessory was a hollow cylinder about 2 cm in diameter and about 3 mm in depth.

A reference spectrum for normalization purposes was collected by measuring the energy source reflected off two polished mirrors. The second polished mirror is necessary because the collection mirror of the praying mantis device does not "see" the specular reflection off a smooth sample.

Discussion of Results

Figures 8-1 through 8-6 contain normalized reflectance data for lanes 1 through 6, respectively, plotted as a function of wavelength. Note, however, that these results are not total reflectance data, as an integrating sphere reflectance accessory was not available for these measurements. Therefore, they cannot be used to calculate material emissivities.

When available, a single sample from the north end, the middle, and the south end of each lane was analyzed; hence, the “N”, “M”, and “S” designation on the key for each figure. The relative magnitudes of each curve are different for any number of reasons, the most likely being that no attempt was made to ensure that each sample had the same distribution of particle sizes. The optical properties of powdered samples are often affected by particle size (Salisbury et al. 1987), as well as packing effort.

Interpretation of these data is left to the reader, with the exception of noting the pronounced *reststrahlen* effect in the quartz-laden soils of lanes 1 and 6. *Reststrahlen* (German for “residual radiation”) is most correctly defined as the selective absorption and reradiation in an otherwise transparent material (The New Encyclopedia Britannica 1987). However, as it is used, today, it seems to have evolved into a term that identifies decreases in emissivity (increases in reflectivity) while still retaining the selective absorption idea. In quartz the absorption is attributed to a resonance in the Si-O bonds at about 8.5 μm. Hence, one sees a region of increased reflectance between 8 and 10 μm on Figures 8-1 and 8-6, with a sharp drop because of Si-O resonance at about 8.5 μm. This region is often referred to as a reflectance doublet. On a plot of emissivity, the same feature is called an emissivity doublet, or an emissivity trough.

As for the interpretation of other features in the diffuse reflectance spectra, one should refer to other references for explanations and additional data (Salisbury et al. 1991; The Aster Spectral Library 1999).

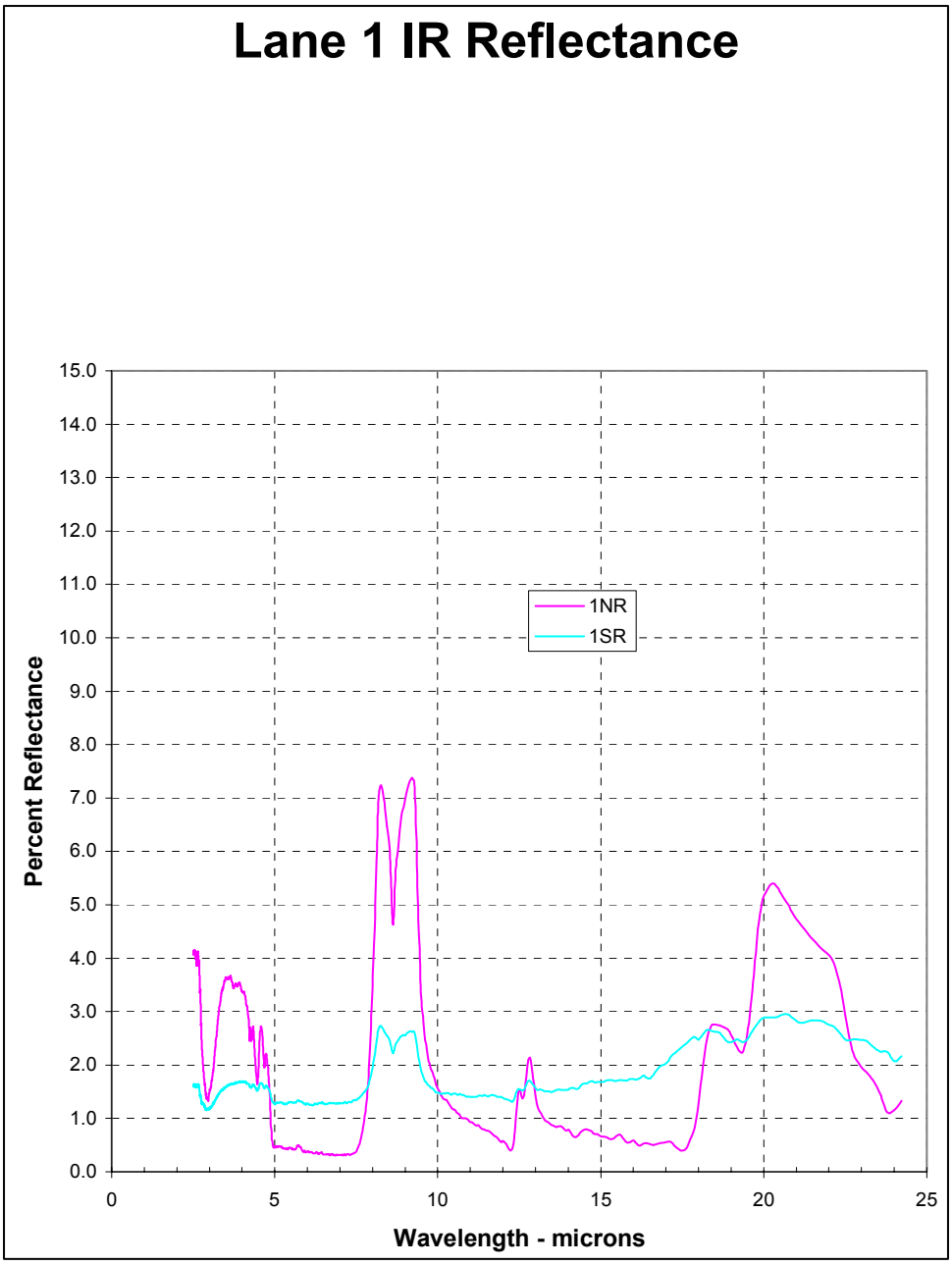

Figure 8-1. Broadband infrared reflectance, lane 1

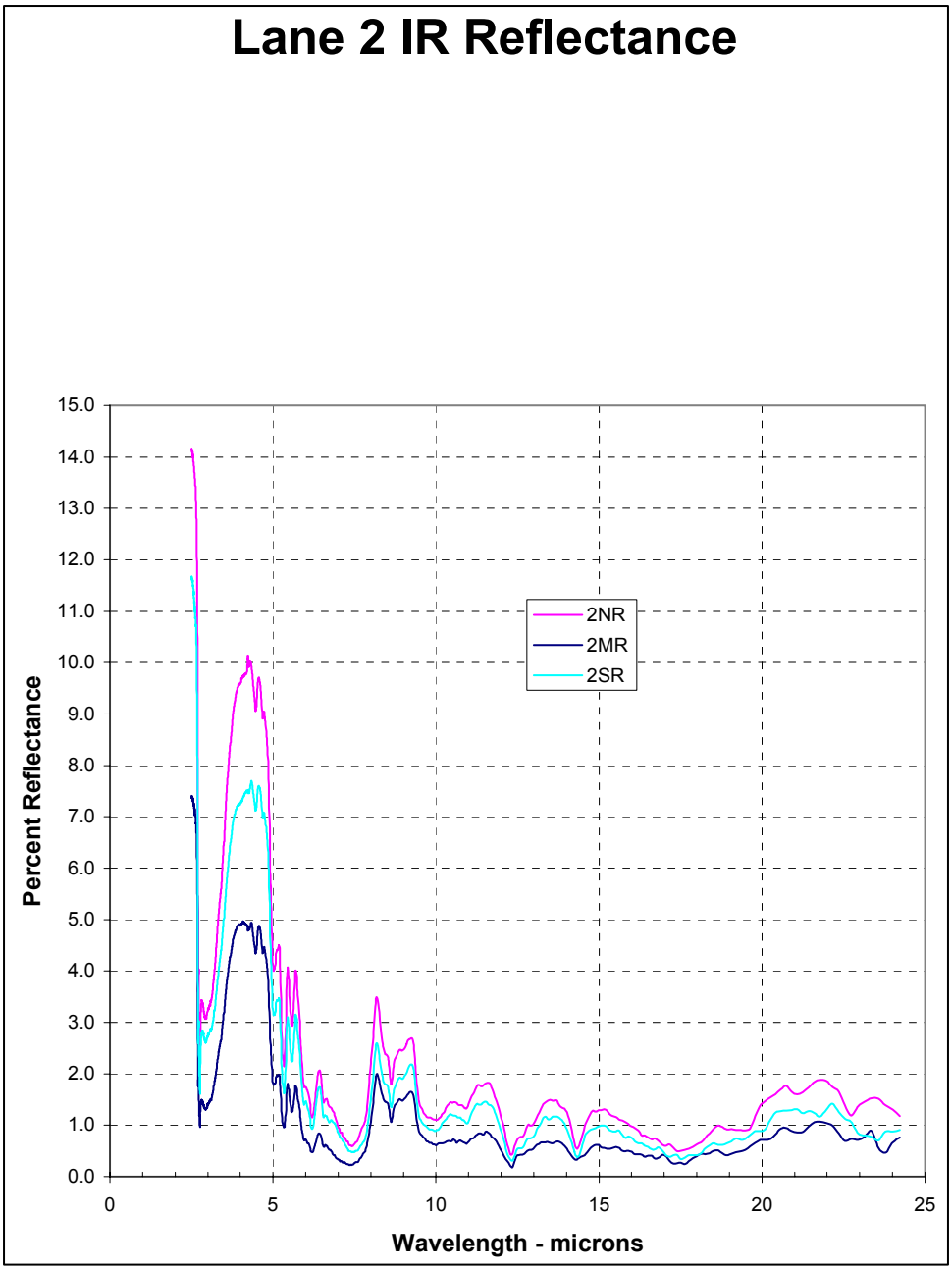

Figure 8-2. Broadband infrared reflectance, lane 2

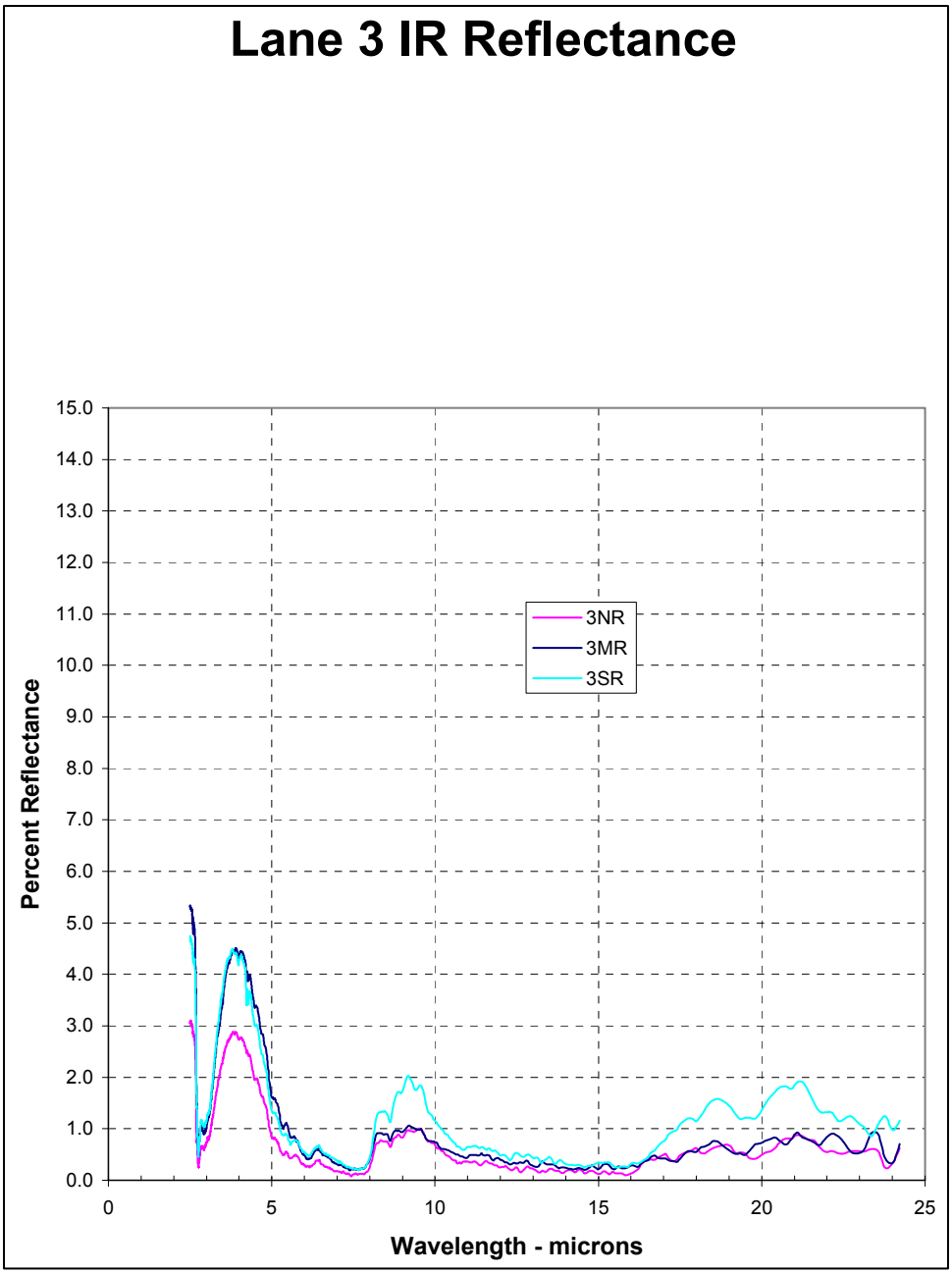

Figure 8-3. Broadband infrared reflectance, lane 3

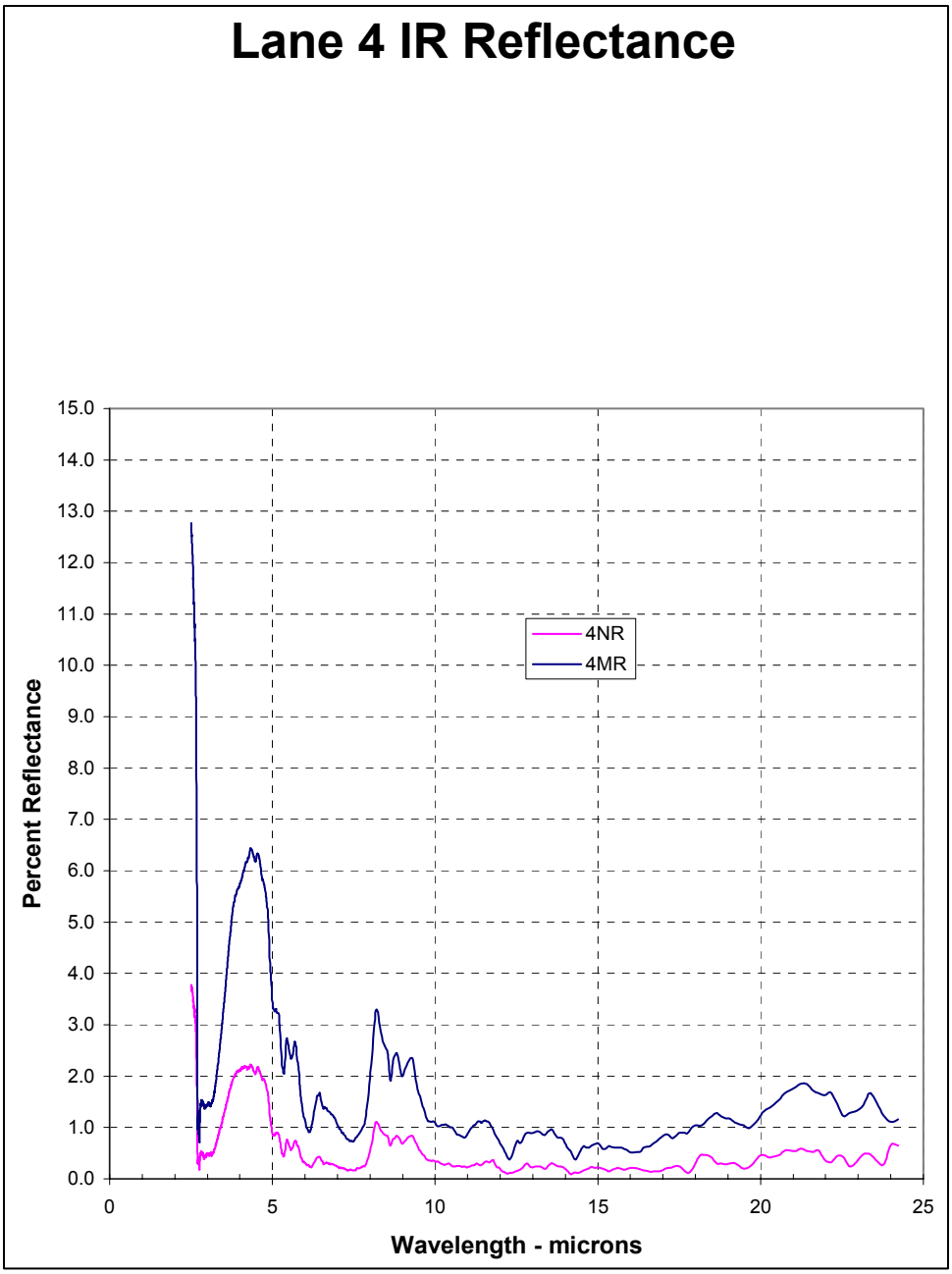

Figure 8-4. Broadband infrared reflectance, lane 4

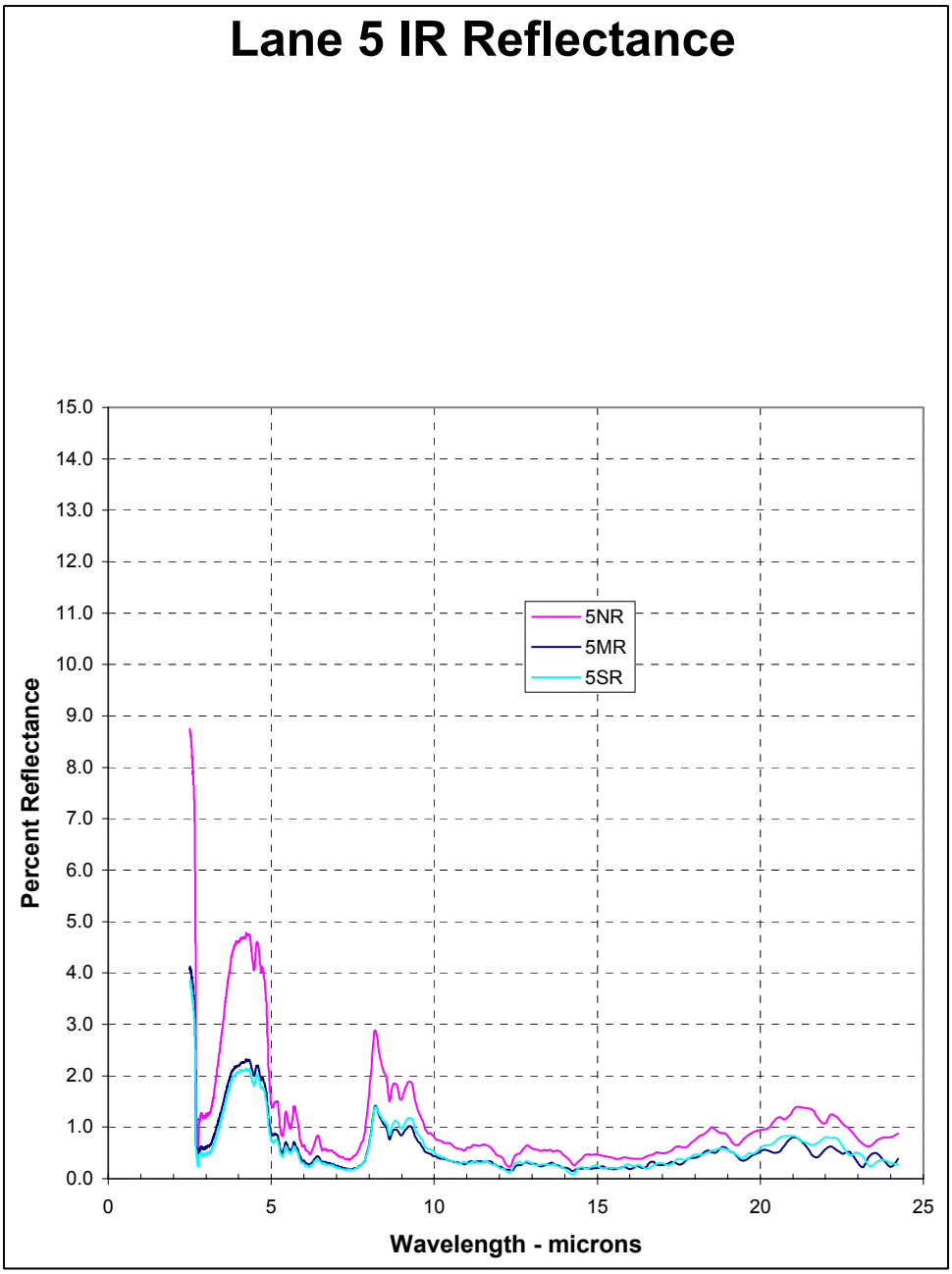

Figure 8-5. Broadband infrared reflectance, lane 5

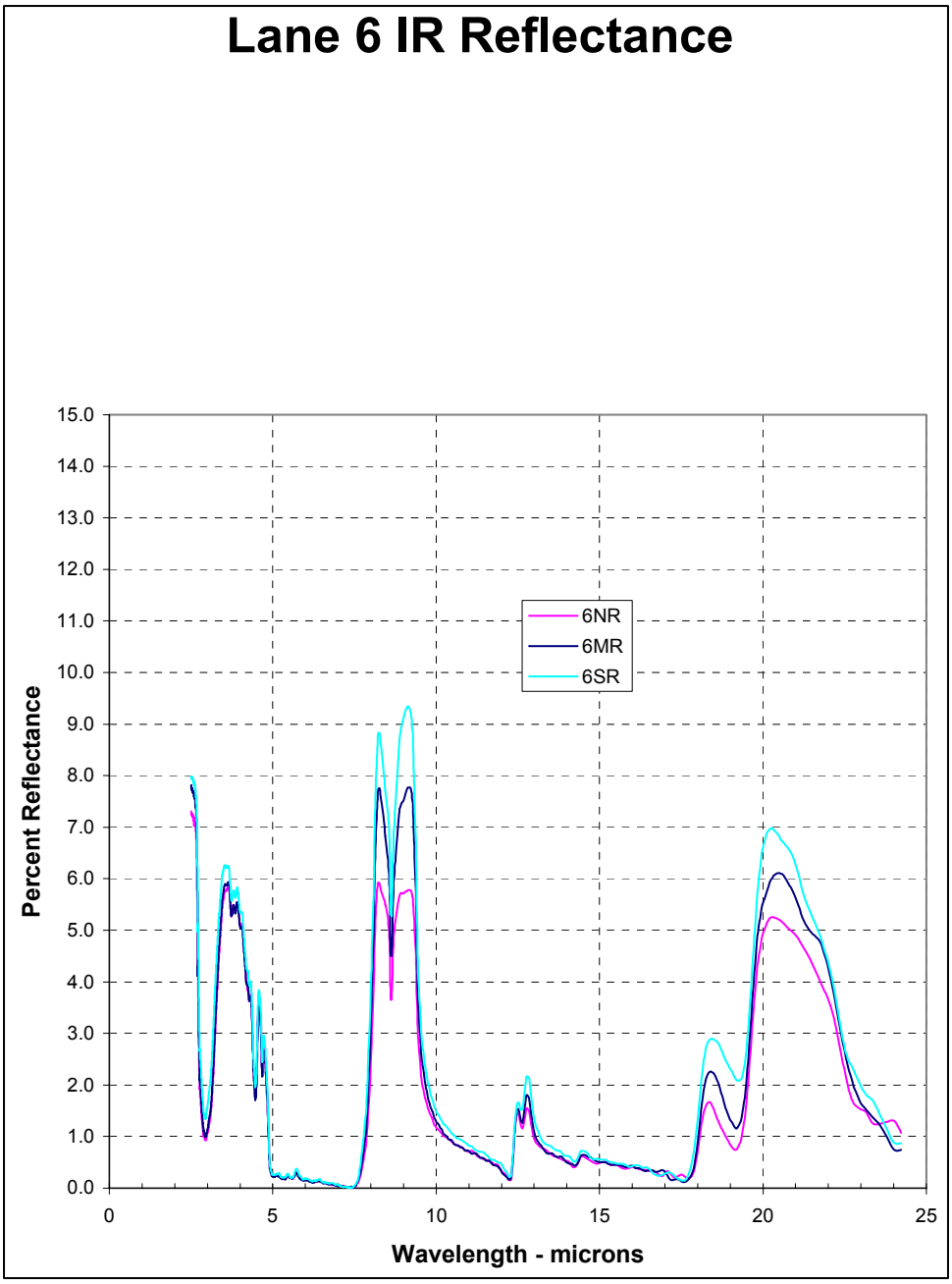

Figure 8-6. Broadband infrared reflectance, lane 6

References

Burger, H. Robert. (1972). *Exploration geophysics of the shallow subsurface.* Prentice Hall, Englewood Cliffs, NJ.

Curtis, John O. (2001a). "A Durable laboratory apparatus for the measurement of soil dielectric properties," *IEEE Transactions on Instrumentation and Measurement,* 50 (5), 1364-1369.

Curtis, John O. (2001b). "Moisture effects on the dielectric properties of soils," *IEEE Transactions on Geoscience and Remote Sensing,* 39 (1), 125-128.

Dearing, John A. (1999). *Environmental magnetic susceptibility using the Bartington MS2 system*. Chi Publishing, London, England.

Headquarters, Department of the Army, Office of the Chief of Engineers. (1970). "Laboratory Soils Testing," Engineer Manual 1110-2-1906, Washington, DC.

Kraus, John D. (1984). *Electromagnetics.* 3rd ed, McGraw Hill, New York.

Nicolson, A. M., and Ross, G. F. (1970). "Measurement of the intrinsic properties of materials by time-domain techniques," *IEEE Transactions on Instrument and Measurement,* IM-19 (4), 377-382.

Salisbury, John W., Hapke, B., and Eastes, John W. (1987). "Usefulness of weak bands in midinfrared remote sensing of particulate planetary surfaces," *Journal of Geophysical Research,* 92 (B1), 702-710.

Salisbury, John W., Walter, Louis S., Vergo, Norma, D'Aria, Dana M. (1991). *Infrared (2.1-25 micrometers) spectra of minerals.* Johns Hopkins University Press.

The ASTER Spectral Library. (1999). Jet Propulsion Laboratory, California Institute of Technology, Pasadena, CA.

The New Encyclopedia Britannica. (1987). 15th ed.

Appendix A
Frequency-Domain Dielectric Property Data

NVESD Mine Lanes

Lane 1 , North End

File : 5Sep21504

Volumetric Moisture (%) : 1.2

Dry Density (g/cc) : 1.82

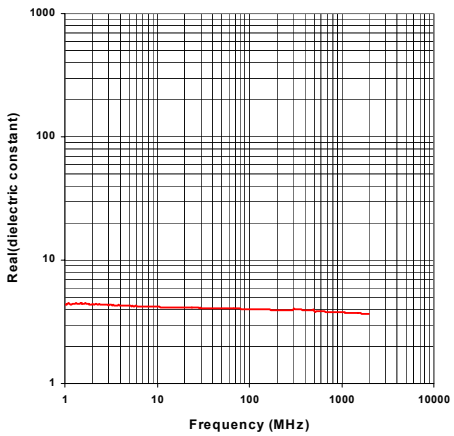

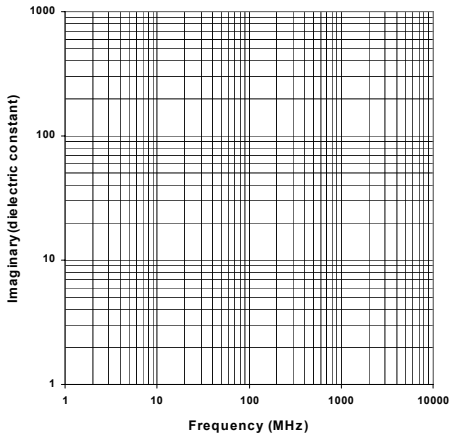

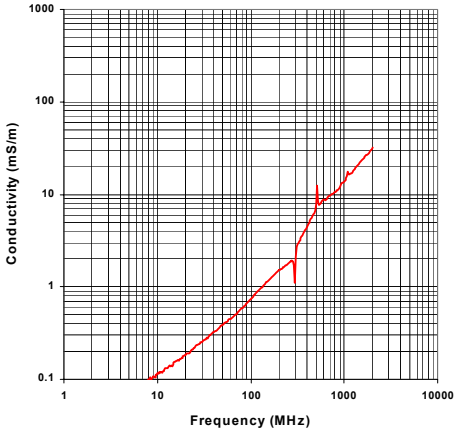

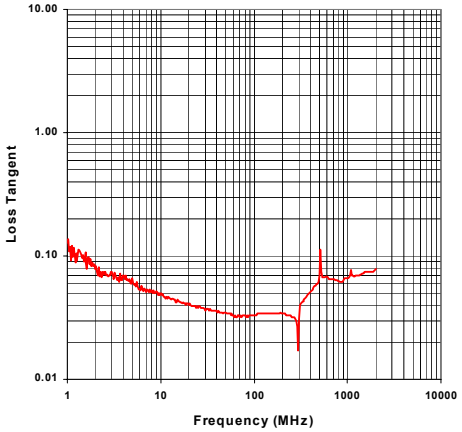

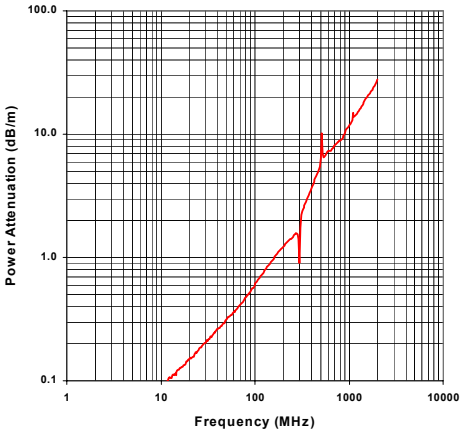

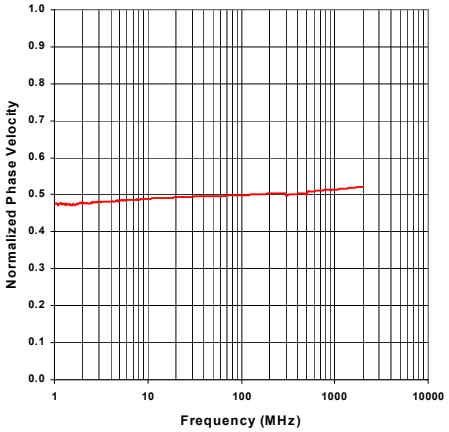

NVESD Mine Lanes

Lane 1 , North End

File : 6Sep21144

Volumetric Moisture (%) : 12.1

Dry Density (g/cc) : 1.82

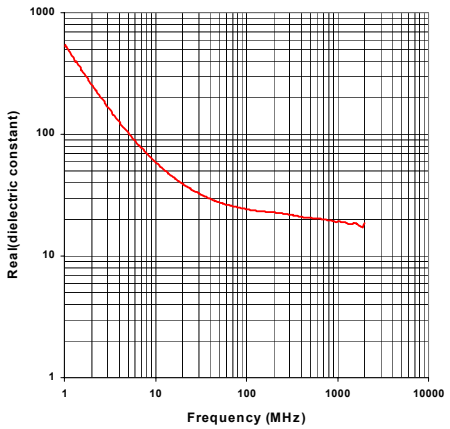

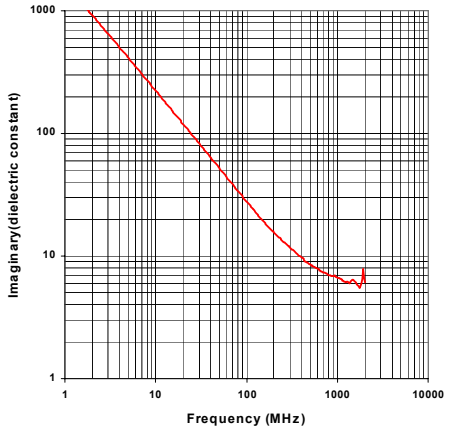

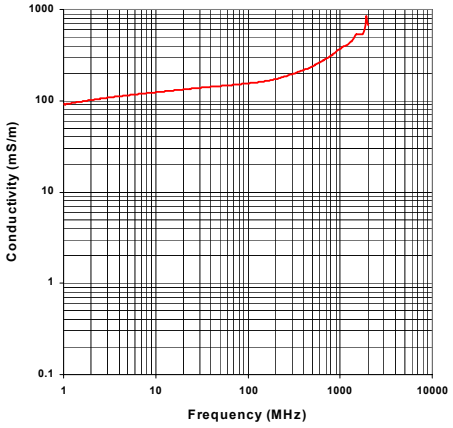

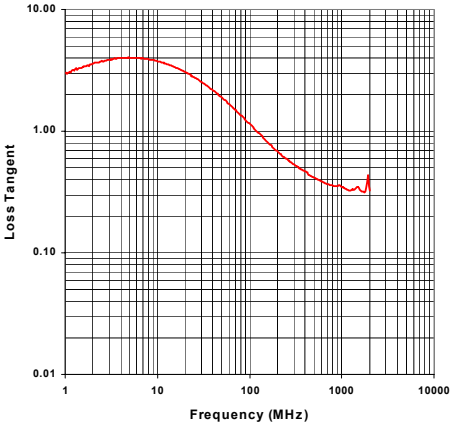

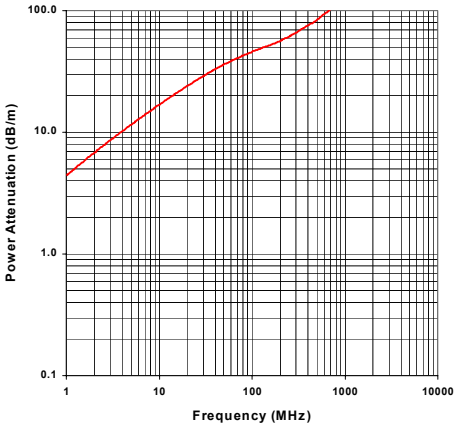

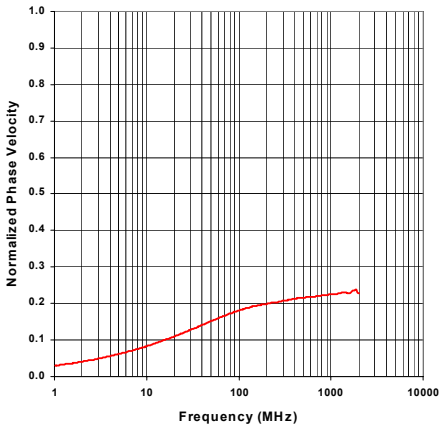

NVESD Mine Lanes

Lane 1 , North End

File : 6Sep21237

Volumetric Moisture (%) : 32.4

Dry Density (g/cc) : 1.82

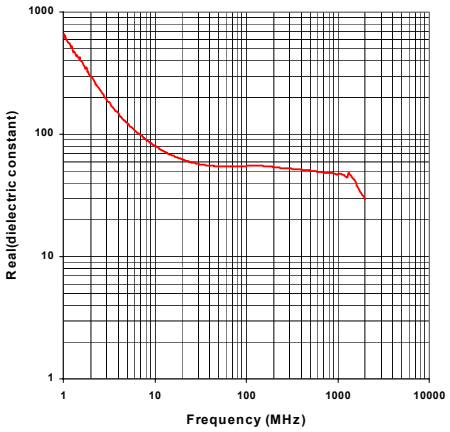

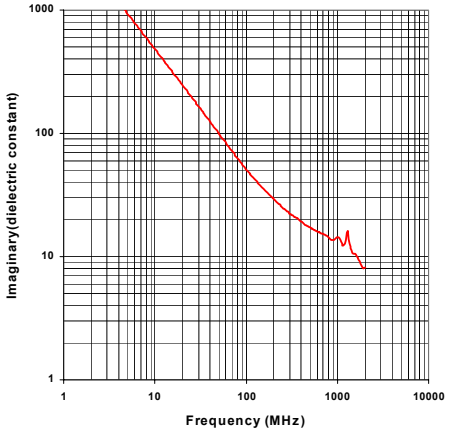

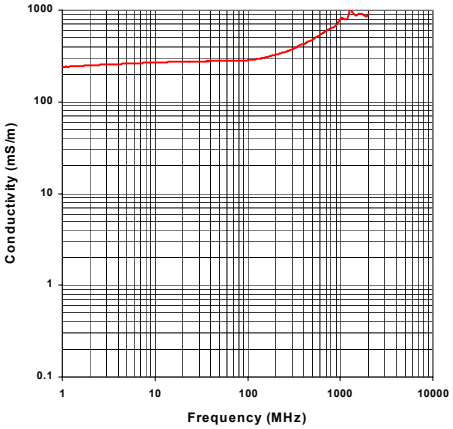

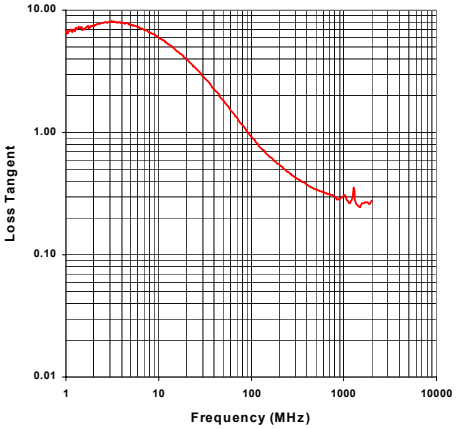

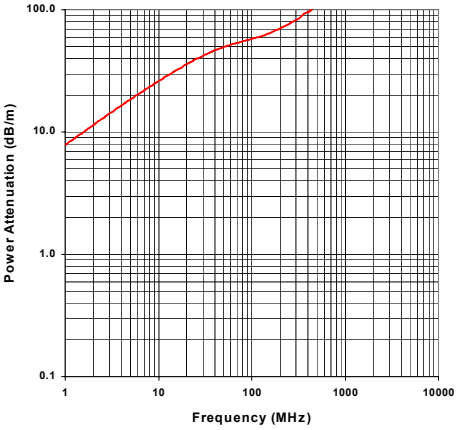

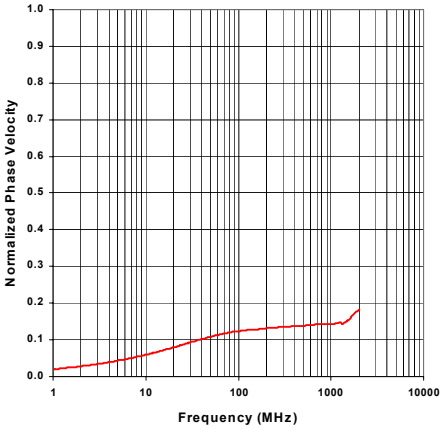

NVESD Mine Lanes

Lane 1 , North End

File : 6Sep21601

Volumetric Moisture (%) : 33.1

Dry Density (g/cc) : 1.82

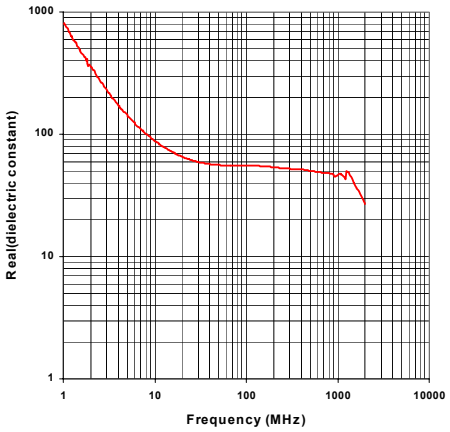

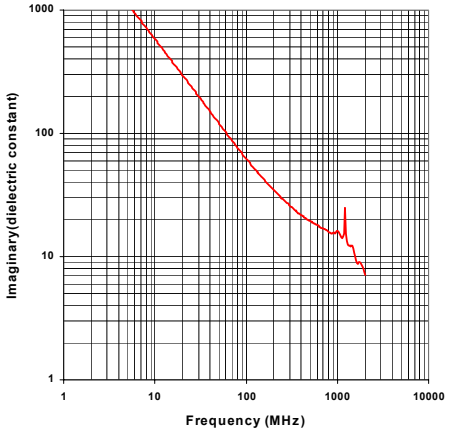

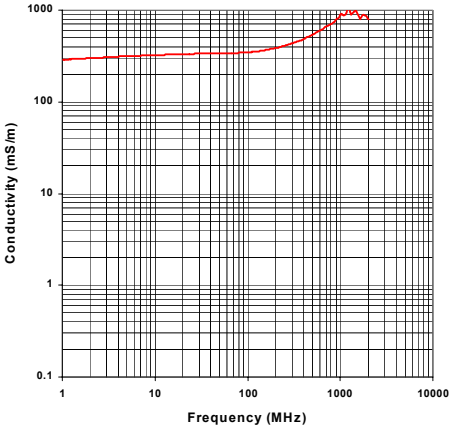

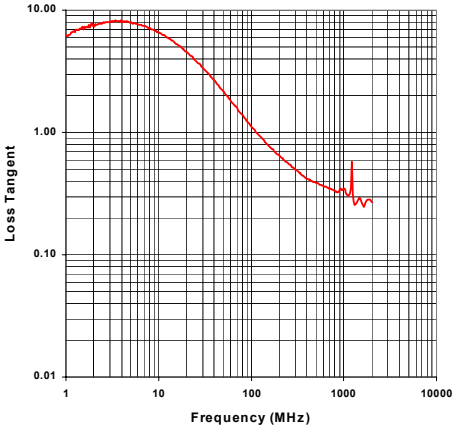

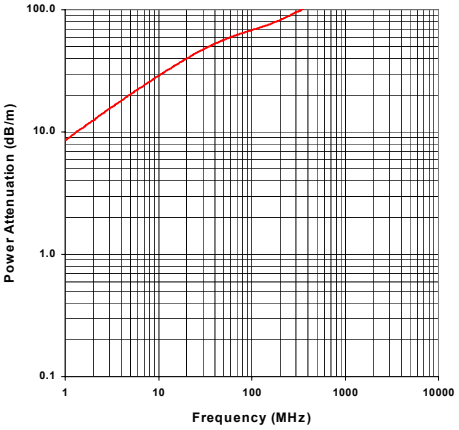

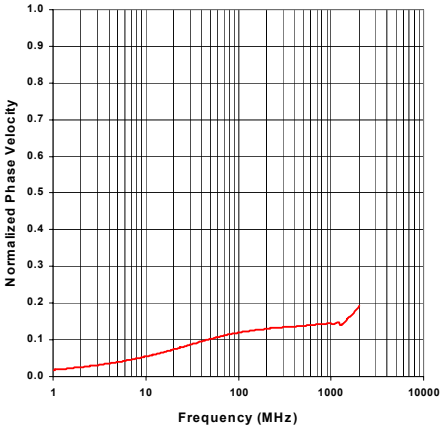

NVESD Mine Lanes

Lane 1 , South End

File : 17Sep21539

Volumetric Moisture (%) : 0.1

Dry Density (g/cc) : 1.81

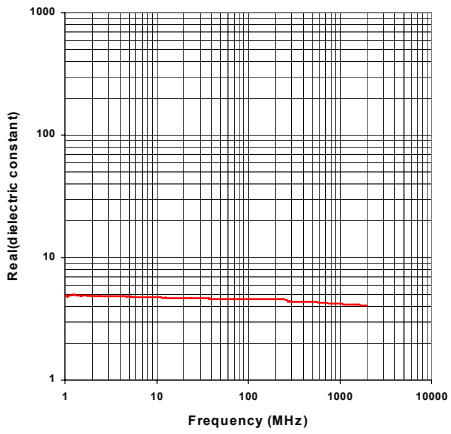

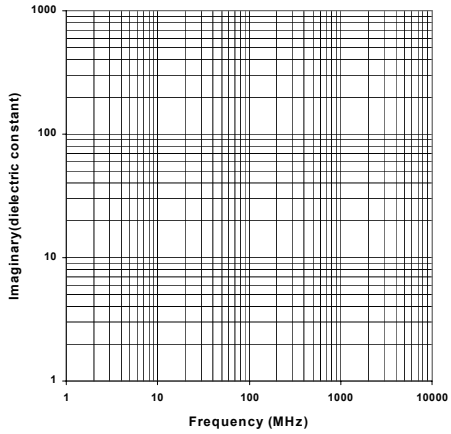

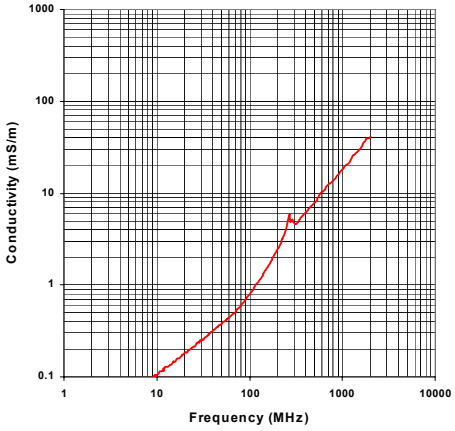

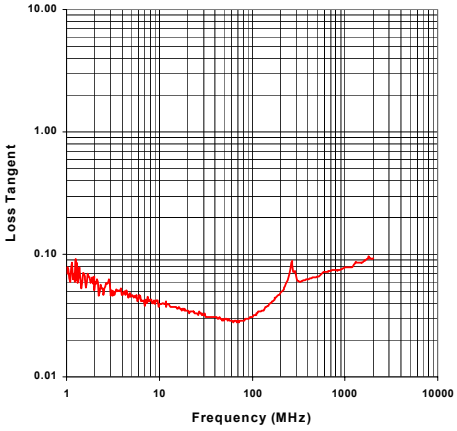

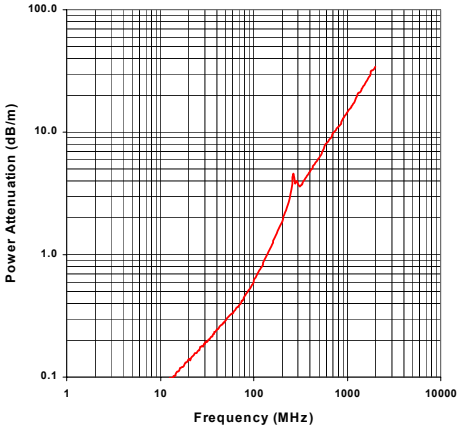

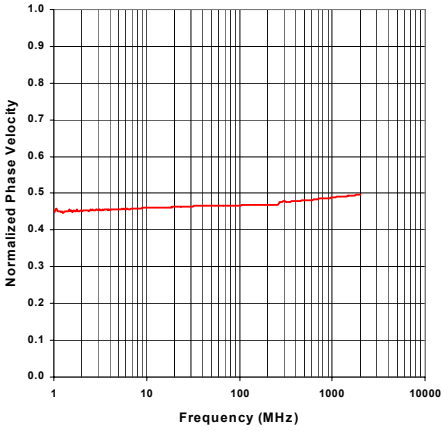

NVESD Mine Lanes

Lane 1 , South End

File : 13Sep21550

Volumetric Moisture (%) : 0.9

Dry Density (g/cc) : 1.81

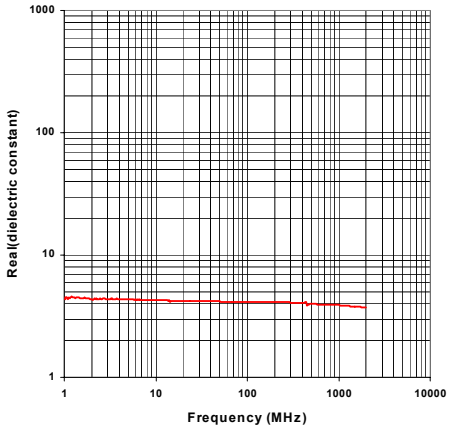

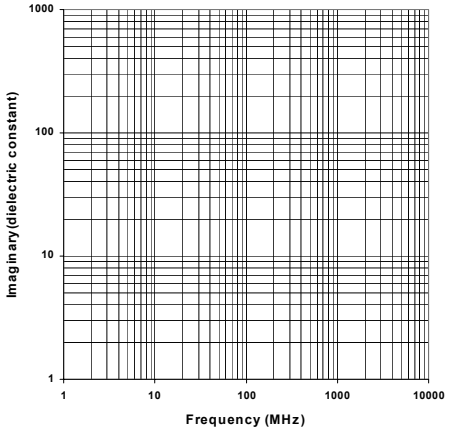

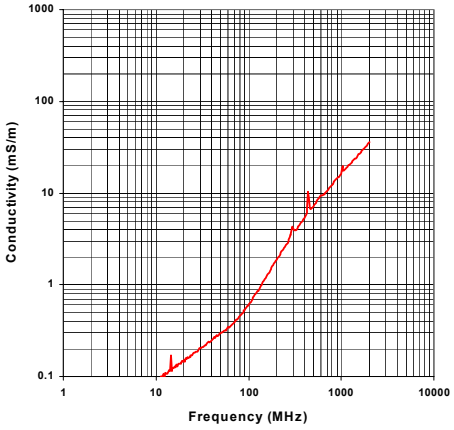

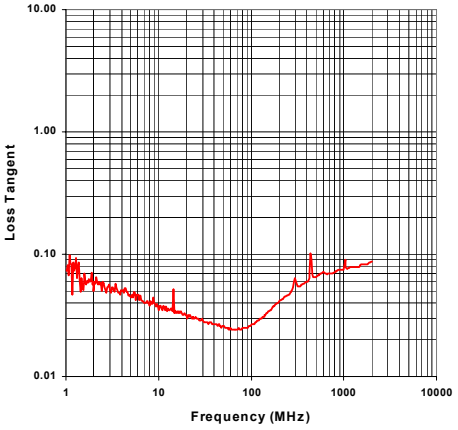

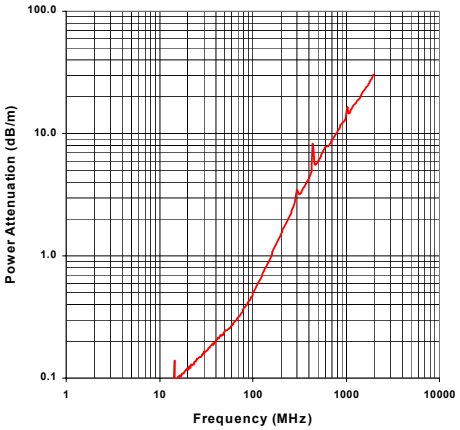

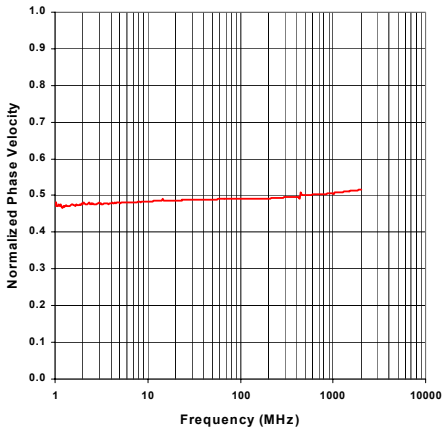

NVESD Mine Lanes

Lane 1 , South End

File : 13Sep21642

Volumetric Moisture (%) : 18.3

Dry Density (g/cc) : 1.81

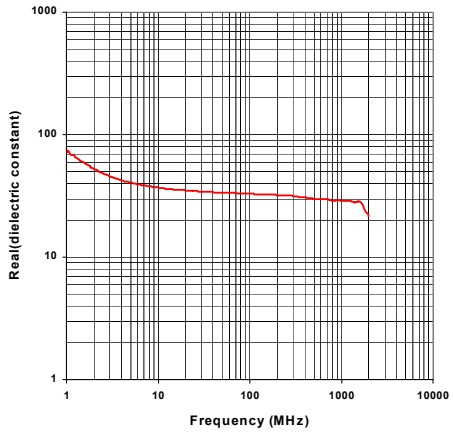

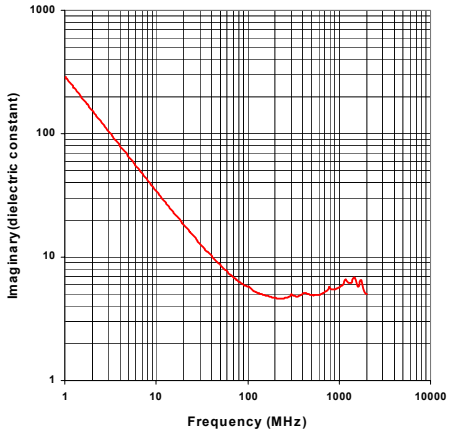

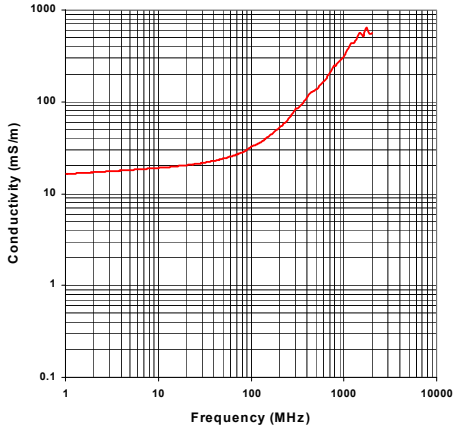

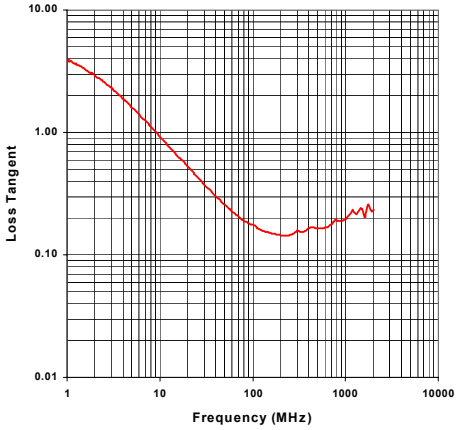

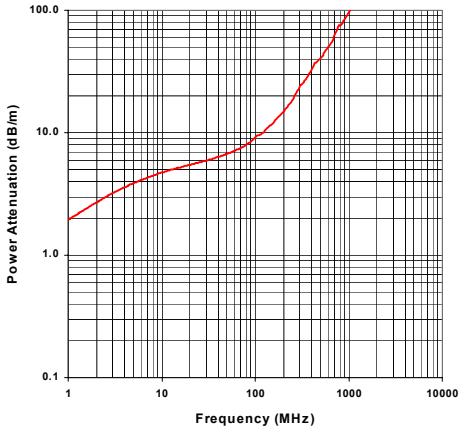

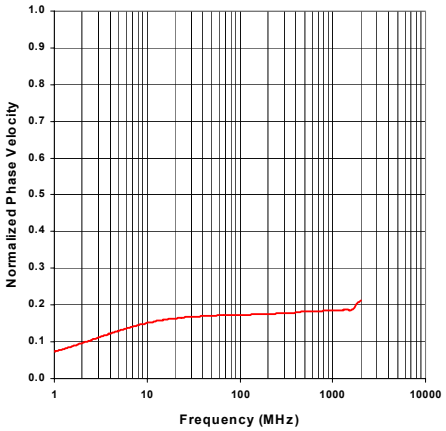

NVESD Mine Lanes

Lane 1 , South End

File : 13Sep21648

Volumetric Moisture (%) : 31.2

Dry Density (g/cc) : 1.81

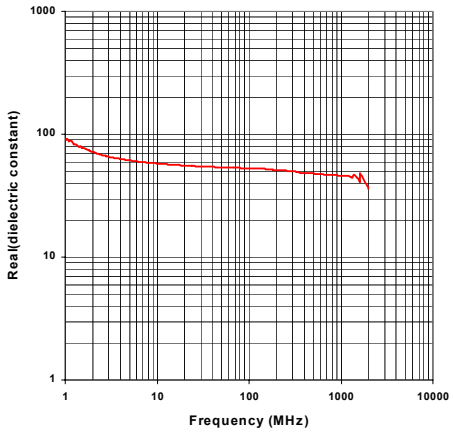

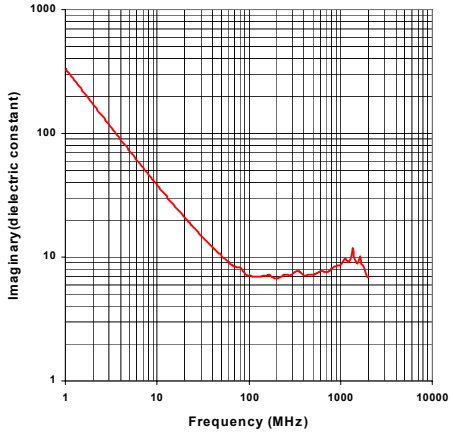

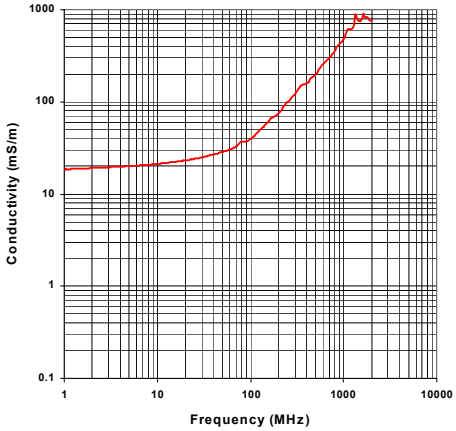

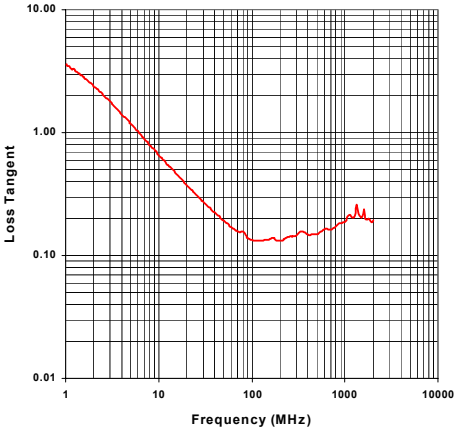

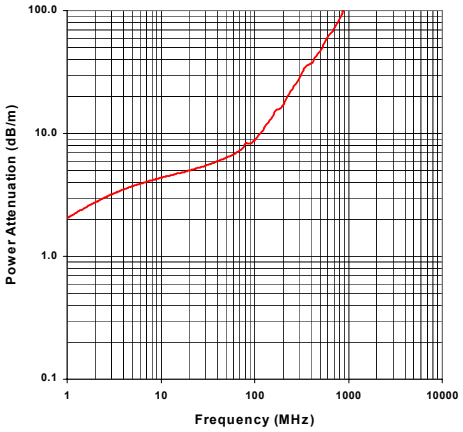

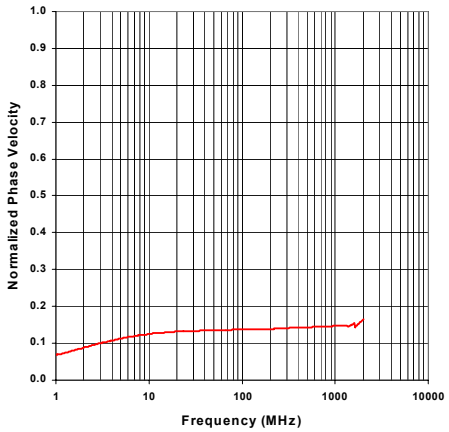

NVESD Mine Lanes

Lane 2 , North End

File : 6Sep21150

Volumetric Moisture (%) : 2.7

Dry Density (g/cc) : 1.36

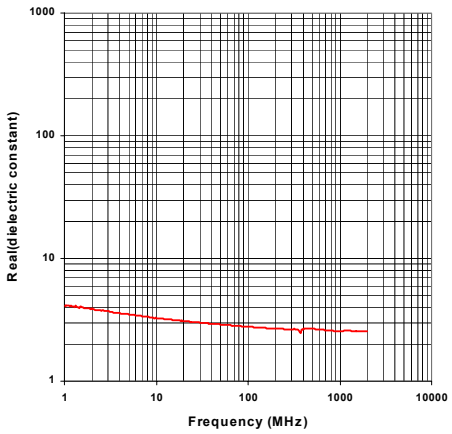

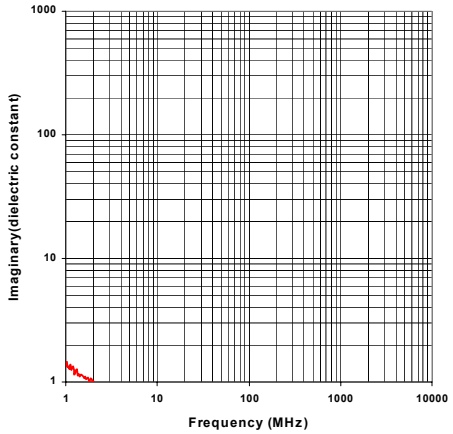

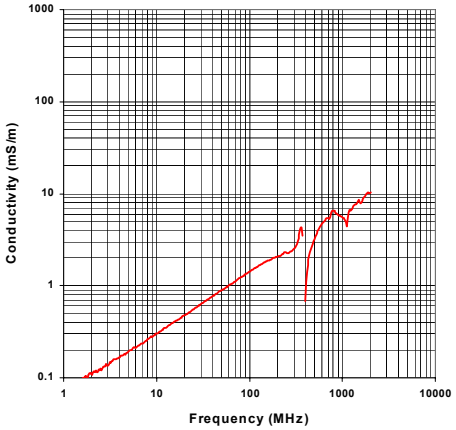

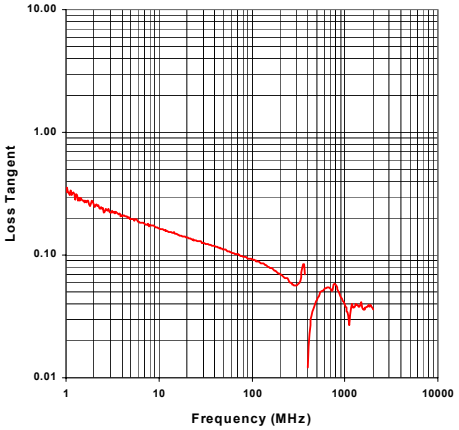

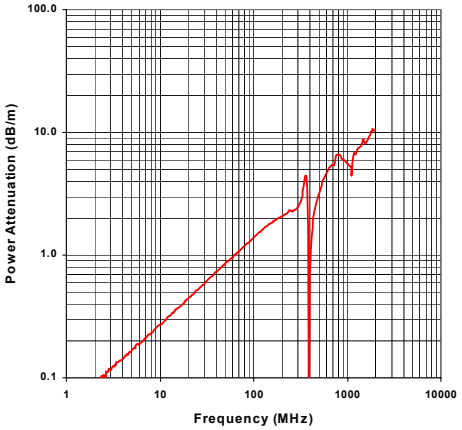

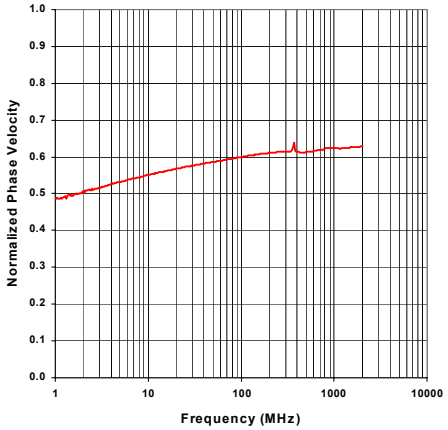

NVESD Mine Lanes

Lane 2 , North End

File : 5Sep21511

Volumetric Moisture (%) : 13.2

Dry Density (g/cc) : 1.36

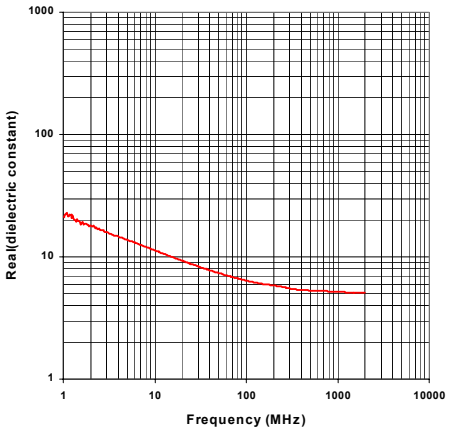

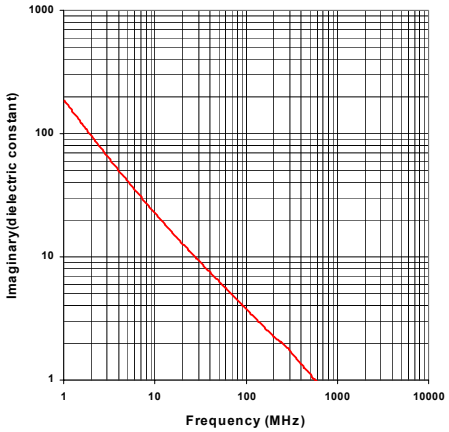

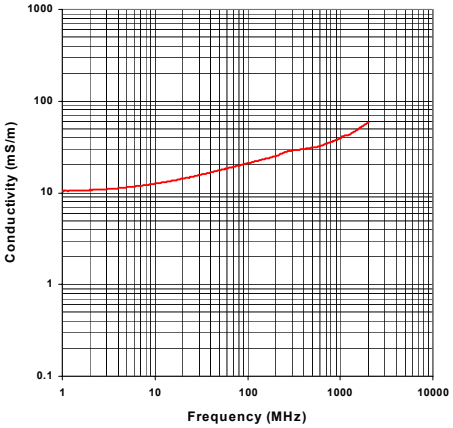

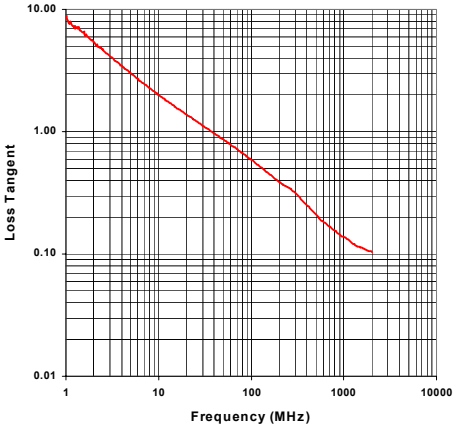

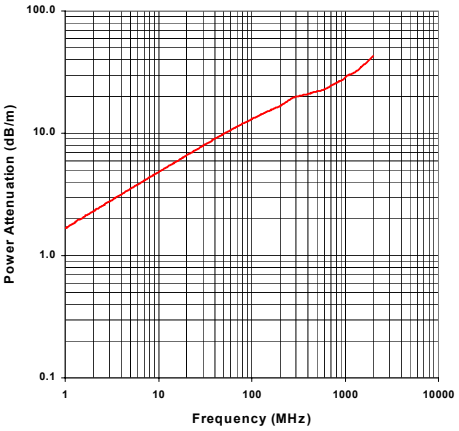

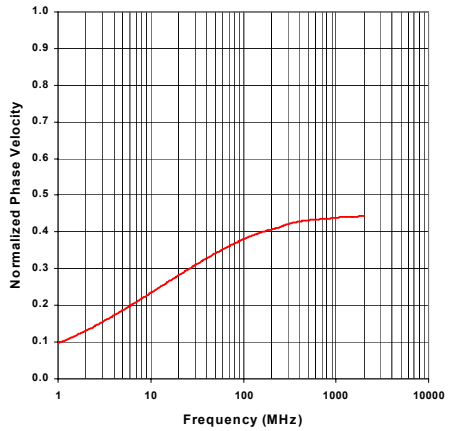

NVESD Mine Lanes

Lane 2 , North End

File : 6Sep21244

Volumetric Moisture (%) : 36.7

Dry Density (g/cc) : 1.36

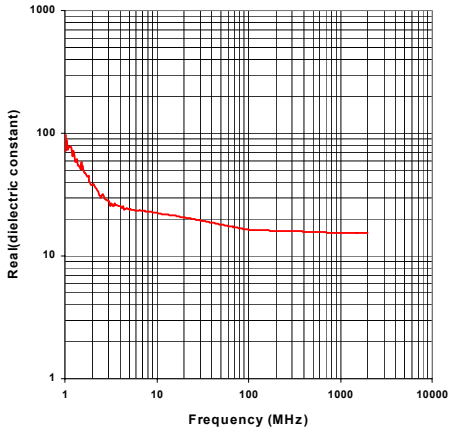

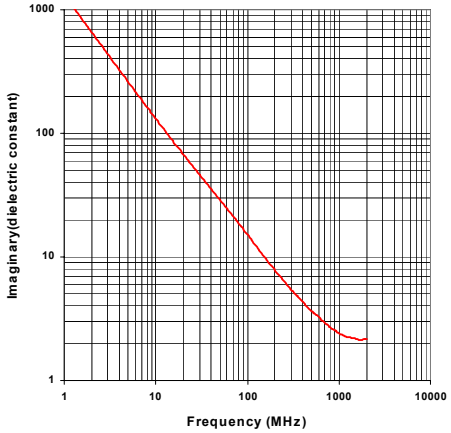

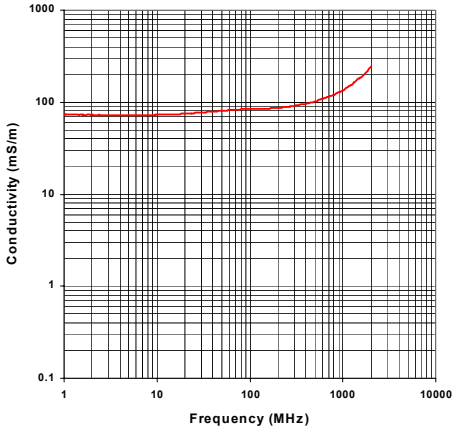

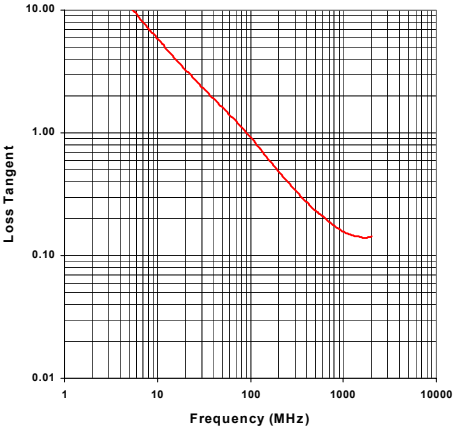

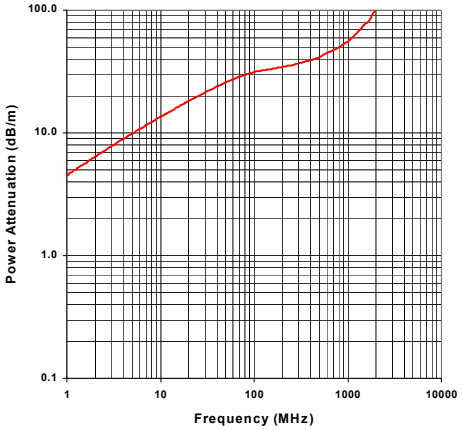

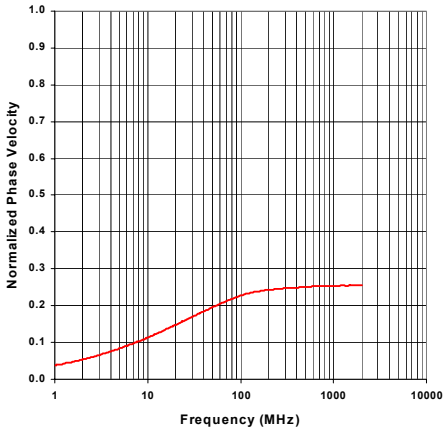

NVESD Mine Lanes

Lane 2 , North End

File : 6Sep21607

Volumetric Moisture (%) : 36.9

Dry Density (g/cc) : 1.36

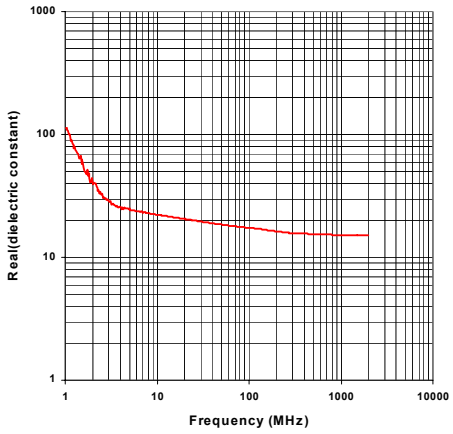

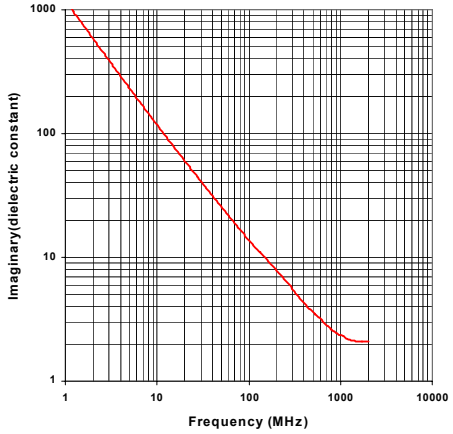

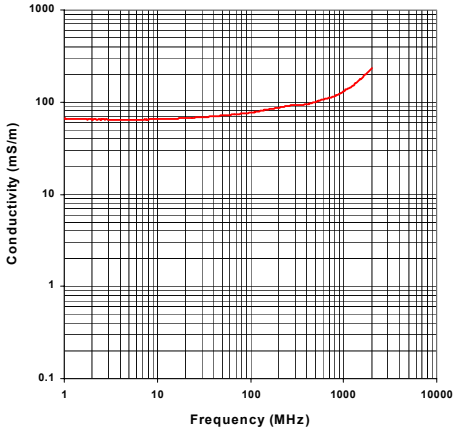

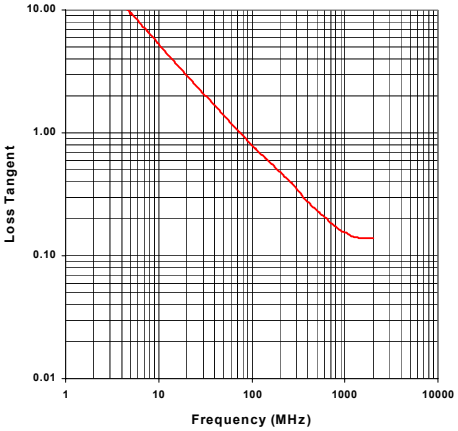

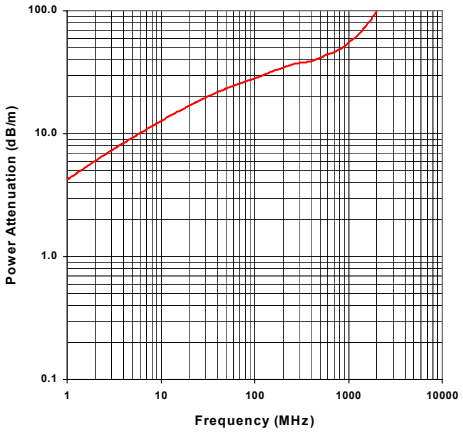

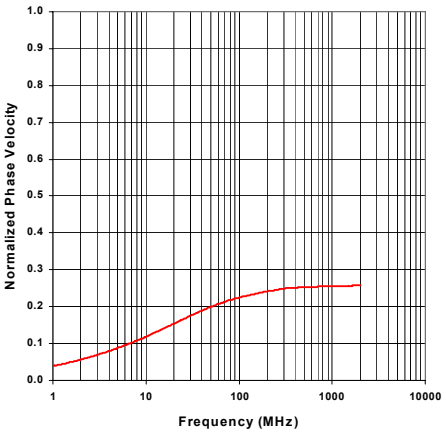

NVESD Mine Lanes

Lane 2 , Middle

File : 17Sep21547

Volumetric Moisture (%) : 2.2

Dry Density (g/cc) : 1.4

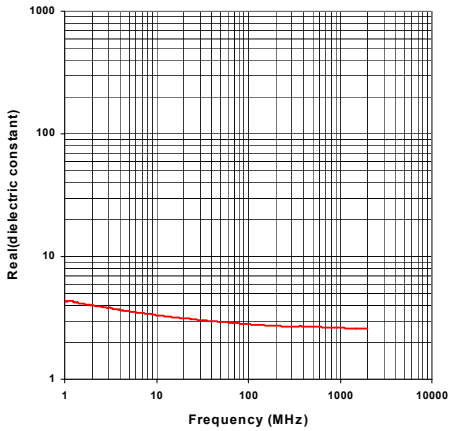

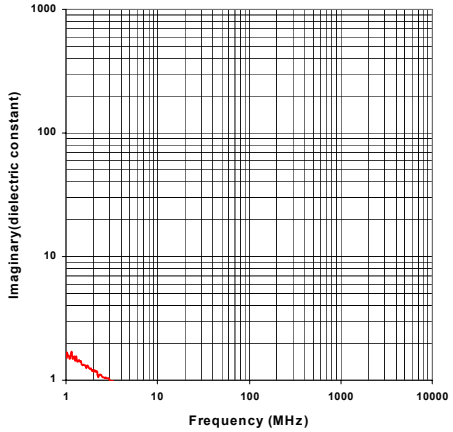

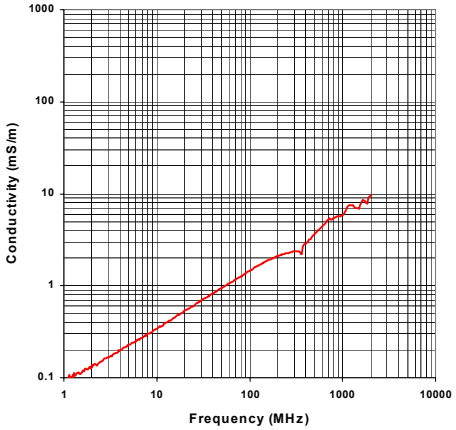

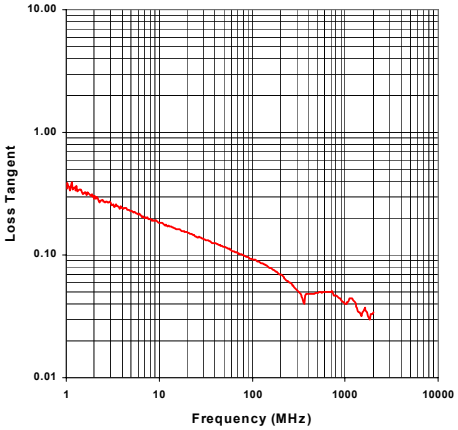

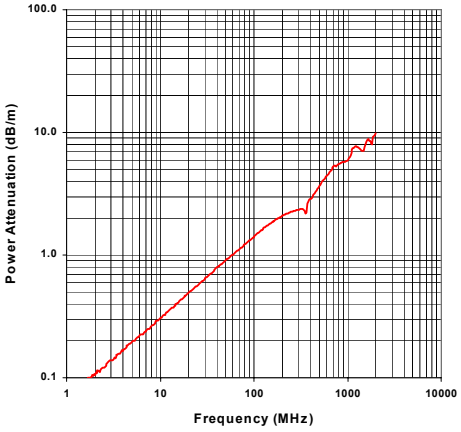

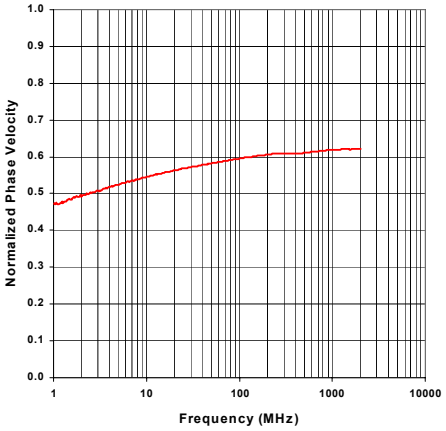

NVESD Mine Lanes

Lane 2 , Middle

File : 13Sep21556

Volumetric Moisture (%) : 13.6

Dry Density (g/cc) : 1.4

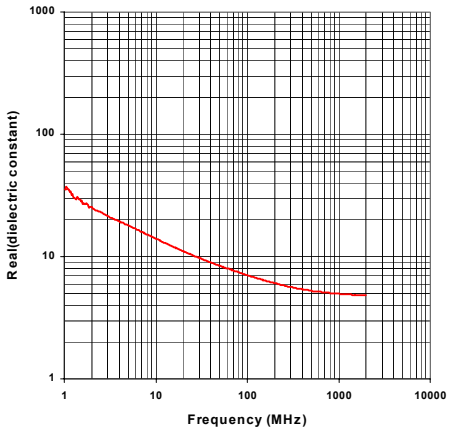

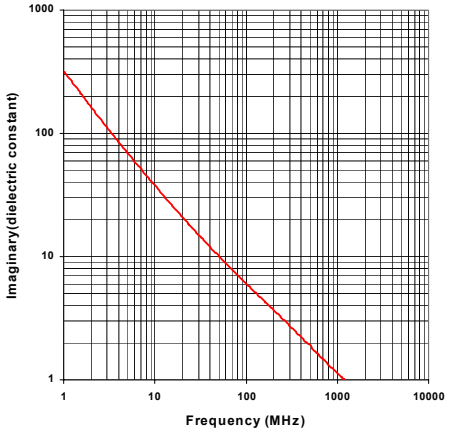

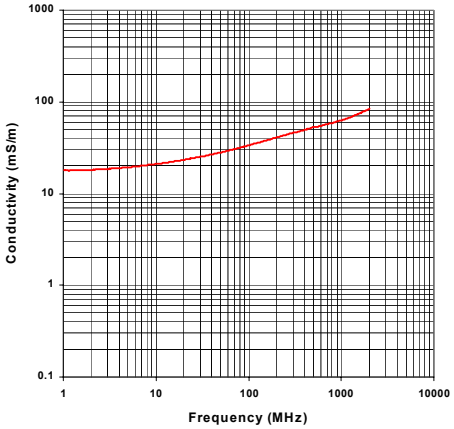

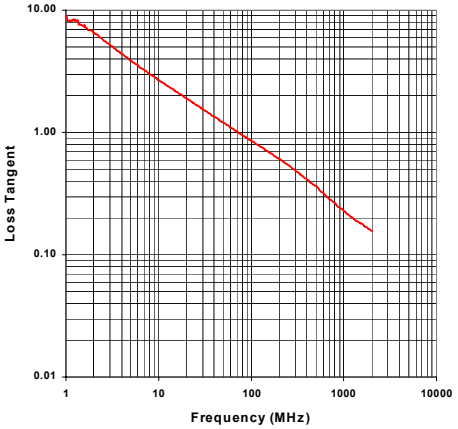

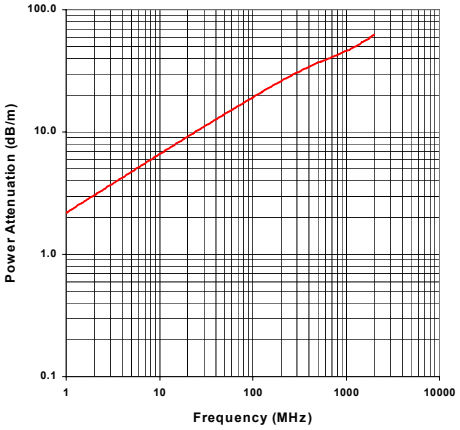

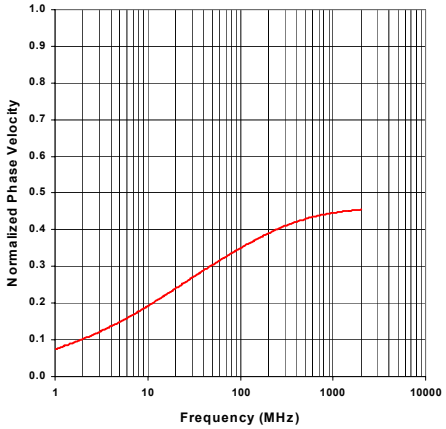

NVESD Mine Lanes

Lane 2 , Middle

File : 13Sep21654

Volumetric Moisture (%) : 41.1

Dry Density (g/cc) : 1.4

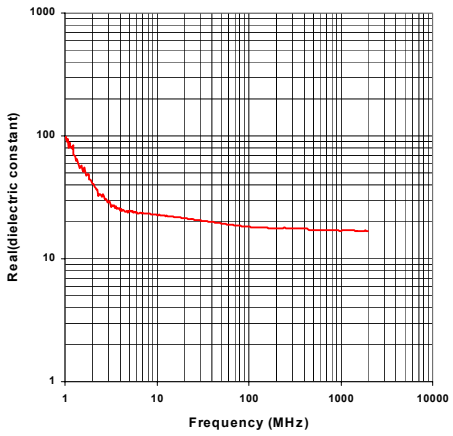

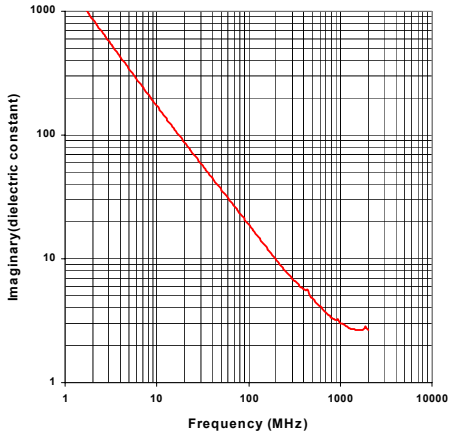

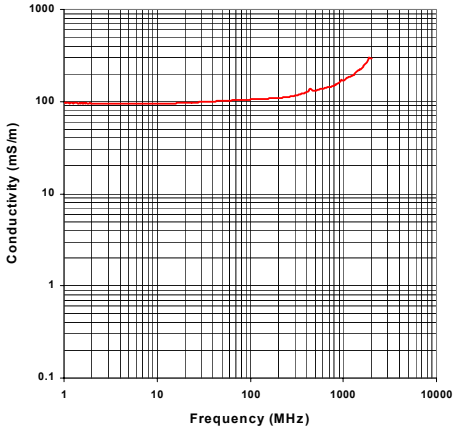

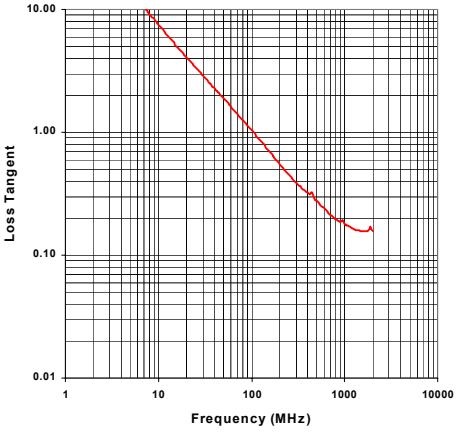

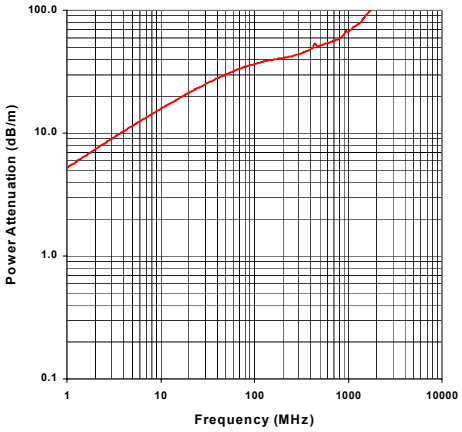

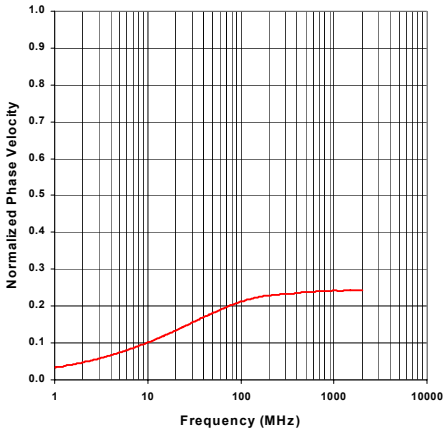

NVESD Mine Lanes

Lane 2 , South End

File : 20Sep21127

Volumetric Moisture (%) : 1.6

Dry Density (g/cc) : 1.3

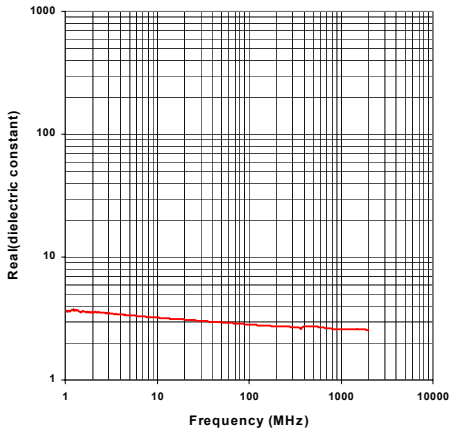

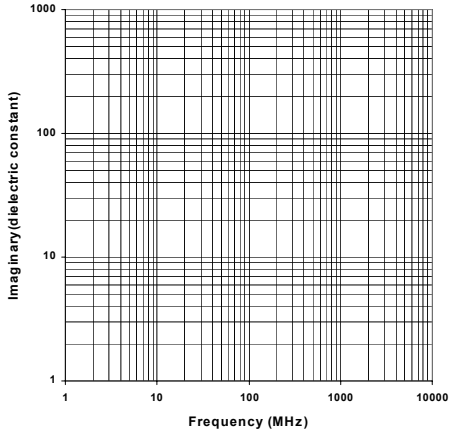

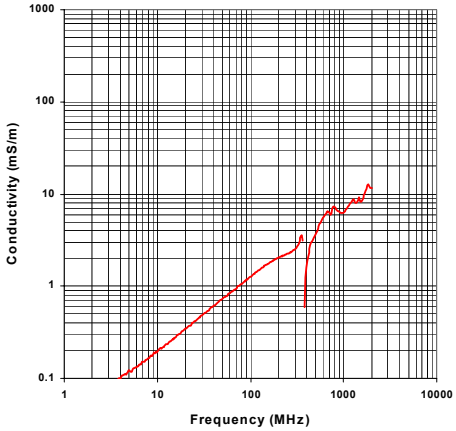

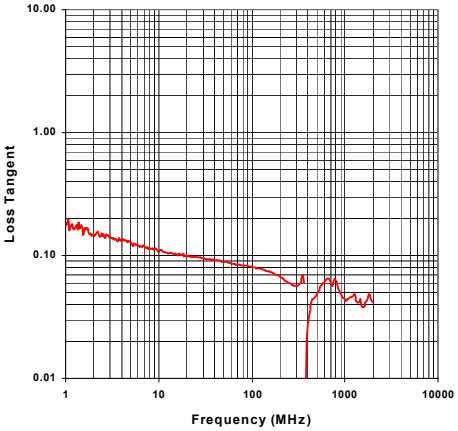

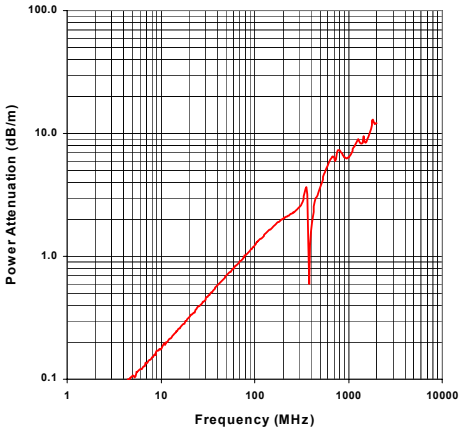

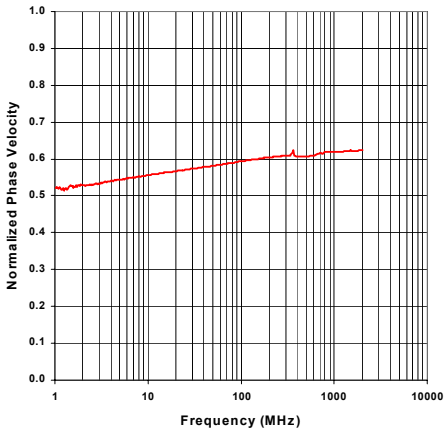

NVESD Mine Lanes

Lane 2 , South End

File : 19Sep21511

Volumetric Moisture (%) : 12.5

Dry Density (g/cc) : 1.3

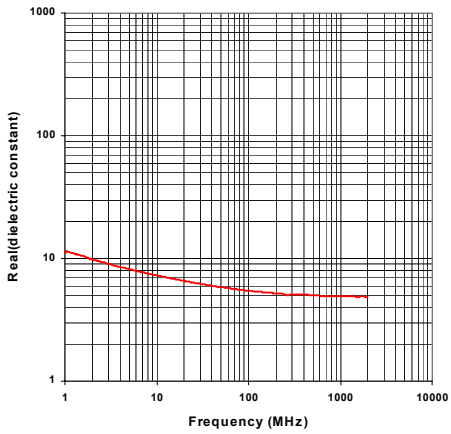

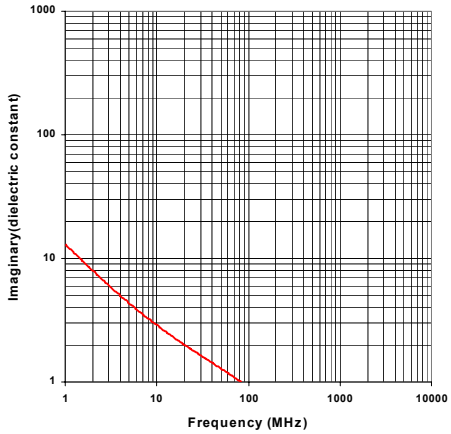

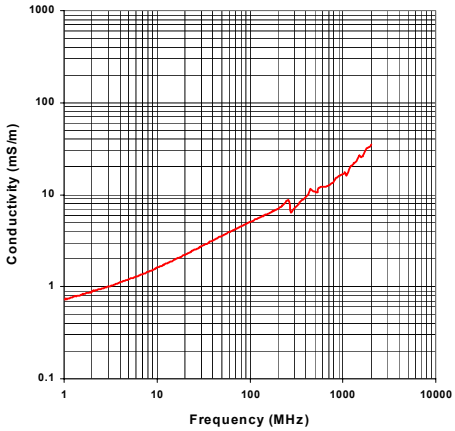

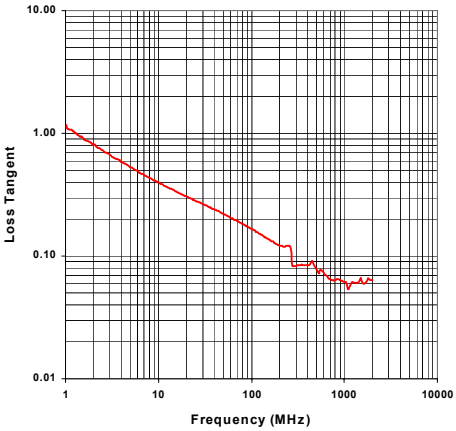

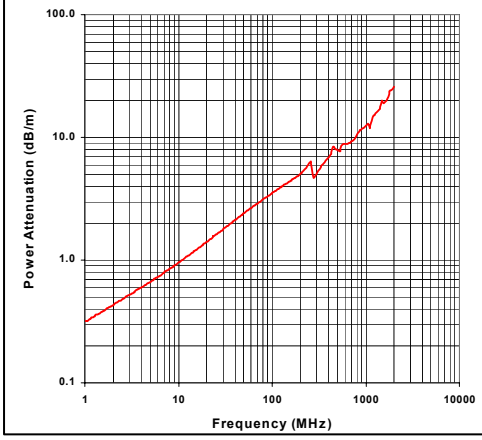

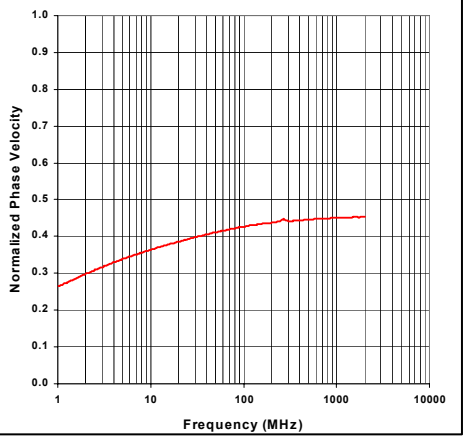

NVESD Mine Lanes

Lane 2 , South End

File : 19Sep21557

Volumetric Moisture (%) : 30.4

Dry Density (g/cc) : 1.3

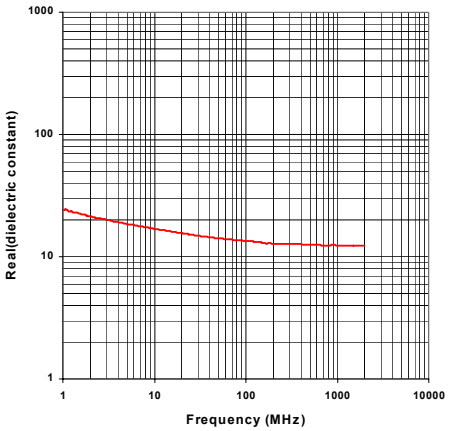

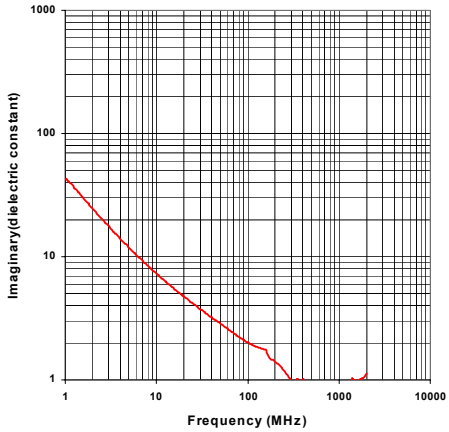

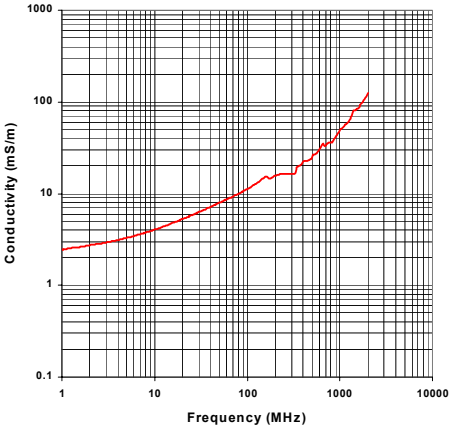

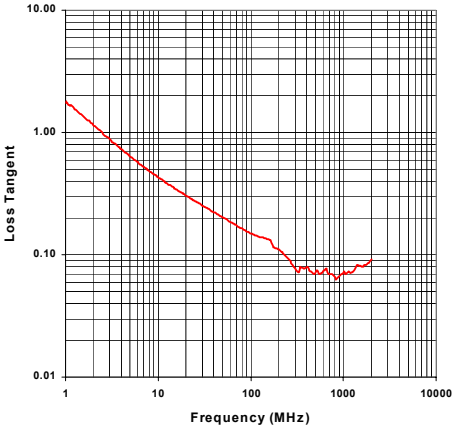

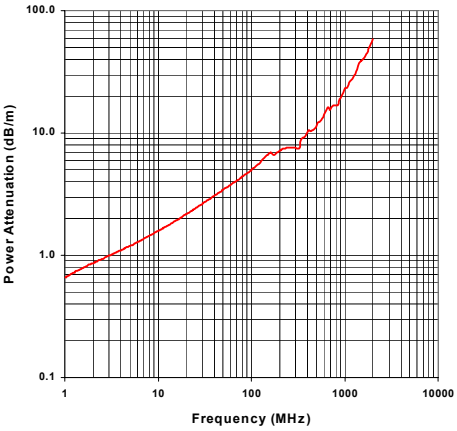

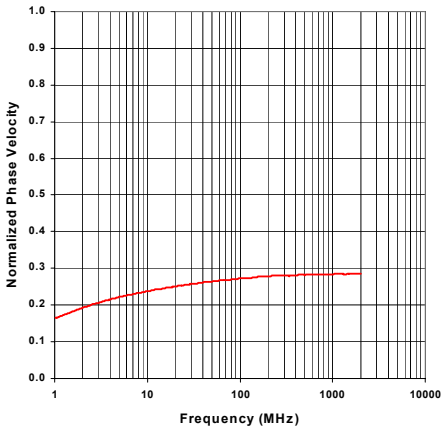

NVESD Mine Lanes

Lane 3 , North End

File : 6Sep21157

Volumetric Moisture (%) : 2.5

Dry Density (g/cc) : 1.77

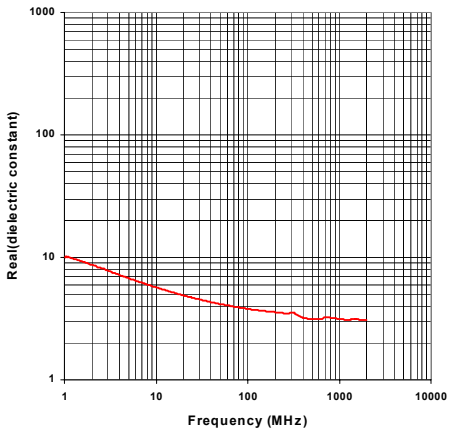

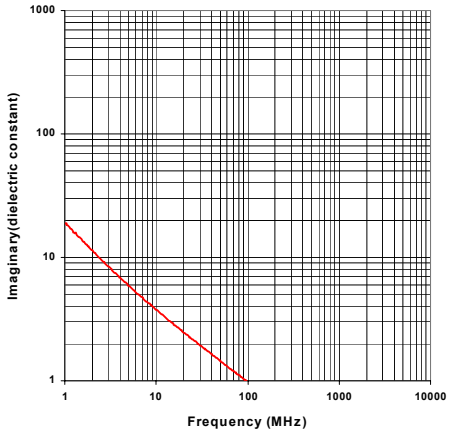

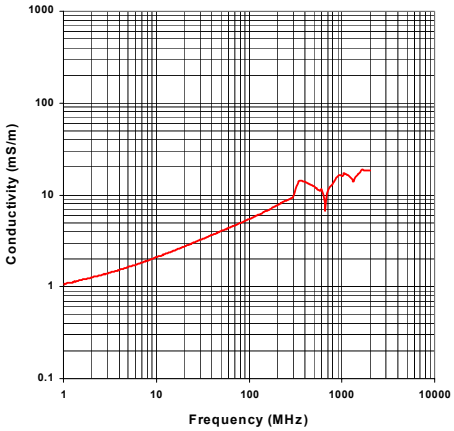

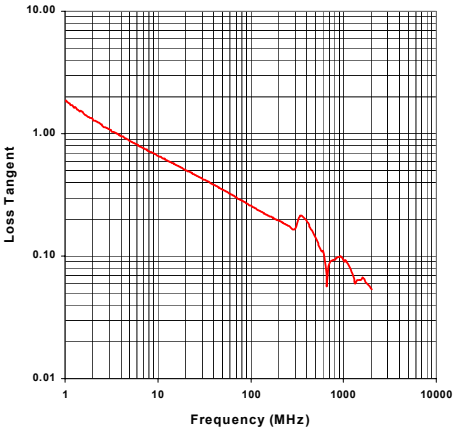

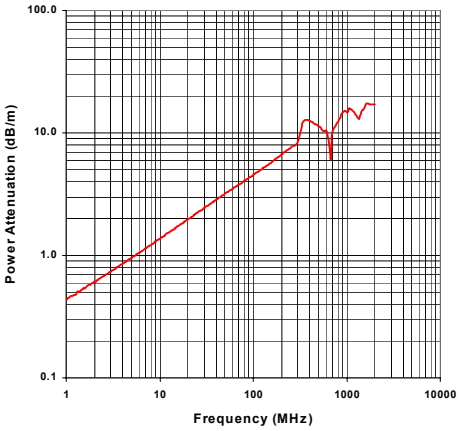

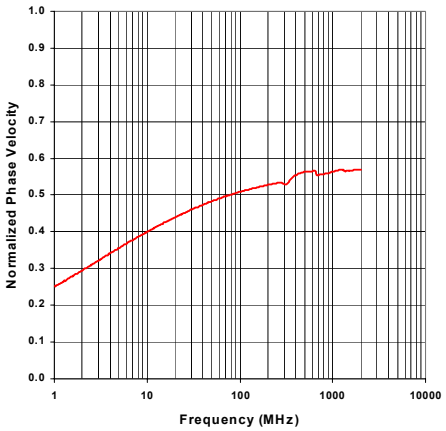

NVESD Mine Lanes

Lane 3 , North End

File : 5Sep21517

Volumetric Moisture (%) : 15.8

Dry Density (g/cc) : 1.77

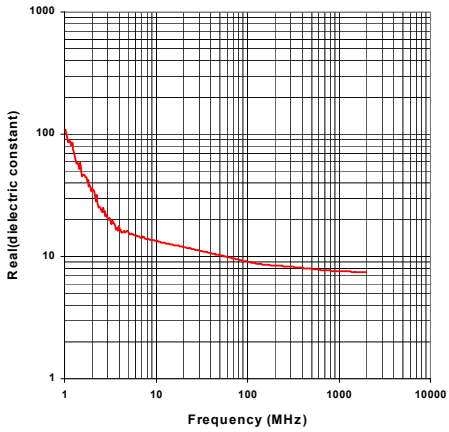

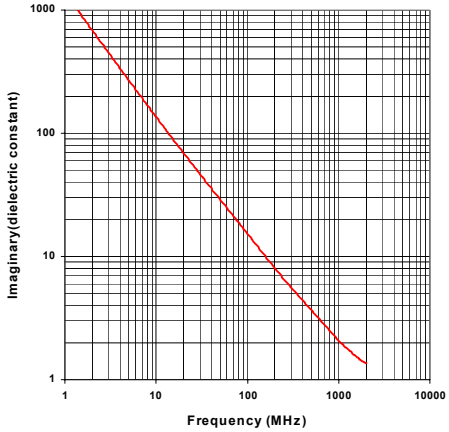

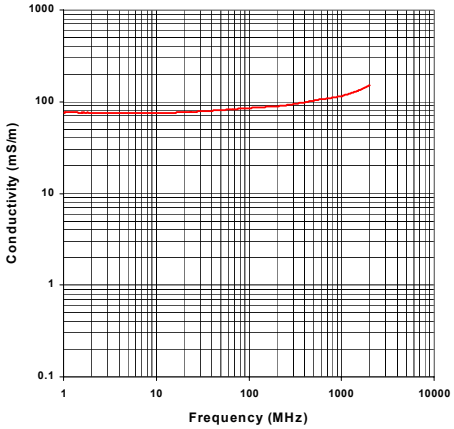

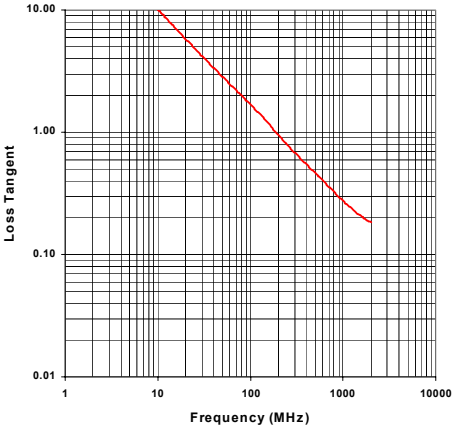

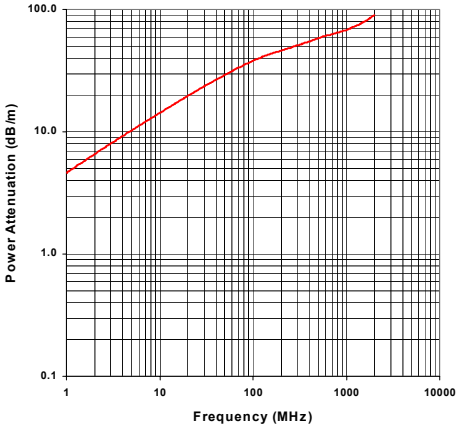

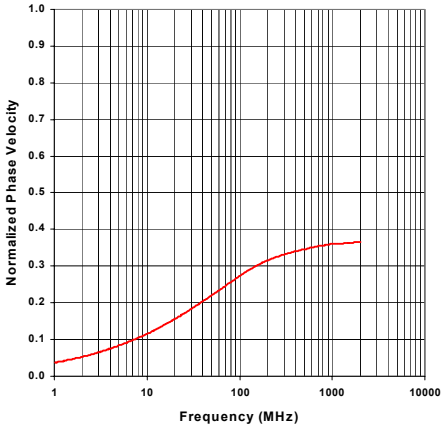

NVESD Mine Lanes

Lane 3 , North End

File : 6Sep21613

Volumetric Moisture (%) : 30.3

Dry Density (g/cc) : 1.77

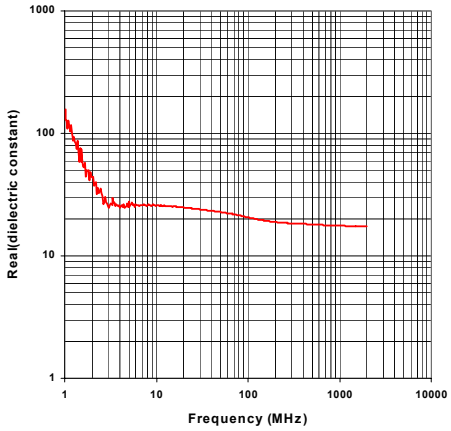

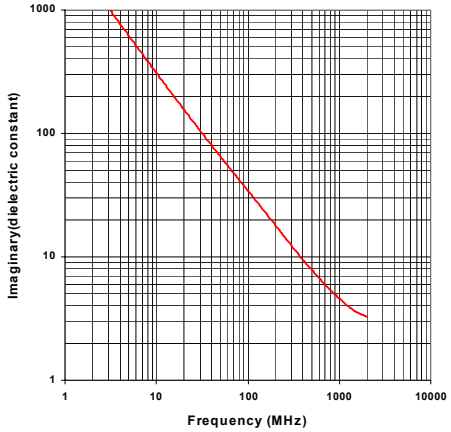

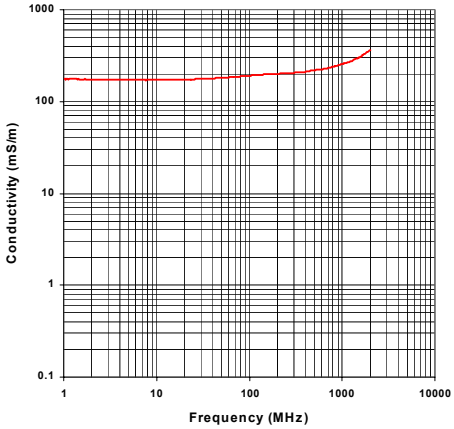

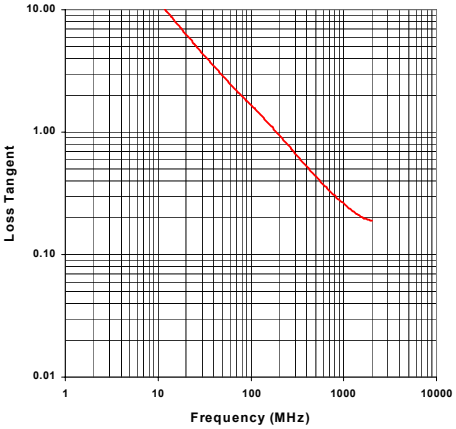

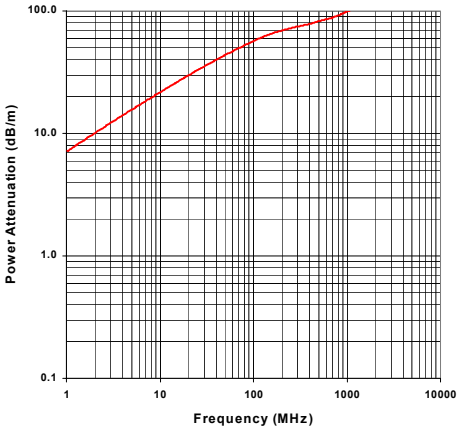

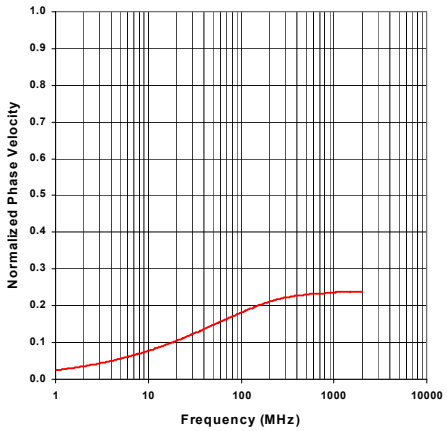

NVESD Mine Lanes

Lane 3 , Middle

File : 17Sep21556

Volumetric Moisture (%) : 0.8

Dry Density (g/cc) : 1.61

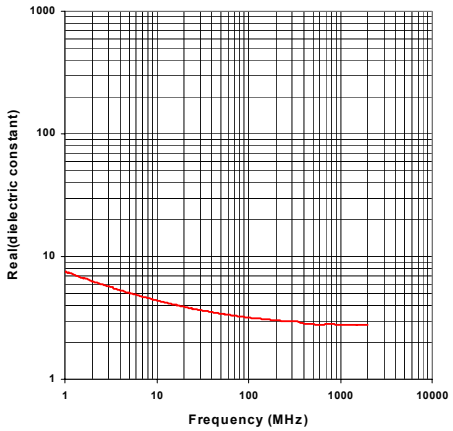

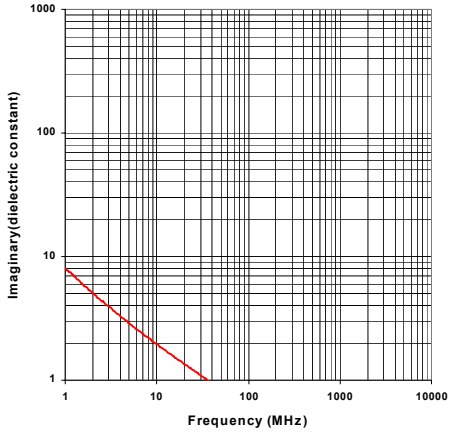

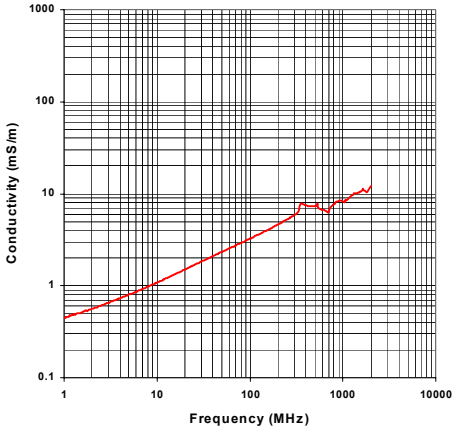

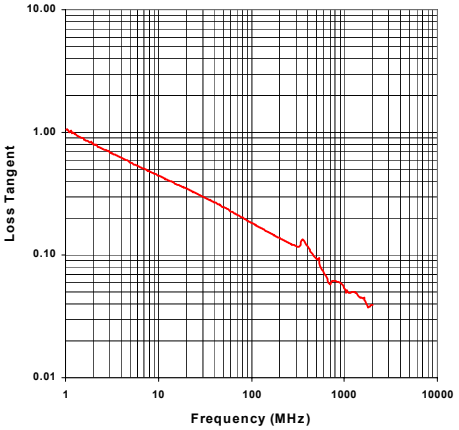

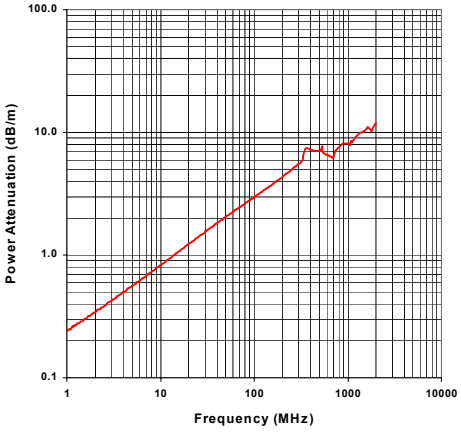

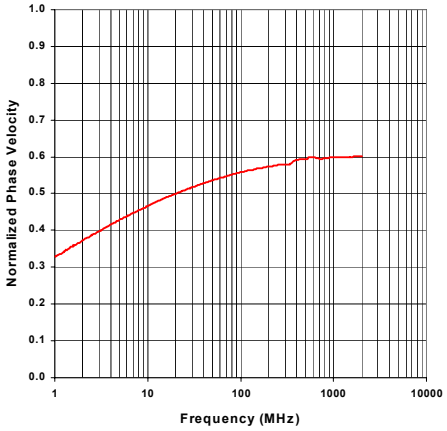

NVESD Mine Lanes

Lane 3 , Middle

File : 13Sep21602

Volumetric Moisture (%) : 8.3

Dry Density (g/cc) : 1.61

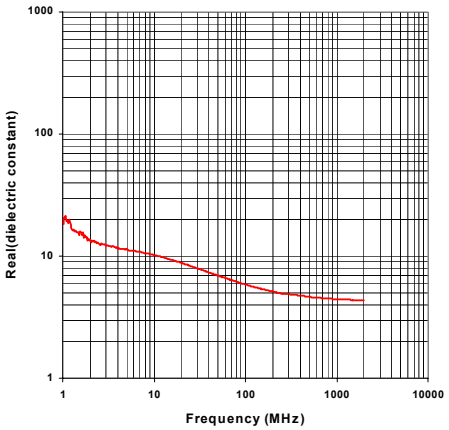

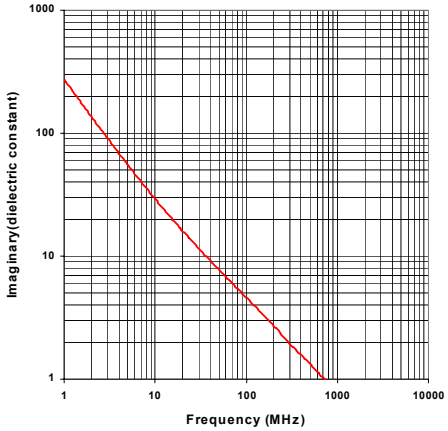

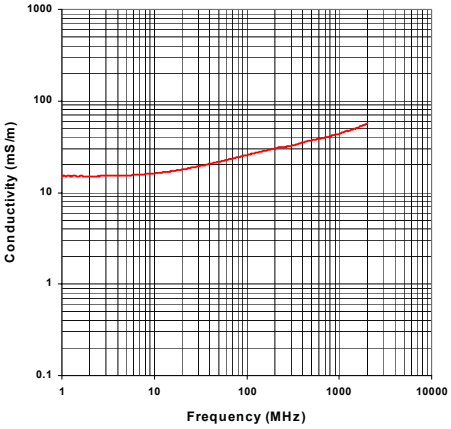

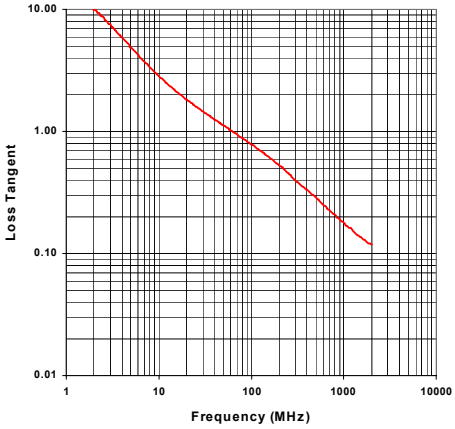

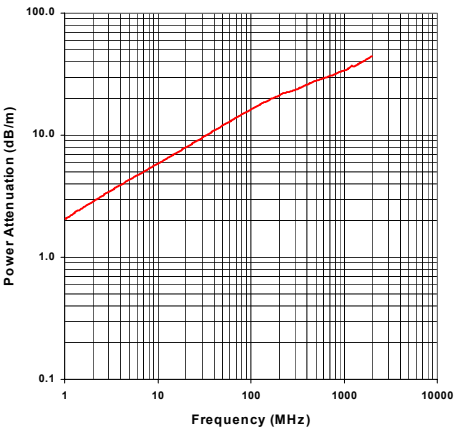

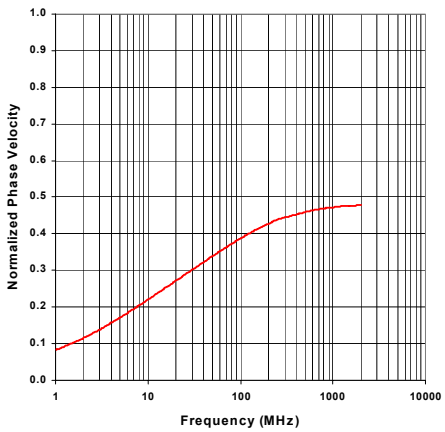

NVESD Mine Lanes

Lane 3 , Middle

File : 13Sep21659

Volumetric Moisture (%) : 33.1

Dry Density (g/cc) : 1.61

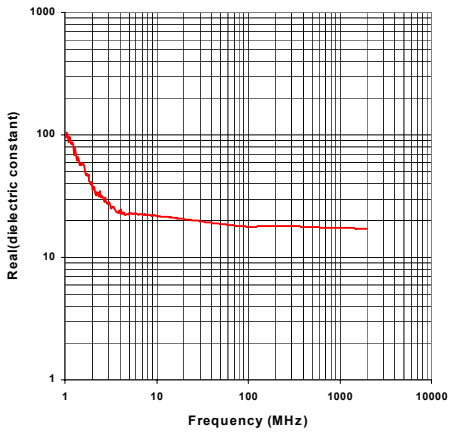

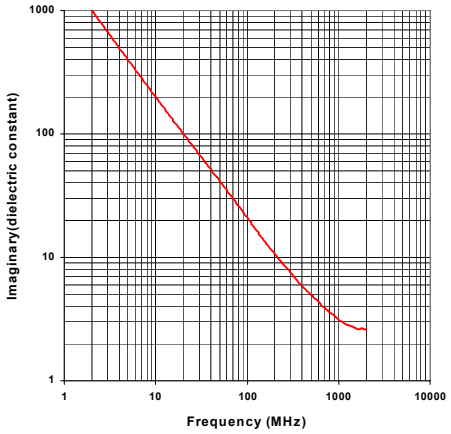

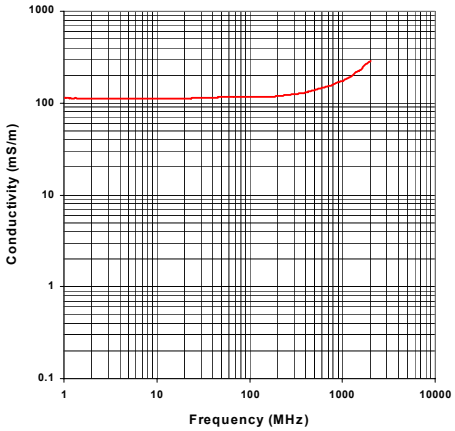

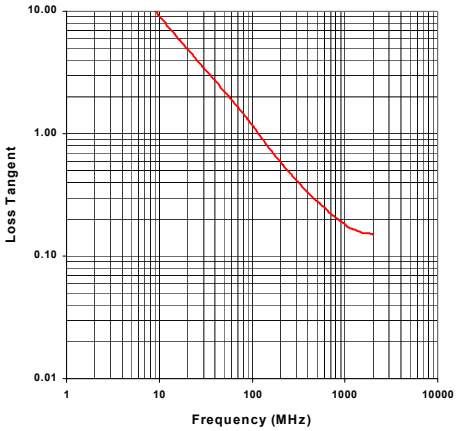

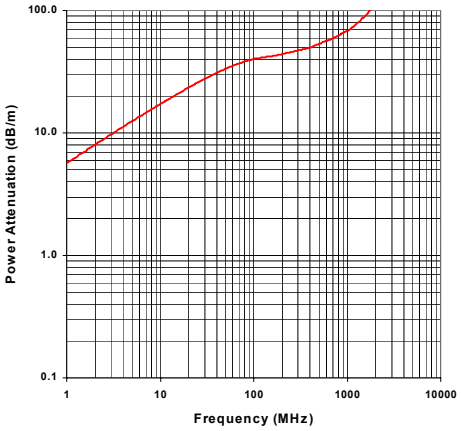

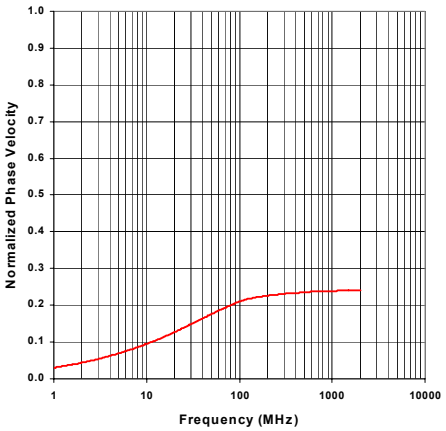

NVESD Mine Lanes

Lane 3 , S end

File : 20Sep21146

Volumetric Moisture (%) : 0.7

Dry Density (g/cc) : 1.69

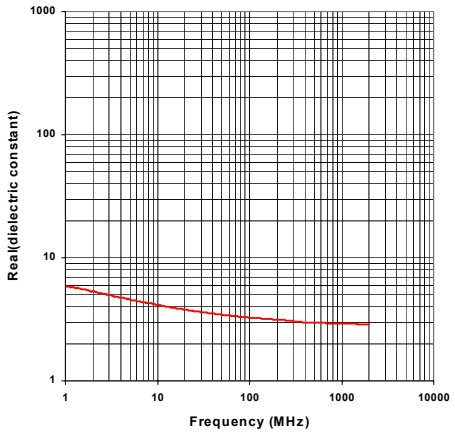

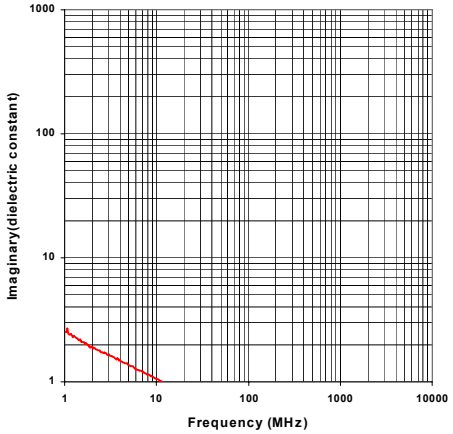

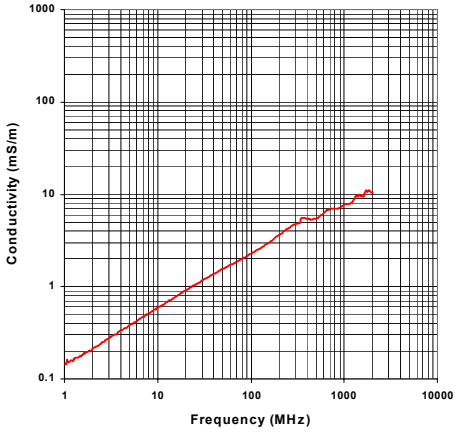

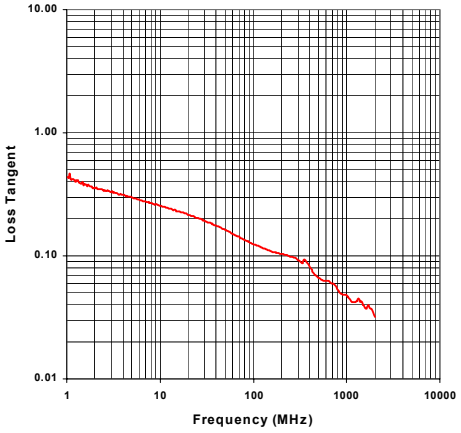

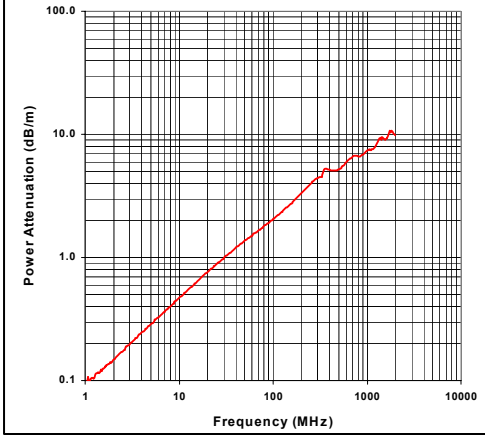

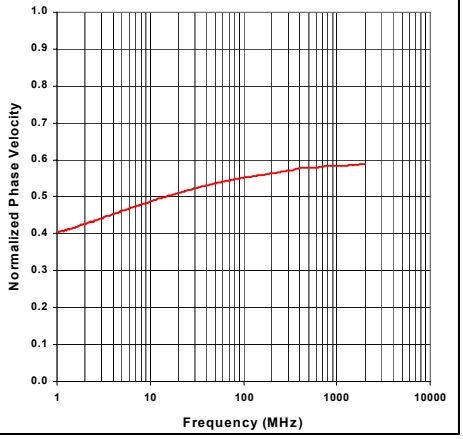

NVESD Mine Lanes

Lane 3 , S end

File : 19Sep21518

Volumetric Moisture (%) : 9.6

Dry Density (g/cc) : 1.69

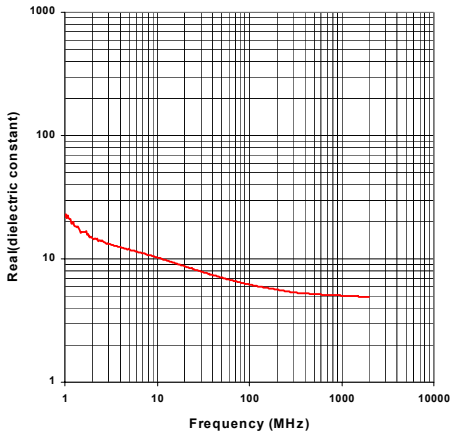

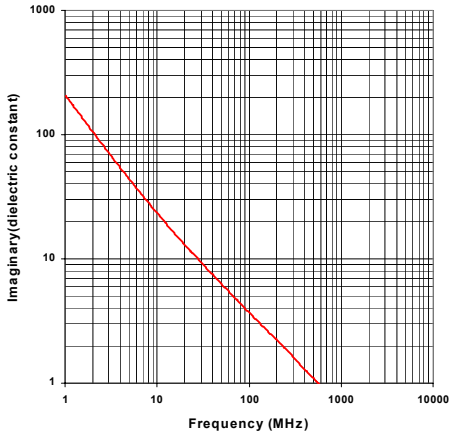

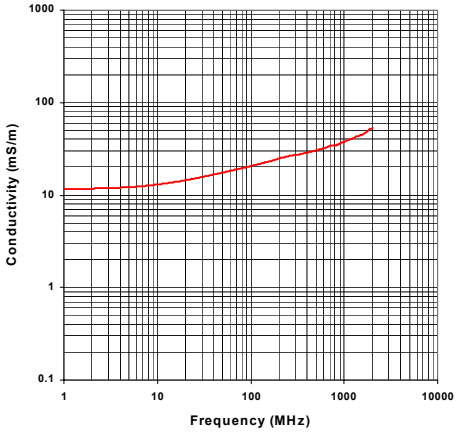

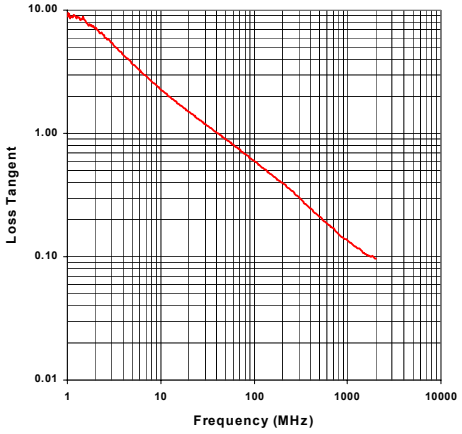

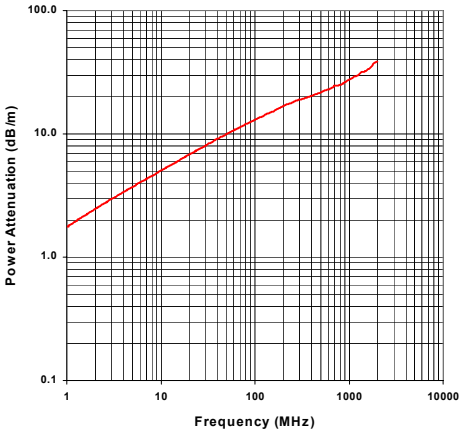

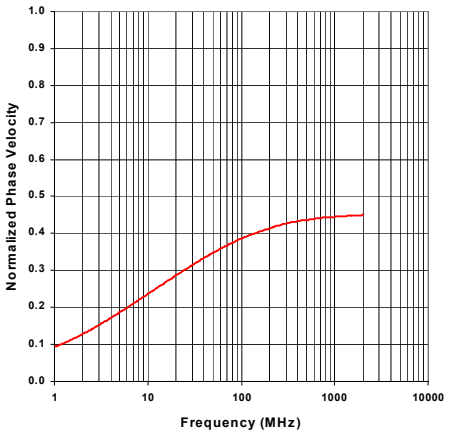

NVESD Mine Lanes

Lane 3 , S end

File : 19Sep21602

Volumetric Moisture (%) : 29.6

Dry Density (g/cc) : 1.69

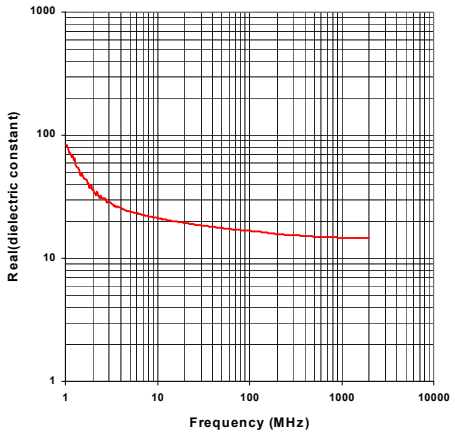

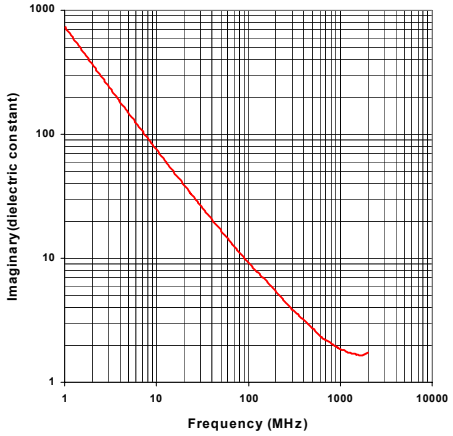

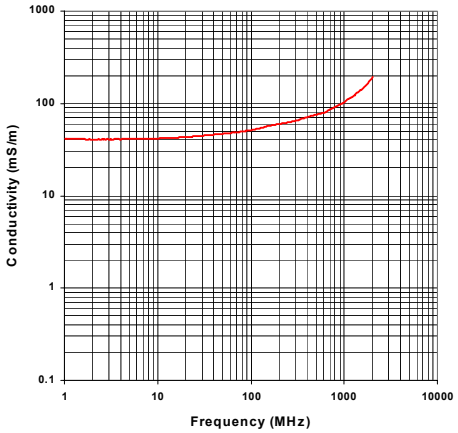

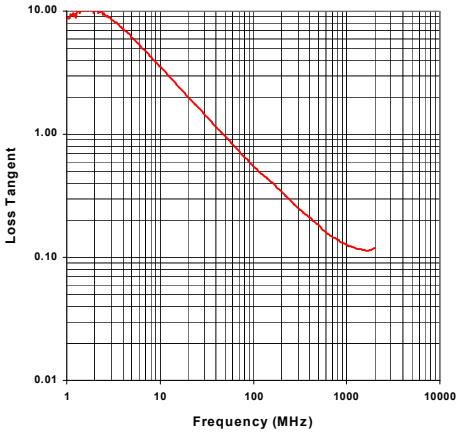

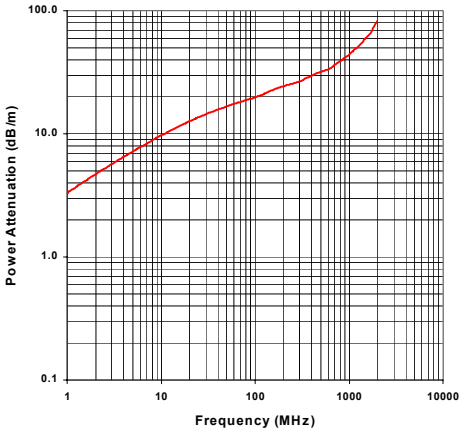

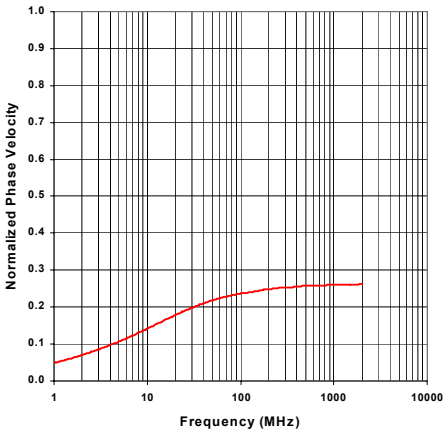

NVESD Mine Lanes

Lane 4 , N end

File : 6Sep21204

Volumetric Moisture (%) : 5.4

Dry Density (g/cc) : 1.5

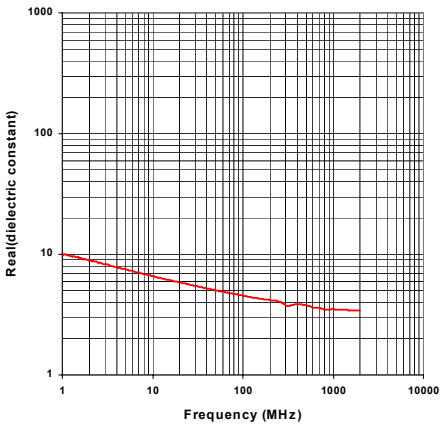

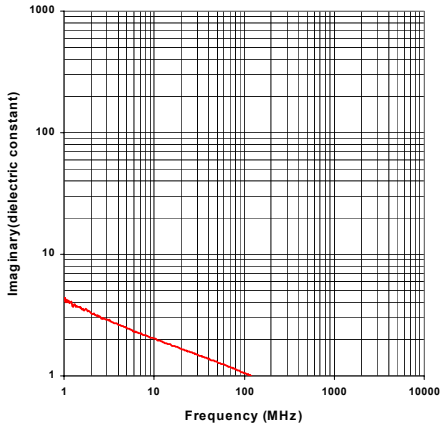

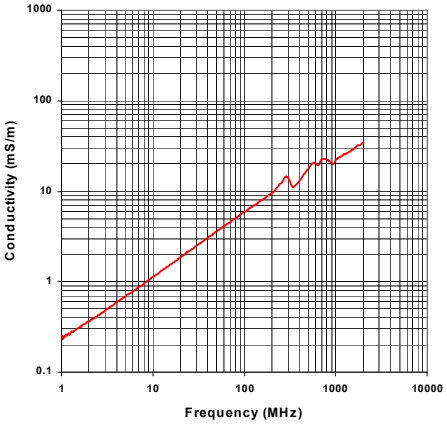

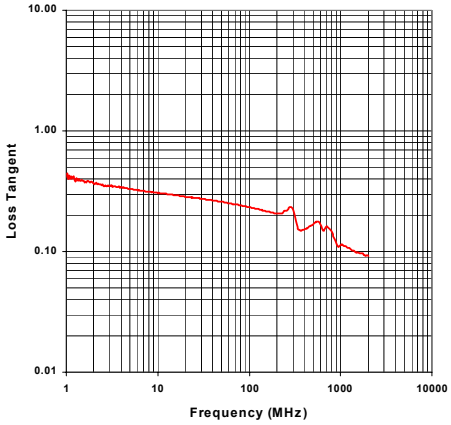

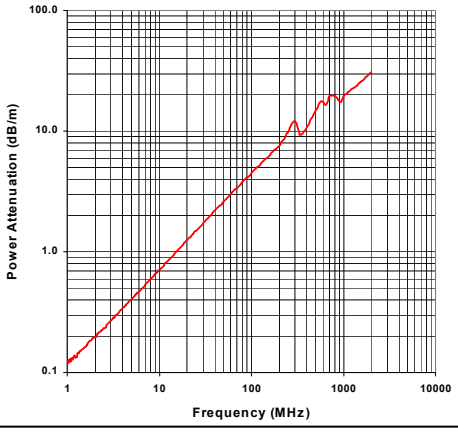

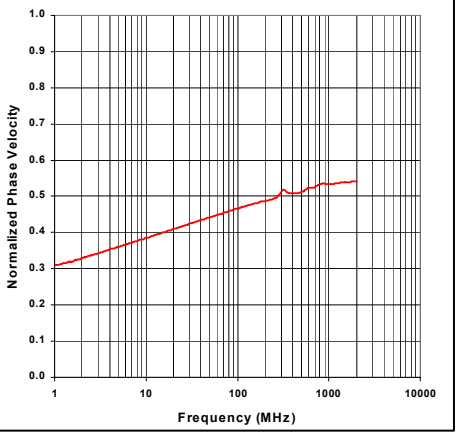

NVESD Mine Lanes

Lane 4 , N end

File : 5Sep21523

Volumetric Moisture (%) : 45.7

Dry Density (g/cc) : 1.5

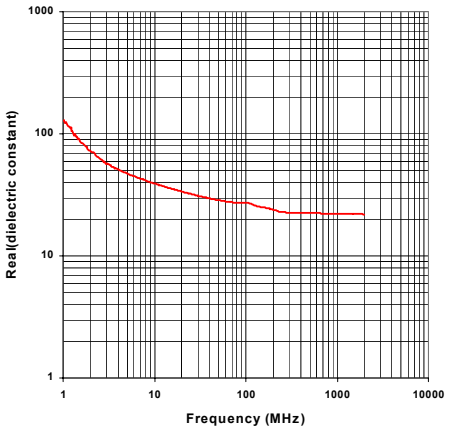

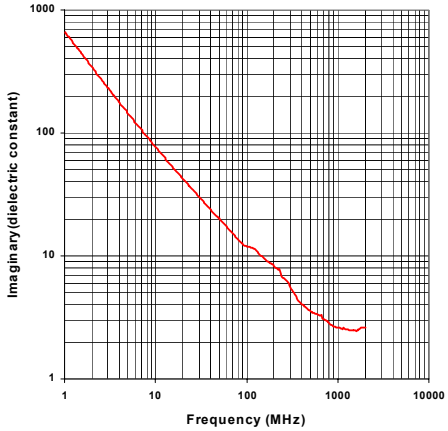

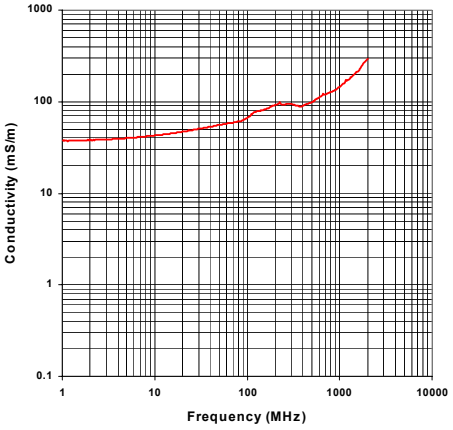

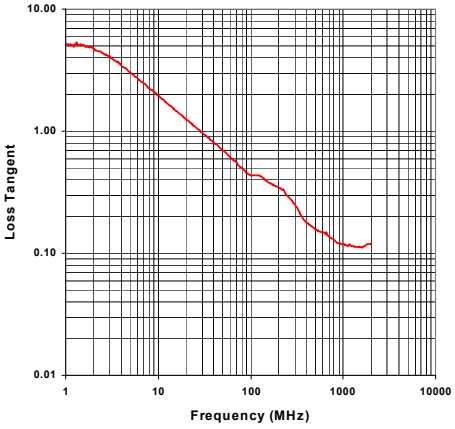

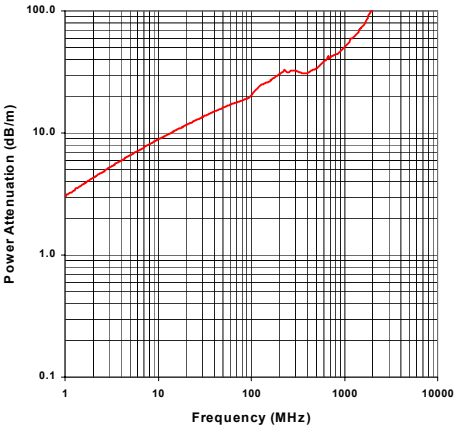

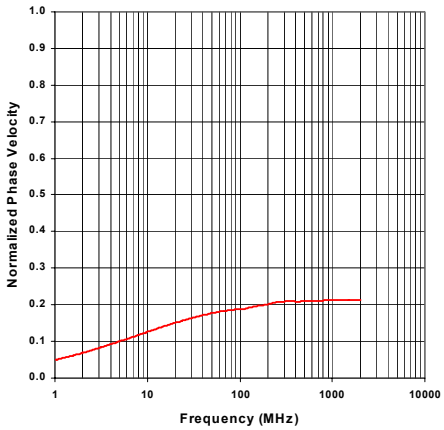

NVESD Mine Lanes

Lane 4 , N end

File : 17Sep21525

Volumetric Moisture (%) : 2

Dry Density (g/cc) : 1.18

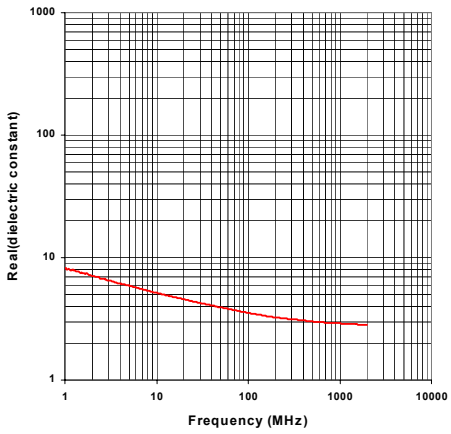

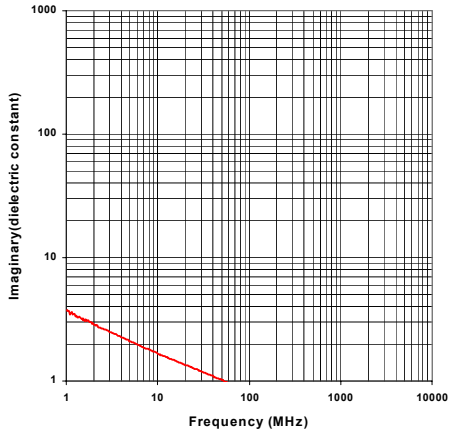

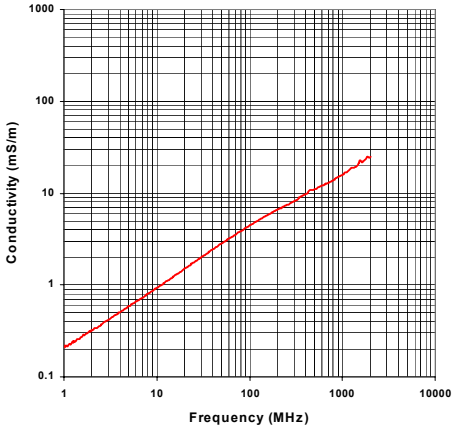

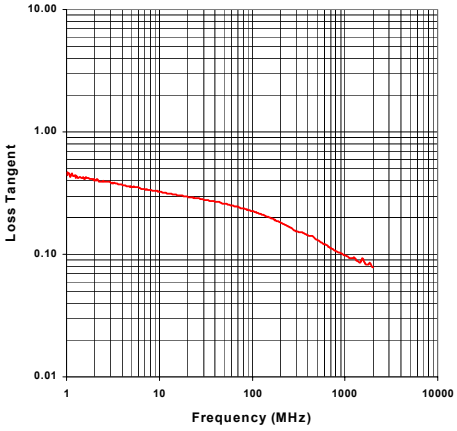

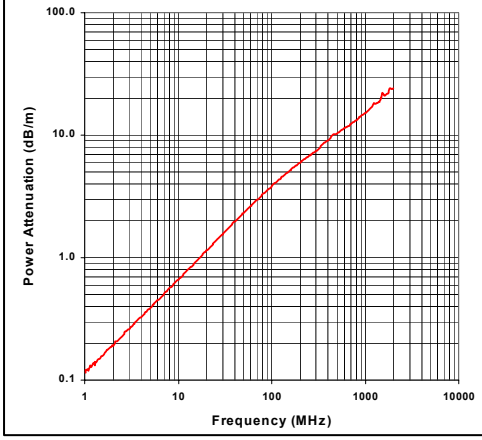

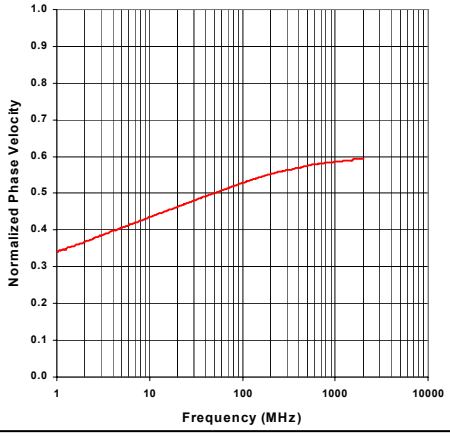

NVESD Mine Lanes

Lane 4 , N end

File : 13Sep21537

Volumetric Moisture (%) : 17.2

Dry Density (g/cc) : 1.18

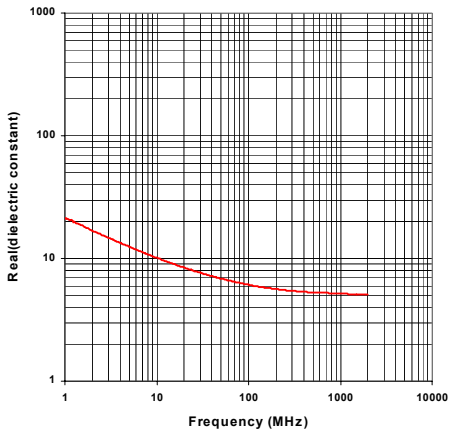

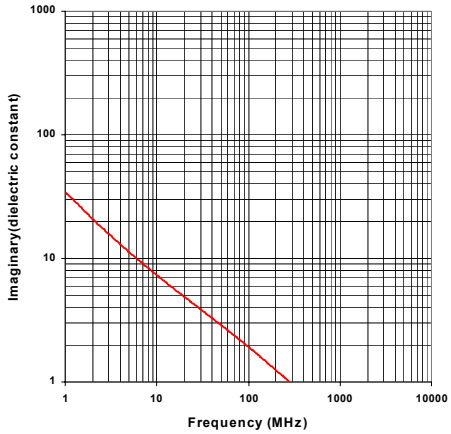

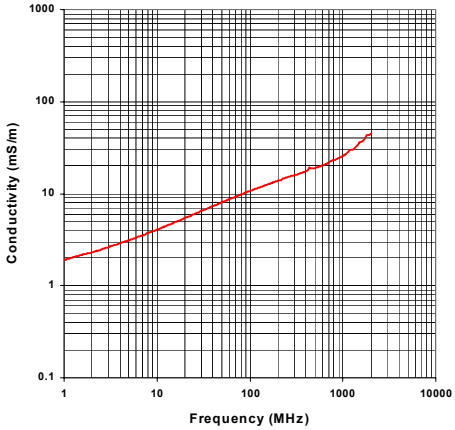

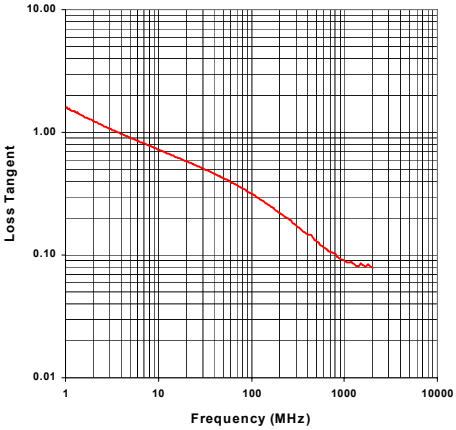

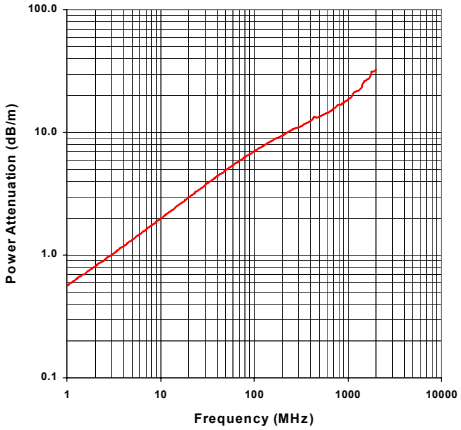

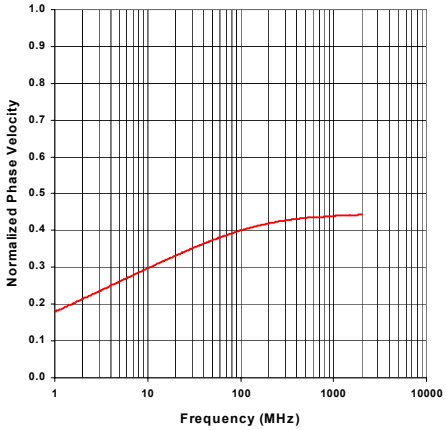

NVESD Mine Lanes

Lane 4 , N end

File : 13Sep21625

Volumetric Moisture (%) : 37.7

Dry Density (g/cc) : 1.18

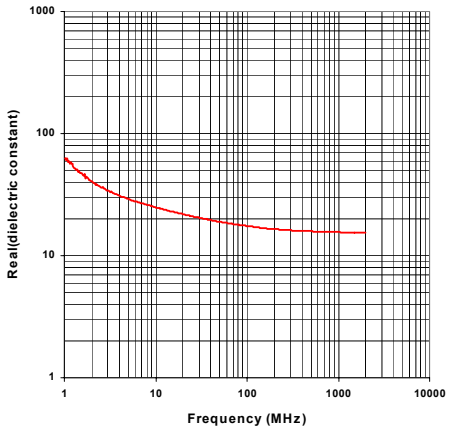

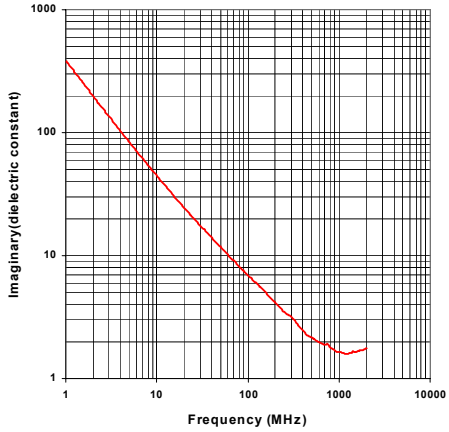

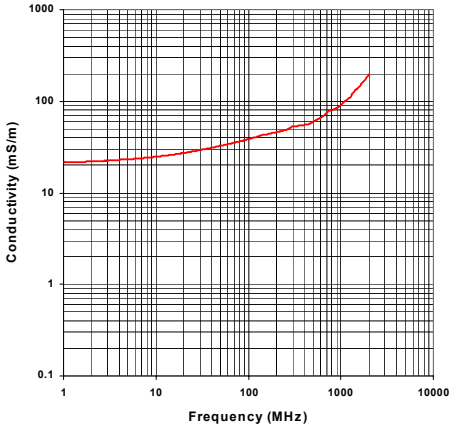

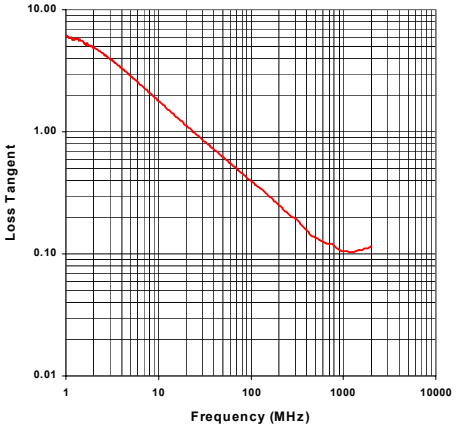

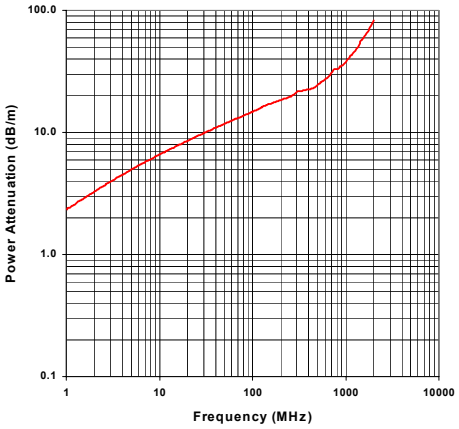

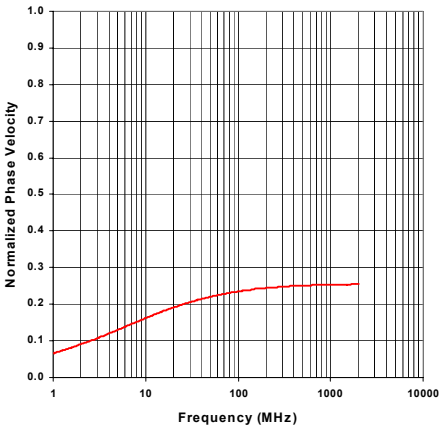

NVESD Mine Lanes

Lane 4 , Middle

File : 17Sep21603

Volumetric Moisture (%) : 4.6

Dry Density (g/cc) : 1.2

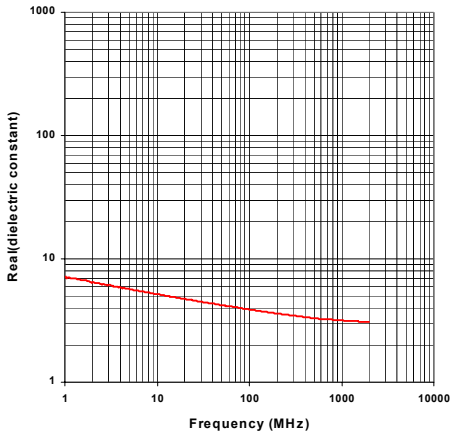

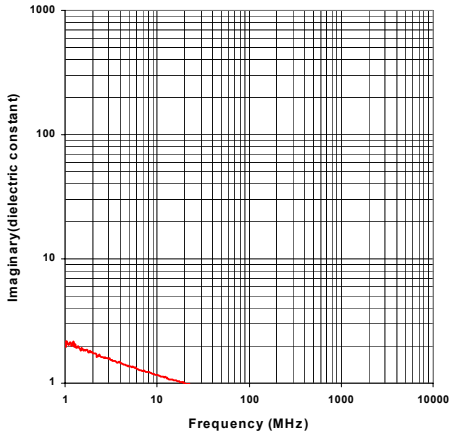

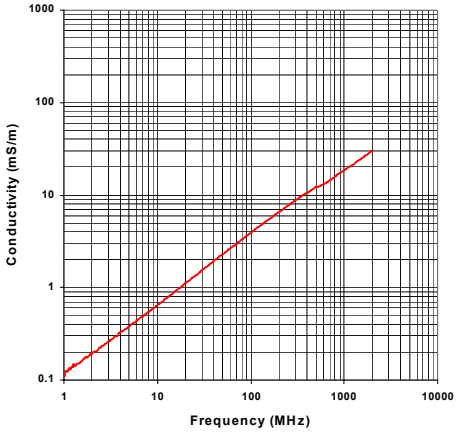

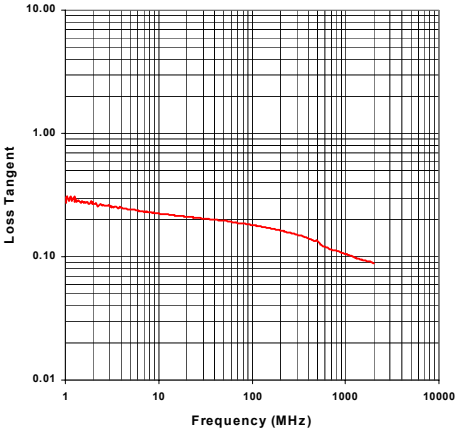

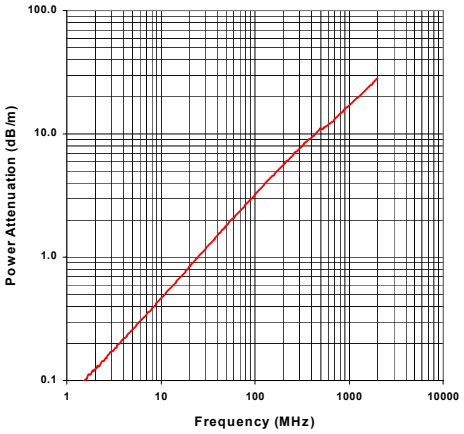

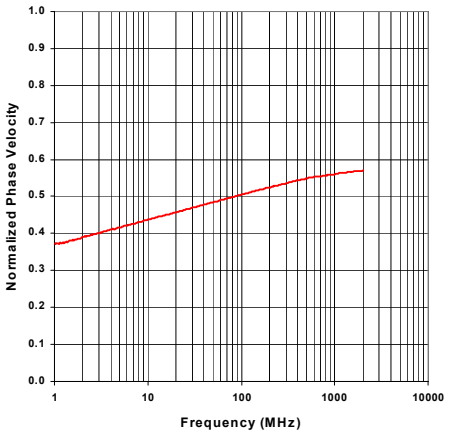

NVESD Mine Lanes

Lane 4 , Middle

File : 13Sep21614

Volumetric Moisture (%) : 20.3

Dry Density (g/cc) : 1.2

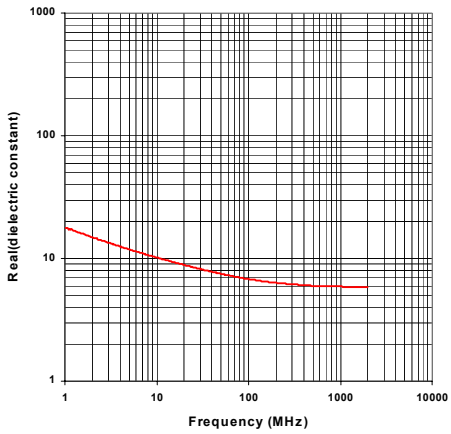

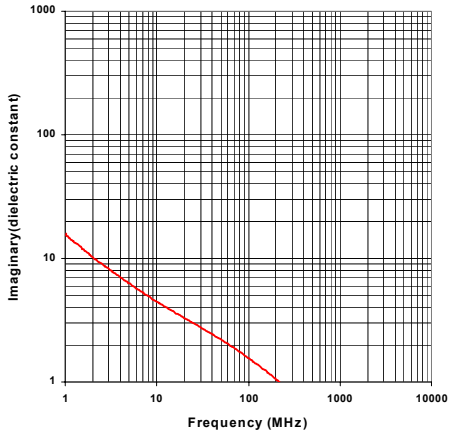

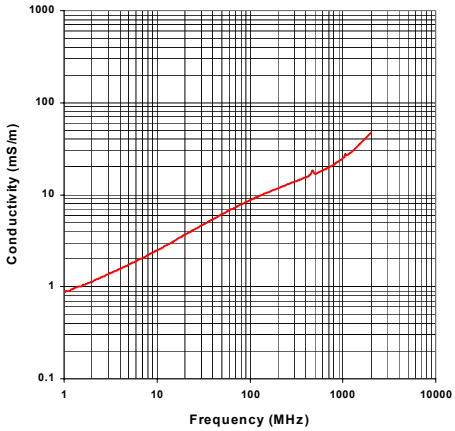

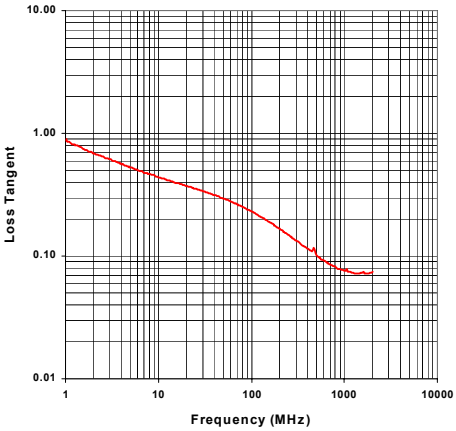

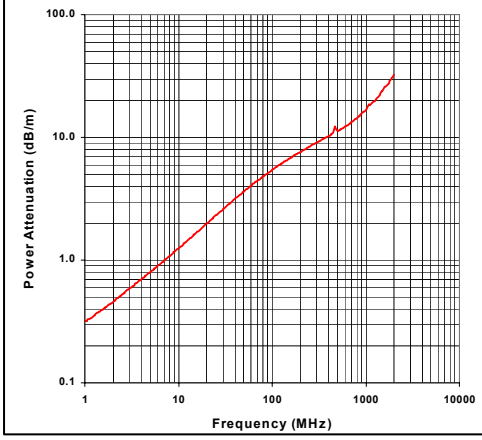

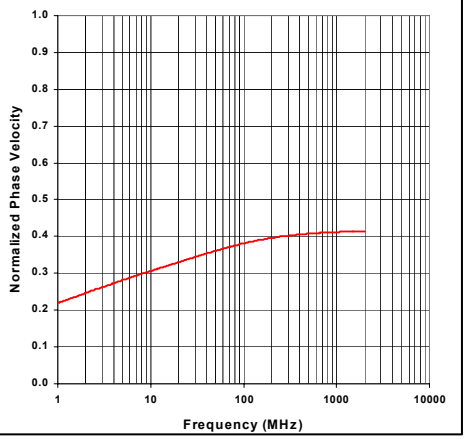

NVESD Mine Lanes

Lane 4 , Middle

File : 13Sep21707

Volumetric Moisture (%) : 44.4

Dry Density (g/cc) : 1.2

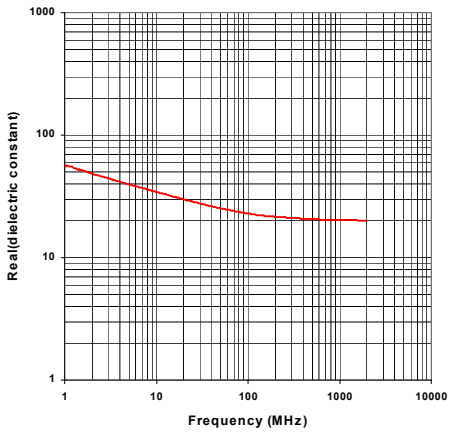

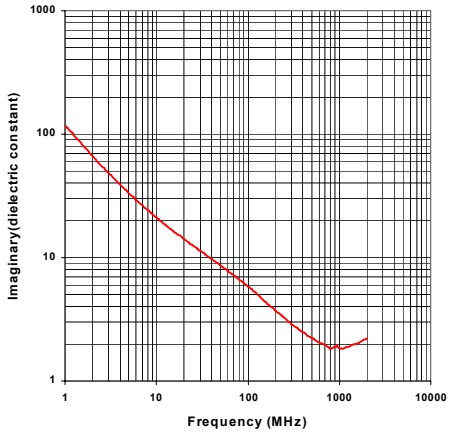

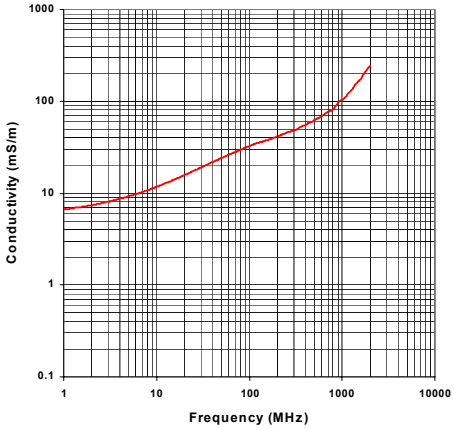

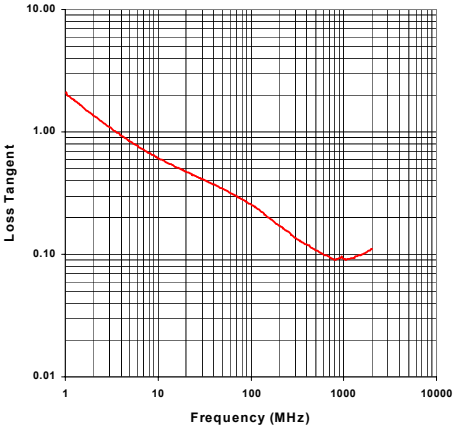

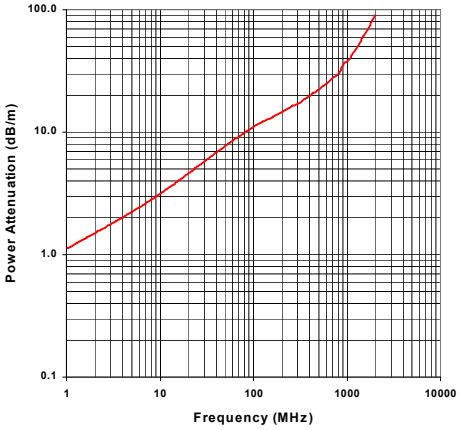

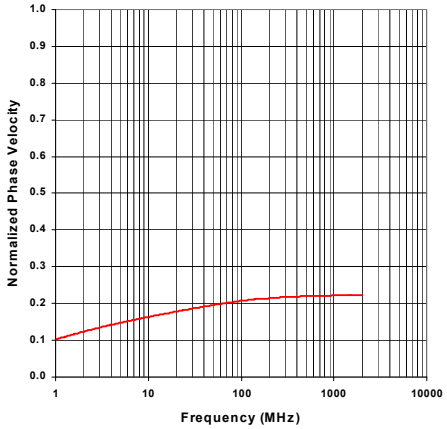

NVESD Mine Lanes

Lane 5 , N end

File : 6Sep21211

Volumetric Moisture (%) : 3

Dry Density (g/cc) : 1.58

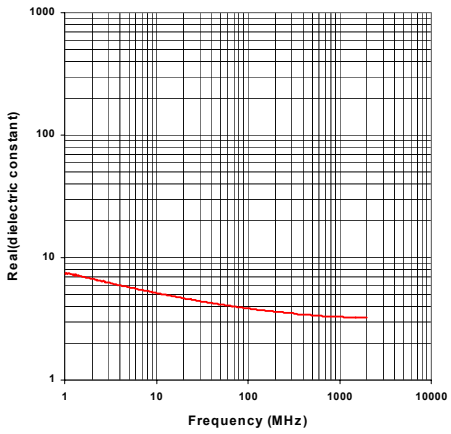

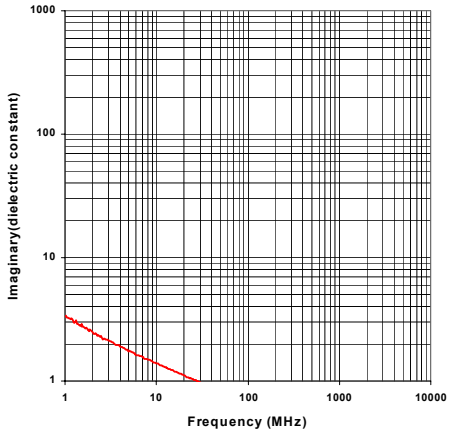

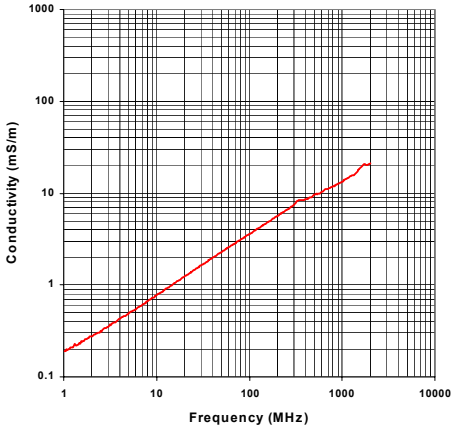

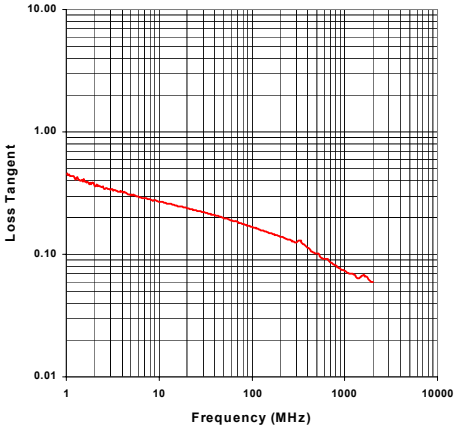

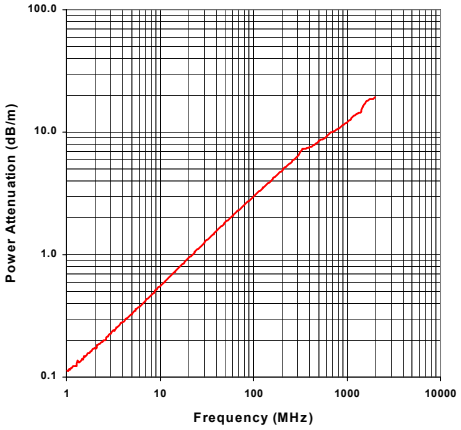

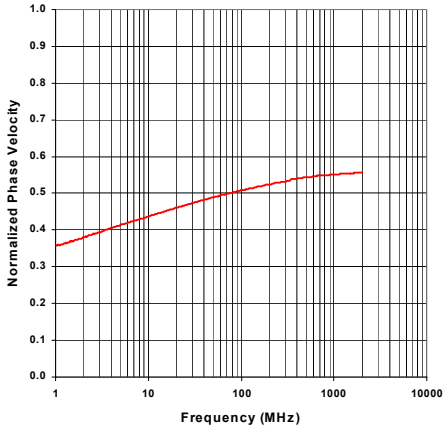

NVESD Mine Lanes

Lane 5 , N end

File : 5Sep21529

Volumetric Moisture (%) : 20.7

Dry Density (g/cc) : 1.58

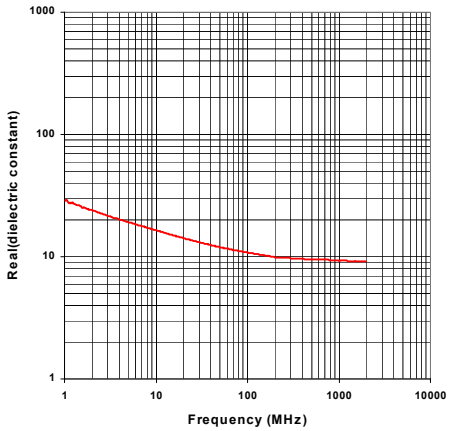

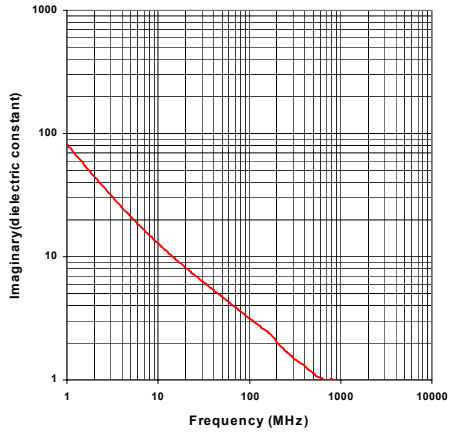

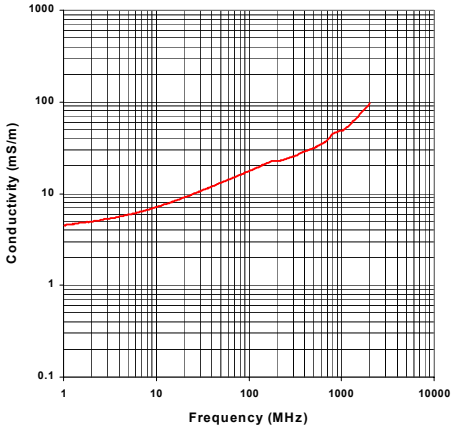

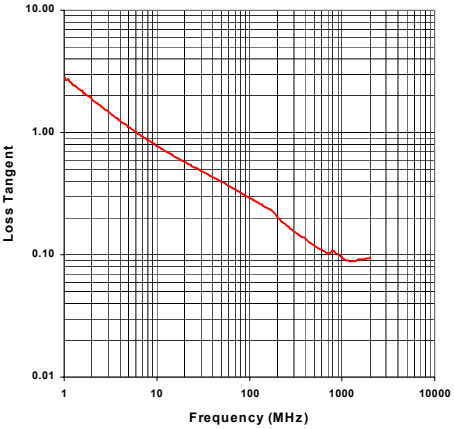

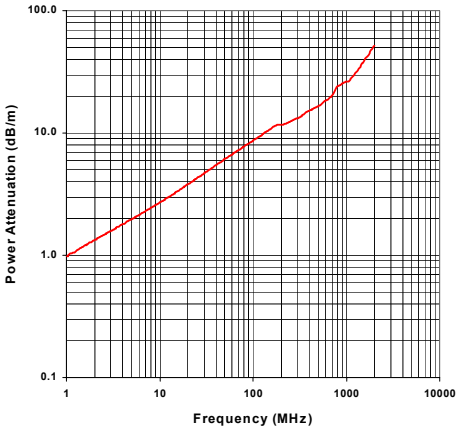

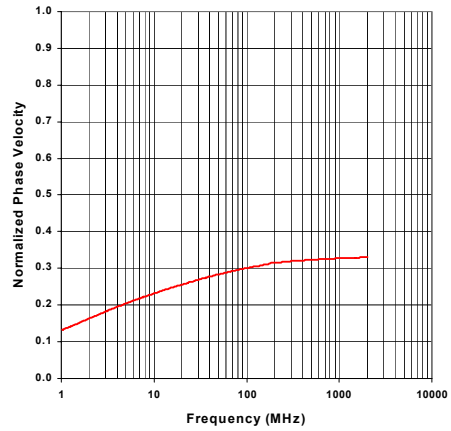

NVESD Mine Lanes

Lane 5 , N end

File : 6Sep21626

Volumetric Moisture (%) : 28.6

Dry Density (g/cc) : 1.58

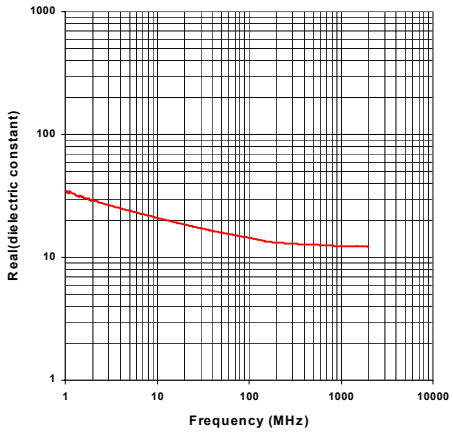

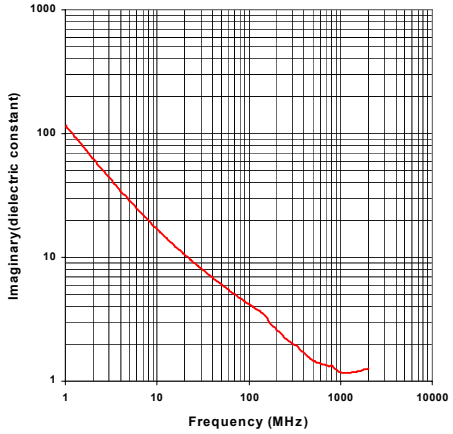

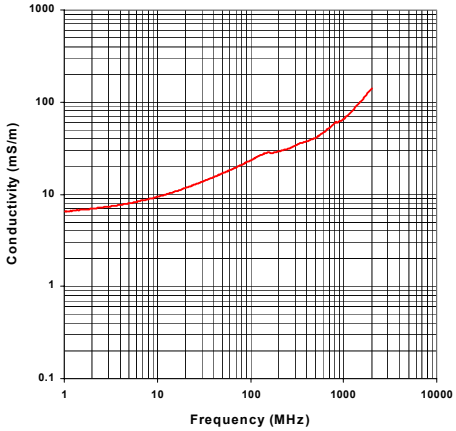

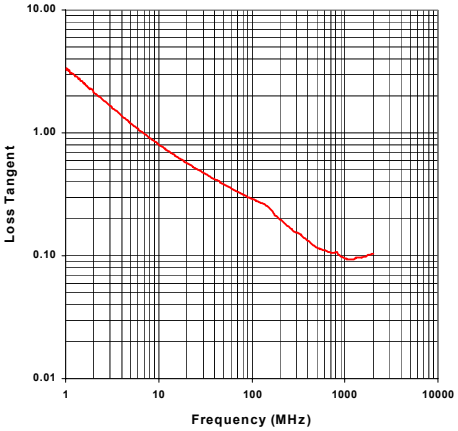

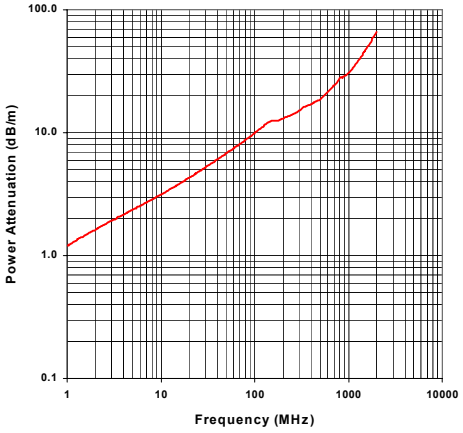

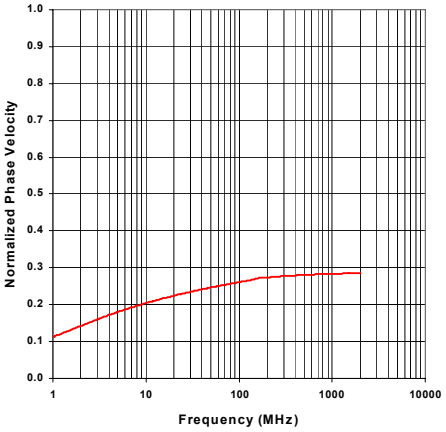

NVESD Mine Lanes

Lane 5 , Middle

File : 6Sep21225

Volumetric Moisture (%) : 4.1

Dry Density (g/cc) : 1.49

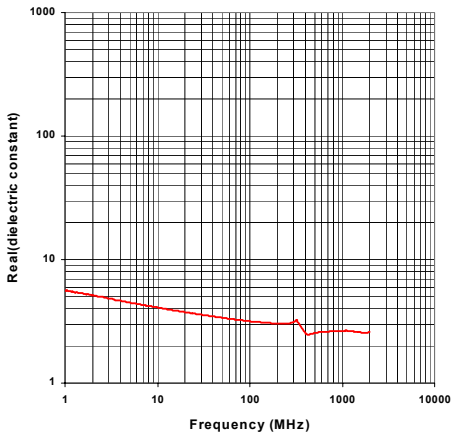

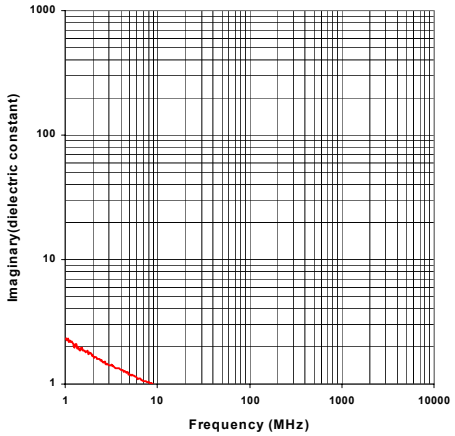

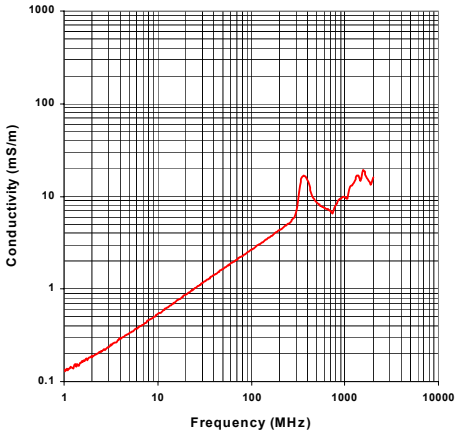

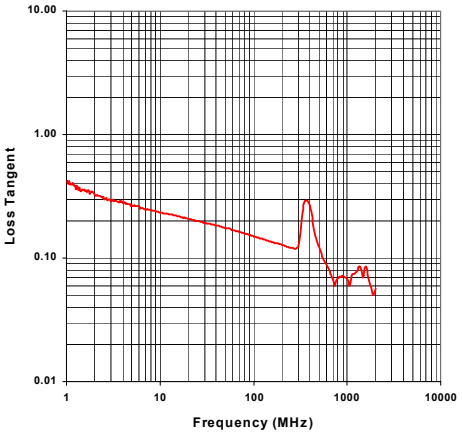

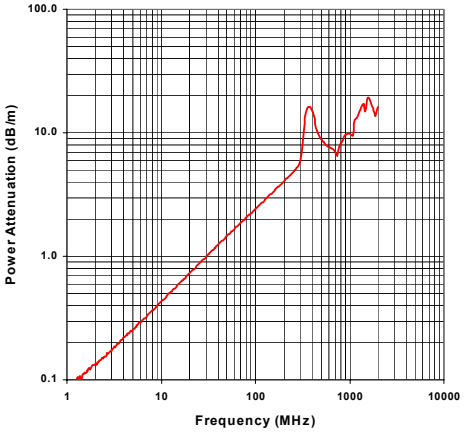

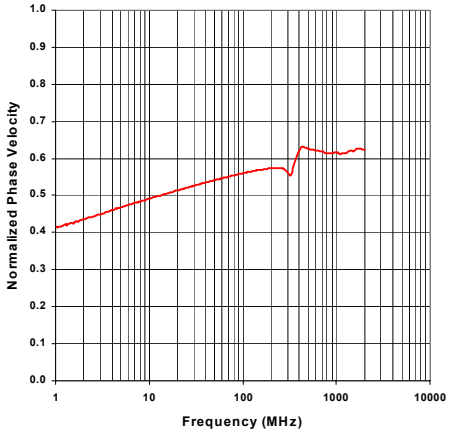

NVESD Mine Lanes

Lane 5 , Middle

File : 5Sep21541

Volumetric Moisture (%) : 25.1

Dry Density (g/cc) : 1.49

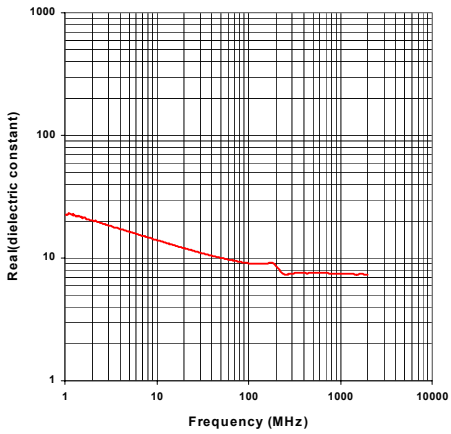

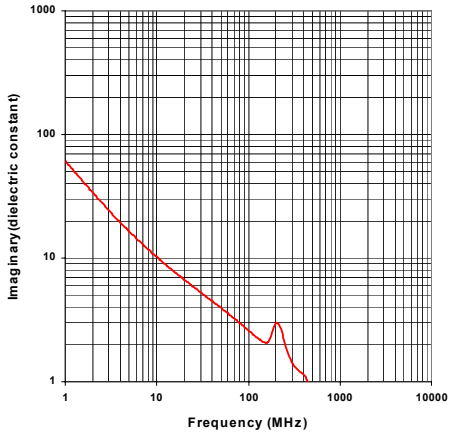

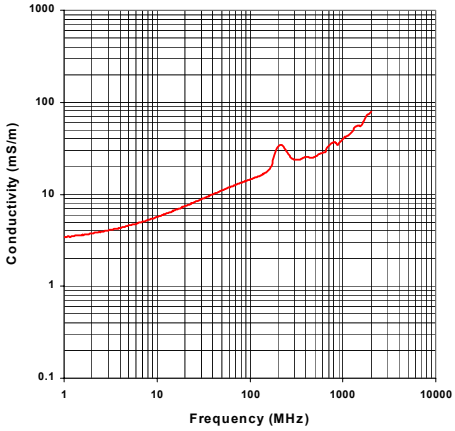

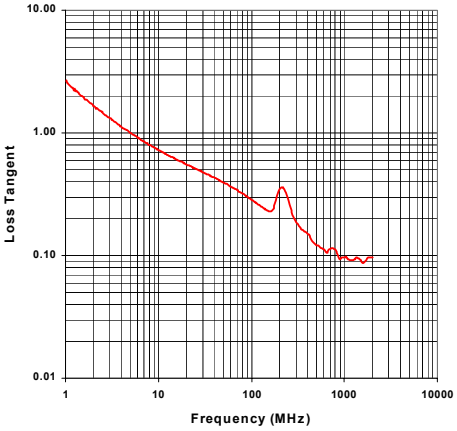

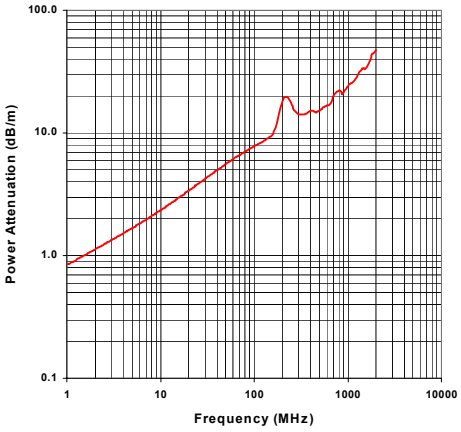

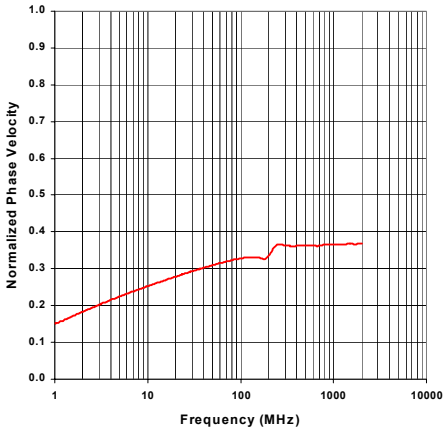

NVESD Mine Lanes

Lane 5 , Middle

File : 6Sep21637

Volumetric Moisture (%) : 36.7

Dry Density (g/cc) : 1.49

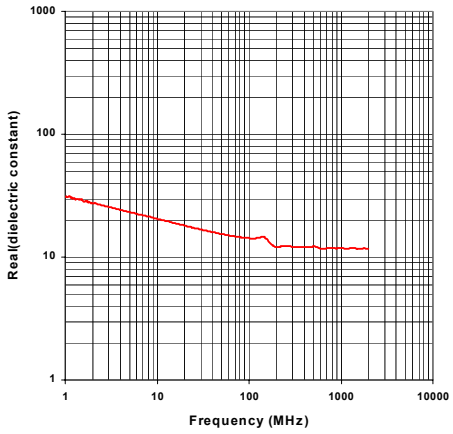

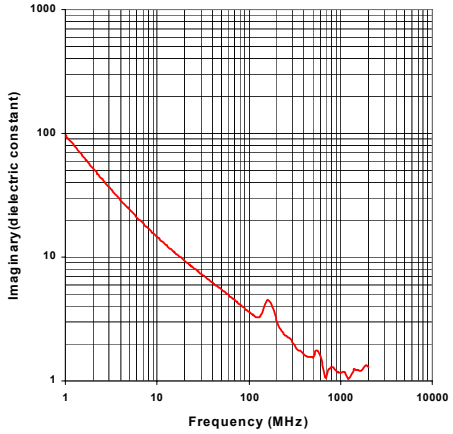

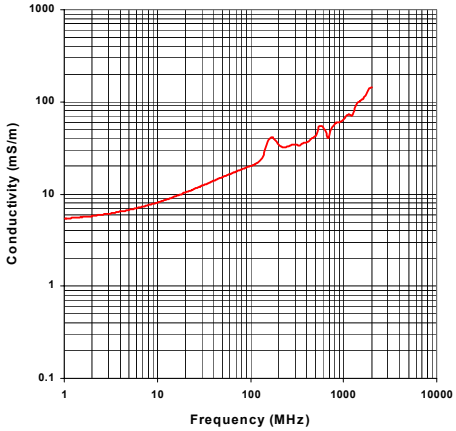

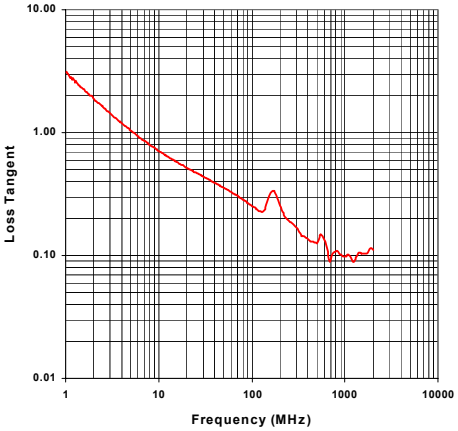

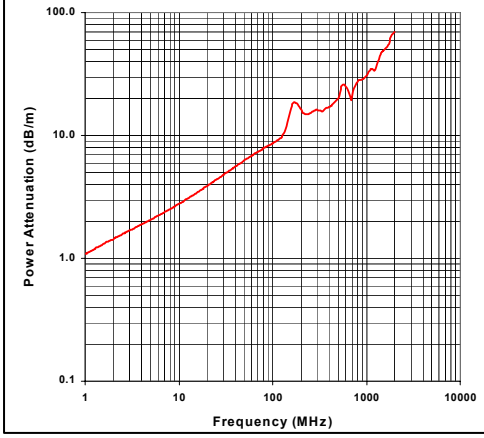

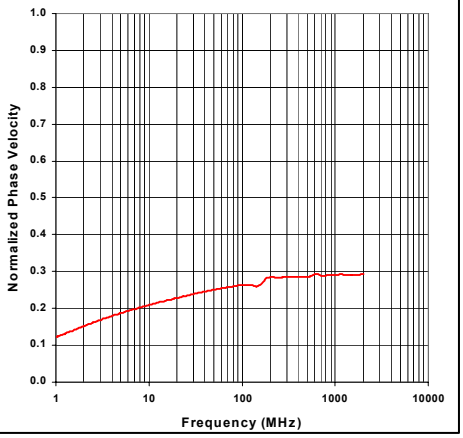

NVESD Mine Lanes

Lane 5 , S end

File : 17Sep21608

Volumetric Moisture (%) : 3.9

Dry Density (g/cc) : 1.33

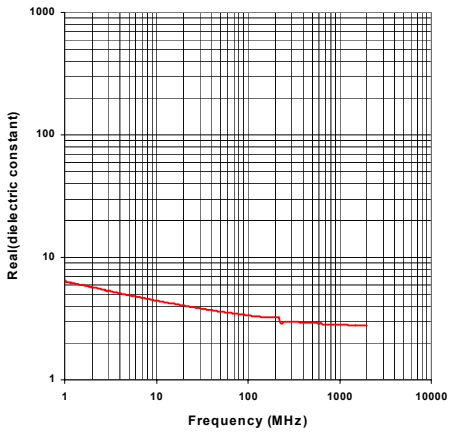

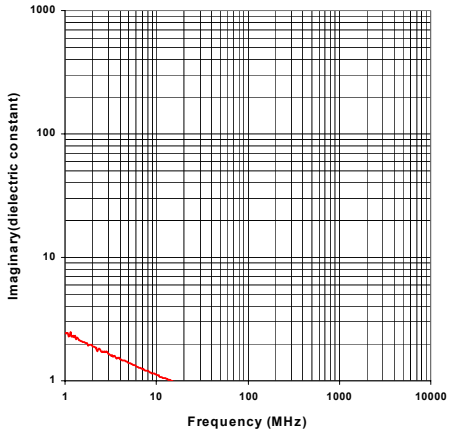

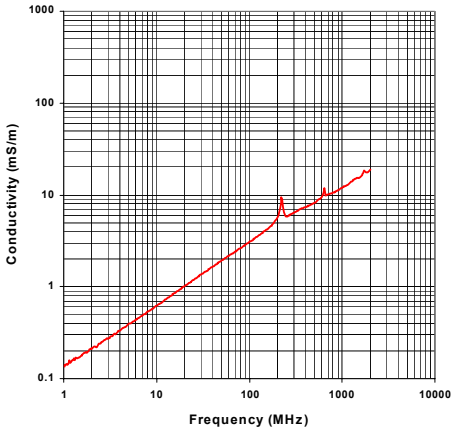

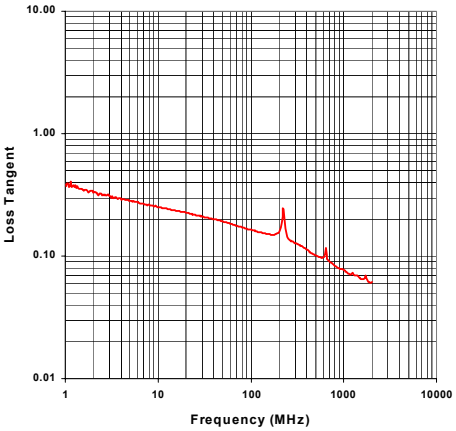

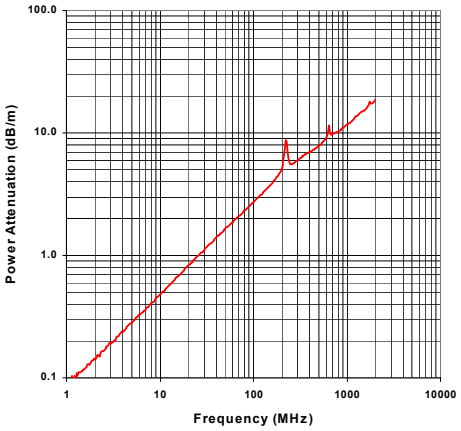

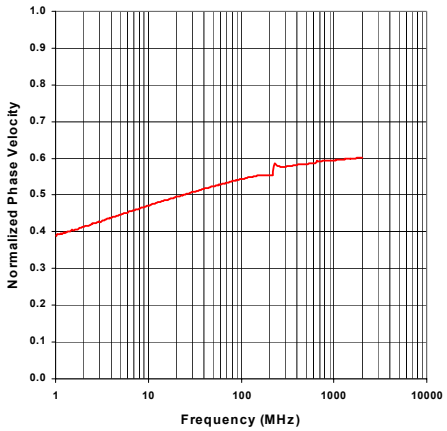

NVESD Mine Lanes

Lane 5 , S end

File : 13Sep21620

Volumetric Moisture (%) : 16.4

Dry Density (g/cc) : 1.33

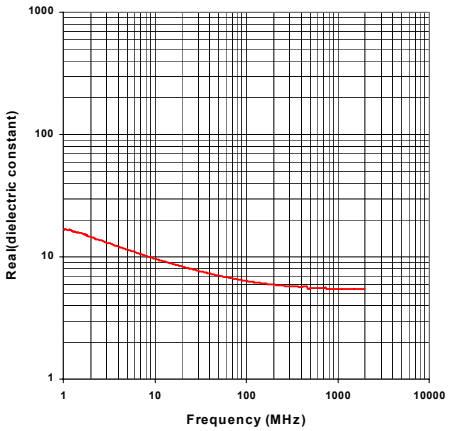

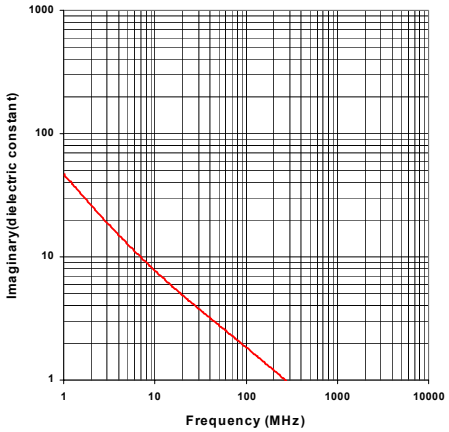

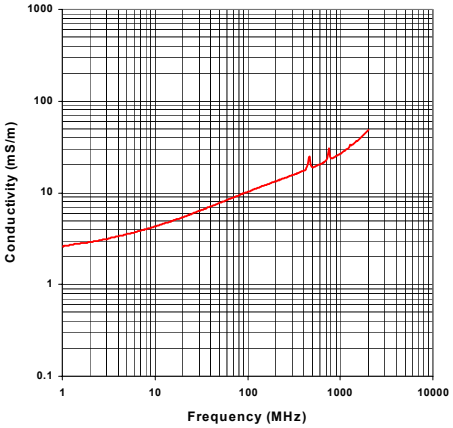

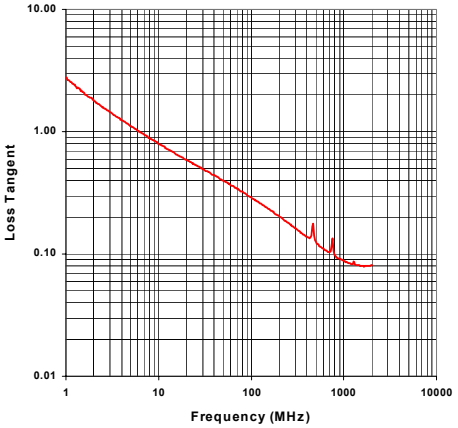

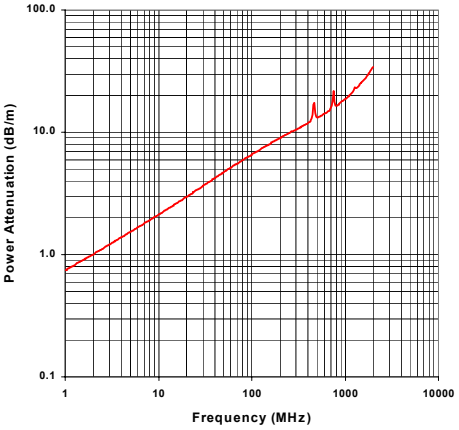

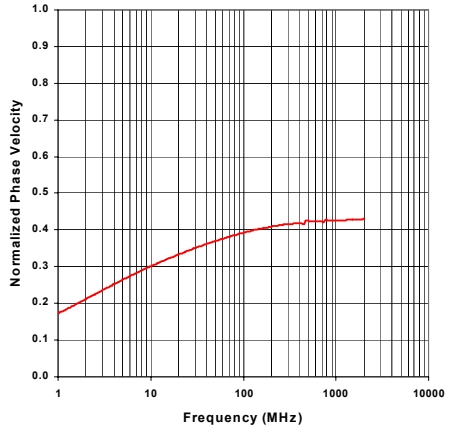

NVESD Mine Lanes

Lane 5 , S end

File : 13Sep21713

Volumetric Moisture (%) : 37.8

Dry Density (g/cc) : 1.33

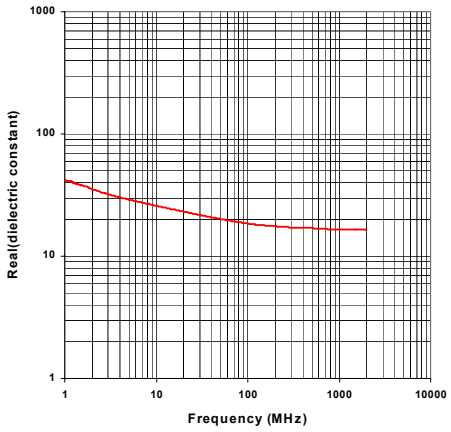

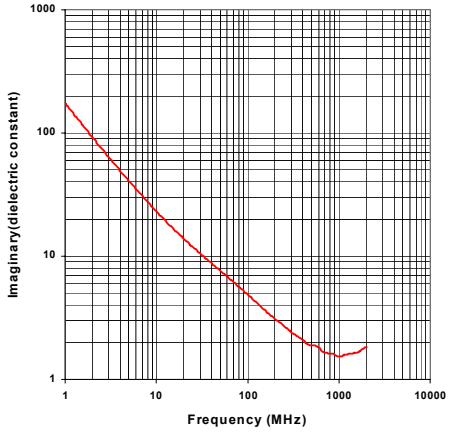

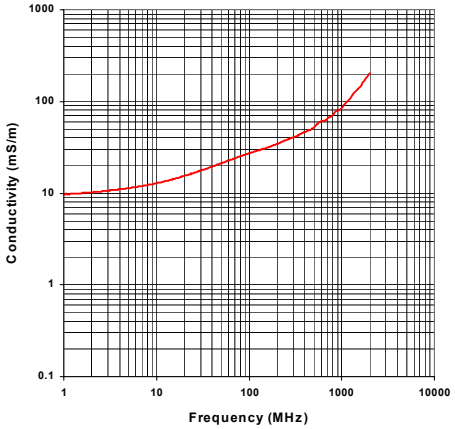

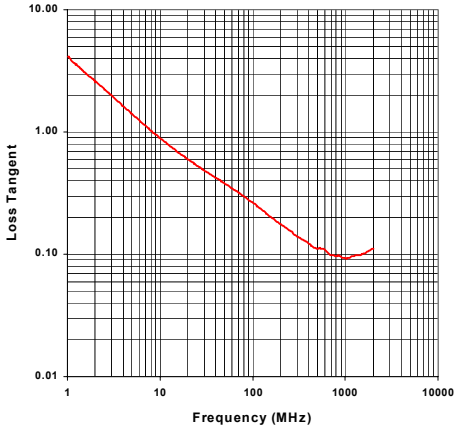

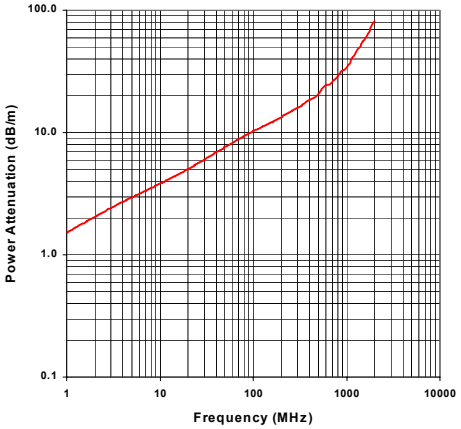

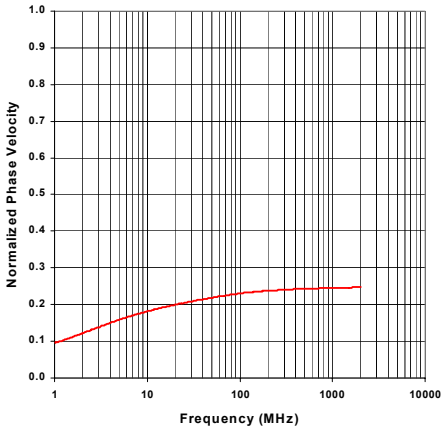

NVESD Mine Lanes

Lane 6 , N end

File : 5Sep21535

Volumetric Moisture (%) : 1.8

Dry Density (g/cc) : 1.6

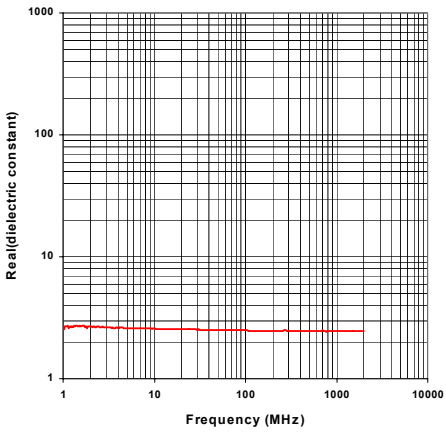

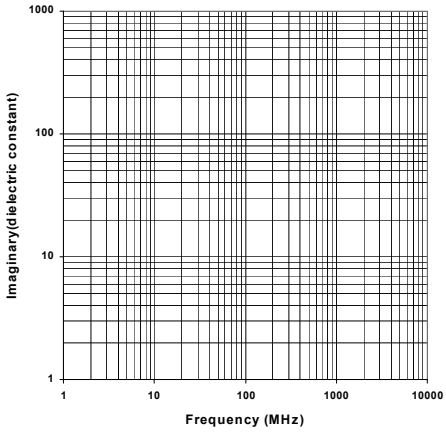

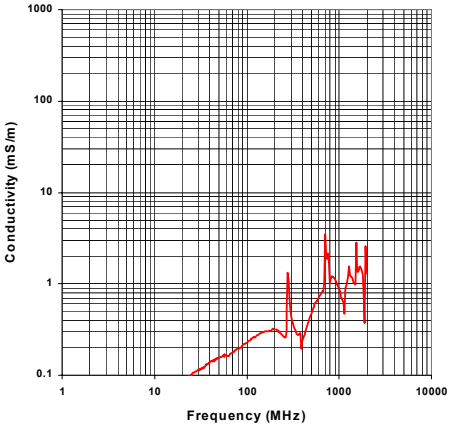

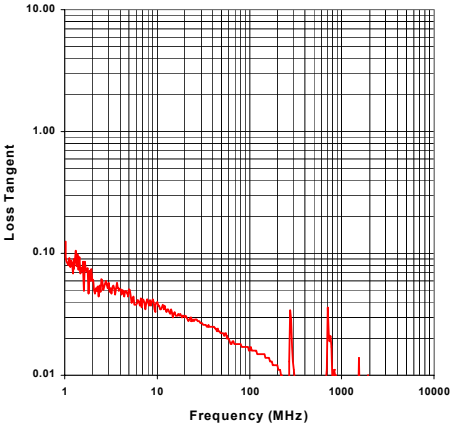

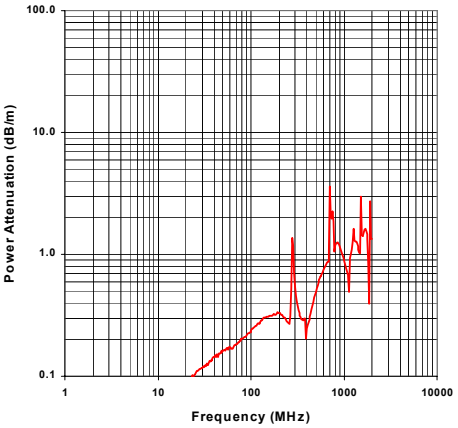

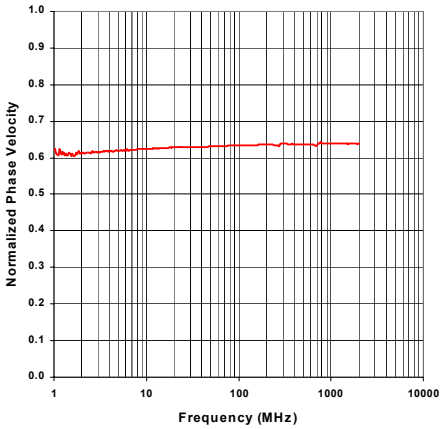

NVESD Mine Lanes

Lane 6 , N end

File : 6Sep21217

Volumetric Moisture (%) : 17.9

Dry Density (g/cc) : 1.6

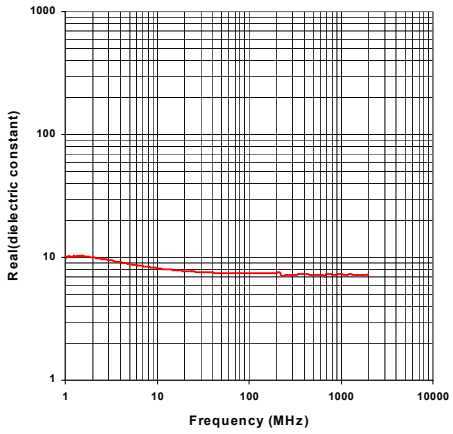

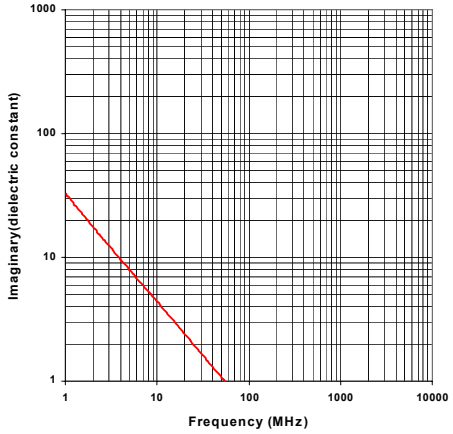

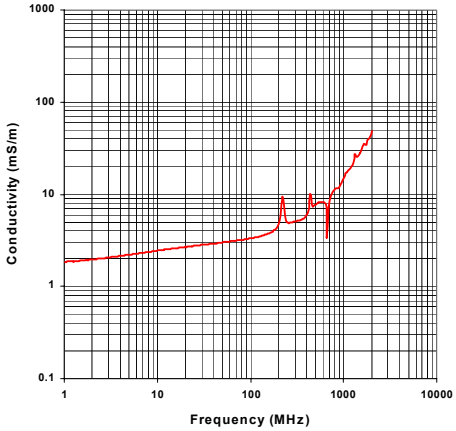

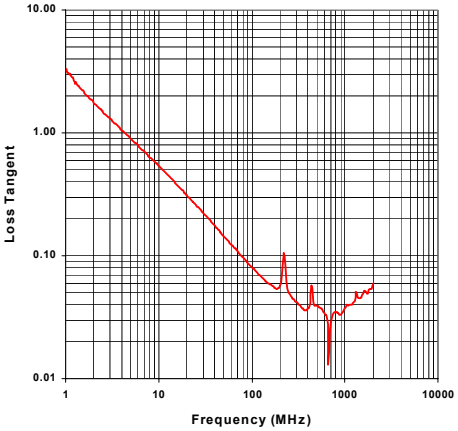

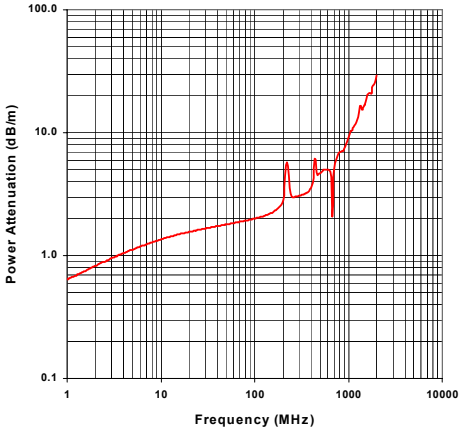

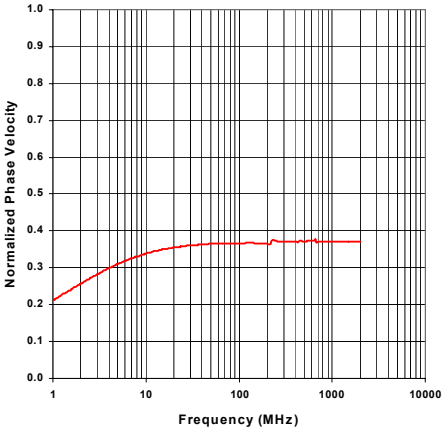

NVESD Mine Lanes

Lane 6 , N end

File : 6Sep21631

Volumetric Moisture (%) : 44.1

Dry Density (g/cc) : 1.6

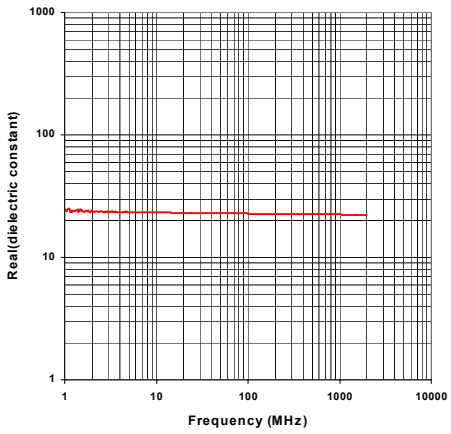

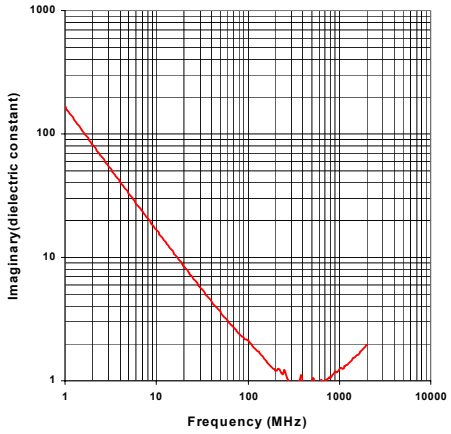

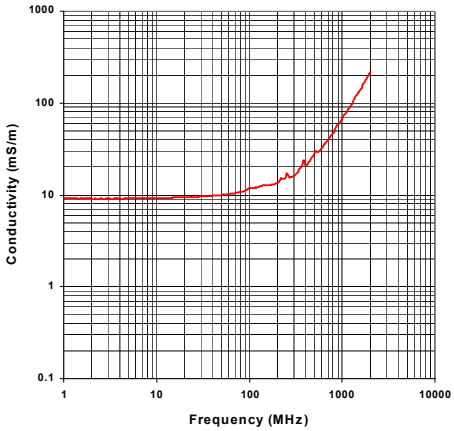

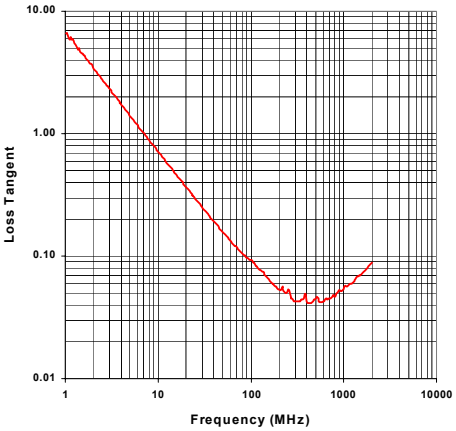

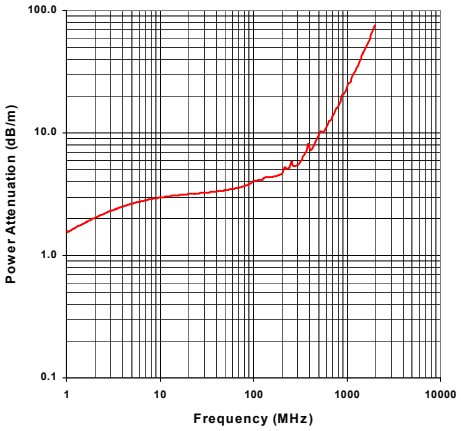

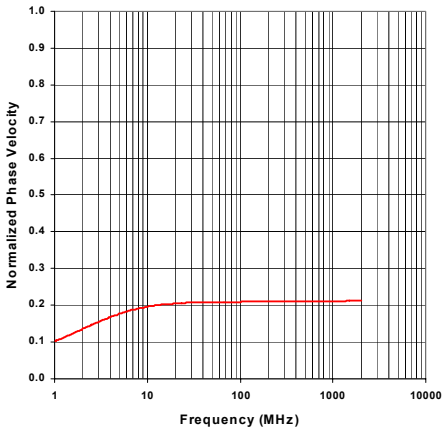

NVESD Mine Lanes

Lane 6 , N end

File : 6Sep21312

Volumetric Moisture (%) : 45.4

Dry Density (g/cc) : 1.6

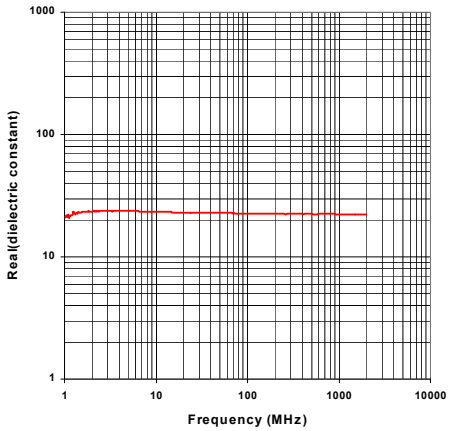

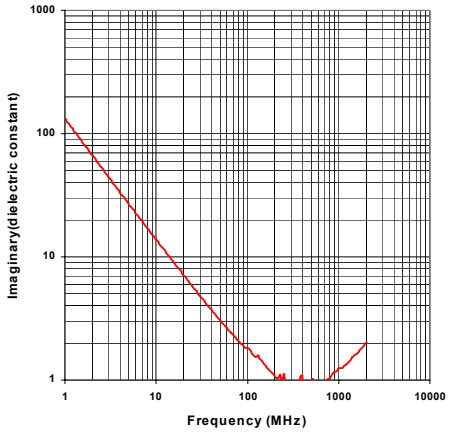

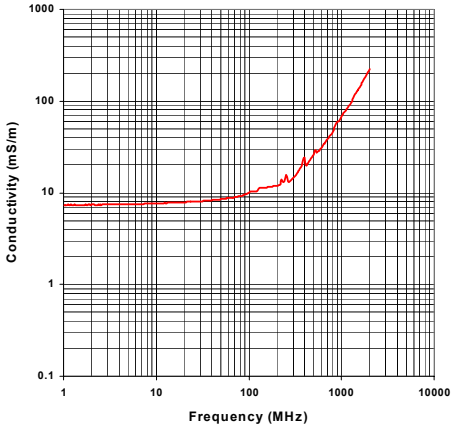

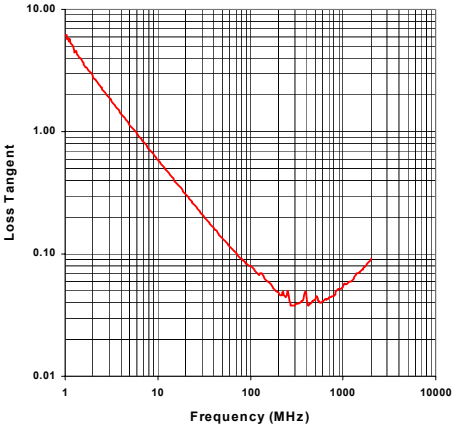

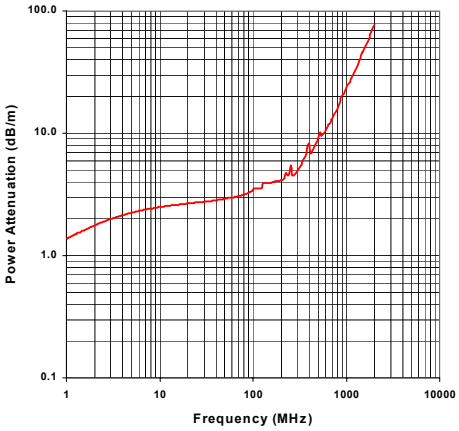

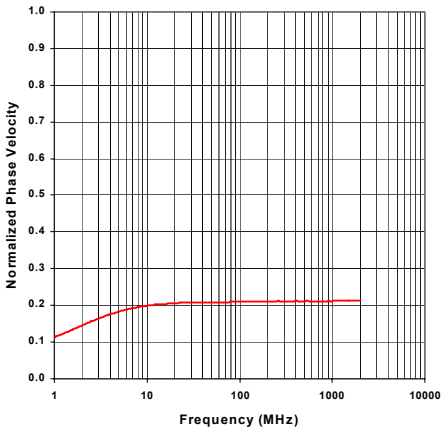

NVESD Mine Lanes

Lane 6 , N end

File : 13Sep21544

Volumetric Moisture (%) : -0.1

Dry Density (g/cc) : 1.68

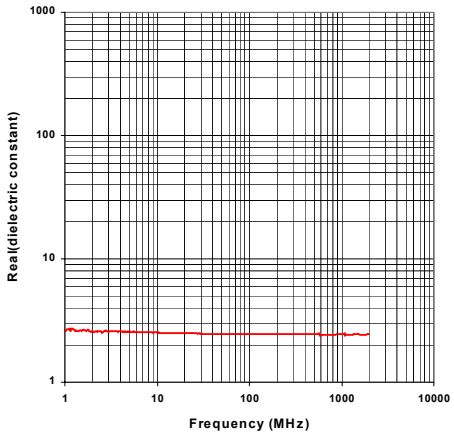

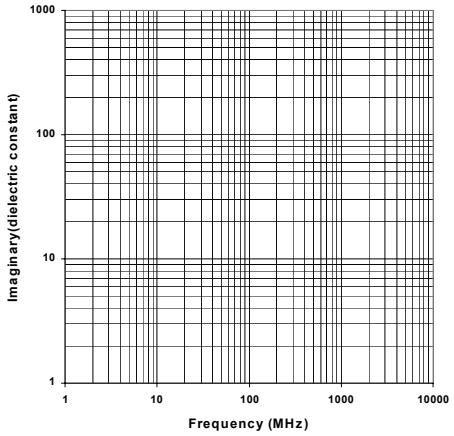

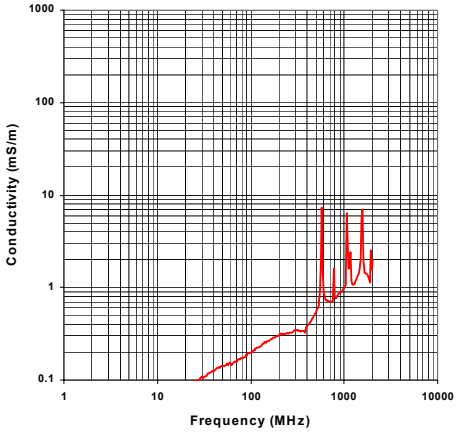

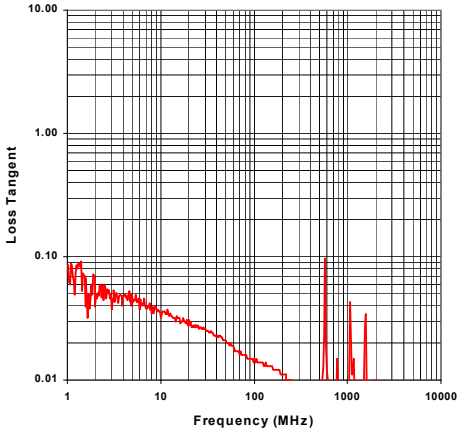

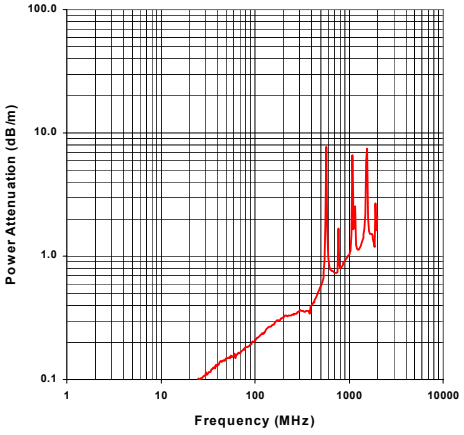

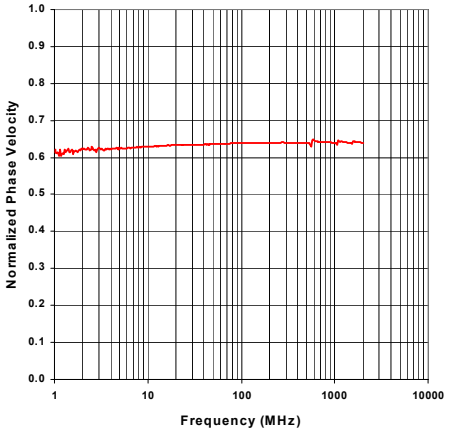

NVESD Mine Lanes

Lane 6 , N end

File : 17Sep21534

Volumetric Moisture (%) : -0.1

Dry Density (g/cc) : 1.68

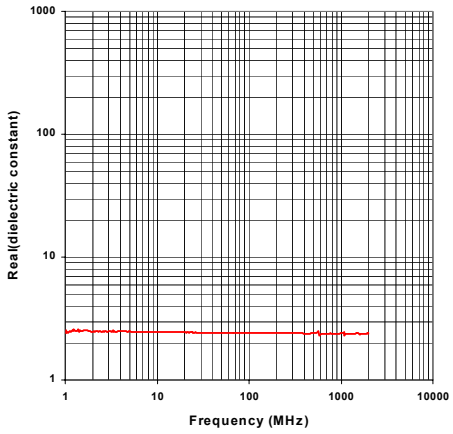

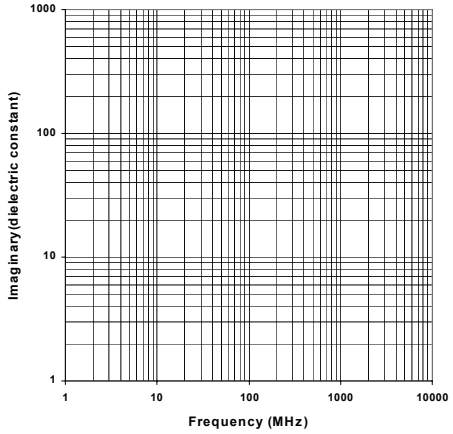

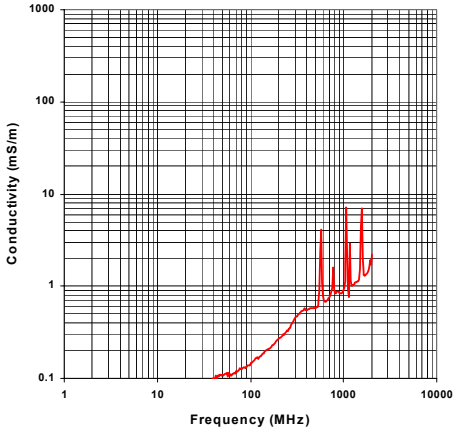

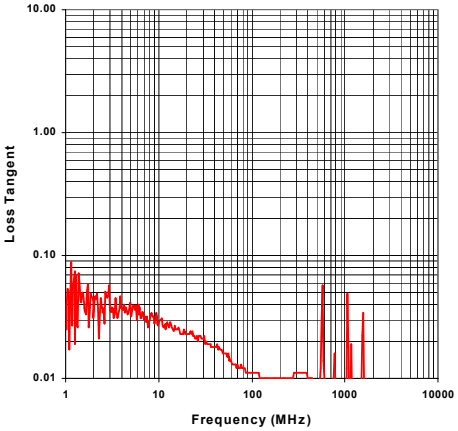

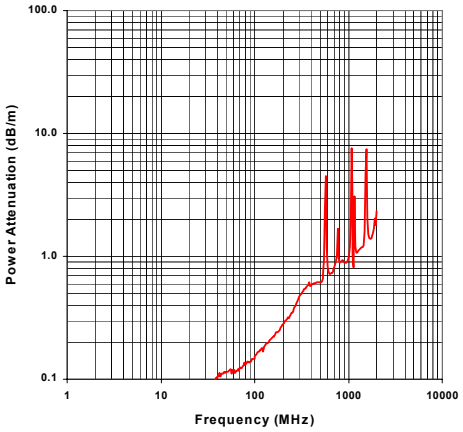

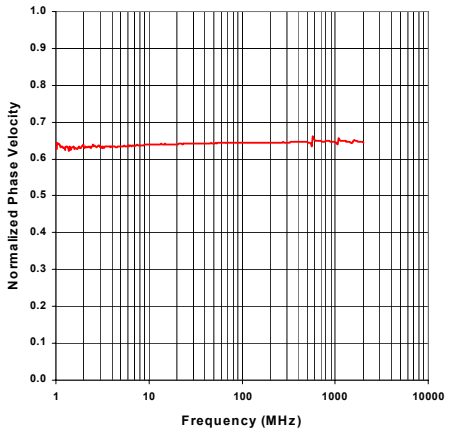

NVESD Mine Lanes

Lane 6 , N end

File : 13Sep21631

Volumetric Moisture (%) : 20.1

Dry Density (g/cc) : 1.68

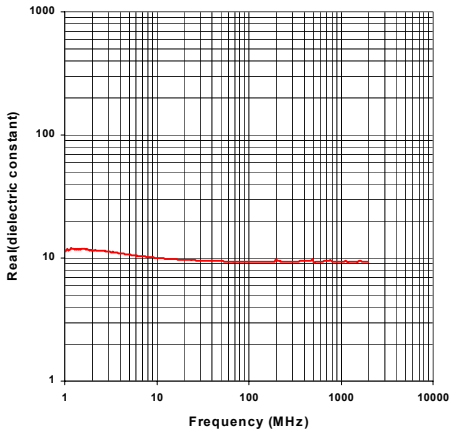

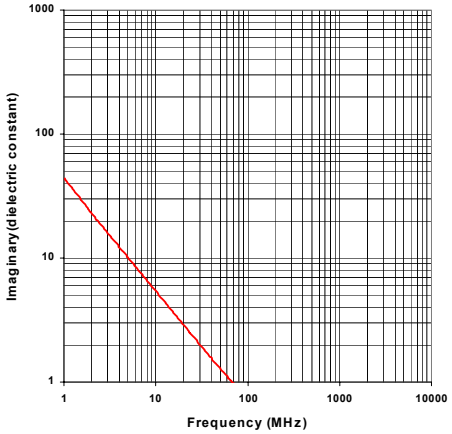

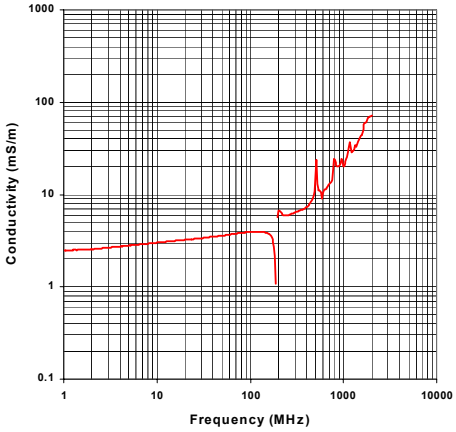

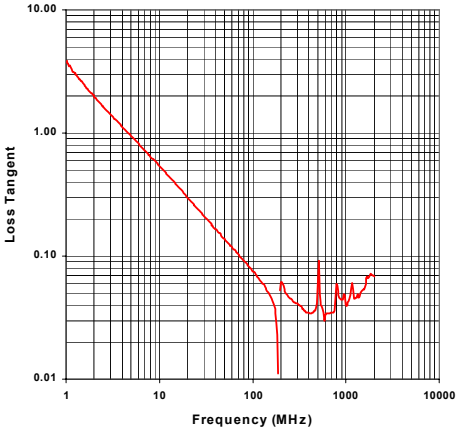

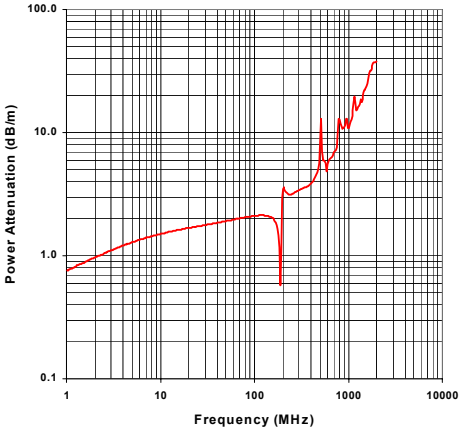

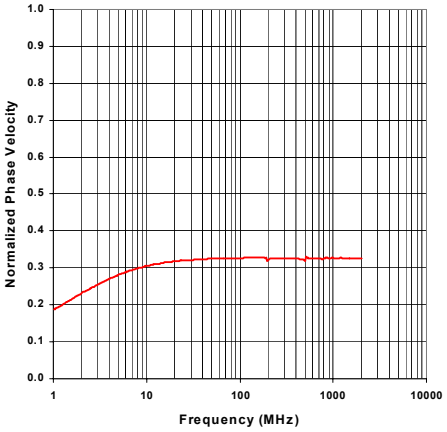

NVESD Mine Lanes

Lane 6 , N end

File : 13Sep21637

Volumetric Moisture (%) : 37.8

Dry Density (g/cc) : 1.68

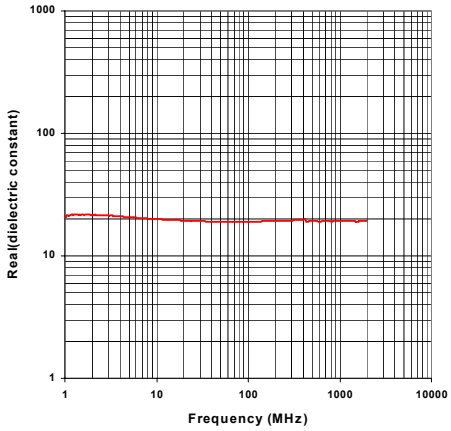

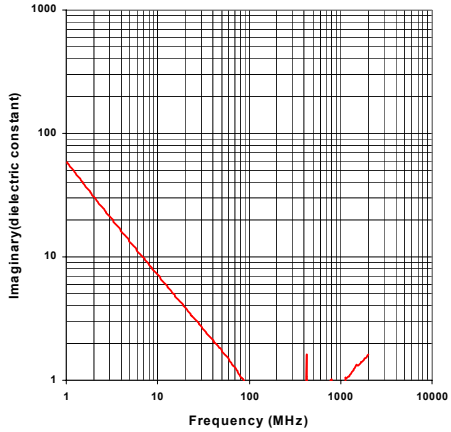

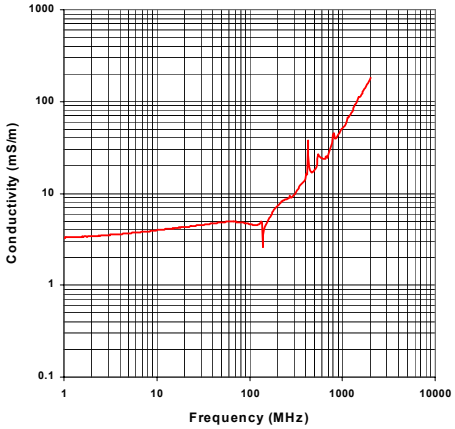

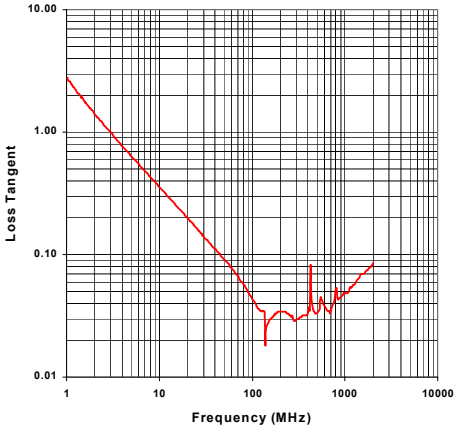

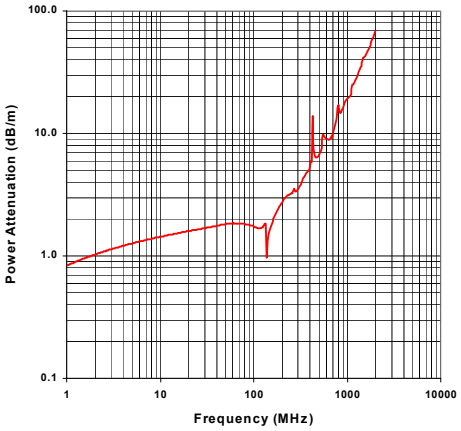

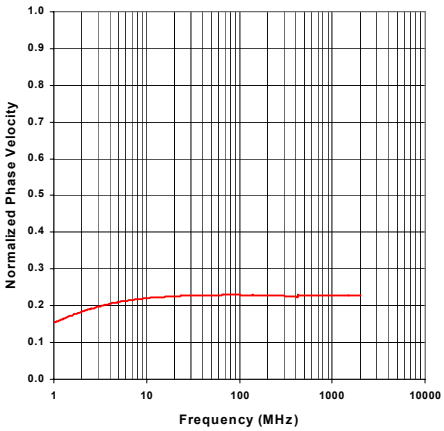

NVESD Mine Lanes

Lane 6 , Middle

File : 19Sep21524

Volumetric Moisture (%) : 0.5

Dry Density (g/cc) : 1.67

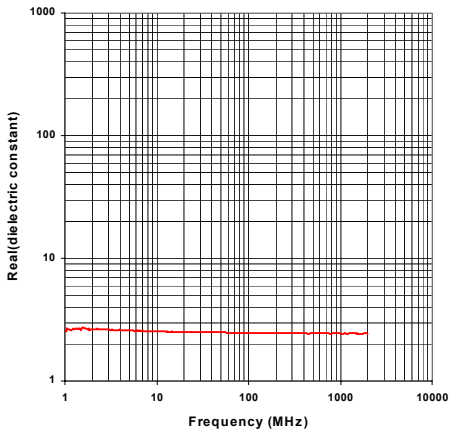

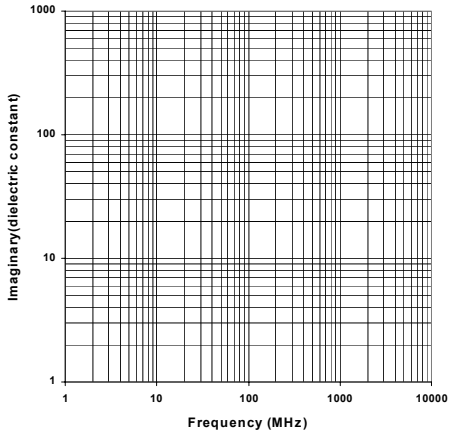

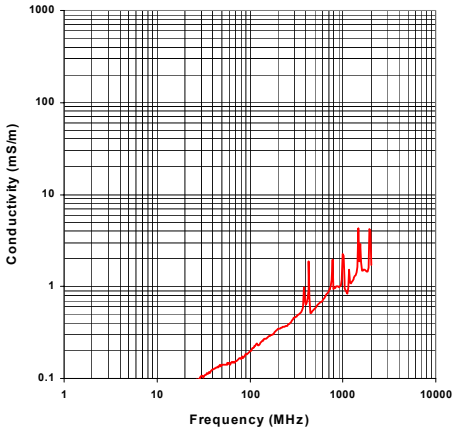

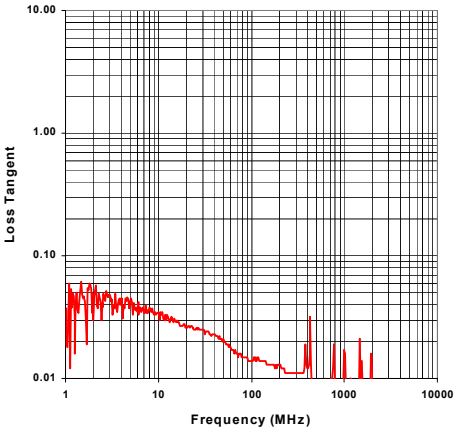

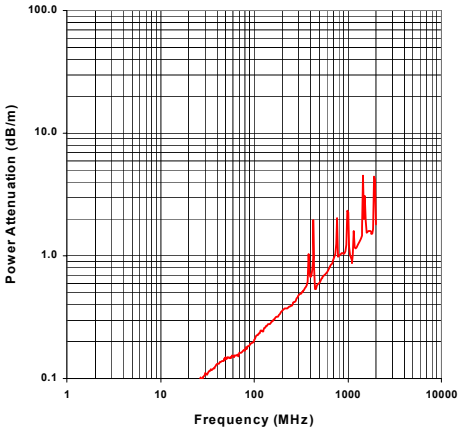

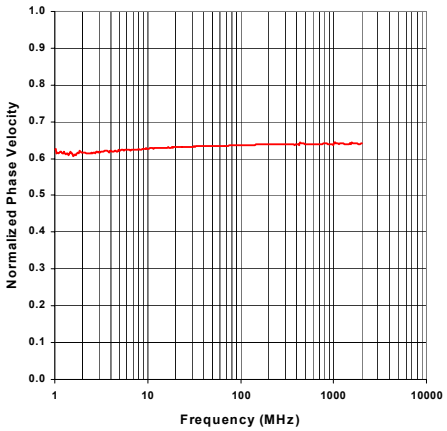

NVESD Mine Lanes

Lane 6 , Middle

File : 19Sep21629

Volumetric Moisture (%) : 16.7

Dry Density (g/cc) : 1.67

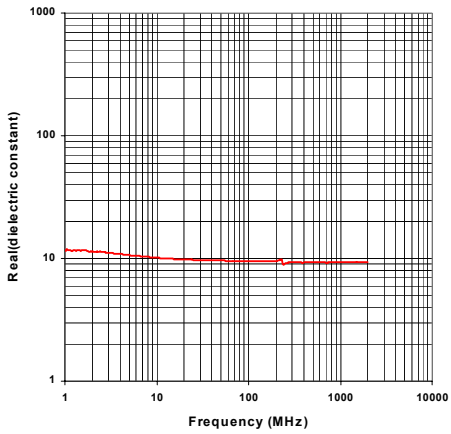

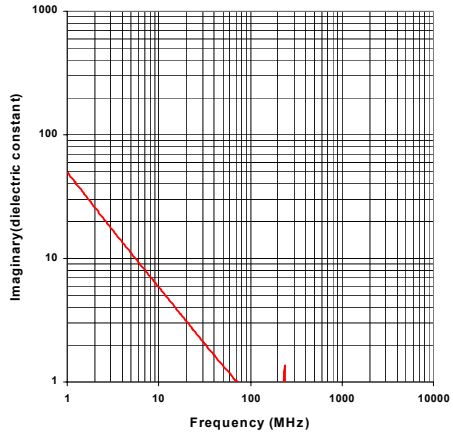

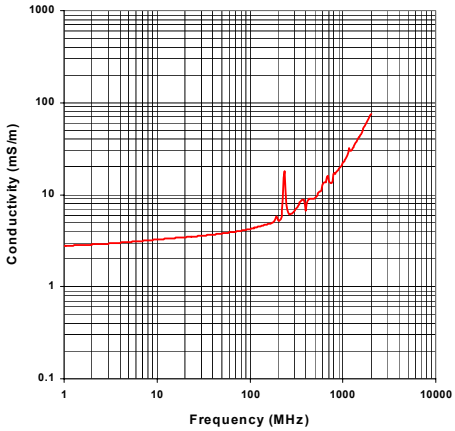

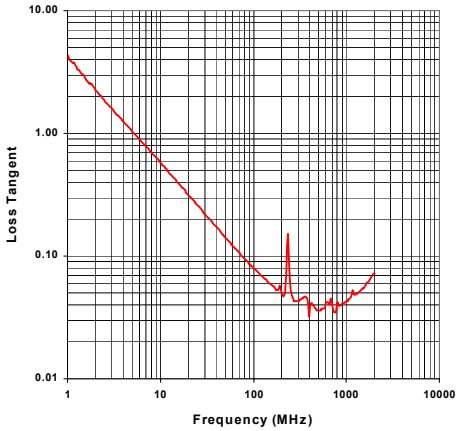

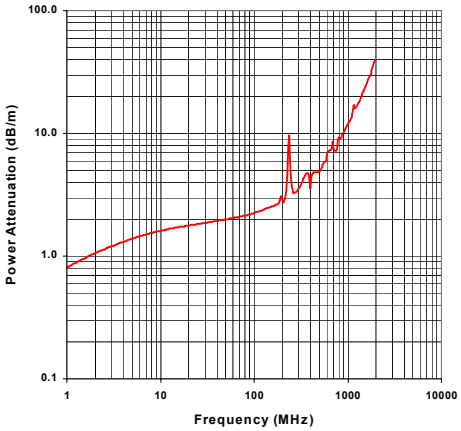

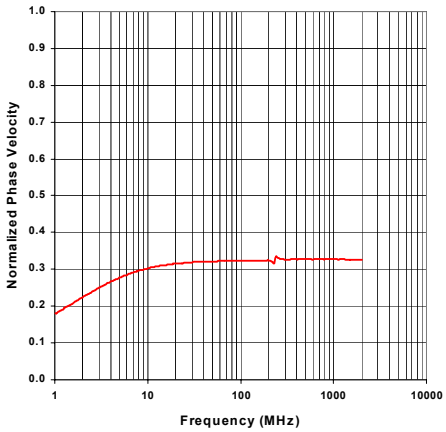

NVESD Mine Lanes

Lane 6 , Middle

File : 20Sep21036

Volumetric Moisture (%) : 26

Dry Density (g/cc) : 1.67

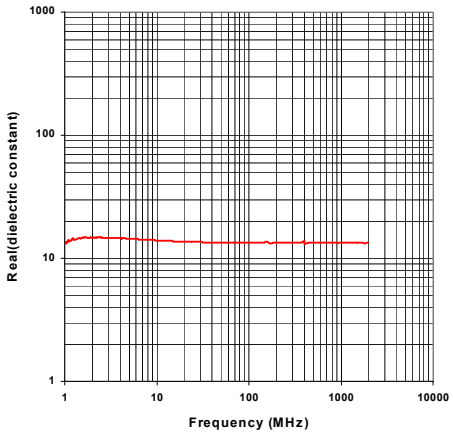

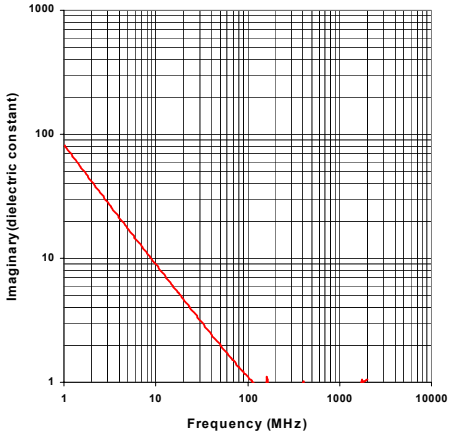

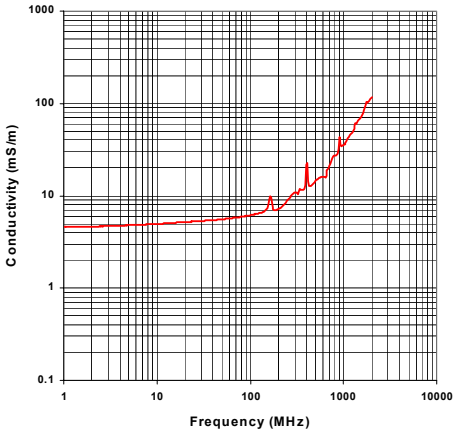

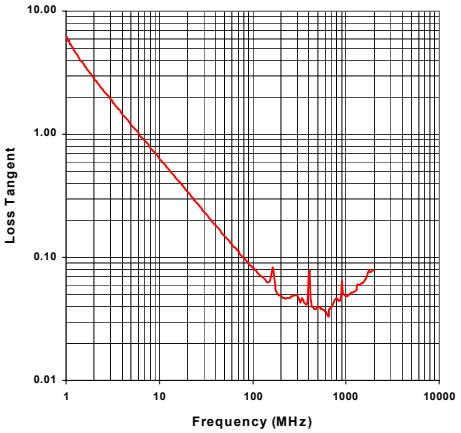

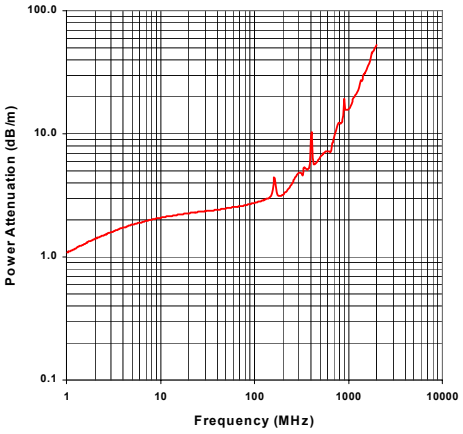

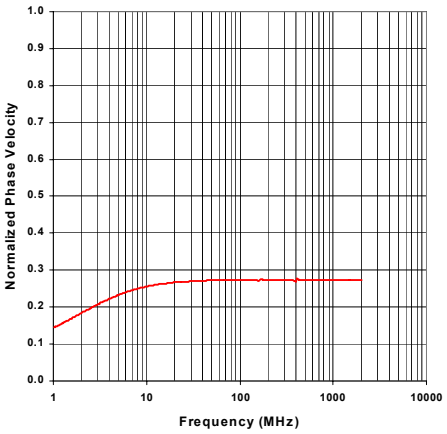

NVESD Mine Lanes

Lane 6 , S end

File : 19Sep21531

Volumetric Moisture (%) : 1.9

Dry Density (g/cc) : 1.62

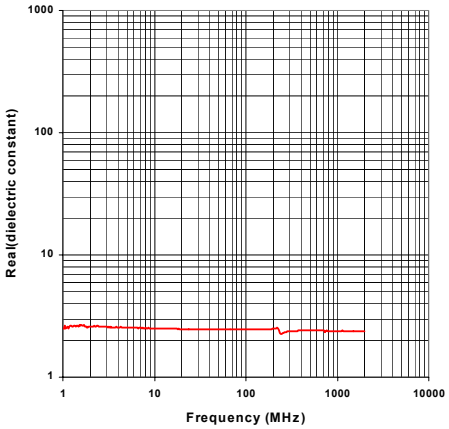

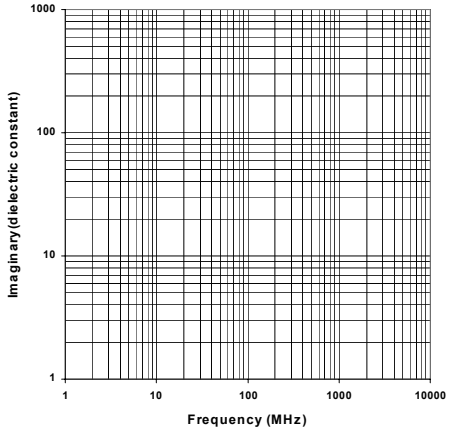

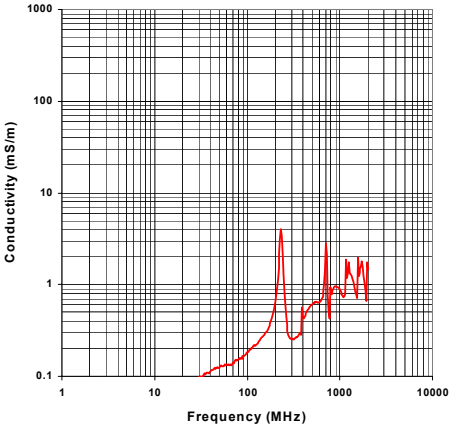

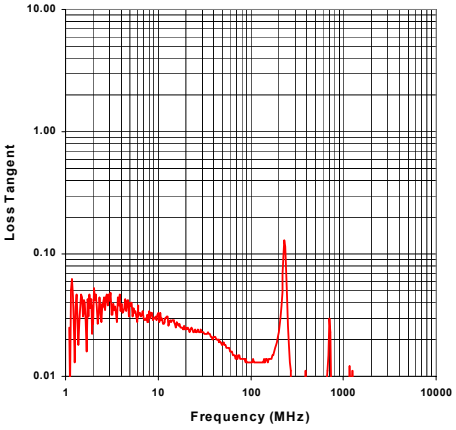

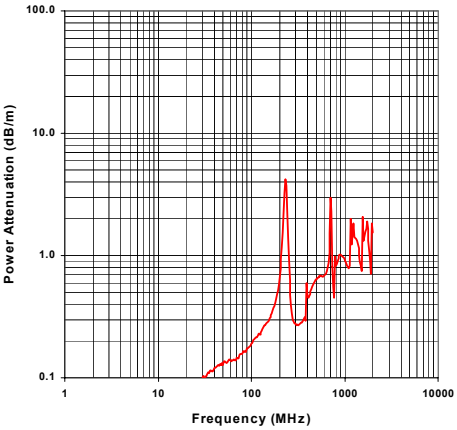

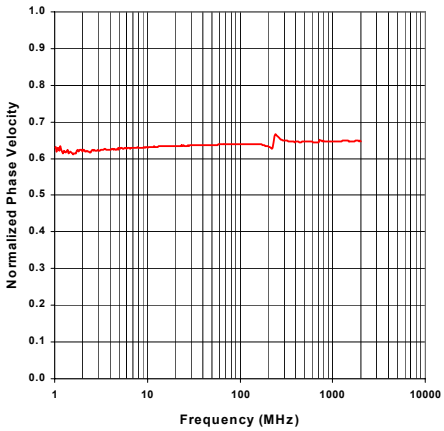

NVESD Mine Lanes

Lane 6 , S end

File : 20Sep21051

Volumetric Moisture (%) : 28.7

Dry Density (g/cc) : 1.62

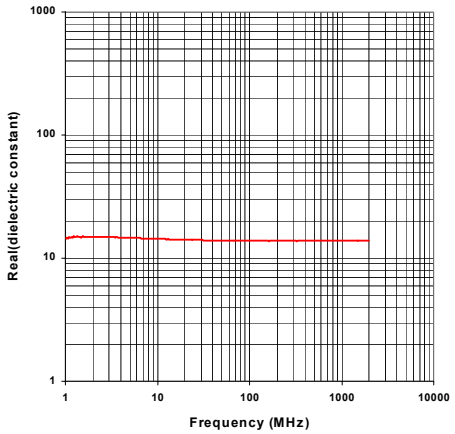

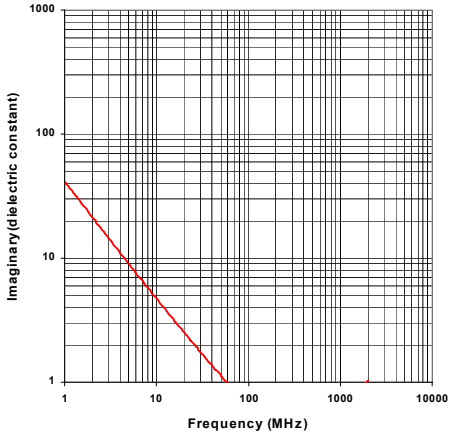

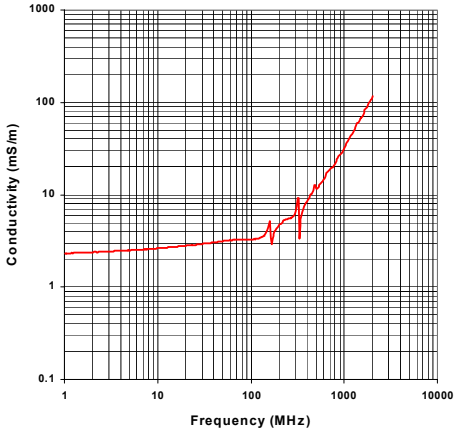

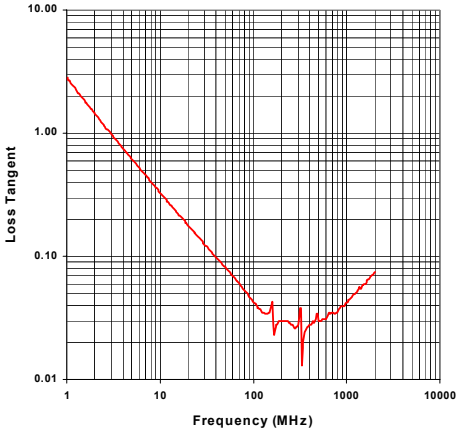

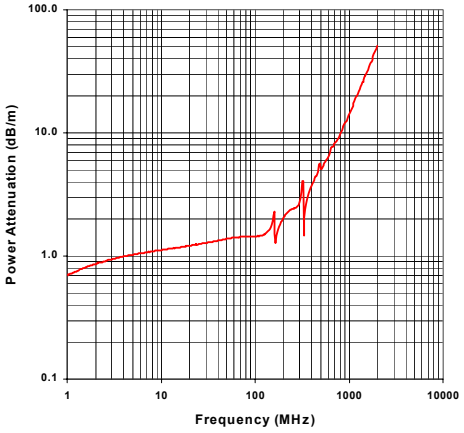

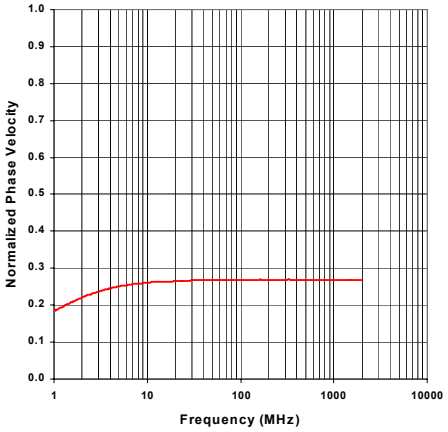

NVESD Mine Lanes

Lane 6 , S end

File : 19Sep21635

Volumetric Moisture (%) : 21.4

Dry Density (g/cc) : 1.62

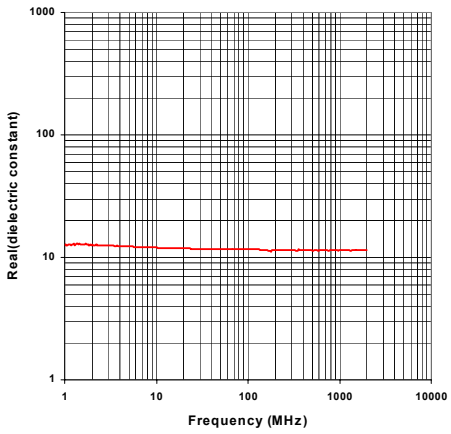

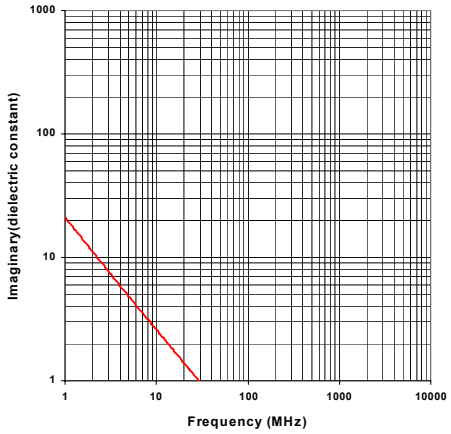

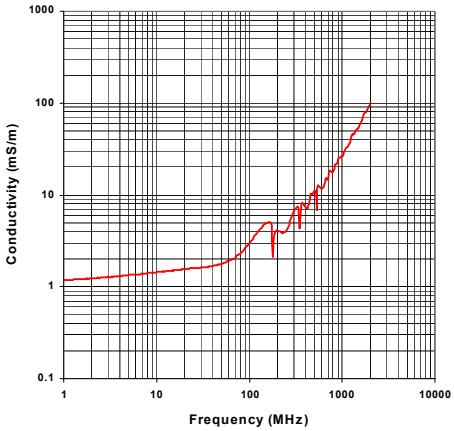

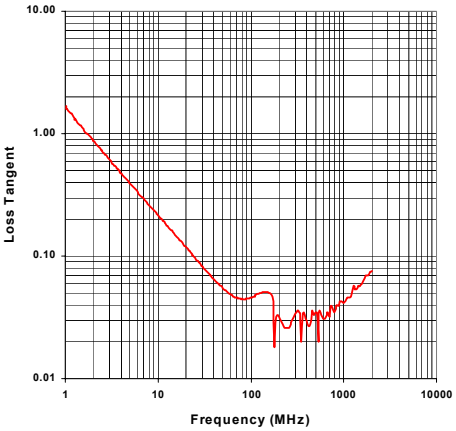

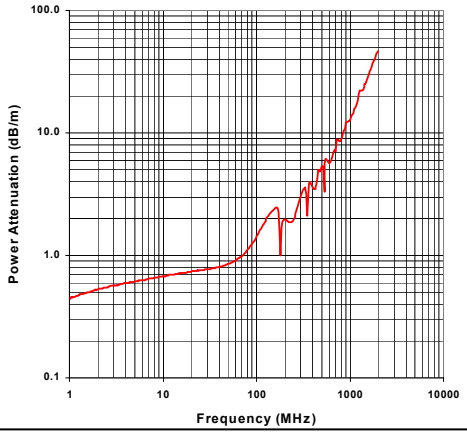

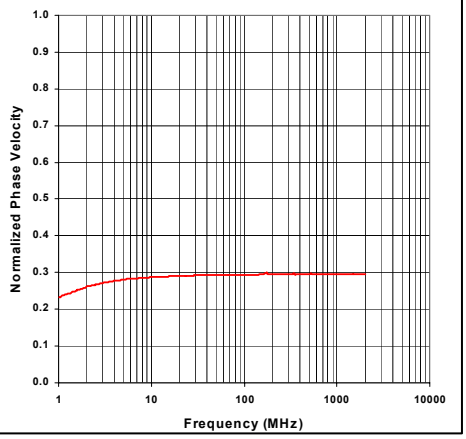

REPORT DOCUMENTATION PAGE

Form Approved
OMB No. 0704-0188

1. REPORT DATE *(DD-MM-YYYY)*	2. REPORT TYPE	3. DATES COVERED *(From - To)*
December 2004	Final report	

4. TITLE AND SUBTITLE

Characterization of Soils from the Night Vision and Electronic Sensors Directorate Mine Lane Facility, Fort Belvoir, VA

5a. CONTRACT NUMBER

5b. GRANT NUMBER

5c. PROGRAM ELEMENT NUMBER

6. AUTHOR(S)

John O. Curtis, Dan Leavell, Charles Weiss, Ryan North, Eric Smith, Javier Cortes, Ray Castellane, and Morris Fields

5d. PROJECT NUMBER

5e. TASK NUMBER

5f. WORK UNIT NUMBER

7. PERFORMING ORGANIZATION NAME(S) AND ADDRESS(ES)

Environmental Laboratory and Geotechnical and Structures Laboratory
U.S. Army Engineer Research and Development Center
3909 Halls Ferry Road, Vicksburg, MS 39180-6199

8. PERFORMING ORGANIZATION REPORT NUMBER

ERDC TR-04-6

9. SPONSORING / MONITORING AGENCY NAME(S) AND ADDRESS(ES)

U.S. Army Corps of Engineers
Washington, DC 20314-1000

10. SPONSOR/MONITOR'S ACRONYM(S)

11. SPONSOR/MONITOR'S REPORT NUMBER(S)

12. DISTRIBUTION / AVAILABILITY STATEMENT

Approved for public release; distribution is unlimited.

13. SUPPLEMENTARY NOTES

14. ABSTRACT

In support of mine detection sensor development programs at the U.S. Army Night Vision and Electronic Sensors Directorate, both onsite and laboratory measurements of soil properties were conducted on soils from the Fort Belvoir, VA, indoor mine lane facility. The lanes contain six distinctly different soils. In an effort to characterize these soils for both current and anticipated sensor technologies, measurement activities included onsite seismic refraction data collection and laboratory measurements of physical property data, complex dielectric constants, magnetic susceptibilities, visual specular reflectances, broadband infrared reflectances, and soil mineralogy and chemistry.

15. SUBJECT TERMS

Dielectric constant
Infrared reflectance
Magnetic susceptibility
Seismic refraction
Soil chemistry
Soil minerology
Soil properties
Visual reflectance

16. SECURITY CLASSIFICATION OF:			17. LIMITATION OF ABSTRACT	18. NUMBER OF PAGES	19a. NAME OF RESPONSIBLE PERSON
a. REPORT	b. ABSTRACT	c. THIS PAGE			19b. TELEPHONE NUMBER *(include area code)*
UNCLASSIFIED	UNCLASSIFIED	UNCLASSIFIED		174	